2021

Not Black and White: BMP Signaling Drives Melanocyte Differentiation Down Stream of Stem Cell Activation

Nicole Rai Infarinato

NOT BLACK AND WHITE: BMP SIGNALING DRIVES MELANOCYTE DIFFERENTIATION DOWNSTREAM OF STEM CELL ACTIVATION

A Thesis Presented to the Faculty of
The Rockefeller University
in Partial Fulfillment of the Requirements for
the degree of Doctor of Philosophy

by
Nicole Rai Infarinato
June 2021

NOT BLACK AND WHITE: BMP SIGNALING DRIVES MELANOCYTE DIFFERENTIATION DOWNSTREAM OF STEM CELL ACTIVATION

Nicole Rai Infarinato, Ph.D.
The Rockefeller University 2021

Tissue stem cells (SCs) maintain, regenerate, and repair the body over the course of an organism's lifetime. To preserve their long-term function, SCs must exert precise control over their cell state dynamics as they move from quiescence to activation and commit to full differentiation. My graduate research has been centered on investigating the molecular mechanisms that fuel these transitions in melanocyte stem cells (McSCs), a unique neural crest-derived SC population located in the hair follicle (HF). Through periodic bouts synchronous with HF cycling, quiescent McSCs become activated to proliferate, giving rise to committed proliferative progeny (McCP) that differentiate into mature pigment-producing melanocytes. The signaling factors and gene expression programs that orchestrate these cellular changes are still incompletely understood. To elucidate new insights into this process, I developed fluorescence-activated cell sorting strategies to isolate quiescent, activated, and differentiating McSC lineage cells from the mouse skin at discrete stages of the hair cycle. I then performed single cell RNA-sequencing (scRNA-seq) to reveal the evolving transcriptional signatures of the lineage with high resolution. Comparative bioinformatic analyses suggested that BMP and WNT signaling increase concomitantly throughout differentiation. I then sought to understand the role of BMP signaling in McSC lineage progression and whether this pathway engages in crosstalk with WNT signaling. To do so, I performed conditional lineage-specific genetic ablation of *Bmpr1a* to extinguish BMP signaling, which resulted in gray hair. However, McSCs remained intact and functional in these mutant animals, indicating dysfunction in their differentiating progeny. ScRNA-seq and pseudotime analysis of *Bmpr1a* null cells indicated a block in the differentiation program just downstream of the early McCP stage, and I detected further signs of melanocyte immaturity using immunofluorescence and electron microscopy analyses. Seeking mechanistic understanding, I interrogated changes in transcription factor expression at this blockage point. I found reduced nuclear levels of the master regulator MITF and WNT mediator LEF1. Using WNT mutant mouse models, cell culture systems, and chromatin profiling, I provide evidence demonstrating cooperation of BMP and WNT signaling to trigger complete differentiation of McCP into melanocytes through MITF and LEF1 activity. Altogether, I have generated a thorough characterization of the transcriptional and chromatin landscape changes that temporally define McSC lineage commitment *in vivo*. My findings underscore a critical role for signaling through BMPR1a to achieve full melanocyte differentiation in the HF. These findings raise intriguing questions about the role of BMP in hair and coat color variation, age-related hair graying, and melanoma initiation and progression.

For Ryan, who shows me what courage and ambition looks like.

Thank you for helping me do hard things.

ACKNOWLEDGEMENTS

This dissertation has only been possible through the support and guidance of my mentor, Dr. Elaine Fuchs. What an incredible privilege it has been to learn and work alongside such a scientific powerhouse. Elaine is fearless in the questions she pursues and tireless in her commitment to accomplish our collective goals in the lab. She has taught me that in order to grow, you must have the courage to be uncomfortable, which requires a little grace towards yourself and trust in the process. Thank you for continuously challenging me and pushing me to think differently. I will carry the lessons I have learned in your lab for the rest of my life.

Katie Stewart has been the most committed collaborator and postdoc mentor I could ever ask for. Our friendship and scientific partnership formed organically, and her contributions were absolutely critical to this body of work. Katie went above and beyond to push the data forward and was extremely invested in learning and implementing new bioinformatic analyses along the way. Our discussions invigorated me to approach my experiments in creative ways and encouraged me when I needed it most. I am so grateful to you.

Thank you to Drs. Sohail Tavazoie and Mary Beth Hatten for serving on my Thesis Committee and consistently providing valuable feedback and support during my training. Thank you to Dr. Ya-Chieh Hsu, whose work I have long admired, for kindly agreeing to participate as my External Examiner. I am grateful to Sohail for allowing me to rotate in his lab, where I was able to work on a wide range of projects and really learn to take initiative to figure out new experimental systems and techniques. Similarly, I thank Mary Beth for graciously offering me her lab's resources and knowledge to approach my experiments differently when I hit hurdles. It has been such a pleasure discussing my science with you all throughout the years.

One of the most enjoyable and advantageous aspects of training in the Fuchs Lab has been spending every day with an incredibly brilliant and diverse group of colleagues. Nick Gomez was instrumental in helping me conceptualize and shape my thesis project. I am especially grateful for his excellent advice in building effective presentations. Through Nick, I was so lucky to meet Megan Gomez, who quickly became one of my closest friends and an immense source of joy, laughter, support, and understanding. My bay mate Leo Yuan has been one of my most dependable and generous friends, and I am thankful that we have been able to go through this program side-by-side. While all members of the lab (past and present) have impacted me and contributed to my training in some way, I am especially grateful for scientific discussions and experimental help from Yihao Yang, Brian Hurwitz, Sanjee Baksh, Rene Adam, Stephanie Ellis, Phoenix Miao, Shruti Naik, Melanie Laurin, Samantha Larson, Irina Matos, Rachel Niec, Shiri Gur-Cohen, Hanseul Yang, Vince Fiore, Anita Kulukian, and Kevin Gonzales. Many of my lab mates are not only excellent colleagues, but are also my dear friends.

I sincerely thank all members of the amazing Fuchs Lab staff and animal team, who make doing science here efficient and seamless. While our staff is always indispensable for the research we do, this has never been more true than in the face of COVID-19. During the shutdown and at every stage of reopening, June Racelis, Ellen Wong, Maria Nikolova, Lisa Polak, Lynette Hidalgo, Megan Sribour, John Levorse, and Prashant Nasseir all contributed to maintaining and reinventing operations in the lab to keep everyone safe and enable our projects to move forward. This pandemic has presented extraordinary challenges to how we function personally and collectively as a lab, and I appreciate all of our team's efforts to adapt and look out for one another.

I owe an enormous debt of gratitude to my support networks in and outside of Rockefeller. All members of the Deans Office have been incredible since the time I was just a prospective

student, and I am thankful for their reliability and accessibility. Drs. Emily Harms and Andrea Morris and Cristian Rosario have been exceptionally helpful. Over the years, Andrea and I have developed a close relationship, and I have counted on her for guidance with everything from navigating research collaborations and developing my manuscript to exploring career opportunities. Similarly, Occupational Health Services has been such a lifeline; I feel enormously privileged to have had access to the care of Lauren Rosenblum and Drs. Nisha Mehta-Naik and Daniel Knoepflmacher. I would also like to thank Iris Taylor and Ann Campbell for showing me such care and compassion. Thank you to my college biochemistry professor, Dr. Dontarie Stallings, who believed in me in the very beginning and advised me to pursue a Ph.D. I am endlessly grateful to Dr. Yael Mossé for her steadfast support and my first real opportunity in biomedical research. Yael's palpable, tireless commitment for research to advance pediatric cancer treatments ignited my desire to pursue a career in science. For allowing me to explore a different side of science, I thank the *Journal of Cell Biology*, especially Drs. Rebecca Alvania and Melina Casadio. Finally, my friends at Rockefeller and beyond continue to bring me so much joy and insight; thank you especially to Hannah Ryles, Priya Khurana, McKenna Storey, Emily Schlick, Pascal Maguin, Melissa Jarmel, and Kimberly Patricia.

Thank you a million times now and always to my family: my Mama, Dad, Kelly, Matthew, and Sophie. You kept me laughing through the most difficult days and made me strong with all your love, hugs, and homecooked food. Dad, your mastery of French, engaging teaching style, and humor have shown me how I could build incredible abilities with education, and how important it is to share what you know in ways that get other people excited. Mama, you have shown me how much one woman is capable of, and watching you light up your clients' faces with your remarkable talent, hard work, and huge heart have taught me the importance of finding a career where you can

stand fully in your purpose. Kelly, my first best friend, the challenges you face as a teacher and the way you serve your students shows me how much of a difference one person can make in someone else's life, and I am reminded of that in my interactions with my lab mates. By your example, I am inspired to advocate for myself, even when I am really intimidated. Matty, thinking of your grit and determination through engineering school and now on your journey to medicine has kept me going in times when I was fed up with failing and wanted to quit. Sophie, your wisdom, commitment to your art, and alignment with your instincts have put you on a beautiful path, and I am inspired to find out what that looks like for me. I am also very fortunate to have a large and supportive extended family, headed by our queen Nonnie, who cares so deeply about all of us and expresses such interest in my science. Spending time with my grandparents, aunts, uncles, and cousins always leaves me feeling loved and bolstered. During my time in graduate school, I have lost two incredible grandparents, my Poppy and my Grammy Carm, as well as our sweet golden girl, Lucy. I miss and love you all tremendously.

And of course, thank you to my partner in life, Ryan Platt, for being the home I come back to every night. Through the years since we have teamed up, we have rubbed off on one another and continue to grow together. I am emboldened by your bravery, wild ambition, and faith in your ability to learn. I love you and our little man Remy more than I can say. I cannot wait to see what the future has in store for us next.

Significant Contributions

The work presented here was published in its original form in *Genes & Development* (Infarinato et al., 2020) and represents a collaborative effort. I sincerely thank each contributor for making this work possible. Dr. Katherine Stewart performed the scRNA-seq analysis, with the assistance of Dr. Nicholas Gomez in data preprocessing. Yihao Yang was especially helpful during revisions with cell culture experiments, and he also performed the predictive motif analysis on differentially expressed genes. Lynette Hidalgo and Lisa Polak maintained the mice colonies and trained me in procedures related to animal work. Many of these experiments relied on the expertise and equipment of the Rockefeller Resource Core facilities. Thank you to the Flow Cytometry Resource Center, especially Drs. Svetlana Mazel and Songyan Han and Stanka Semova for performing countless cell sorts on my often difficult samples. Dr. H. Amalia Pasolli and Nadine Saplop in the Electron Microscopy Core were critical in preparing, imaging, and analyzing my samples to assess melanosome ultrastructure. Dr. Thomas Carroll, head of the Bioinformatics Resource Center, was instrumental in analyzing the bulk RNA-seq and ATAC-seq datasets. The Genomics Resource facilities at both Rockefeller and Weill Cornell were essential for these high-throughput sequencing experiments. I also thank the members of the Bio-imaging Resource Center, especially Tao Tong for guidance on image processing and quantification. Relevant sections of **Chapter 5** (Materials and Methods) were written by Drs. Katherine Stewart and Thomas Carroll and Yihao Yang for the publication of our manuscript, and these sections have been slightly reworded and edited for the purpose of this thesis. Finally, all authors of the Infarinato et al., 2020 paper provided essential intellectual input in the form of valuable discussions, ideas for experiments, and troubleshooting.

TABLE OF CONTENTS

LIST OF FIGURES

Chapter1

Chapter 2

Chapter 3

LIST OF TABLES

LIST OF ABBREVIATIONS

α-MSH	Alpha-melanocyte-stimulating hormone
Acvr2a	Activin A receptor type 2A
ADRB2	β-2 adrenergic receptor
ALK	Activin Receptor-Like Kinase
Alx3	Aristaless-like homeobox 3
aMcSC	Activated melanocyte stem cell
AP-1	Activator protein 1
ASIP	Agouti signaling protein
Ana	Anagen
ATAC-seq	Assay for Transposase Accessible Chromatin with sequencing
BMP	Bone morphogenetic protein
Bmpr1a/BMPR1a	Bone morphogenetic protein receptor 1A
BRAF	V-raf murine sarcoma viral oncogene homolog B1
BrdU	Bromodeoxyuridine
Bu	Bulge
C	Cluster
cAMP	Cyclic adenosine monophosphate
CD	Cluster of differentiation
cKO	Conditional knockout
COL17A1	collagen XVII
C→T	Cytosine to thymine
CUT&RUN	Cleavage Under Targets and Release Using Nuclease
CXCR4	C-X-C Motif Chemokine Receptor 4
Dct/DCT	Dopachrome tautomerase
DP	Dermal papilla(e)
E	Embryonic day
EDN	Endothelin
EdU	5-Ethyl-2′-deoxyuridine
eGFP	Enhanced green fluorescent protein
EM	Electron microscopy
ERCC	External RNA controls consortium
FACS	Fluorescence-activated cell sorting
FDR	False discovery rate
FoxD3	Forkhead Box D3
GDF6	Growth differentiation factor 6 (also known as BMP13)
GEO	Gene Expression Omnibus
GO	Gene ontology
Gpr143	G Protein-Coupled Receptor 143 (also known as *Oa1*, ocular albinism 1)
G→T	Guanine to thymine
HB	Hair bulb
Het	Heterozygote/heterozygous
HF	Hair follicle
HFSC	Hair follicle stem cell
HG	Hair germ

Id1/2/3	Inhibitor of DNA Binding
IMF	Immunofluorescence
IP	Intraperitoneal (injection)
k-NN	k-nearest neighbors
Kb	Kilobases
KO	Knockout
LacZ	β-galactosidase
Lef1/LEF1	Lymphoid Enhancer Binding Factor 1
Mc1r/MC1R	Melanocortin 1 receptor
McCP	Melanocyte stem cell committed, proliferative progeny
McSC	Melanocyte stem cell
Mitf/MITF	Microphthalmia-associated transcription factor
Msx1/2	Msh homeobox
NF1	Neurofibromin 1
NRAS	Neuroblastoma RAS viral oncogene homolog
Oca2	Oculocutaneous albinism II
ORS	Outer root sheath
P	Postnatal day
p53	Tumor protein P53
Pax3/PAX3	Paired box 3
PBS	Phosphate buffered saline
PCA	Principle component analysis
PI3K	Phosphoinositol 3-kinase pathway
PMEL	Premelanosome protein
POMC	Proopiomelanocortin
pP38	Phosphorylated p38 MAP kinase
pSMAD1/5/9	Phosphorylated SMAD1/5/9
PTEN	Phosphatase-and-tensin homologue
qMcSC	Quiescent melanocyte stem cell
R26YFP	*Rosa-26* yellow fluorescent protein
RAC1	Ras-related C3 botulinum toxin substrate 1
RBP-J	Recombination signal binding protein for immunoglobulin kappa J
RFP	Red fluorescent protein
RT-qPCR	Real time quantitative polymerase chain reaction
SC	Stem cell
SCF	Stem cell factor (also known as KIT ligand)
scRNA-seq	Single cell RNA-sequencing
SDF-1	Stromal cell-derived factor 1
SHH	Sonic hedgehog
Slc45a2	Solute carrier family 45 member 2
Sox10/SOX10	Sex determining region Y-box 10
SMAD	*C. elegan*s Sma and the *Drosophila* Mothers against decapentaplegic
TACs	Transit-amplifying cells
Telo	Telogen
TCF	T cell factor
TGF-β	Transforming growth factor beta

TF	Transcription factor
TPM	Transcripts per million
TSS	Transcription start site
Tyr/TYR	Tyrosinase
TyrCreER	*Tyrosinase* estrogen receptor Cre recombinase
TYRP1	Tyrosinase-related protein 1
UMAP	Uniform manifold approximation and projection
UV	Ultraviolet (light/radiation)
WNT	Wingless-related integration site
WT	Wild type
YFP	Yellow fluorescent protein

CHAPTER 1:
INTRODUCTION

1.1 Melanocytes and their embryonic origins

Looking across the animal kingdom, there is astonishing variety in hair, fur, skin, and feather pigmentation and patterning. These shades and their unique organization have myriad functions including protection from ultraviolet (UV) light, thermoregulation, camouflage, sexual selection, and communication (Caro and Mallarino, 2020). Underlying this phenotypic diversity are melanocytes, a specialized cell type found in vertebrates that synthesize and transfer black-brown eumelanin and red-yellow pheomelanin pigment (Mort et al., 2015). Given the overt visible effects induced by changes in this lineage, melanocytes and their precursor cells have long been an attractive system for developmental and cell biologists and geneticists to harness. From the wide array of coat colors in "fancy mice" to animals recapitulating human cancer and disease, mice continue to be an excellent model organism in which to study this unique lineage.

The cells that terminally differentiate into melanocytes initially emerge during embryonic development from the trunk region of the neural crest. A small number of founder progenitor cells called melanoblasts are specified in a process governed chiefly by WNT signaling (Luciani et al., 2011; Thomas and Erickson, 2008). WNT induces neural crest formation and also directs downstream specification of melanoblasts. WNT1 and WNT3a ligands are expressed in the dorsal neural tube, and double knockout (KO) mice show defects in melanocyte specification, along with other neural crest-derived lineages (Ikeya et al., 1997). Consistently, neural crest-specific KO of downstream WNT mediator β-catenin using *Wnt1-Cre* causes loss of melanocytes (Hari et al., 2002; Hari et al., 2012). BMP signaling appears to act antagonistically, and BMP4 is downregulated in the neural tube at the time of melanoblast specification. Cultured neural crest cells treated with WNT3a adopt a melanocyte fate, while BMP4 drives cells instead towards a neural fate (Jin et al., 2001). Transcription factors (TFs) SOX10 and PAX3 are expressed in both

melanocyte and glial fated cells, while WNT/β-catenin activates the master regulator of the melanocyte lineage microphthalmia-associated transcription factor (MITF) (Dorsky et al., 2000; Takeda et al., 2000). Differentiation between these two lineages occurs via FOXD3, which represses MITF to favor neuron and glial cell fates (Thomas and Erickson, 2009). SOX10 and PAX3 then in turn regulate MITF (Potterf et al., 2000).

Around embryonic day (E) 9 in mice, melanoblasts begin to depart from the neural crest and embark on a spectacular migratory journey to colonize their destination niches throughout the body. They move along two major routes: the dorsolateral and ventral pathways. In the more well-characterized dorsolateral pathway, melanoblasts travel between the somites and ectoderm in what appears to be a first wave of migration (Erickson and Goins, 1995). It was later discovered that bipotent precursor cells with the capacity to differentiate into either melanoblasts or Schwann cells migrate along developing nerve sheaths in a second wave to populate the limbs with melanocytes (Adameyko et al., 2009). In cells migrating along the dorsolateral pathway, the expression of lineage-specific markers such as MITF and melanogenic enzyme dopachrome tautomerase (DCT) occurs around E10.5 (Larue et al., 2013; Mort et al., 2015).

By E11.5, melanoblasts begin to cross the basement membrane from the dermis to invade the epidermis. Their migration and invasion relies on several cytoskeletal organization factors such as RAC1 (Li et al., 2011; Mort et al., 2015). Outside of intrinsic migratory factors, melanoblasts presumably require external guidance cues to find the epidermis, although the identity and timing of such factors are largely unknown. However, evidence from 3-dimensional culture systems suggests that the membrane-bound form of stem cell factor (SCF, also known as kit ligand, KITL) expressed in the basal layer of the developing epidermis may direct melanoblasts to localize at this

juncture (Tabone-Eglinger et al., 2012). While many melanoblasts cross into and expand in the epidermis, a subset of cells persist in the dermis.

As melanoblasts migrate throughout the developing embryo, they undergo massive proliferation (Larue et al., 2013). Again, WNT/β-catenin signaling is critical here, driving proliferation in both the epidermal and dermal compartments (Luciani et al., 2011). Lineage-specific ablation studies *in vivo* have revealed other key genes and pathways regulating melanoblast migration and proliferation, with mutant animals displaying loss of pigmentation and white spotting phenotypes. Endothelin 3 (EDN3) is expressed in mesenchymal cells and signals through endothelin receptor-B (EDNRB) on melanoblasts, driving their proliferation in the dermis as well as their migration (Larue et al., 2013; Lee et al., 2003; Shin et al., 1999). SCF/c-KIT signaling also plays an essential role in proliferation, as well as in cell survival and migration (Yoshida et al., 1996a, Yoshida et al., 1996b). This crucial ligand is expressed by the mesenchyme and epidermis during embryonic development, driving melanoblast expansion specifically once cells reach the epidermis.

By E15.5, melanoblasts cluster around developing hair follicles (HFs) and sweat glands through a process that is still poorly characterized. There is some evidence that the chemokine receptor CXCR4 expressed on melanoblasts plays a role in their positioning, as disruption of this receptor *in vivo* results in melanoblasts aggregating abnormally in the epidermis. In culture, the CXCR4 ligand SDF-1 functions as a chemoattractant (Belmadani et al., 2009). Experiments using *Dct*-LacZ embryonic skin explants and ligand-coated beads demonstrated that while SCF serves as a chemokinetic factor facilitating melanoblast migration, it does not act as an attractive force (Jordan and Jackson, 2000). However, given the complex dynamics of morphogenesis, it is likely

that a plethora of other factors in addition to SDF-1 and SCF instruct melanoblast localization to their target destinations.

Once at the HFs, these progenitors migrate towards the base of the down-growing hair bulb and continue to differentiate into pigment-producing melanocytes that supply melanin for the first round of hair growth. However, a fraction of the migrating melanoblasts associate with the mid-portion of the HF in a specialized region known as the bulge where hair follicle stem cells (HFSCs) reside. Here, melanoblasts are maintained in an immature and quiescent state. It is still not understood how these colonizing melanoblasts initially become segregated into two compartments of bulge-associated immature and hair bulb matrix-associated differentiating cells.

The major localization of melanocytes is the skin, where they reside in both HFs and the basal layer of the epidermis. However, melanocytes are found in other organs, including the eye, inner ear, brain, and heart. While their primary purpose is to generate melanin pigment for UV protection, their unexpected locations in other sites throughout the body seem to suggest that melanocytes may have surprising auxiliary functions. While melanocytes in the kidney marrow of fish shield hematopoietic stem and progenitor cells from UV damage (Kapp et al., 2018), analogous to their role in the skin, conversely, melanocytes in the ear are actually critical for hearing and are thought to modulate the chemical composition of endolymph (Price and Fisher, 2001). Future studies on these unconventional melanocyte-lineage populations may lend further insight into other potential roles these cells play in the skin.

1.2 Tissue melanocyte stem cells (McSCs) and their progeny in the HF

Adult tissue-specific stem cells (SCs) are populations of long-lived cells that maintain and regenerate tissues in homeostasis and injury over the course of an organism's lifetime. For many

decades, researchers posited that a pool of SCs must exist in order to replenish the melanocytes of the HF, which are eliminated at the end of each hair cycle (Nishimura, 2011). Furthermore, so-called "amelanotic melanocytes" were observed in the ORS of human HFs (Staricco, 1959). In 2002, Nishimura et al. demonstrated that the melanoblasts that initially localize to the bulge region fulfill the criteria for tissue SCs. These *Dct*-LacZ^{+} cells remained immature and unpigmented through adulthood and were slow-cycling, as demonstrated by their ability to retain bromodeoxyuridine (BrdU) in pulse-chase experiments. After depletion of their differentiating progeny with KIT blocking antibody, these immature cells in the bulge survived and were able to both self-renew and repopulate the hair bulb compartment with differentiating melanocytes in the subsequent hair cycle. In hair reconstitution assays using whisker follicle fragments, only implants with the lower permanent portion of HFs (where these undifferentiated *Dct*-LacZ^{+} cells were localized) gave rise to pigmented hair in albino animals. This population of cells are hence referred to as melanocyte stem cells (McSCs) (Nishimura et al., 2002; Nishimura, 2011)

To achieve growth of pigmented hair, HFSCs, which fuel the growth and regeneration of the HF, and McSCs must coordinate their behavior. Hair growth occurs through stages of rest, active growth, and regression **(Fig. 1.1)** (Gonzales and Fuchs, 2017). In telogen, hair follicles are at rest, with both HFSCs and neighboring McSCs in quiescence. At the onset of anagen, or active hair growth, HFSCs at the base of the bulge and nearby McSCs become activated to proliferate. HFSCs of the hair germ (HG) give rise to short-lived proliferative progeny that envelope the mesenchymal dermal papilla (DP), forming a hair bulb of matrix cells. HFSCs in the bulge generate the downward growing outer root sheath (ORS), creating distance from the proliferating hair bulb and DP and restoring quiescence to the bulge and upper ORS compartments (Hsu et al., 2014; Yang et al., 2017). Similarly, in early anagen, activated McSCs (aMcSCs) enter a brief

window of proliferation to give rise to committed, proliferative progeny (McCP). The McCP become spatially segregated from the SC compartment and associate with the DP and hair matrix. Here in the hair bulb, McCP continue to differentiate into melanocytes that produce and transfer pigment to neighboring hair cells, imparting color to the growing hair. Finally, in catagen, the destructive phase of the hair cycle, mature melanocytes undergo apoptosis alongside the lower two thirds of the follicle (Tobin et al., 1998).

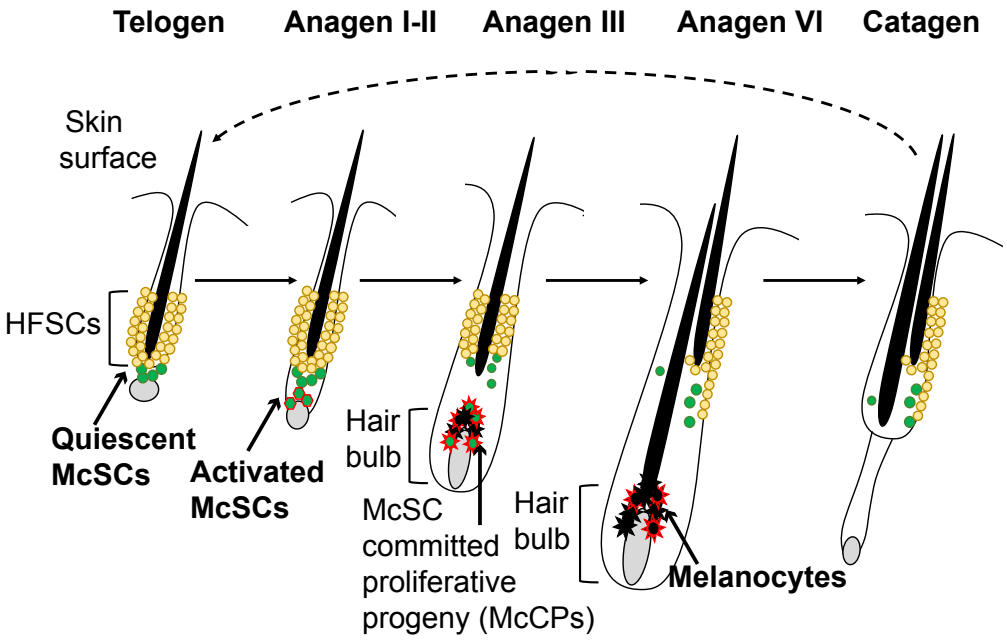

Figure 1.1 McSCs undergo periodic bouts of quiescence, activation, and differentiation throughout the hair cycle.

Hair cycling in mice is highly predictable and can be easily tracked and manipulated through method such as hair plucking, which induces anagen. Given that the tissue SC populations residing in the HF exhibit periodic bouts of activity in sync with cycling, the mouse skin is an excellent system with which to temporally investigate SC quiescence (reversible cell cycle exit), activation (proliferation), lineage commitment, and differentiation *in vivo*. While HFSCs have been thoroughly studied and profiled in this context, less is known about the dynamic behavior of

McSCs. Here, mouse models present an additional advantage, because unlike human skin, mouse back skin lacks epidermal melanocytes. Unlike the melanocyte progeny generated by McSCs in the HF, epidermal melanocytes divide infrequently and produce and transfer melanin depending on the skin's UV exposure (Davis et al., 2019). Therefore, the mouse skin provides a simplified system in which to specifically probe McSCs and their lineage. A more complete understanding of melanocyte lineage progression under homeostatic conditions is a critical prerequisite to achieving greater insight into melanocyte-related pathologies like melanoma and eventually developing novel therapeutic approaches for such conditions.

1.3 Key regulators of McSC quiescence, activation, and melanocyte differentiation

Tissue SCs protect their long term potential through precisely controlling their transitions between quiescence, activation, and differentiation. Like Muscle SCs, hematopoietic SCs, neural SCs, and HFSCs, McSCs exhibit periodic activity (van Velthoven and Rando, 2019). Dysregulation of the cellular states of SCs occurs during aging and can contribute to declining tissue repair and fitness, as well as in disease states characterized by excessive cell proliferation, such as cancer. Regulation of these states and the transitions between them occurs at both the cell intrinsic and extrinsic levels.

Lineage and cell state-specific TF expression is a defining feature of cell-intrinsic regulation. Master regulator MITF directs diverse cellular processes at all stages of development, including survival, proliferation, and melanocyte differentiation (Goding and Arnheiter, 2019). It coordinates these myriad functions by acting differently at low, medium, and high levels (Carreira et al., 2006), as well as by interacting with other TFs (Goding and Arnheiter, 2019). Its expression is regulated by the TFs PAX3 and SOX10 (Lang et al., 2005; Harris et al., 2013; Potterf et al.,

2000). In McSCs, PAX3 is thought to both restrict lineage potential and prevent differentiation (Lang et al., 2005). SOX10 is necessary for McSC maintenance, but if levels are too high, SCs prematurely differentiate and are lost (Harris et al., 2013). In addition to these critical TFs, expression of the anti-apoptotic protein BCL2 is necessary for McSC maintenance and is especially critical as cells return to quiescence (Nishimura et al., 2005). During McSC activation, B-RAF and C-RAF kinases together are essential for cell cycle entry (Valluet et al., 2012).

Ultimately, the role of the niche and the extrinsic cues it provides are indispensable for the appropriate regulation of McSC activity, converging on these TFs to control cellular behavior. Functional studies in mice have demonstrated that neighboring HFSCs to which McSCs adhere are a crucial component of their specialized microenvironment. HFSCs express the hemidesmosomal transmembrane collagen, COL17A1, which is essential for their maintenance, quiescence, and expression of transforming growth factor beta (TGF-β) (Tanimura et al., 2011). While COL17A1 is essential for the structural integrity of the McSC niche, TGF-β from HFSCs promotes McSC quiescence (Nishimura et al., 2010; Tanimura et al., 2011). Cell-cell interactions are again important for Notch signaling, which is necessary for McSC maintenance (Moriyama et al., 2006; Schouwey et al., 2007). At the same time, Notch signaling through RBP-J in HFSCs regulates levels of retinoic acid, changes in which sensitize McSCs to differentiation (Lu et al., 2020).

At the onset of anagen, WNT/β-catenin signaling activates both HFSCs and McSCs. Additional crosstalk occurs here, as activated HFSCs secrete EDN-1 which further induces McSC proliferation (Rabbani et al., 2011; Takeo et al., 2016). Loss of the TF NFIB in HFSCs leads to expression of EDN-2, causing expansion of McSCs and precocious differentiation (Chang et al., 2013). As anagen progresses, HF lineages continue to guide McSC differentiation. WNT/β-catenin

signaling continue to be essential, as mice lacking β-catenin in the melanocyte lineage show reduced proliferation of McSCs in the bulge as well as in their progeny in the hair bulb, which fail to fully differentiate (Rabbani et al., 2011). Proliferating and differentiating lineage cells (McCP) express c-KIT receptor, and overexpression of its ligand stem cell factor (SCF) increases the number of melanocytes in the hair bulb. Conversely, interrupting this signaling cascade with c-KIT blocking antibody induces hair graying due to reduced melanocytes and impaired differentiation (Botchkareva et al., 2001). In their landmark study identifying McSCs, Nishimura et al. (2002) employed this blocking antibody to show that McSCs persist and replenish differentiating progeny in subsequent hair cycles. Later, *Krox20*-expressing hair shaft progenitors in the matrix were found to be a key source of essential SCF that fuels melanocyte differentiation (Liao et al., 2017).

However, HFSCs and their lineage are not the only niche cell types that influence McSC activity. Groundbreaking work by Zhang et al. (2020) investigating the link between stress and hair graying revealed the influence of sympathetic nerves on McSC activity. qMcSCs express ADRB2, which receive stress signals from nerves via the neurotransmitter norepinephrine, inducing proliferation, migration, and differentiation out of the bulge niche. The mesenchymal DP of the HF is also a key regulator and source of SCF (Yoshida et al., 1996). Wnt/β-catenin activity in the DP directs pigment-type production in melanocytes via agouti signaling protein (ASIP) or agouti-inhibitor corin expression. Melanocortin 1 receptor (MC1R) is expressed on melanocyte lineage cells and binds either alpha-melanocyte-stimulating hormone α-MSH or ASIP to induce eumelanin or pheomelanin production, respectively, via cAMP activity (Enshell-Seijffers et al., 2010).

The melanocyte lineage can also be regulated on a systemic level. Hormones like proopiomelanocortin (POMC)-derived neuropeptides adrenocorticotropic hormone (ACTH) and several MSHs are produced in the pituitary gland and can induce pigment production in melanocytes of the skin (Ito et al., 2005; Suzuki et al., 1996). Interestingly, a form of epidermal hyperpigmentation known as melasma can be triggered by fluctuations in sex hormones from pregnancy or medication (Filoni et al., 2019). There is also evidence of an emerging role of McSC crosstalk with the innate immune system via MITF (Harris et al., 2018).

Throughout the animal kingdom, regulators of the McSC lineage are manipulated to achieve hair color variations and patterns with functions beyond UV protection, including camouflage, inter- and intra-species signaling, mating rituals, and thermoregulation. Different colors can be achieved through loss of key components of pigment production (i.e. mutation of *Tyr* in CD-1 mice, resulting in albinism), or through more global mechanisms impacting the McSC differentiation trajectory. For example, the back stripe pattern of the African mouse *Rhabdomys pumilio* is achieved through differential expression of the TF *Alx3*, which suppresses MITF-induced differentiation to produce regions with lighter hair (Mallarino et al., 2016). Differential regulation and timing of SC activity and differentiation to achieve patterning has also been demonstrated in birds, where nonpigmented melanocyte progenitors in the lower bulge region of feather follicles periodically give rise to transit-amplifying progeny that differentiate as they move upward into the so-called barb region (Lin et al., 2013).

1.4 Dysfunction in McSCs and their lineage in aging and disease

As is the case for other tissue SC types throughout the body, dysfunction in how and when McSCs undergo these cell state transitions occurs in aging and can result in disease. Interest in

correcting abnormalities in this lineage stem from cosmetic to life-saving motivations. Over the course of aging, humans exhibit hair graying and also areas of skin hyper- and hypopigmentation. This reduced pigmentation can compromise UV protection, contributing to increased damage and decline of the skin tissue overall. With advanced age, the prevalence of melanoma also increases. Melanoma is the deadliest form of skin cancer, with cutaneous cases accounting for 55,500 deaths per year, as of 2018 (Schadendorf et al., 2018). Therefore, understanding how McSCs and their melanocyte lineage can go awry in these contexts is important not only for SC biology, but also for combatting serious clinical issues.

1.4.1 Natural mechanisms of McSC depletion

Dysfunction in the McSC lineage in the HF results in hair graying (also known as canities), one of the most ubiquitous and visible signs of aging (Nishimura, 2011). Gray or white hair phenotypes in mice can occur through two major routes: 1) dysfunction or loss of cells in the McSC compartment, or 2) in the differentiating progeny **(Fig. 1.2 A-B)**. Some have posited that age-related hair graying is caused by oxidative stress in melanocytes of the hair bulb, where reactive byproducts of melanin biosynthesis damage cells over time and lead to their eventual loss (Wood et al., 2009). However, Nishimura et al. (2005) demonstrated that in both humans and mice, age-related hair graying can result from loss of McSCs. Without the bulge SC reservoir, during active hair growth, fewer or no pigment-producing progeny can be generated, leading to irreversible loss of hair color.

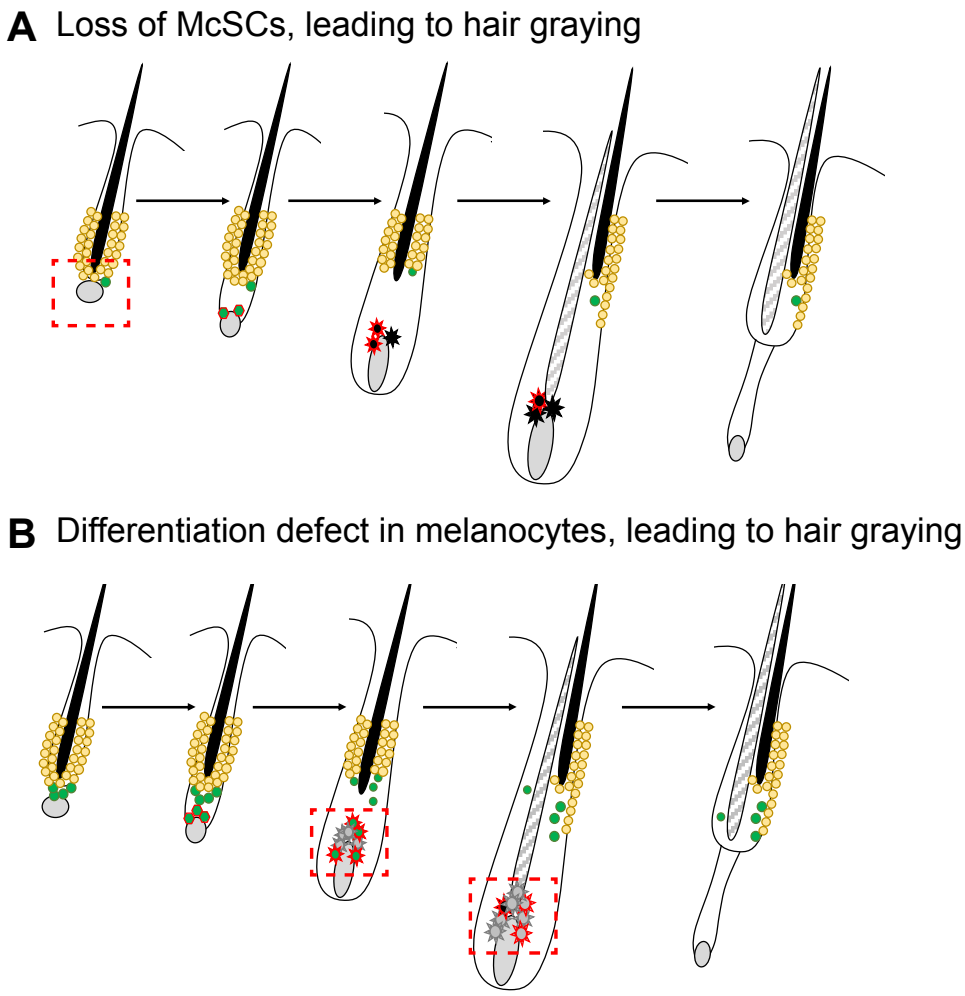

Figure 1.2 Loss of hair color can occur through defects in McSCs or their progeny. (A) Loss or dysfunction in McSCs results in the generation of fewer or no differentiating progeny to make pigment. **(B)** Alternatively, problems downstream in the differentiating progeny themselves can result in reduced pigment production and or transfer.

There are several causes and mechanisms through which McSCs can be depleted. The accumulation of genotoxic damage in qMcSCs can lead to ectopic differentiation in the bulge and compromised self-renewal, and mice lacking ataxia-telangiectasia mutated (ATM) kinase are sensitized to McSC differentiation upon ionizing radiation (Inomata et al., 2009; Ueno et al. 2014). Indeed, individuals with progeria syndromes have impaired DNA damage response mechanisms and often show premature hair graying (Nishimura, 2011). During acute stress, experiences of

which accumulate over an organism's lifetime, norepinephrine is secreted by sympathetic nerves and induces McSC proliferation and migration to the epidermis, depleting the bulge population and resulting in gray hair (Zhang et al., 2020). At the same time, the aging HF niche and epidermis can compromise McSCs as well as differentiated melanocytes. In human and mouse skin, COL17A1 levels are reduced with age, leading to McSC differentiation in HFs and loss of epidermal melanocytes (Liu et al., 2019; Matsumura et al., 2016; Tanimura et al., 2011).

On a more local scale, McSCs can be affected by insults to the skin such as wounding, UV exposure, and inflammation. Dermatologists and patients have long noticed the presence of hyperpigmentation around wounded and scarred areas of the skin. While epidermal melanocytes are likely also affected here, Chou et al. (2013) demonstrated that after excisional wounding and UVB irradiation in mice, McSCs migrate out of the HF niche. They do so without self-renewing, moving upward into the epidermis where they differentiate into melanocytes and are thought to provide additional UV protection to vulnerable damaged cells during wound healing. This phenomenon results in white hairs in the wound area due to permanent McSC depletion from HFs. UVB-induced McSC migration is in fact the basis of a form of re-pigmentation phototherapy used to treat vitiligo, a skin condition characterized by depigmented patches of skin due to loss of epidermal melanocytes (Nishimura, 2011). Multiple causes of melanocyte destruction have been proposed, from cell detachment to oxidative stress, but the prevailing notion is that it occurs through autoimmune attack (Bergqvist and Ezzedine, 2020). Follicular McSCs appear to be spared from these assaults and can therefore be stimulated by UV light therapy to migrate to the epidermis and differentiate into melanocytes to replenish skin pigmentation. A recent study has provided new insights into how the melanocyte lineage normally defends itself against the immune system. McSCs from *Mitf* heterozygous mice were found to express higher levels of type I interferon genes

relative to control. Curiously, when viral mimics were introduced into *Sox10* overexpressing mice to raise an innate immune response, hair graying was induced through an unknown mechanism (Harris et al., 2018). These findings indicate that MITF plays a role in repressing interferon signature genes normally, and in certain circumstances, a heightened immune response can contribute to hair graying.

Finally, there is currently scant evidence for the how autophagy, a self-degradation process whereby cells clear damaged organelles or proteins, affects McSCs. However, given its role in protecting against oxidative stress, which is increased by melanin production, and protecting the integrity of other long-lived tissue and quiescent SCs (van Velthoven and Rando, 2019), disrupted autophagy is a plausible route through which McSCs might become compromised in aging. As the body's first line of defense, the skin will encounter various challenges over the course of an organism's lifetime. It is likely that many if not all of the mechanisms discussed culminate to contribute to the overall depletion of McSCs and dysfunction of their melanocyte progeny.

1.4.2 Melanoma and its SC properties

On the other end of the spectrum is cancer, a pathologic shift towards overactivation and unrestrained proliferation. Melanoma is a highly aggressive form of skin cancer prone to metastatic spread. It can occur in cutaneous, acral (on the palms of hands, soles of feet, or nailbeds), mucosal, uveal, and conjugtival forms. Common oncogenic driver mutations include $BRAF^{V600E}$, *NRAS*, *NFI,* and genes in cell cycle regulation, with loss-of-function mutations in tumor suppressors genes like *P53* and *PTEN* (Schadendorf et al., 2018). Such mutations induce overactivation of several pathways like MAPK and PI3K signaling. Different melanomas exhibit distinct mutational signatures and molecular features (Trucco et al., 2019), depending on body location, disease stage progression, and complex interactions between the tumor and its microenvironment and the

immune system. For instance, UV-induced cutaneous melanomas exhibit a high mutational burden characterized by C→T and G→T mutations, while non-UV induced acral and mucosal melanomas often have fewer mutations but higher incidence of structural variants like copy number variation. (Alexandrov et al., 2013; Hayward et al., 2017; Schadendorf et al., 2018; Trucco et al., 2019). As primary lesions progress, they are prone to metastasize through the lymphatics (Ubellacker et al., 2020) to the lymph nodes and then to the blood circulation to disseminate throughout the body. Once a patient has progressed to metastatic disease, prognosis and survival outcomes are significantly worse (Davis et al., 2019).

These cancer cells exhibit a high degree of plasticity and are able to undergo "phenotype switching" to oscillate between more or less proliferative and or differentiated states, which is often dictated by levels of MITF (Carreira et al., 2006; Cheli et al., 2011). This agility can be exploited to change behavior throughout melanoma progression (i.e. proliferative cancer cells in the tumor switching to a more stem-like state during invasion) and may in some cases confer drug resistance. For example, in response to inflammatory cytokines released by T cells, melanomas can dedifferentiate and downregulate their expression of melanocytic antigens in order to evade immunotherapy (Landsberg et al., 2012). Another aspect of this plasticity centers on heterogeneity within the tumor (Tirosh et al., 2016) and the concept of a subpopulation of "melanoma stem cells" endowed with unique properties that allow them to self-renew and both sustain and repopulate tumors (Schatton et al., 2008). These cells may be identified by expression of distinct markers, and although often slow-cycling, drive tumor growth through supplying proliferative progeny (Boiko et al., 2010; Fang et al., 2005; Roesch et al., 2010).

A popular hypothesis that has been proposed to explain the deadly propensities of melanoma for plasticity and metastasis is that transformed cells are able to re-access their neural

crest and or SC programs. The capacities of melanoblasts for exponential proliferation and impressive migration and colonization during embryogenesis are tightly regulated, but if transformed cells could tap into these developmental mechanisms without proper restraints, the results would be disastrous. Gupta et al. (2005) demonstrated that when transformed with the same oncogenes, melanocytes give rise to melanomas that metastasize, but fibroblasts and mammary epithelial cells produce tumors that rarely lead to metastatic disease. These findings point to the importance of the melanocyte lineage cellular context in endowing these aggressive capabilities. Studies in zebrafish have been particularly illuminating here, highlighting the neural crest features that underlie melanoma initiation, invasion, and drug resistance (Fazio et al., 2021; Johansson et al., 2020; Kaufman et al., 2016; Santoriello et al., 2020). For example, a key study by Kaufman et al. (2016) employed a *crestin-eGFP* reporter to demonstrate that *p53* and *BRAF* mutant cells induce a neural crest gene signature during melanoma initiation (Kaufman et al., 2016). Similarly, global embryonic melanoblast transcriptomic data has recently been mined to uncover novel regulators of melanoma metastasis (Marie et al., 2020).

Given the striking parallels between melanomas and their neural crest and melanoblast precursors, the field has debated whether adult McSCs in HFs and sweat glands can act as the melanoma cell-of-origin. Indeed, McSCs not only give rise to proliferative progeny but retain migratory capacity, abilities that in a malignant context are akin to fueling tumor expansion and metastasizing, respectively. McSC quiescence is also interesting here, as melanoma cells that have metastasized are able to exist in a state of dormancy for years in distal sites of the body before being reactivated to generate a metastatic tumor. Curiously, immunocompromised patients can develop melanoma after receiving organ transplants, suggesting that their immunocompetent donors had dormant cancer cells lurking in that organ, but appeared healthy otherwise (Strauss and

Thomas, 2010). Furthermore, there are melanotic (pigmented) and amelanotic (unpigmented) forms of melanoma, which seems to suggest the possibility of both melanocyte (pigmented) and McSC (unpigmented) precursor cells.

Several recent studies have sought to tackle this controversial cell-of-origin question using mouse models. Using *TyrCreER* to drive mutant $Braf^{V600E}$ and *Pten* loss-of-function in McSCs and their lineage, Moon et al. (2017) demonstrated that McSCs could give rise to melanoma, but to do so required their activation. Upon UV exposure and inflammation, transformed McSCs migrated to the epidermis where they expanded and generated down-growing melanomas. The authors claim that SC quiescence is tumor suppressive in this context. In a back-to-back report, Köhler et al. (2017) approached a similar question using this mouse model, but focused on the tail, where amelanotic and mature epidermal melanocytes reside (Glover et al., 2015). Their evidence suggests that melanocytes can give rise to melanomas, but that they undergo transcriptional reprogramming to dedifferentiate during this process. Analogous to the results of Moon et al. in qMcSCs, the quiescent amelanotic population of cells in the tail appear refractory to melanomagenesis. Later, using a new *c-Kit-CreER* driver to more specifically transform the SC compartment, Sun et al. (2019) further substantiated and extended evidence suggesting that McSCs can serve as the melanoma cell-of-origin. Outside of cutaneous skin, the palms and soles of feet lack HFs but are also common sites for melanoma. Given their ability to divide and migrate to the epidermis upon oncogenic stress, the immature and slow-cycling lineage cells that reside in the secretory portion of sweat glands are intriguing candidates for acral melanoma tumor-initiators (Okamoto et al., 2014). At this point, there is compelling evidence in mice that melanomas can originate from either McSCs or their progeny, but whether this actually occurs in human cancers remains to be definitively demonstrated.

1.5 Summary

Melanoblasts, tissue McSCs, and their melanocyte progeny have been an attractive model system with which to approach myriad questions, ranging from those pertaining to basic genetics to embryonic development to mechanisms of migration and proliferation to organelle biogenesis and trafficking. In my thesis research, I have harnessed the tractable model of the mouse skin and HF to elucidate the molecular mechanisms that underlie McSC quiescence, their transition to activation and proliferation, and their complete differentiation into pigment-producing cells. A more thorough understanding of this lineage and how in functions normally *in vivo* is a critical parallel to studies being conducting in abnormal cell states like melanoma and vitiligo. Such studies may not only inform our understanding of disease, but may have broader implications across other types of adult tissue SCs, especially those that cycle between quiescent and activated states to generate transit amplifying progeny in response to periodic tissue demands. For the McSCs and their lineage, there is still much to learn about how the differentiation process is accomplished, especially with regard to the intermediate transit-amplifying stages and how different signaling inputs are integrated. To unearth new insights, I sought temporal and single cell-level information about transcription and chromatin states, prioritizing experiments that could be performed in the native mammalian tissue context.

CHAPTER 2:
ELUCIDATING THE TRANSCRIPTIONAL DYNAMICS OF MELANOCYTE LINEAGE PROGRESSION THROUGH STEM CELL ACTIVATION AND DIFFERENTIATION

2.1 Introduction

McSCs move from quiescence to activation and differentiation in step with hair cycle progression. Given its predictability and ease of manipulation, the murine HF is an attractive model system with which to interrogate McSC behavior. While elegant functional studies in mice have yielded important discoveries regarding the specific pathways involved in McSC lineage progression, unbiased approaches like high throughput sequencing provide an opportunity to uncover novel insights about complex biological processes. Previous studies have used single-cell qPCR of qMcSCs, melanocytes, and embryonic melanoblasts (Osawa et al. 2005), bulk RNA-sequencing of McSCs (Joshi et al., 2019; Moon et al., 2017; Zhang et al., 2020) or single-cell comparisons of McSCs and melanoma using 10X Genomics (Sun et al., 2019).

In my investigation of this lineage, I also wanted to start with a more global vantage point with which I could establish my own datasets and address gaps in our understanding. Broadly, I hypothesized that distinct transcriptional programs fueled by specific TFs drive quiescence, activation, and differentiation. In my approach, I wanted to have single cell resolution that would allow me to delineate the intermediate and likely heterogenous activation and differentiation steps. To best accomplish this, I also needed a sequencing method that would afford high depth of coverage to discern maximal transcriptional differences between these related cell types.

To this end, I implemented transgenic mice expressing fluorescent proteins in the melanocyte lineage and characterized the activity and localization of McSCs and their progeny throughout hair cycling. I then designed fluorescence-activated cell sorting (FACS) strategies to isolate lineage cells from the skin at three discrete time points and performed single cell RNA-seq (scRNA-seq) with Smart-Seq2 (Picelli et al., 2013; Picelli et al., 2014). With this approach, I

obtained high quality transcriptional data with which to perform comparative gene expression and pathway analyses, illuminating both expected and novel insights into this differentiation process.

2.2 Results

2.2.1 Characterizing McSC lineage activity during hair cycling in the mouse skin

To facilitate the visualization and FACS-based isolation of McSCs and their progeny, I took advantage of the *Dct*-eGFP mouse strain (Gong et al., 2003). DCT is a melanogenic enzyme and ubiquitous lineage marker expressed by approximately E10.5. in mice (Mort et al., 2015). Using immunofluorescence (IMF) analysis of the skin, I confirmed that eGFP expression overlapped with endogenous DCT and was present in both McSCs in the bulge region and in their differentiating progeny in the anagen hair bulb **(Fig. 2.1 A)**. In second telogen, or approximately postnatal day 60 (P60), qMcSCs in the bulge region were the only melanocyte lineage present in the skin **(Fig 2.1 A, left)**. To assess the timing of peak McSC proliferation and enable isolation of aMcSCs, I measured incorporation of 5-ethynyl-2-deoxyuridine (EdU) within a 24 hour pulse at time points spanning from late first telogen through early anagen progression (P20-23) in *Dct*-eGFP mice **(Fig. 2.1 B-C)**. Quantification of EdU^+ endogenous DCT^+ cells indicated that McSC proliferative activity peaked during anagen I-II, which occurred at P21 in males of this background strain **(Fig. 2.1 C-D)**. At this point, morphologically, HG expansion and DP engulfment was minimal in HFs, and the majority of aMcSCs had not yet become spatially segregated from the bulge region. Later on in anagen III, HGs had developed into hair bulbs distanced from the bulge, which allowed for evaluation McCP behavior during differentiation **(Fig. 2.1 C, E)**. At P23, approximately 30% of DCT^+ cells in the hair bulbs were proliferating, suggesting continued expansion of progeny after initial McSC activation **(Fig. 2.1 F)**.

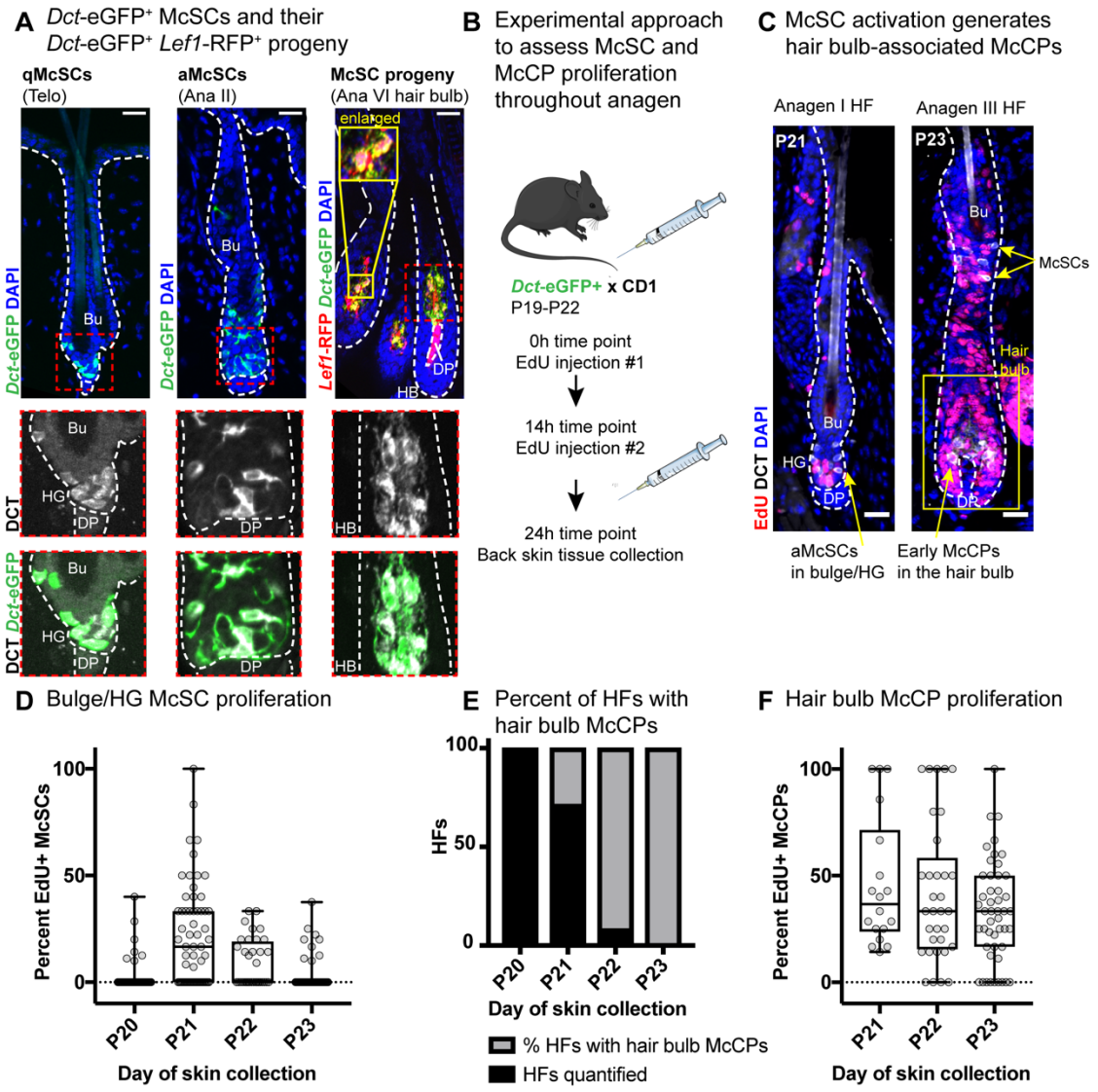

Figure 2.1 Characterization of McSC activity and differentiation into melanocytes throughout the hair cycle reveals time points at which to capture different cellular states. (A) IMF images of qMcSCs (left, 2nd telogen (telo) ~P60), aMcSCs (middle, anagen II (ana II) at P21), and hair bulb McSC progeny (right, anagen VI at P10); red dashed box indicates enlarged areas below. **(B)** Experimental schematic used to assess proliferation of McSCs and McCPs through EdU incorporation over 24 hours. **(C)** Representative IMF images of HFs at P21 and P23. Minimum value displayed was adjusted for DCT channel to reduce background. **(D)** Quantification of percent EdU$^+$ McSCs. **(E)** Percent of HFs counted that had developed hair bulb-associated McCPs with corresponding **(F)** percent EdU$^+$ McCPs in the developing hair bulb. [P20 n=53 HFs; P21 n=63 HFs; P22 n=36 HFs; P23 n=48 HFs (P20 n=1 mouse; P21-23 n=2 mice)]. For all IMF, scale bars=25 μm, white dashed line outlines HFs at the epithelial-mesenchymal junction, Bu=bulge.

By full anagen (anagen VI), differentiating pigment-producing melanocyte progeny were present in the hair bulb. However, both McSCs and their progeny express *Dct*-eGFP, so to distinguish these differentiating cells from their SCs using FACS, an additional fluorescent marker was necessary. For this purpose, I crossed *Dct*-eGFP mice to lymphoid enhancer factor 1(*Lef1*)-RFP mice that express RFP in the WNT-responsive differentiating melanocytes but not in McSCs **(Fig. 2.1 A, right)** (Rendl et al., 2005). In full anagen hair bulbs at P10, *Lef1*-RFP was expressed in melanocyte lineage cells and the DP, but melanocytes could be distinguished by co-expression of *Dct*-eGFP. By characterizing McSC lineage activity in the mouse skin, I could then use these time points and fluorescent proteins as the basis upon which to develop cell isolation protocols.

2.2.2 McSCs can be purified from mouse skin

Having established the optimal time points and fluorescent markers with which to label qMcSCs, aMcSCs, and their differentiating progeny (including mature melanocytes), I next designed FACS strategies to isolate these populations. Using well-established protocols from the Fuchs Lab, I mechanically and chemically digested dissected mouse back skin according to the hair cycle stage to generate a single cell suspension **(Fig. 2.2 A)**. For all purification schemes, I used antibodies against cell surface markers of contaminating cell types in the skin, including endothelial ($CD31^+$), immune ($CD45^+$), fibroblast, platelet, and adipocyte ($CD140a^+$), epidermal and HF infundibulum ($Sca\text{-}1^+$) and bulge HFSC ($CD34^+$) cells. After gating against these cell types, qMcSCs from second telogen skin were defined as *Dct*-$eGFP^+$ integrin $\alpha\text{-}6^{medium\text{-}low}$ cells; in anagen I-II (P21), I collected *Dct*-$eGFP^+$ integrin $\alpha\text{-}6^{all}$ cells, in case changes in integrin expression occurred during this dynamic and heterogeneous activation state **(Fig. 2.2 B, top)**. Finally, in anagen VI (P10), differentiating lineage cells were identified as *Dct*-$eGFP^+$, *Lef1*-RFP^+, and c-KIT $(CD117)^+$ cells **(Fig. 2.2 B, bottom)**.

For initial validation of these strategies, I used RT-qPCR followed by bulk RNA-sequencing of the "bookend" populations of telogen qMcSCs and anagen VI differentiating McSC progeny. These RNA-seq data showed high reproducibility between biological replicates, and compared to published HFSC RNA-seq data, there was robust expression of known lineage markers including *Dct*, *Sox10*, and *c-Kit* **(Fig. 2.2 C)**. Differential gene expression analysis with DESeq2 (Love et al., 2014) revealed thousands of significant transcriptional differences between qMcSCs and their differentiating progeny (2,385 genes up in qMcSCs; 2,819 up in differentiating progeny, padj≤0.001, $\log_2$fold≥1) **(Fig. 2.2 D;** see also Table S1 of Infarinato et al., 2020**)**. Notably, these included several previously described population-specific gene expression differences, including *Bcl2* in qMcSCs and *Oca2* and *Mc1r* in the differentiating progeny.

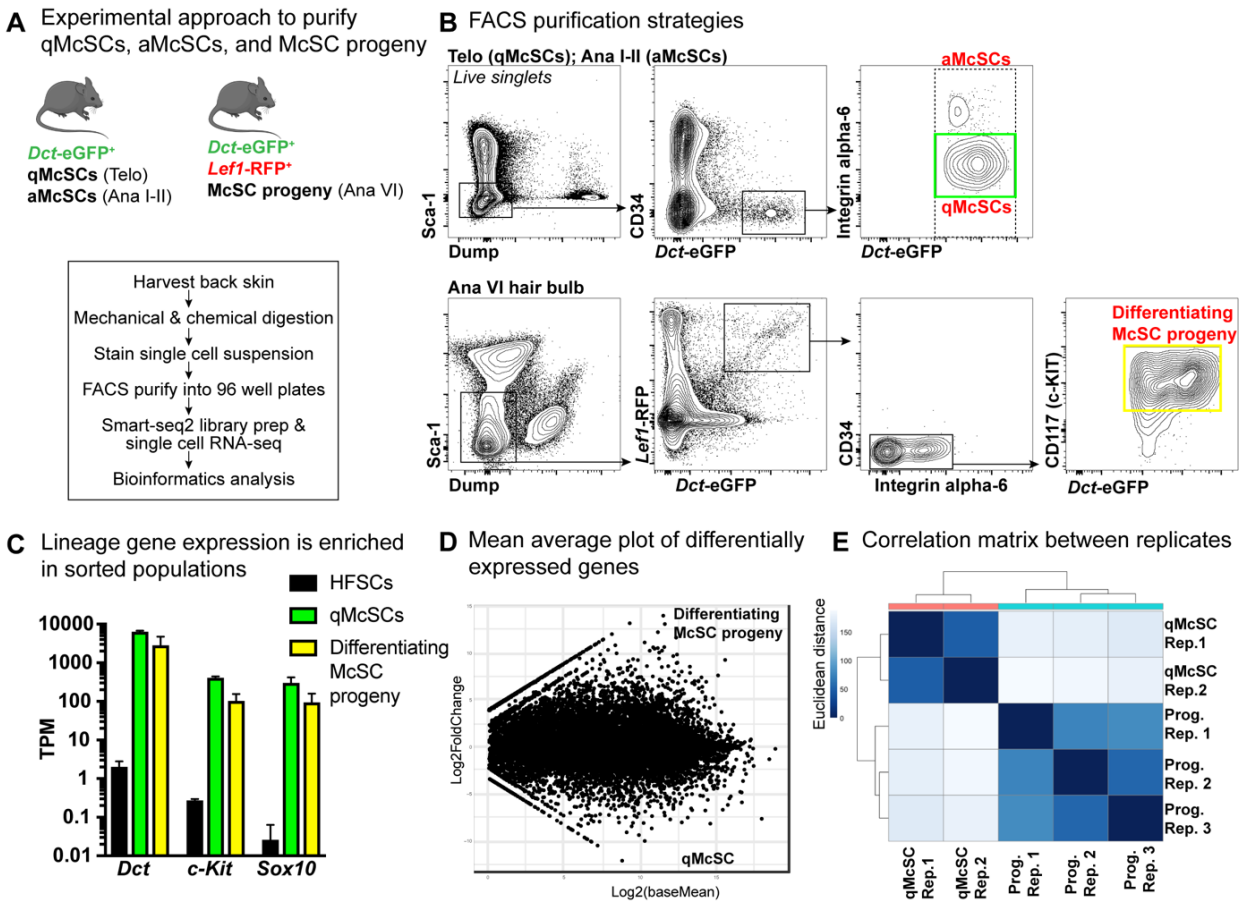

Figure 2.2 McSCs and their differentiating progeny can be isolated from mouse skin. (A) Experimental approach used to isolate McSC lineage and perform transcriptional profiling. **(B)** FACS purification schemes for McSCs (top) and differentiating hair bulb McSC progeny (bottom). **(C)** Validation of sorting strategies by bulk RNA-seq. Bar graph shows Transcripts Per Million (TPM) mean values relative to HFSCs. Error bars represent standard deviation (HFSCs n=2, qMcSCs n=2, hair bulb McSC progeny n=3). **(D)** Mean average plot of differentially expressed genes between qMcSCs (negative fold change) and their differentiating progeny (positive fold change). **(E)** Correlation matrix illustrating Euclidean distances between biological replicates (prog.=differentiating McSC progeny).

While these data provided a solid foundation for my study and showed good correlation between biological replicates **(Fig. 2.2 E)**, I suspected that even in these carefully purified populations, there might be transcriptional heterogeneity due to intermediate transition steps in the lineage and asynchrony of cells passing through each stage, as well as some degree of contamination from other cell populations in the skin. The ability to detect these differences would

be especially critical at the activation and transit-amplifying steps, where my IMF analyses indicated the presence of non-cycling and cycling McSCs and early McCP populations in the hair bulb **(Fig. 2.1 C-F)**. To both capture this heterogeneity and ensure high purity, we performed scRNA-seq with Smart-Seq2, which provides higher depth of coverage than Drop-seq or 10X Genomics (Picelli et al., 2013) on telogen qMcSCs, anagen I-II aMcSCs, and anagen VI differentiating progeny **(Fig. 2.2 A)**. To minimize the capture of non-lineage cells for this purpose, I also implemented more stringent FACS gating.

2.2.3 McSCs and their progeny exhibit distinct transcriptional signatures throughout lineage progression *in vivo*

Single cell mRNA libraries were prepared according to the Smart-Seq2 protocol (Picelli et al., 2013; Picelli et al., 2014) and subjected to sequencing. Prior to comparative analyses, a variety of quality control tests and filtering parameters were performed **(Fig. 2.3)**. External RNA (ERCC) spike-ins were implemented to discern technical noise associated with library preparation and sequencing from biological variability **(Fig. 2.3 A)** (Brennecke et al., 2013). To eliminate low quality libraries from further analysis, cells with transcript reads from <1,250 genes were removed. Any *Dct*^{low} (logTPM+1<6) or *Krt15*$^{+}$ (logTPM+1>6) cells were assumed to be non-melanocyte lineage cells and were also eliminated from further analysis. The retained cells had an average of $1x10^5$ reads/cell, with few reads from the full datasets mapping to the mitochondrial genome, suggesting good cell viability **(Fig. 2.3 B)**. Libraries were processed in multiple rounds of sequencing, so to determine the impact of batch effect, cells were visualized according the biological replicate (mouse) from which they originated **(Fig. 2.3 C, left and middle)**. McSCs from telogen and anagen I-II exhibited strongly overlapping profiles; for anagen VI differentiating progeny, where slight variations in age and rapidly progressing hair cycle stage might influence

transcriptional profiles, cells from individual mice were still most closely related to each other and showed a considerably degree of overlap. Finally, telogen qMcSCs displayed the least complex transcriptome **(Fig. 2.3 B, middle and C, right)**, consistent with a previous report by Osawa et al. (2005) using single cell RT-qPCR. Furthermore, this low complexity transcriptome was also observed in a fraction of the anagen I-II McSCs, where a subset of cells are expected to remain quiescent during SC activation. These results suggest that reduced transcription is likely a genuine feature of qMcSCs, similar to what been described for several other types of quiescent SCs (van Velthoven and Rando, 2019).

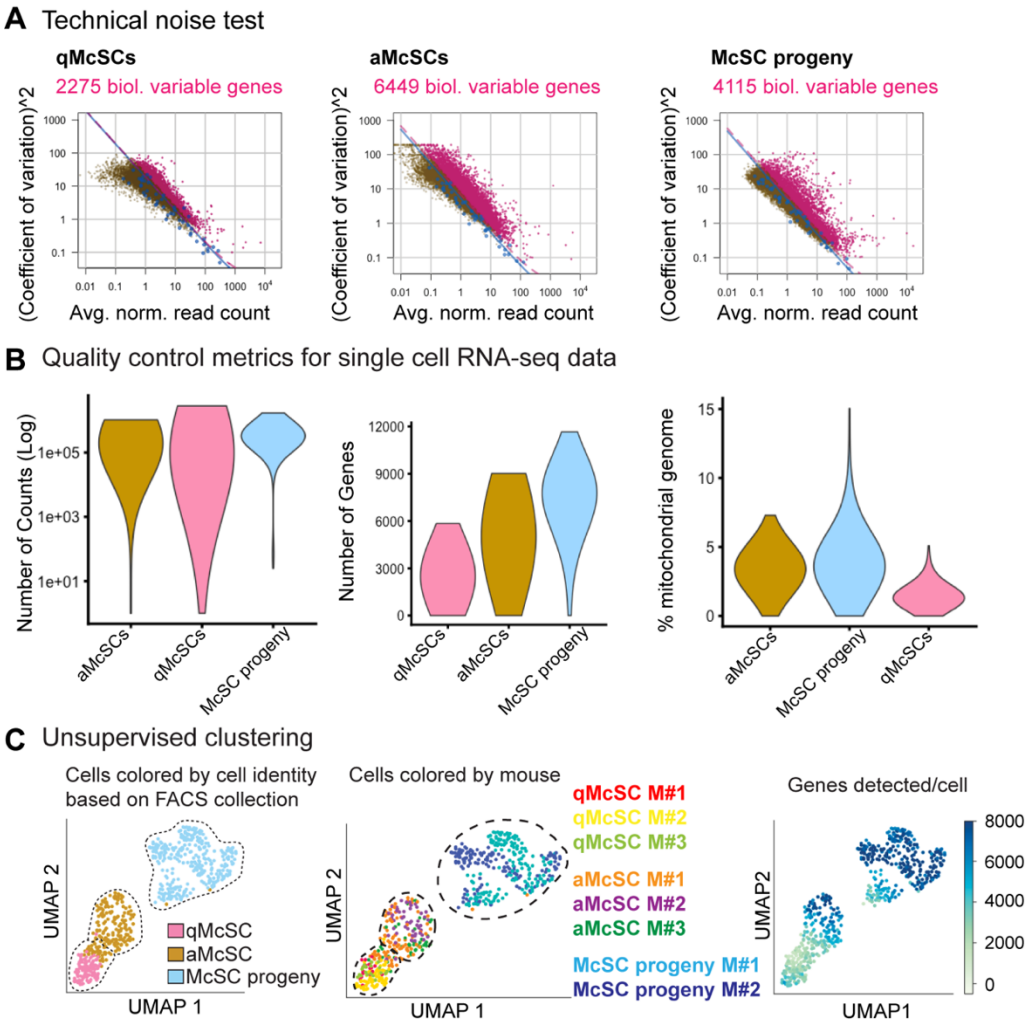

Figure 2.3 scRNA-seq data from purified cells are of high quality. (A) Technical noise tests relative to ERCC spike-ins detects biologically variable genes for each population. **(B)** Quality control tests showing log number of counts, genes detected per cell, and percentage of mitochondrial reads for unfiltered datasets. **(C)** Unsupervised k-NN based clustering of melanocyte lineage cells colored by group identity (left), individual mouse (middle), and number of genes detected per cell (right).

Principle component analysis (PCA) with uniform manifold approximation and projection (UMAP) (Becht et al., 2019) coupled with k-Nearest Neighbors (k-NN) based community detection (Blondel et al., 2008) was used to visualize these datasets. Cells segregated into three distinct clusters, all of which showed robust expression of lineage markers such as *Dct* and *Mitf* **(Fig. 2.4 A)**. As expected, clustering indicated that telogen and anagen I-II McSC populations (C1,

C2) were more similar to one another than to the anagen VI differentiating progeny (C3). To first understand what are the major transcriptional differences driving this separation and define features of stemness versus differentiation, differential gene expression and gene ontology (GO) analyses were performed on the combined cells of C1 and C2 versus C3 **(Fig. 2.4 B; Table 2.1;** see also Table S2 of Infarinato et al., 2020**)**.

In this comparison, McSCs showed selective upregulation of transcripts for genes with known importance in stemness, such as *Bcl2* (Nishimura et al., 2005) and *Pax3* (Lang et al., 2005; Potterf et al., 2000). Unexpectedly, activator protein-1 (AP-1) family TFs (*Fosb*, *Fos*, *Junb*, *Jun*) featured prominently. At the same time, McSCs showed a striking upregulation of immunomodulatory genes (*Socs3*, *Stat3*, *Stat5a*, *Il6st*). Among these genes was *Cd274*, encoding programmed death-ligand 1 (PD-L1), an immune checkpoint protein that binds to PD1 receptor on T cells to inhibit their activation.

On the other side, the differentiating progeny of C3 showed robust upregulation of genes involved in melanogenesis including key melanin production enzymes (*Tyrp1*, *Tyr*) and melanosome proteins (*Pmel*, *Gpr143, Oca2*) and transporters (*Rab38*). Transcripts from well-known melanocyte differentiation pathways were also enriched, including SCF/c-KIT (*Kitl*) (Botchkareva et al., 2001; Liao et al., 2017), MC1R/α-MSH/ASIP (*Mc1r*) (Enshell-Seijffers et al., 2010), and WNT signaling (*Lef1*) (Rabbani et al., 2011). Consistent with their increased activity compared to SCs, differentiating progeny showed upregulation of several genes encoding enzymes involved in multiple forms of cellular metabolism as well as genes involved in semaphorin-plexin signaling *(Plxna1/2/4*, *Sema6d*).

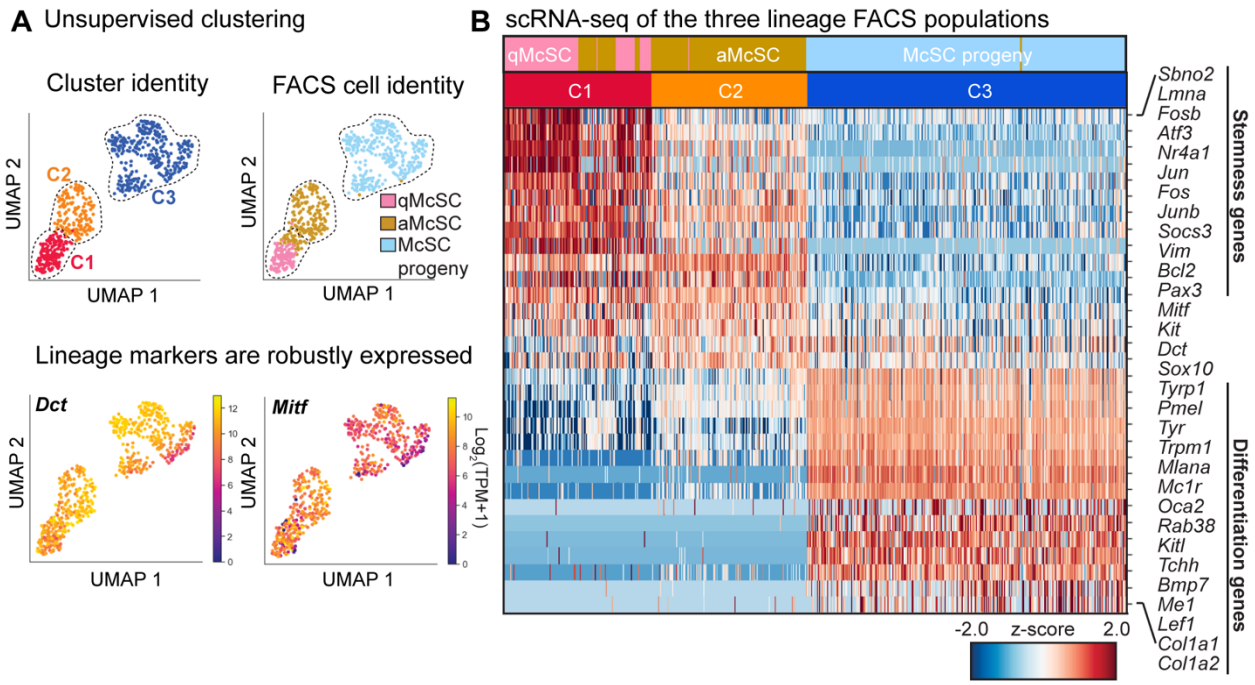

Figure 2.4 McSCs and their progeny exhibit distinct transcriptional signatures. (A) UMAP representation and unsupervised k-NN based clustering of single cell data. Each dot represents a cell colored by its cluster ("C") and known cell identity. For FACS cell identity, pink dots are telogen "qMcSCs" (n=104 cells, n=3 mice), gold are anagen I-II "aMcSCs" (n=193 cells, n=3 mice), and light blue are anagen VI "hair bulb McSC progeny" (n=308 cells, n=2 mice). Below, expression plots for the lineage markers, *Dct* and *Mitf*, across all three melanocyte populations. **(B)** Heatmap illustrating select differentially expressed genes between McSCs (C1 and C2) and McSC progeny (C3).

2.2.4 Transcriptional heterogeneity increases throughout differentiation

Having established the key transcriptional features that broadly define stemness and differentiation, I next turned to investigating the presence of intrapopulation heterogeneity, a concept that had received little attention in the McSC and melanocyte field. This was achieved through further sub-clustering of the original three clusters, maintaining conservative parameters so as to break down clusters based on the most prominent transcriptional differences. This analysis detected the presence of six distinct subpopulations and suggested that transcriptional heterogeneity increases as cells move from quiescence to activation and differentiation. C1

remained as one cluster, C2 split into C2a and C2b, and C3 broke into C3a, C3b, and C3c **(Fig. 2.5 A)**.

To understand the features of these six sub-clusters, the stemness and differentiation signature genes in the initial comparison of C1 and C2 versus C3 were used to generate global scoring system **(Fig. 2.5 B)**. Consistent with my IMF characterization of the lineage throughout the hair cycle **(Fig. 2.1)**, these six sub-clusters could be delineated on the basis of differences in proliferation and melanogenesis gene expression. Therefore, a group of proliferation genes was also used to establish an overall score **(Fig. 2.5 C, left)**. These analyses indicated that C1 had the highest stemness score, and C2 sub-clusters showed marked differences, where C2a was more stem-like than C2b. Consistently, a fraction of the C2b cells had positive differentiation scores, which were all high in the C3 clusters, especially in C3b and C3c. Global proliferation scoring provided further insight, suggesting that sub-cluster C2a was less quiescent than C1, but sub-clusters C2b and C3a were particularly enriched for cell cycling transcripts. Cell phase scoring provided further resolution, indicating signatures for G1/S, S, G2/M, and M stages **(Fig. 2.5 C)**. Some cell cycle transcripts remained elevated in the more differentiated C3b and C3c sub-clusters, but overall, these were substantially lower than in C3a. At the same time, C3c expressed the highest levels of melanin biosynthetic and melanosome organization pathway genes, marking these as the most mature melanocytes in the dataset **(Fig. 2.6 A-C)**. Based on these stemness, proliferation, and differentiation gene expression patterns, as well as the hair cycle stage at which they were isolated, it was possible to delineate these sub-clusters as qMcSCs (C1), aMcSCs (C2a), a transitional state from aMcSCs to early McCP (C2b), later McCP of the hair bulb (C3a), and differentiated melanocytes (C3b, c) **(Fig. 2.6D)**. This provided high resolution with which to explore temporal changes in transcription throughout the differentiation trajectory.

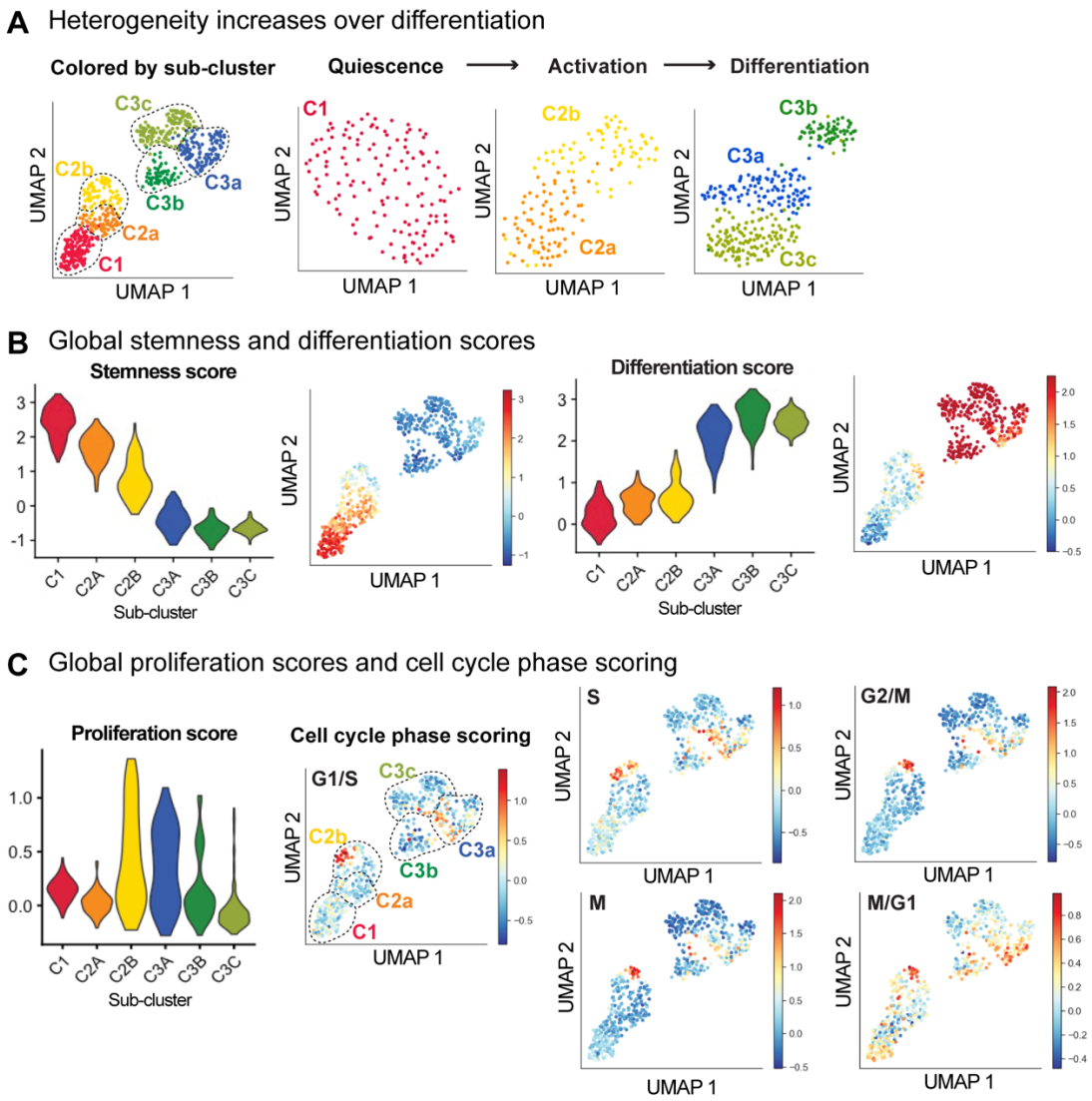

Figure 2.5 Transcriptional heterogeneity increases throughout lineage progression. (A) Sub-clustering of each original cluster from Fig. 2.4 A. **(B)** Violin and UMAP plots depicting global stemness and differentiation scores throughout the six sub-clusters. **(C)** Violin plot of proliferation scores with cell cycle phase scoring.

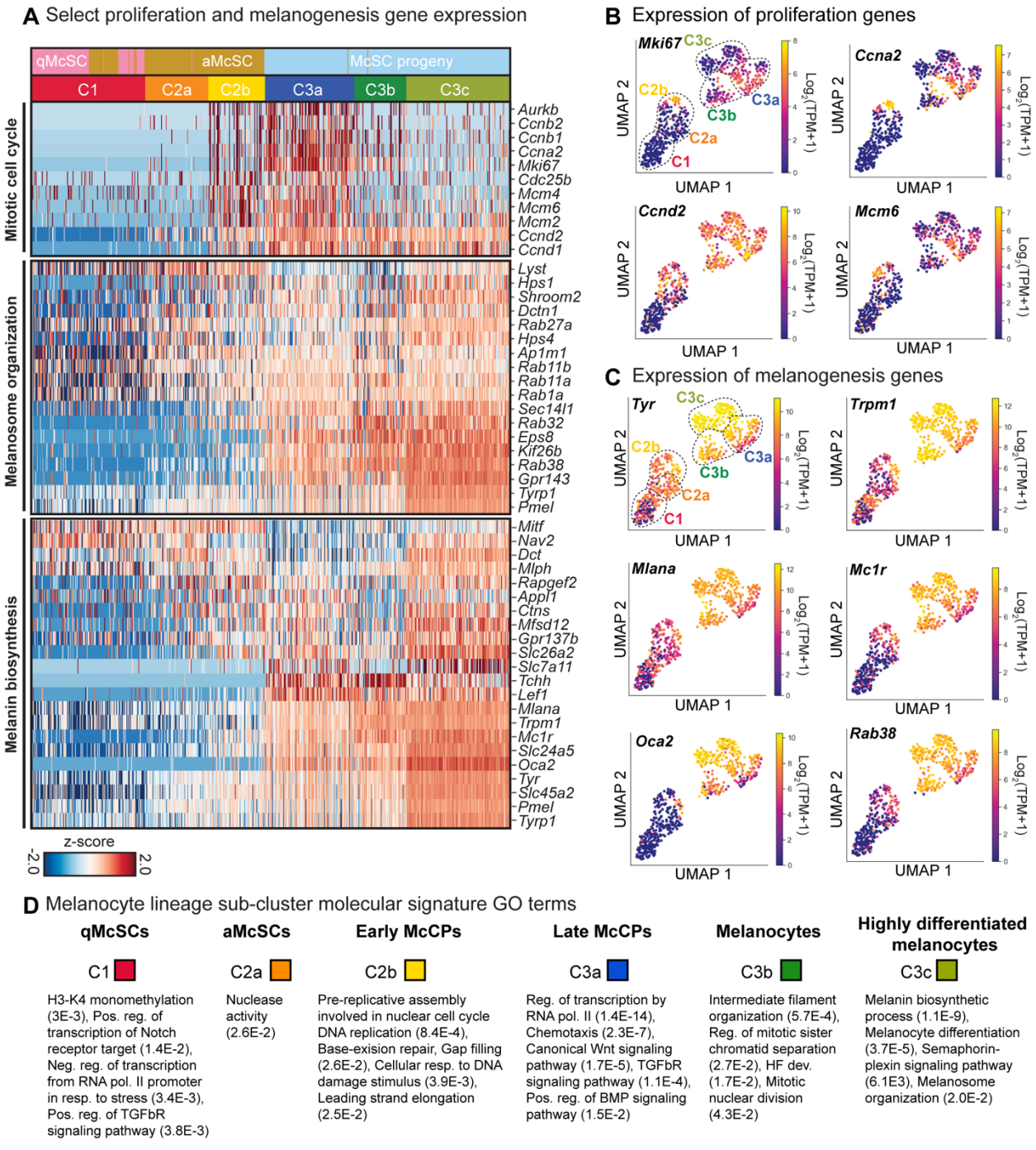

Figure 2.6 Melanogenesis, cell cycling genes, and GO analysis further delineate sub-cluster identities. (A) Heatmap of select proliferation and melanogenesis mRNAs. **(B)** Expression plots of example proliferation genes and **(C)** melanogenesis genes. **(D)** Selected GO terms for each sub-cluster with False Discovery Rate (FDR).

2.2.5 Analysis of signaling pathways and biological processes associated with each sub-cluster

As a next step to understand the biological features of these distinct sub-clusters, GO analysis was implemented. Sub-clusters were compared against one another using differential gene expression analysis, and the resulting gene lists were subject to GO term processing using PANTHER (Mi et al., 2019; Thomas et al., 2006) and DAVID 6.8 (Huang et al., 2009a; Huang et al., 2009b) **(Fig. 2.6 D,** select PANTHER terms with FDR; see also Table S3-6 of Infarinato et al., 2020**)**. When qMcSCs (C1) were compared to all anagen I-II McSCs/early McCPs (C2), expected pathways such as Notch (Moriyama et al., 2006) and TGF-βR signaling (Nishimura et al., 2010) were enriched. Genes and processes involved in "negative regulation of cell proliferation" (1.1E-7) and "autophagy" (p=1.7E-5) (DAVID 6.8) were also detected, consistent with the "common quiescence signature" that has been described for other types of tissue SCs (van Velthoven and Rando, 2019). In line with their transition to an activated state, C2 was dominated by cell division terms, and a few melanogenesis genes were significantly increased, including *Oca2, Mc1r*, and *Rab32*. To delineate the cellular processes that change as aMcSCs become early McCP, C2a was compared to C2b. This highlighted elevated nuclease activity and regulation of cell migration in C2a, while C2b showed enrichment of cell cycling and DNA replication and repair pathways, characteristic of a transit-amplifying cell population.

To dissect the differences between the three sub-clusters of McSC differentiating progeny in the anagen VI hair bulb, differential gene expression was performed on C3a late McCP versus C3c highly differentiated melanocytes and C3b melanocytes versus C3c. In both analyses, melanin biosynthesis and related processes comprised the top terms for C3c. C3a, the late McCP, showed upregulation of an intriguing number of cell signaling pathways, and C3b showed enrichment of cytoskeletal organization and cell division-related processes.

2.2.6 BMP and WNT signaling gene expression increases through differentiation

Turning to genes and pathways likely to be involved in lineage commitment and progression, I focused on cohorts of genes that robustly changed in expression during the less understood transitional stages of differentiation. Subdividing the McSC lineage into six transcriptionally distinct sub-clusters now revealed with higher resolution when specific signaling pathways became activated.

An interesting feature that became apparent was that WNT signaling and response were particularly elevated at the juncture between the anagen I-II C2b McCP and the anagen VI late McCP (C3a) in the hair bulb **(Fig. 2.7 A, top)**. This marked transition was also reflected by the significantly enriched (FDR=$1.7E^{-5}$) "canonical WNT signaling pathway" GO term in sub-cluster C3a when compared to C3c melanocytes **(Fig. 2.6 D)**. Of further intrigue was a similar dramatic elevation of bone morphogenetic protein (BMP) pathway response genes at this same juncture **(Fig. 2.7 A, bottom)**, and also the significant (FDR=$1.5E^{-2}$) term "positive regulation of BMP signaling pathway" in the C3a McCP sub-cluster analysis **(Fig. 2.6 D)**. Probing deeper into WNT pathway activation throughout the lineage revealed elevated levels of genes such as *Lef1, Wif1, Me1* and *Wnt5a* within the McCP/melanocyte populations **(Fig. 2.7 B)**. Similarly, there was robust upregulation of BMP target genes *Id1/2* and *Msx1/2* and ligands *Bmp2/7* in these differentiating populations **(Fig. 2.7 C-D)**, consistent with their BMP receptor expression **(Fig. 2.7 D-E)**.

WNT activity drives McSC expansion and downstream melanocyte differentiation (Rabbani et al., 2011). BMPs have been reported to elicit ligand and context-specific effects on melanin production in cultured cells (Bilodeau et al., 2001; Hsu et al., 2005; Jin et al., 2001; Kawakami et al., 2008; Park et al., 2009; Singh et al., 2012; Yaar et al., 2006; Yang et al., 2014). However, the role of this pathway in the native tissue microenvironment, as well as whether it

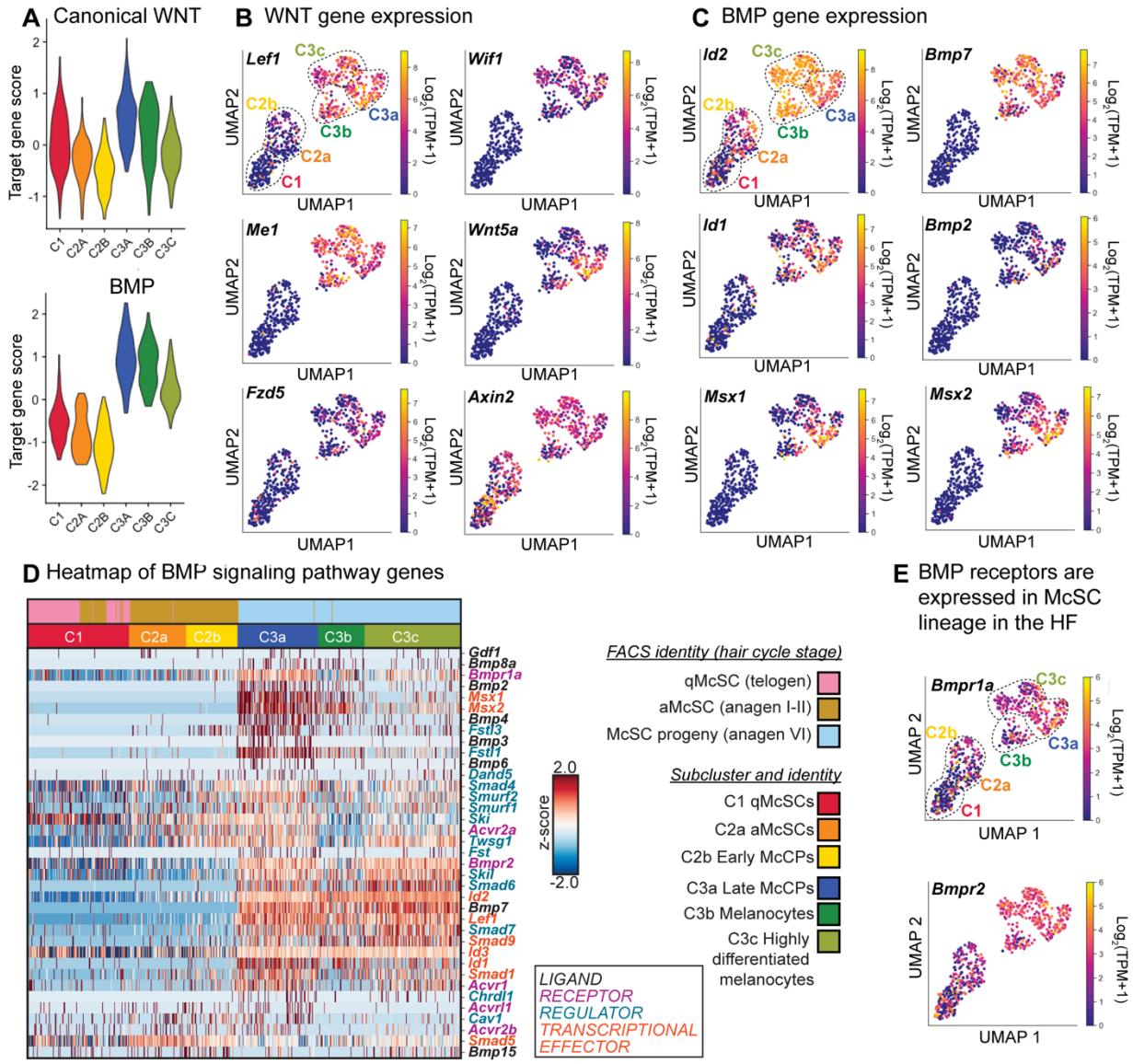

Figure 2.7 WNT and BMP signaling increase during melanocyte differentiation. (A) Violin plots of canonical WNT and BMP target gene pathway scores in each sub-cluster. **(B)** Expression plots of WNT and **(C)** BMP pathway genes. **(D)** Heatmap of BMP ligand, receptor, and transcriptional effectors over differentiation. **(E)** Expression plots of BMP receptors.

might engage with crosstalk with other niche signaling components was not well understood. Therefore, I endeavored to investigate the role of BMP signaling in melanocyte lineage progression *in vivo* and explore possible interplay with WNT. These studies are the subject of **Chapter 3**.

2.3 Discussion

In harnessing an unbiased approach and profiling cells from their native niche throughout lineage progression, this study represents a significant advance in our understanding of the transcriptional underpinnings of McSC quiescence, activation, and differentiation. It revealed the presence of six distinct transcriptional profiles, suggesting that the lineage increases in complexity as cells progress through differentiation. Further studies will be necessary to delineate whether these different profiles, especially those three sub-clusters in the differentiating C3 cluster, represent a continuum of states through which all cells pass, or perhaps also indicate differences in spatial organization within the HF and hair bulb niche, resulting in different extracellular cues and cell-cell adhesion. For example, cells in more direct contact with the DP might receive different levels of signals from the mesenchyme than those further out and closer to matrix TACs.

One significant argument for studying the dynamic developmental trajectory of this lineage is to gain insight into how normal features might be exploited or perturbed in disease. In this regard, several aspects of the McSC signature underscore the concept that melanomas harness SC programs. AP-1 factors regulate several cellular processes, but the particular upregulation in SCs was intriguing in light of their implications in cancer. For instance, in melanoma, c-JUN and MITF are thought to act antagonistically (Riesenberg S et al., 2015), and FOSL1 has been shown to induce melanocyte reprogramming and transformation, also downregulating MITF (Maurus et al., 2017). Given these striking parallels and the paucity of information regarding their role in the normal physiological context, AP-1 family TFs in the McSC lineage merit further study.

Furthermore, the upregulation of immune-related genes in McSCs might also suggest that the ability of melanoma to modulate and evade immune detection is rooted in a physiological SC property. Indeed, with regard to gaining potential insights into malignant traits, one major

advantage of studying adult tissue McSCs versus embryonic melanoblasts is understanding these SCs in the context of an immune-competent niche. Curiously, work by Riesenberg et al. (2015) suggest that dedifferentiated $MITF^{low}$ melanoma cells have higher expression of inflammatory genes. In this regard, the selective upregulation of *Cd274* (encoding PD-L1) in McSCs in my dataset was particularly striking. PD-L1 is upregulated on melanoma cells to protect against immune attack, and targeting this interaction with immunotherapy has revolutionized melanoma treatment (Sharma and Allison, 2015). It is tempting to speculate that McSCs might harness molecules like PD-L1 to protect themselves from immune attack in situations when the protective HF niche might be compromised (i.e. wounding, inflammation) or during migration out of the follicle and into the epidermis. Indeed, McSC crosstalk with the immune system is an area of emerging study. Harris et al. (2018) demonstrated that MITF suppresses interferon signature genes. My data appear to be consistent, as qMcSCs with lower levels of MITF protein, show upregulation of many immune-related genes relative to their differentiating progeny, which accumulate nuclear MITF. Overall, these results add to the body of literature that report shared molecular features of McSCs and melanoma, and point to genes whose role in normal and transformed cells could be elucidated in future functional studies.

Considering such interactions raises further questions regarding how transcriptional changes in the McSC lineage impacts other cell types in the surrounding microenvironment, especially HFSCs and their lineage. Numerous studies have described mechanisms through which HFSCs and their HF lineage cells dictate the behavior of McSCs and melanocytes, but whether the reverse scenario is true (outside of providing UV protection) is not well understood. Given that hair growth is not dependent on functional McSCs or their progeny (white hair can grow), the implications of melanocytic signals might be subtle, but perhaps still present. These scRNA-seq

data provide a list of candidate factors that could serve as a starting point for such investigations. Conversely, it still remains to be determined which components of the bulge and HF niche are triggering these gene expression changes in the McSC lineage, as opposed to those that are intrinsically controlled.

Finally, in their cyclic quiescence, activation, transit amplification, and differentiation, McSCs mirror the developmental trajectory of HFSCs. Hsu et al. (2014) demonstrated that HF matrix TACs signal back to quiescent SCs via Sonic hedgehog (SHH) signaling to induce their self-renewal. This begs an intriguing question: do McSC TAC progeny (McCP) provide feedback to their parent SCs in the way that HFSCs do? Based on the timing of this signaling for matrix TACs, the data obtained from aMcSCs and early McCPs in anagen I-II might present clues. Indeed, to create banded patterns in feathers, it is believed that mature melanocytes engage in a negative feedback loop, signaling back to undifferentiated proliferative progenitor cells to stop their progression and achieve cyclic maturation and pigmentation (Inaba and Chuong, 2020).

In summary, these new data contribute a more complete and high resolution picture of McSC transcription throughout differentiation. Notably, this dataset affords a high depth of coverage to discern maximal differences between cell types, and it includes intermediate stages of lineage progression, namely aMcSCs and McCP. Recently, Smart-Seq2 data has been generated for human melanocytes isolated from different patient ages and body sites (Belote et al., 2020). Future cross-species analyses will likely provide useful new insights for the field's understanding of this lineage.

However, transcription is just one level of regulation impacting cellular dynamics; global proteomic and epigenetic studies at the single cell level will provide further insight into how these different McSC states are achieved and how chromatin state, transcription, and translation

intersect. This work would inform questions concerning whether some qMcSCs, while appearing transcriptionally homogeneous, are actually poised for activation, while another pool is more deeply quiescent. These differential gene expression and pathway analyses implicated both known and novel genes and biological processes at each stage, allowing me to form more specific hypotheses about how McSCs pass through activation and differentiation, which is the subject of **Chapter 3** and centers on BMP and WNT signaling **(Chapter 2.2.6)**. At the same time, this body of work raises several diverse hypotheses, and will hopefully form the foundation for future studies in the McSC lineage during homeostasis and in disease.

CHAPTER 3:
BMP SIGNALING DRIVES FULL DIFFERENTIATION OF MELANOCYTES DOWNSTREAM OF STEM CELL ACTIVATION AND LINEAGE COMMITMENT

3.1 Introduction

By performing high sensitivity scRNA-seq on McSC lineage cells at multiple developmental time points, I gained temporal insight on not only the gene expression changes during lineage progression, but also when signaling pathways seem to become activated. In narrowing the focus of my project to study the pathways and downstream TFs that were likely to impact lineage progression and differentiation, both BMP and WNT signaling featured prominently **(Chapter 2.2.6)**. When compared to the most highly differentiated melanocytes in the dataset (C3c), the later McCP of the anagen VI hair bulb (C3a) showed significant upregulation of genes involved in both pathways. This was intriguing given the essential role of WNT signaling in McSC activation and downstream melanocyte maturation (Rabbani et al., 2011), and also given reports of both cooperative and antagonistic effects of WNT and BMP pathways in SC biology.

Simply described, canonical WNT signaling occurs through the binding of WNT ligands to frizzled (FZD) and lipoprotein receptor-related protein (LRP) receptors, disrupting the cytoplasmic β-catenin degradation complex. Stabilized β-catenin can then translocate to the nucleus and bind with TCF/LEF family TFs to regulate gene expression (Nusse and Clevers, 2017). WNT plays an essential role in the melanocyte lineage, from embryonic specification of melanoblasts, where it appears to act antagonistically with BMP signaling (Hari et al., 2002; Hari et al., 2012; Jin et al., 2001), to activation of HF McSCs and downstream proliferation and differentiation of melanocytes in the hair bulb (Rabbani et al., 2011).

BMP signaling occurs through the binding of BMP ligands to complexes of BMP type I and type II cell surface receptors, triggering their serine/threonine kinase-mediated phosphorylation of SMAD1/5/9 proteins. Phosphorylated SMAD1/5/9 then bind SMAD4 and translocate to the nucleus to regulate target gene expression (Wang et al., 2014). Through genetic

manipulation of *Bmpr1a* (*ALK3*), the Fuchs Lab has shown that this pathway is critical for HF lineage regulation. BMP signaling both maintains HFSCs in quiescence and promotes the differentiation of HF TACs (Genander et al., 2014; Kobielak et al., 2007). However, the role of BMP signaling in McSC lineage commitment was not well understood, with most insights resting on cell culture studies (Bilodeau et al., 2001; Jin et al., 2001; Kawakami et al., 2008; Park et al., 2009; 2005; Singh et al., 2012; Yaar et al., 2006; Yang et al., 2014); the few studies in mice made the precise contributions of this pathway difficult to interpret (Han et al., 2012; Sharov et al., 2005).

Given the highly context-dependent roles of this pathway, which stem from promiscuity of ligand binding, differential receptor expression and complex combinations, and expression of positive and negative pathway regulators (Wang et al., 2014), I wanted to gain a deeper understand about how BMP works in the lineage in the native tissue microenvironment. Therefore, in my thesis research, I posed the following hypotheses: 1) BMP (BMPR1a) signaling promotes McSC lineage progression and melanocyte differentiation, and 2) BMP signaling coordinates with WNT signaling in the differentiation process. To test these hypotheses, I harnessed genetic mouse models, IMF and ultrastructural analyses, cell culture, scRNA-seq, and chromatin profiling approaches.

3.2 Results

3.2.1 Cocommitant activity of WNT and BMP signaling in the lineage

At the transcript level, there is evidence of increasing WNT and BMP signaling at the late McCP stage. To confirm the acitivty of these pathways at the protein level, I performed IMF analysis of the skin throughout hair cycling. To assay for WNT activity, I interrogated the TF LEF1. While McSCs throughout cycling lacked LEF1, nuclear signal became robust as cells

transitioned to the McCP/melanocyte stages in anagen **(Fig. 3.1 A)**. While inner bulge HFSCs showed robust BMP signaling through pSMAD1/5/9, neighboring McSCs lacked nuclear signal in both their quiescent and activated states. However, as differentiation progressed, McCP/melanocytes in the hair bulb became strongly pSMAD1/5/9^{+}, and this was maintained throughout anagen **(Fig. 3.1 B)**. Together, these RNA and protein analyses were consistent with the hypothesis that BMP signaling acts during differentiation. Furthermore, the concomitant timing of pSMAD1/5/9 and LEF1 nuclear accumulation in McCP/melanocytes in anagen HFs were in agreement with a degree of convergent signaling. On this basis, I proceeded to employ loss-of-function mouse models to investigate the role of BMP signaling in lineage progression and how it might intersect with WNT.

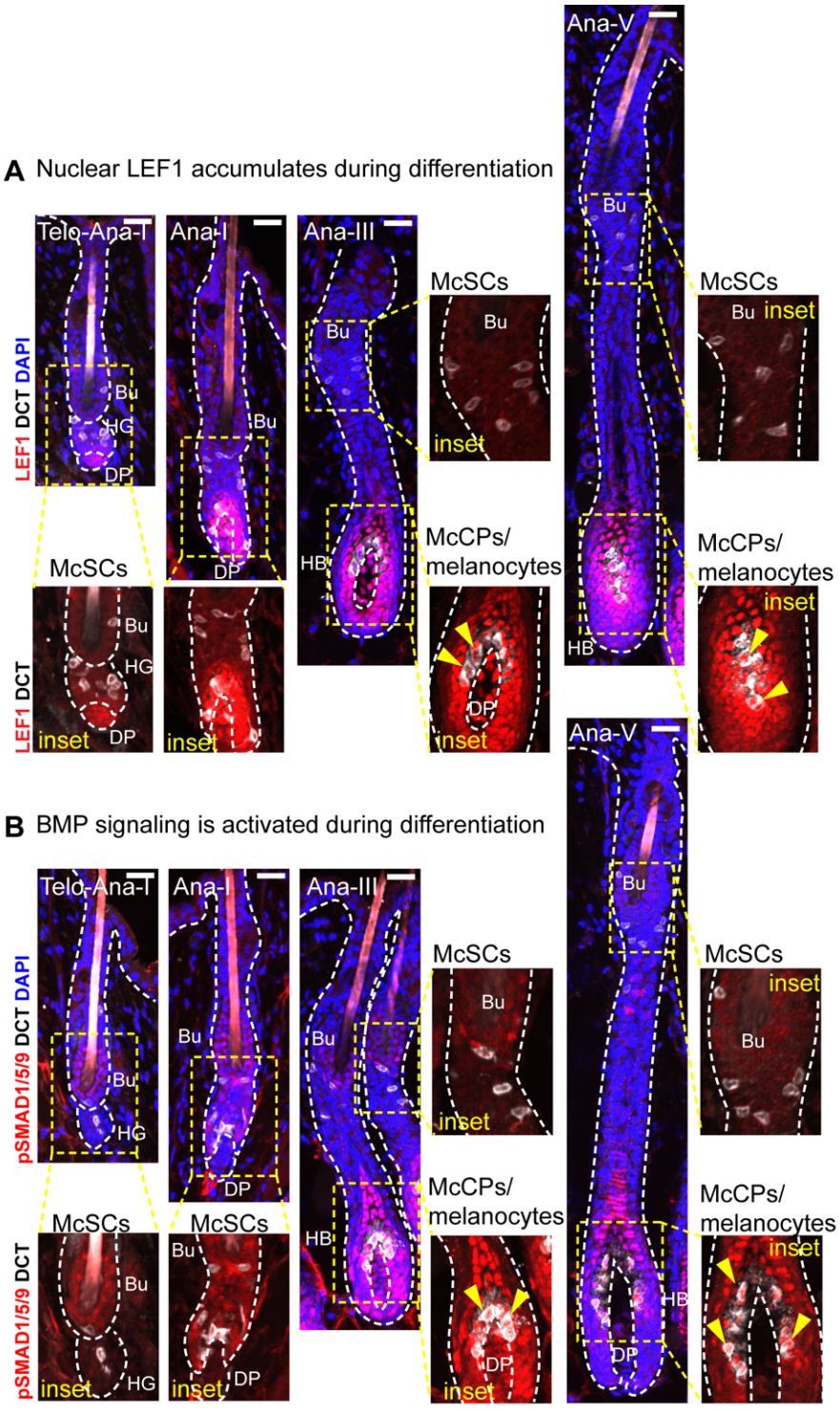

Figure 3.1 WNT/LEF1 and BMP/SMAD signaling is activated in McCP/melanocytes. (A) IMF images showing LEF1 protein expression in the melanocyte lineage throughout hair cycling. Nuclear LEF1 (red) indicated by yellow arrows. **(B)** pSMAD1/5/9 (BMP signaling) is absent in McSCs but becomes nuclear in McCPs/melanocytes (Mcs), indicated by yellow arrows. All scale bars=25μm.

3.2.2 Perturbed WNT signaling in mice results in reduced hair pigmentaiton

To understand the importance of LEF1 in the lineage, I first revisted *Lef1* full body KO mice (Kratochwil et al., 1996; van Genderen et al., 1994). These mice had less pigmented hair compared to their littermates **(Fig. 3.2 A)**. Due to their lack of most HFs, there is abnormal localization of melanocytes in KO skin, including pigmented melanocytes in the dermis and some follicles containing fewer melanocytes. However, in the follicles that did contain DCT^{+} cells in their anagen HFs, hair bulbs and hairs still appeared less pigmented, suggesting that loss of LEF1 impaired melanocyte differentiation **(Fig. 3.2, right)**.

I then used a second, more specific approach to conditionally ablate β-catenin (*Ctnnb1*) in the lineage by generating *TyrCreER Ctnnb1*^{floxed} *R26-YFP*^{floxed} mice (Bosenberg et al., 2006; Brault et al., 2001; Srinivas et al., 2001). This model is similar to that used by Rabbani et al. (2011) to demonstrate that WNT signaling plays key roles in McSC activation and downstream proliferation and differentiation of melanocytes in the hair bulb. Upon tamoxifen treatment, *TyrCreER* drives expression in both McSCs and their differentiating progeny (Bosenberg et al., 2006). At P21, mice were treated with seven consecutive doses of tamoxifen **(Fig. 3.2 B)**. Consistent with the results of Rabbani et al. (2011), by second telogen, *Ctnnb1* conditional KO (cKO) mice had hairs with reduced pigmentation relative to control **(Fig. 3.2 C)**. I then wanted to interrogate the status of BMP signaling in the absence of functional WNT/β-catenin signaling. To analyze the McSC lineage during differentiation, I waxed tamoxifen-treated second telogen mice to induce synchronous hair growth and analyzed tissues one week later in anagen **(Fig. 3.2 B)**. Nuclear pSMAD1/5/9 was still present in *Ctnnb1* null McSC progeny in the hair bulb, indicating that BMP signaling is not dependent on WNT signaling **(Fig. 3.2 D)**.

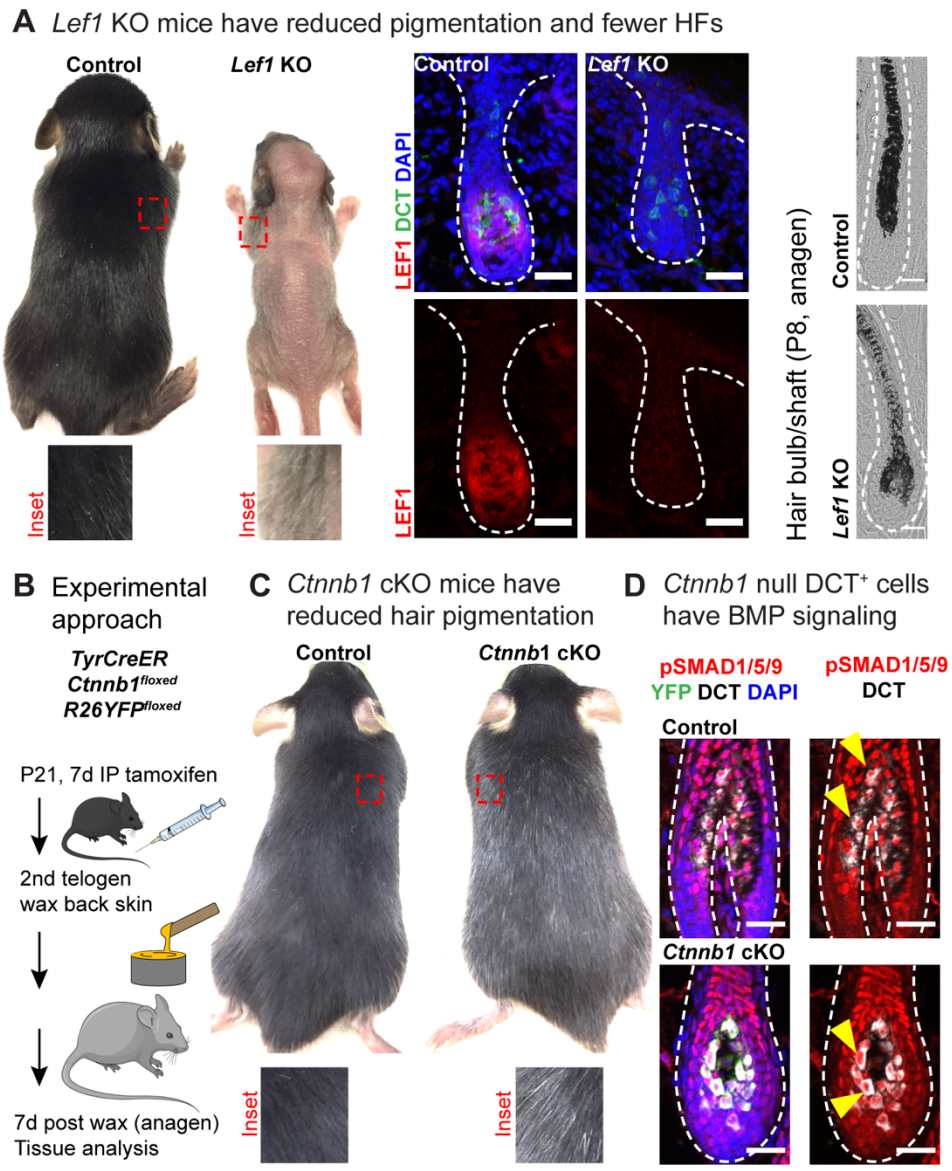

Figure 3.2 WNT mutant mice have reduced pigmentation. (A) Left, phenotype of *Lef1* KO mice at P13, when hair on the skin surface has emerged in KO (control littermate: female, *Lef1* KO: male). Middle, IMF for LEF1 in control and *Lef1* KO skin at P0. Right, brightfield images of P8 anagen HFs. **(B)** Experimental schematic for conditionally ablating β-catenin (WNT) in the melanocyte lineage *in vivo*. **(C)** Phenotype of tamoxifen-treated *TyrCreER Ctnnb1*^{floxed} *R26YFP*^{floxed} mice at 2nd telogen. **(D)** IMF of *Ctnnb1* cKO and control skin 1 week after waxing. BMP signaling through nuclear pSMAD1/5/9 is indicated by yellow arrows. Scale bars=25μm.

3.2.3 Loss of BMP signaling through BMPR1a leads to hair graying

To interrogate the role of BMP signaling in McSC lineage progression, I generated a strain of conditional lineage-specific *Bmpr1a* KO mice, *TyrCreER Bmpr1a*^{floxed} *R26YFP*^{floxed} (Bosenberg et al., 2006; Mishina et al., 2002; Srinivas et al., 2001). BMPR1a is a type I receptor serine/threonine kinase whose loss extinguishes downstream signaling through the pathway. I treated these mice with tamoxifen at P21 and allowed them to progress to second telogen. Strikingly, by this point, *Bmpr1a* cKOs exhibited gray hair, while *Bmpr1a* heterozygotes (*TyrCreER*$^{+}$ *Bmpr1a*$^{fl/+}$) showed no phenotype relative to controls (*TyrCreER*$^{-}$ or *TyrCreER*$^{+}$ *Bmpr1a*$^{+/+}$) **(Fig. 3.3 A)**. To observe the McCP/melanocyte populations in hair bulb compartment, tamoxifen-treated second telogen mice were waxed, and anagen skin was collected after one week of hair growth. As measured by optical density, there was significantly reduced pigmentation in *Bmpr1a* cKO hair bulbs **(Fig. 3.3 A-B)**.

Gray hair phenotypes can occur due to defects in the McSC compartment, including apoptosis, ectopic proliferation and differentiation, or migration out of the niche (Nishimura et al., 2011). Alternatively, abnormalities may occur downstream at other points in differentiation **(Fig. 1.2)**. To ascertain the cause of the gray hair in *Bmpr1a* cKO mice, I waxed second telogen mice to trigger hair growth and McSC activation and differentiation, then analyzed McSCs after one week using IMF. McSCs numbers per HF were comparable between *Bmpr1a* cKO mice and controls **(Fig. 3.3 C)** and seemed to return to quiescence normally after activation, as measured by EdU incorporation during a 4 hour pulse **(Fig. 3.3 D)**. To more conclusively rule out McSC dysfunction, I challenged the SC pool by performing serial waxing. The anterior back skin of second telogen mice was waxed five times in total every three weeks, by which time the waxed region appeared to return to telogen. By four rounds of waxing, the anterior hair coat did not show an appreciable

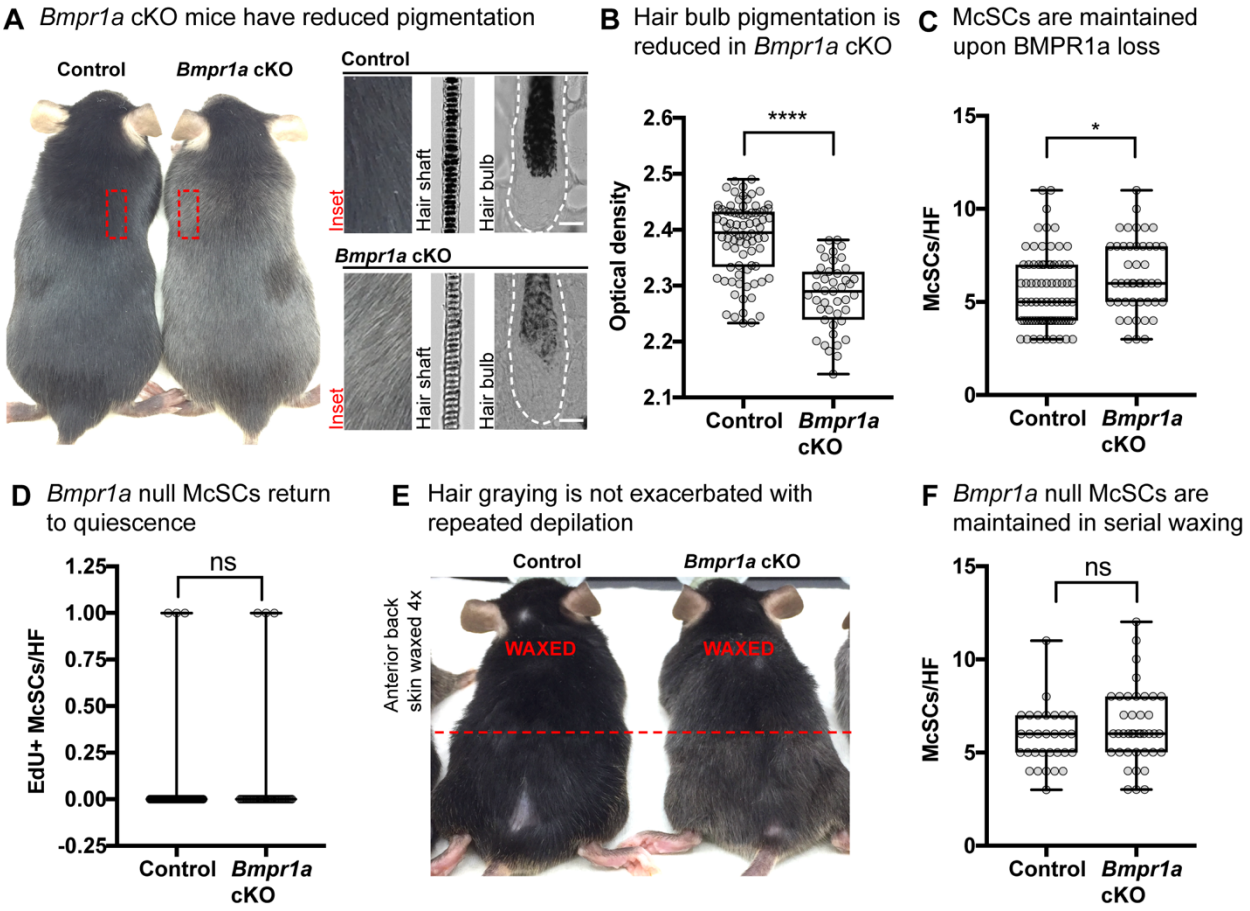

Figure 3.3 Conditional ablation of *Bmpr1a* in the lineage results in gray hair without compromised McSCs. (A) Representative phenotype of *TyrCreER Bmpr1a*^{floxed} *R26YFP*^{floxed} mice tamoxifen-treated mice in 2nd telogen. Scale bars=25μm. **(B)** Quantification of pigment content in hair bulbs measured by optical density. [****p<0.0001, Mann-Whitney test; Control n=80 HFs (n=4 mice); *Bmpr1a* cKO n=43 HFs, (n=3 mice)]. **(C)** Quantification of McSCs numbers per anagen HF 1 week after waxing [*p=0.0184, Mann-Whitney test; Control n=76 HFs (n=5 mice); *Bmpr1a* cKO n=45 HFs (n=4 mice)]. **(D)** Quantification of EdU^{+} McSCs per HF 1 week after waxing [(ns=not significant, Mann-Whitney test; Control n=61 HFs (n=3 mice); *Bmpr1a* cKO n=45 HFs (n=4 mice)] **(E)** Phenotype of control and *Bmpr1a* cKO mice after 4 rounds of waxing on the anterior portion of the back skin, 3 weeks apart. Note that a small skin biopsy was taken from the posterior midline near the time of initial waxing of the anterior. **(F)** Quantification of McSCs per HF after 5 rounds of depilation, quantified in anagen 1 week after the fifth wax [(Mann-Whitney test; Control n=30 HFs (n=3 mice); *Bmpr1a* cKO n=40 HFs (n=4 mice)].

exacerbation of hair graying **(Fig. 3.3 E)**. Anagen skin was collected one week after the fifth wax for IMF, and I found no significant difference in number of McSCs per HF between control and *Bmpr1a* cKO mice **(Fig. 3.3 F)**. These results suggested that McSCs were intact and functional upon *Bmpr1a* loss and were consistent with my scRNA-seq **(Fig. 2.7)** and IMF data **(Fig. 3.1 B)**, which both indicated that this pathway is not activated until the McCP stage.

I therefore turned my attention to identifying defects downstream in the lineage. In *Bmpr1a* cKO mice, DCT^{+} cells populated the McCP/melanocyte compartment of the hair bulb. By IMF, these cells showed loss of nuclear pSMAD1/5/9 as well as pP38, indicating ablation of canonical and non-canonical pathways downstream of BMPR1a, respectively **(Fig. 3.4 A-B)**. To rule out the possibility that hair bulbs were less pigmented because cells were simply delayed in differentiation, I analyzed skin further into anagen. Indeed, 12 days after waxing, *Bmpr1a* cKO hair bulbs were still poorly pigmented **(Fig. 3.4 C)**. These data suggested that without BMP signaling, McSC quiescence and activation were not impacted, but lineage progression and subsequent melanin production were disrupted.

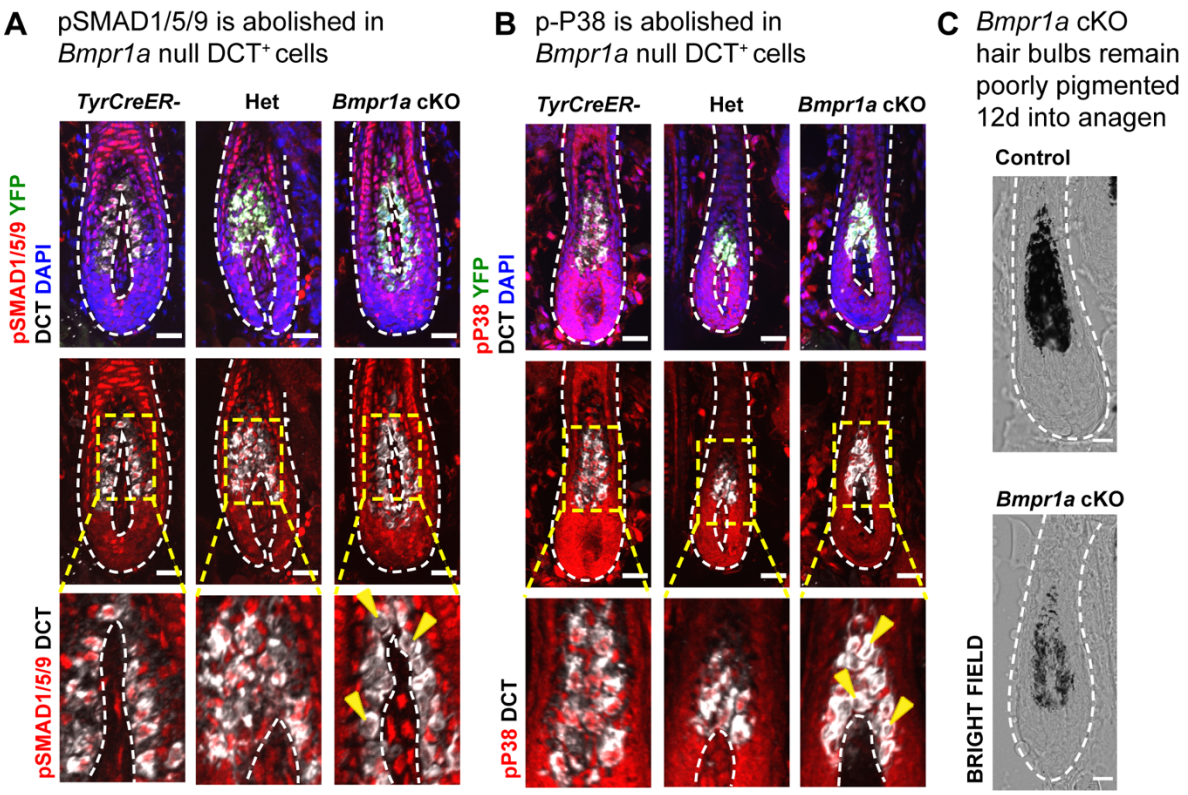

Figure 3.4 McSCs in *TyrCreER*$^{+}$ *Bmpr1a*$^{fl/fl}$ *R26YFP* mice give rise to differentiating progeny that populate the hair bulb. (A) IMF showing loss of BMP-SMAD signaling through pSMAD1/5/9 and **(B)** MAPK through pP38 in *Bmpr1a* null DCT^{+} cells in the hair bulb. **(C)** Bright field images of control and *Bmpr1a* cKO hair bulbs 12 days after waxing. Scale bars=25μm

3.3.4 ScRNA-seq and pseudotime analysis of *Bmpr1a* null cells *in vivo* suggests a block in differentiation between early McCP and mature melanocyte

Given that my *in vivo* results suggested a defect downstream in differentiation, I sought to gain further mechanistic insights using a cultured melanocyte mouse cell line, Melan-a2 (Sviderskaya, et al., 1995). To minimize variability, I first generated a clonal parental line from Melan-a2, then using CRISPR/Cas9, I generated and validated *Bmpr1a* KO and control cloncal cell lines **(Fig. 3.5 A)**. However, while loss of the receptor in culture led to reduced pSMAD1/5/9 upon BMP2 stimulation, signaling was not completely abolished, and BMP6-induced pSMAD1/5/9 signaling was not affected in *Bmpr1a* KO cells **(Fig. 3.5 B)**. At the same time, no apparent change in melanin was observed, suggesting that the *in vivo* phenotype could not be

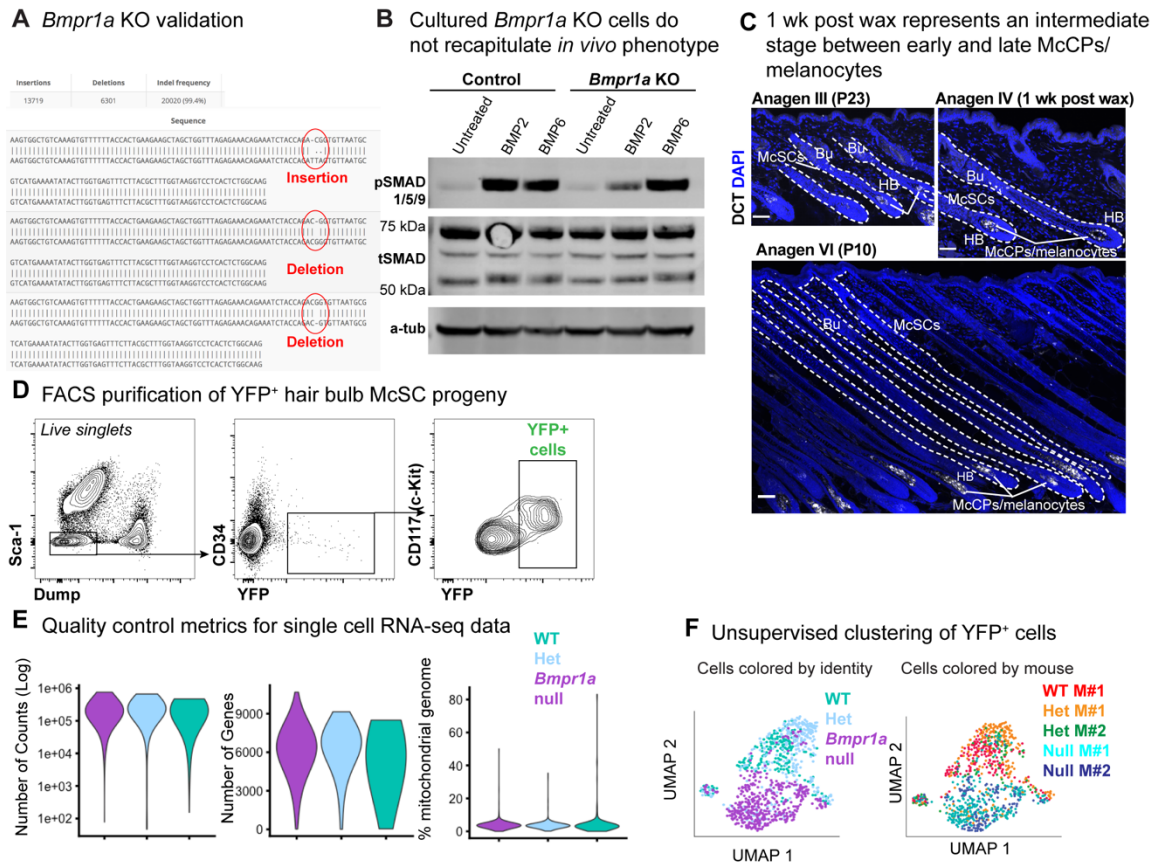

Figure 3.5 FACS purification of i*n vivo Bmpr1a* null cells preserves the molecular profile that results from the dynamic and complex microenvironment. (A) Validation of CRISPR KO of *Bmpr1a* using Cas-analyzer tool on rgenome.net, using MiSeq results. **(B)** Western blot analysis of pSMAD1/5/9 signaling in control and KO Melan-a2 cell lines after 1 hour BMP stimulation (0.5% serum, CT-free media during treatment). **(C)** IMF images of skin at different stages of hair cycling. Bu=bulge, HB=hair bulb. Scale bars=50μm. **(D)** FACS purification schemes for YFP$^+$ populations. **(E)** Quality control metrics showing log number of counts, genes/cell, and percentage of mitochondrial genes for unfiltered datasets. **(F)** Unsupervised k-NN based clustering of control (heterozygous, Het and wild-type, WT) and *Bmpr1a* null cells colored by known identity (left) and individual mouse ("M") (right). For cell identity, purple are WT, (*TyrCreER*$^+$ *Bmpr1a*$^{+/+}$, n=205 cells, n=1 mouse), blue are Het, (*TyrCreER*$^+$ *Bmpr1a*$^{+/fl}$, n=304 cells, n=2 mice) and green are *Bmpr1a* null (*TyrCreER*$^+$ *Bmpr1a*$^{fl/fl}$, n=421 cells, n=2 mice).

accurately recapitulated *in vitro*. This was not surprising given the complexity and context-dependent behavior of this pathway. BMP/TGF-β receptor superfamily members (i.e. activin receptors) can dimerize in multiple combinations and yield signaling responses that differ depending upon the specific ligand, receptors, and intra- and extracellular regulator molecules present (Wang et al., 2014). These differences limited the studies I could perform in culture, but

provided a plausible explanation for the context-dependent behaviors described in this lineage in the literature (Bilodeau et al., 2001; Han et al., 2012; Jin et al., 2001; Kawakami et al., 2008; Park et al., 2009; Sharov et al., 2005; Singh et al., 2012; Yaar et al., 2006; Yang et al., 2014). These findings underscored the importance of taking *in vivo* approach where possible to study this signaling pathway and specific receptor's function.

Therefore, I focused on methods that enabled me to study the effect of BMPR1a loss in mice. To this end, I turned again to FACS purification and scRNA-seq. *Bmpr1a* control (*Bmpr1a* heterozygous +/fl and WT +/+) and cKO mice were treated with tamoxifen at P21, allowed to progress to second telogen, then waxed to induce anagen. At one week post-waxing, HFs were in anagen IV, an ideal time point at which to capture differentiating McCP in the hair bulb when BMP signaling becomes activated **(Fig. 3.5 C)**. Using a digestion protocol to preferentially release cells from the dermis of the skin including hair bulb cells, I FACS purified YFP^+ cells, gating against CD31, CD45, CD140a, Sca-1 and $CD34^+$ cells **(Fig. 3.5 D)** and again performed scRNA-seq. Again, this approach afforded many advantages, including the ability to discern any YFP^+ cells captured that were not actually *Bmpr1a* null (which were consequently clustered appropriately with control cells). ScRNA-seq data were subject to quality control analyses and filtering parameters, where any Dct^{low} and $Krt15^+$ cells were again excluded from further analysis. Overall, cells displayed a similar depth of sequencing with approximately 5,000 genes per cell (consistent with increased transcriptional activity occurring during differentiation), and few reads mapped to mitochondrial transcripts **(Fig. 3.5 E)**. Furthermore, independent replicates exhibited similar clustering **(Fig. 3.5 F)**.

PCA with UMAP and k-NN clustering of these data revealed the presence of two major groups. *Bmpr1a* WT and heterozygous cells showed significant overlap and comprised one of

these two clusters, while *Bmpr1a* null cells formed the second cohort, indicating their unique transcriptome **(Fig. 3.6 A)**. Consistently, expression of direct BMP target genes *Id2* and *Id3* were dramatically downregulated in this *Bmpr1a* null cluster **(Fig. 3.6 B**). To understand what other transcriptional differences were driving this separation, differential gene expression analysis was performed on the control versus *Bmpr1a* null cluster. This indicated that 80 genes were significantly ($q \geq 0.05$) downregulated and 346 genes were upregulated in the absence of *Bmpr1a* **(Fig. 3.6 C-D**; **Table 3.1-3.2;** see also Table S9 of Infarinato et al., 2020**)**. Strikingly, *Bmpr1a* null cells showed diminished expression of genes involved in melanogenesis and melanosome organization, including *Oca2*, *Rab38*, *Gpr143, Shroom2,* and *Mc1r*. At the same time, these cells

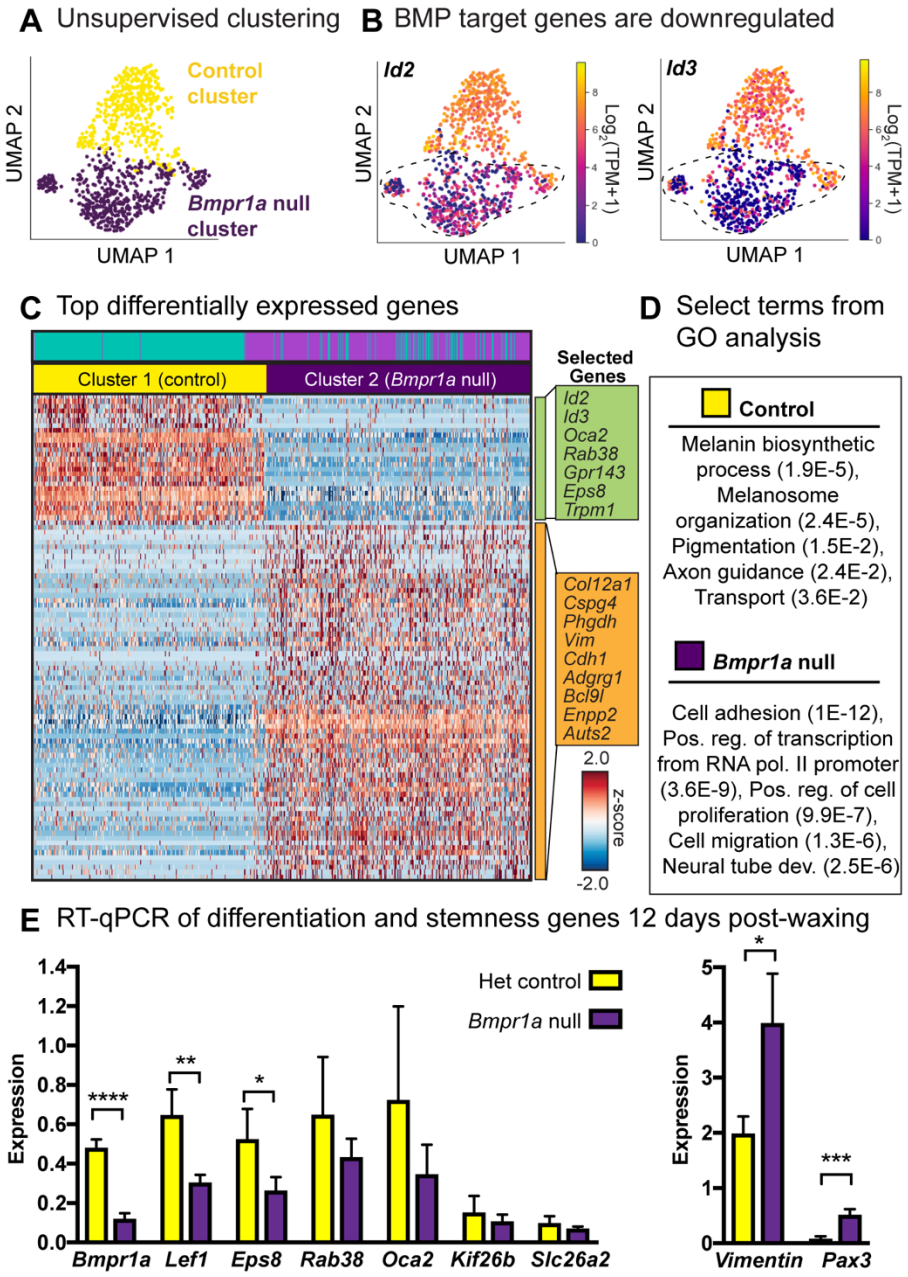

Figure 3.6 *Bmpr1a* null cells downregulate melanogenesis, melanosome, and transport genes. **(A)** UMAP representation and unsupervised k-NN based clustering of control and *Bmpr1a* null cells colored by cluster identity. **(B)** Expression plots of *Id2* and *Id3* in YFP^{+} populations. **(C)** Heatmap of top differentially expressed genes for *Bmpr1a* null versus stage-matched controls and **(D)** selected GO terms (DAVID 6.8) with (p-values). See also Table 3.1-3.2. **(E)** RT-qPCR expression of genes from scRNA-seq list isolated 12 days post waxing [(****p<0.0001 *Bmpr1a*; **p=0.0035 *Lef1*; *p=0.0269 *Eps8*; *p=0.0148 *Vimentin*; ***p=0.0010 *Pax3*, Unpaired t-test; Heterozygous control n=3 mice, *Bmpr1a* cKO n=4 mice)].

showed elevated transcripts of genes involved in stemness (*Pax3*, *Vim*), migration and cellular projections (*Enpp2*, *Tubb2b*), and cell adhesion (*Cspg4*, *Adgrg1)*. To test whether these trends persisted further into anagen, bulk YFP^+ cells were FACS purified 12 days after waxing for RT-qPCR, which produced similar results for several genes **(Fig. 3.6 E)**.

These intriguing results begged another question: if integrated into the original WT McSC lineage dataset **(Chapter 2)**, how would the *Bmpr1a* null cells compare? Pseudotime algorithms can be implemented on scRNA-seq data to gain temporal information about a biological process such as SC differentiation, ordering individual cells in a dataset along an inferred trajectory. Therefore, these experimental datasets were integrated with the six WT lineage sub-clusters (qMcSCs, aMcSCs, early and late McCP, and differentiated melanocytes) and UMAP-based dimensionality reduction and clustering was performed **(Fig. 3.7 A)**. One-third of *Bmpr1a* null cells clustered with early McCP (C2b), suggesting their transcriptional similarity **(Fig. 3.7 B, left)**.

Next, the collective dataset was subject to pseudotime analysis using Monocle3 (Cao et al., 2019), a relatively unbiased method to map differentiation in which all biologically significant genes are considered. As expected based on the hair cycle time point from which cells were isolated and the differentiatial gene expression analyses between sub-clusters **(Fig. 3.7 B)**, qMcSCs (C1) were placed at the start or "root" of the trajectory, followed by aMcSCs, then McCP, with the most differentiated melanocytes (C3c) forming the end point of the "branch." As expected, Monocle3 also indicated that *Bmpr1a* control cells collected from anagen IV hair bulbs were earlier in the differentiation process than all WT McCP/melanocyte (C3) sub-cluster cells isolated from anagen VI hair bulbs. *Bmpr1a* null cells however were placed after early McCP (C2b) from anagen I-II HFs and their stage-matched controls, as well as all other anagen VI McCP/melanocytes (C3).

Their placement in the pseudotime map suggested that *Bmpr1a* null cells were blocked in their differentiation trajectory. To further explore this idea, the expression of established "stemness" and "differentiation" signature genes **(Fig. 2.5 B)** was analyzed relative to the WT lineage sub-clusters **(Fig. 3.7 C)**. *Bmpr1a* null cells showed reduced expression of genes involved in melanogenesis as compared to the WT McCP/melanocytes (C3), as well as genes involved in BMP and WNT signaling pathways, with elevated expression of stemness genes. This is visualized through the global scoring system in the expression plots in **Fig. 3.7 D**, where levels of stemness and differentiation gene scores can also be compared to a small number of YFP^{+} McSCs collected from both *Bmpr1a* control and null groups, which have the highest stemness and lowest differentiation scores. Overall, these analyses suggested that *Bmpr1a* null cells share many transcriptional similarities with early McCP but have elevated melanogenesis and differentiation-associated gene expression, underscoring that these cells are arrested just downstream of the aMcSCs and early McCP stages.

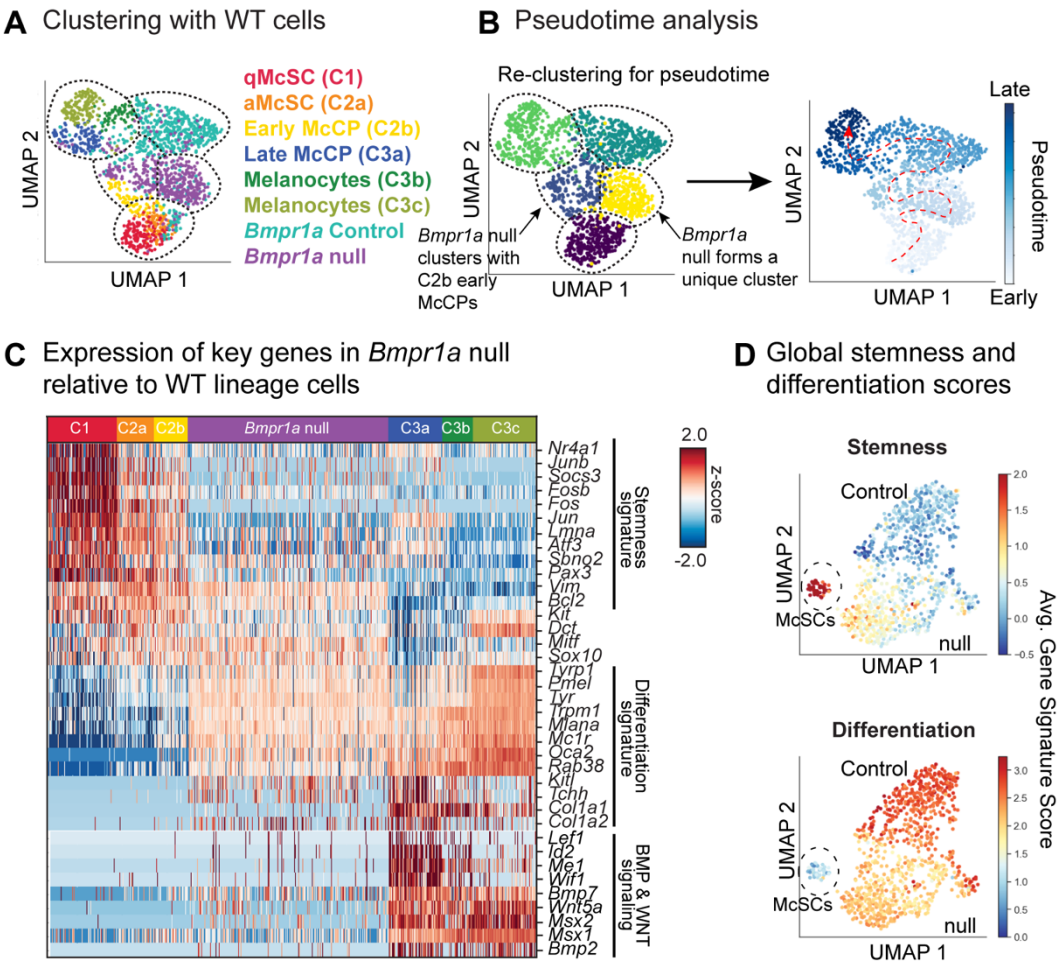

Figure 3.7 Pseudotime analysis of the *Bmpr1a* null cells suggests a block at the juncture after early McCP. (A) Unsupervised k-NN based clustering of original melanocyte lineage populations with *Bmpr1a* null and control cells, colored by sub-cluster identity. **(B)** Pseudotime analysis of combined datasets colored by pseudotime clusters (left) and pseudotime order (right). Cells are colored by progression through pseudotime with dashed red arrow to indicate direction of progression. **(C)** Heatmap showing expression of key signature genes in *Bmpr1a* null cells relative to WT sub-clusters. **(D)** Expression plots of global stemness and differentiation scores for *Bmpr1a* null and control cells.

3.3.5. *Bmpr1a* null cells in the hair bulb exhibit signs of immaturity

My transcriptional data suggested that *Bmpr1a* null lineage cells were blocked in differentiation. Therefore, I performed tissue analyses to test for feautres of melanocyte immaturity. To test for proliferation, I treated mice with tamoxifen at P21, waxed their backskin in second telogen, and collected anagen skin one week later after a 4 hour EdU pulse. In agreement

with their transcriptional similarities to aMcSCs and early McCP, *Bmpr1a* null cells in the hair bulb showed increased EdU incorporation relative to control **(Fig. 3.8 A)**. I confirmed these results in another experiment, where I counted DCT^{+} cells in the hair bulb and found cell numbers to be significantly increased in *Bmpr1a* cKOs **(Fig. 3.8 B)**. This suggested that surprisingly, the reduced pigmentation in the cKO hair bulbs was not due to reduced numbers of McCP/melanocytes. This contrasted from the effect of loss of WNT/β-catenin signaling, which results in reduced proliferation in both the McSC and hair bulb compartments (Rabbani et al., 2011). At the same time, *Bmpr1a* null cells in the hair bulb exhibited increased expression of the McSC signature gene vimentin at the protein level, further indicating their immaturity **(Fig. 3.8 C)**.

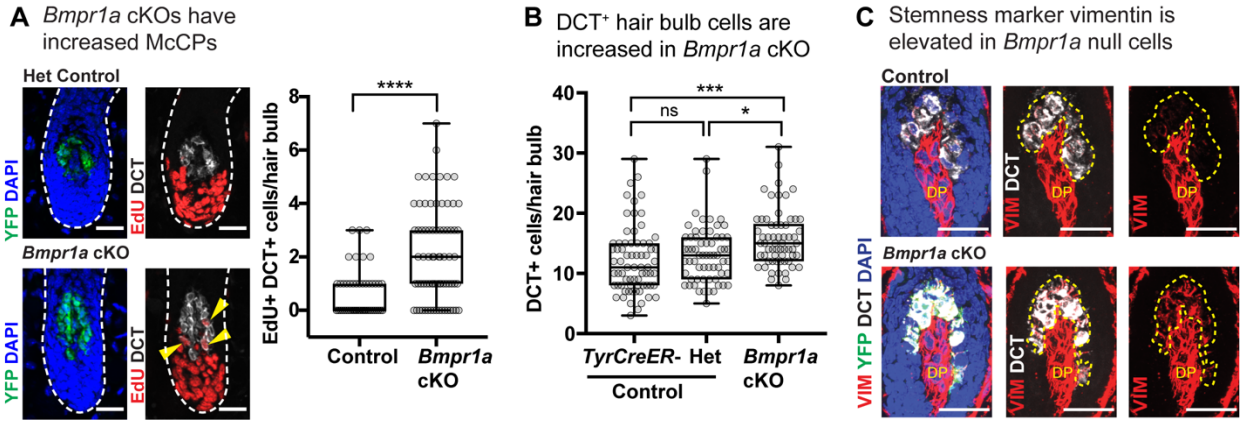

Figure 3.8 *Bmpr1a* null cells in the anagen hair bulb exhibit signs of immaturity. (A) 4 hour EdU pulse experiment with representative IMF images and quantification [****p<0.0001, Mann-Whitney test; control n=50 HFs (n=2 mice); *Bmpr1a* cKO n=75 HFs (n=3 mice)]. Yellow arrow heads indicate proliferating (EdU^{+}) DCT^{+} cells. **(B)** Quantification of DCT^{+} cells per hair bulb 1 week after waxing [****padj<0.0001, *padj=0.0103, Kruskal-Wallis test, Dunn's multiple comparisons test; *TyrCreER*$^{-}$ control n=70 HFs (n=3 mice); Het control n=63 HFs (n=3 mice); *Bmpr1a* cKO n=62 HFs (n=4 mice)]. **(C)** IMF expression of vimentin (red); yellow dashed area encircles DCT^{+} cell area. Scale bars=25μm

Given the presence and increased number of McSC differentiating progeny in *Bmpr1a* cKO hair bulbs, I next tested for the protein expression of the three key melanogenic enzymes: DCT, tyrosinase (TYR), and tyrosinase-related protein 1 (TYRP1). In agreement with my scRNA-seq

data indicating that these enzymes are upregulated earlier on in differentiation, DCT, TYR, and TYRP1 (which was in fact reduced in *Bmpr1a* null cells at the transcript level) were all present by IMF in *Bmpr1a* null cells in the hair bulb **(Fig. 3.9 A-B)**, suggesting that the defect in pigmentation was unlikely attributable to loss of any one critical component of melanin production. Instead, I turned to assessing melanosomes. While PMEL, a structural component of melanosomes involved in organelle maturation, was expressed in *Bmpr1a* null cells, it exhibited a more perinuclear localization compared to control cells, where labeling was seen throughout the cell body and dendritic processes **(Fig. 3.9 B, right)**. This suggested a perturbation in melanosome biogenesis or localization, which was reinforced by the reduced expression of melanosome organization genes seen by scRNA-seq **(Fig. 3.6 C-D)**.

Melanosome biogenesis proceeds through four distinct phases of maturation that are well-defined at the ultrastructural level. Stage I melanosomes largely resemble endosomal multivesicular bodies, stage II melanosomes exhibit parallel intralumenal striations, stage III melanosomes show thickening and darkening of these striations as melanin is deposited, and stage IV mature melanosomes ultimately become opaque (Marks and Seabra, 2001). To investigate the status of melanosomes in *Bmpr1a* null cells, back skin was waxed and collected one week later in anagen for electron microscopy (EM) of lineage cells in the hair bulb. Quantification of total and mature (stage IV) melanosome area densities revealed similarities between control and *Bmpr1a* null cells, but *Bmpr1a* null cells displayed a significantly higher density of immature (stage I-III) melanosomes **(Fig. 3.9 C)**. Together, these results suggest that in the absence of BMPR1a signaling, McSC progeny are suspended in a partially differentiated state characterized by increased proliferation and perturbed melanosome biogenesis and pigment production.

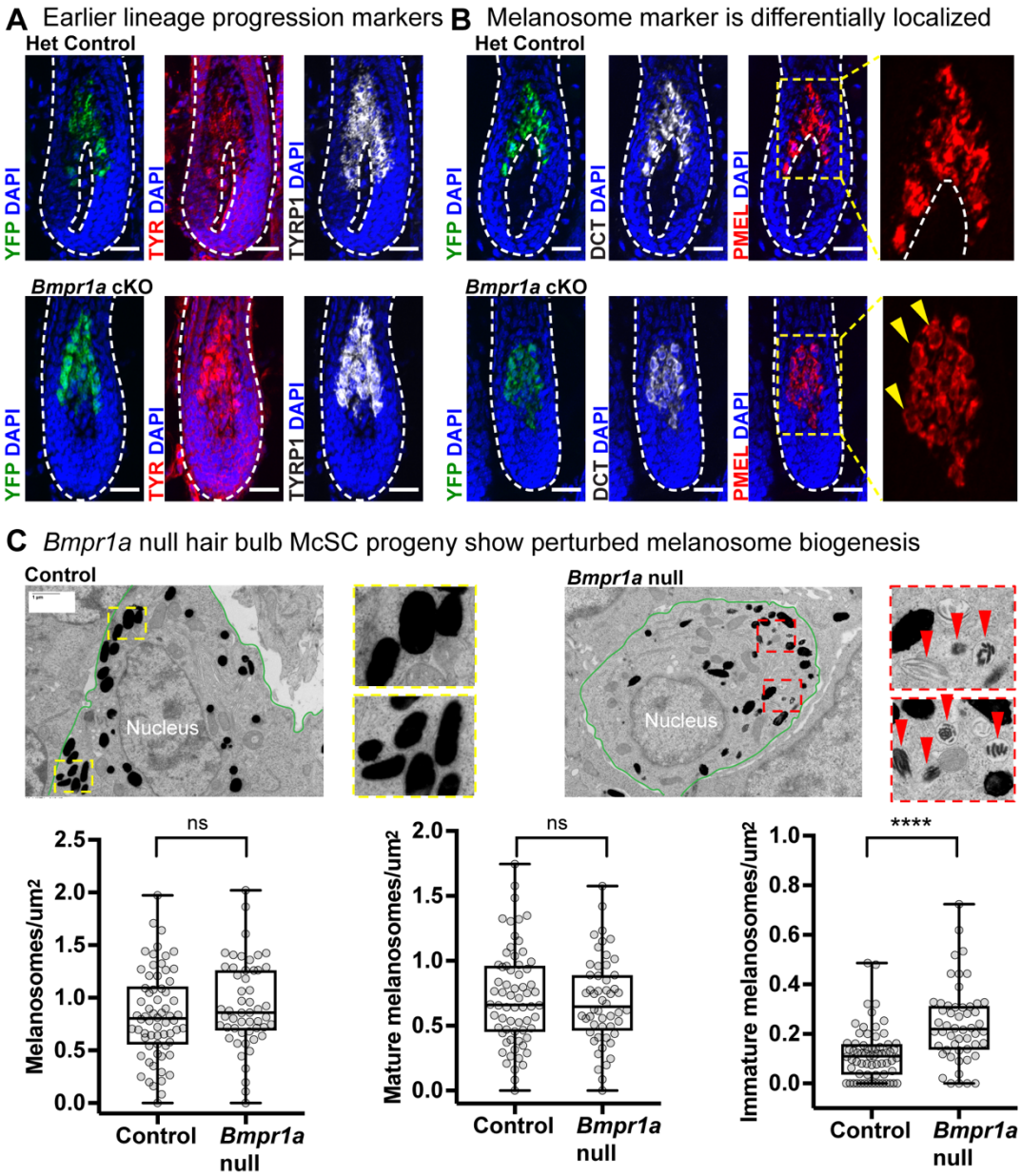

Figure 3.9 *Bmpr1a* null cells are intermediately differentiated. (A) IMF images showing expression of early melanogenic enzymes in control and *Bmpr1a* null cells in the hair bulb. **(B)** IMF image showing expression pattern of PMEL. Area within yellow dashed box is enlarged to the right, with yellow arrows to indicate perinuclear localization of signal. All IMF scale bars=25µm. **(C)** EM images of silver sections with melanocyte lineage cells outlined in green. Dashed box insets are enlarged. Red arrows indicate immature melanosomes. Scale bar=1µm. Lower graphs show quantification of number of melanosomes divided by melanocyte lineage cell area. Left – total melanosomes/µm^2, middle – mature melanosomes/µm^2, right – immature melanosomes/µm^2 [****p<0.0001, Mann-Whitney test; Control n=66 areas (3 mice); *Bmpr1a* cKO n=52 areas (3 mice)].

3.3.6 BMP-regulated *Lef1* may cooperate with MITF to drive full melanocyte differentiation

Given the newfound role of BMPR1a signaling at the juncture downstream of McSC activation/early McCP and upstream of melanocyte differentiation **(Fig. 3.10 A)**, I sought further insight into how this signaling cascade is transmitted to regulate genes involved in differentiation and melanosome organization. My overarching hypothesis for my thesis work was that distinct transcriptional programs are fueled by specific TFs that drive dynamic cellular states throughout differentiation. Therefore, I turned my attention to TFs that were downregulated in *Bmpr1a* null cells by scRNA-seq. Intriguingly, WNT mediator *Lef1* showed a trending downregulation by scRNA-seq **(Fig. 3.10 B, left)** and RT-qPCR **(Fig 3.6 E)**. Consistently, *Bmpr1a* null cells exhibited reduced nuclear LEF1 levels by IMF **(Fig. 3.10 B, right)**.

Probing for further changes in TFs, I interrogated MITF, the master regulator of the melanocyte lineage that is often regulated at the post-transcriptional level (Goding and Arnheiter, 2019). MITF coordinates myriad lineage processes in development, differentiation, and melanoma, including survival, proliferation, and pigment production (Goding and Arnheiter, 2019). Carreira et al. (2006) proposed that in melanoma, MITF functions according to a "rheostat model," where low MITF promotes stemness, intermediate MITF induces proliferation, and high MITF drives differentiation and melanogenesis. While *Mitf* levels were unchanged at the transcript level in *Bmpr1a* null cells relative to control, interestingly, nuclear MITF protein was reduced by IMF **(Fig. 3.10 C)**.

Given the numerous differentiation and pigmentation defects that stem from perturbations or loss of MITF, reduced nuclear MITF in *Bmpr1a* null cells alone might largely explain the block in melanocyte differentiation and resulting gray hair phenotype. However, MITF is known to regulate its diverse cellular processes through cooperation with other TFs (Goding and Arnheiter,

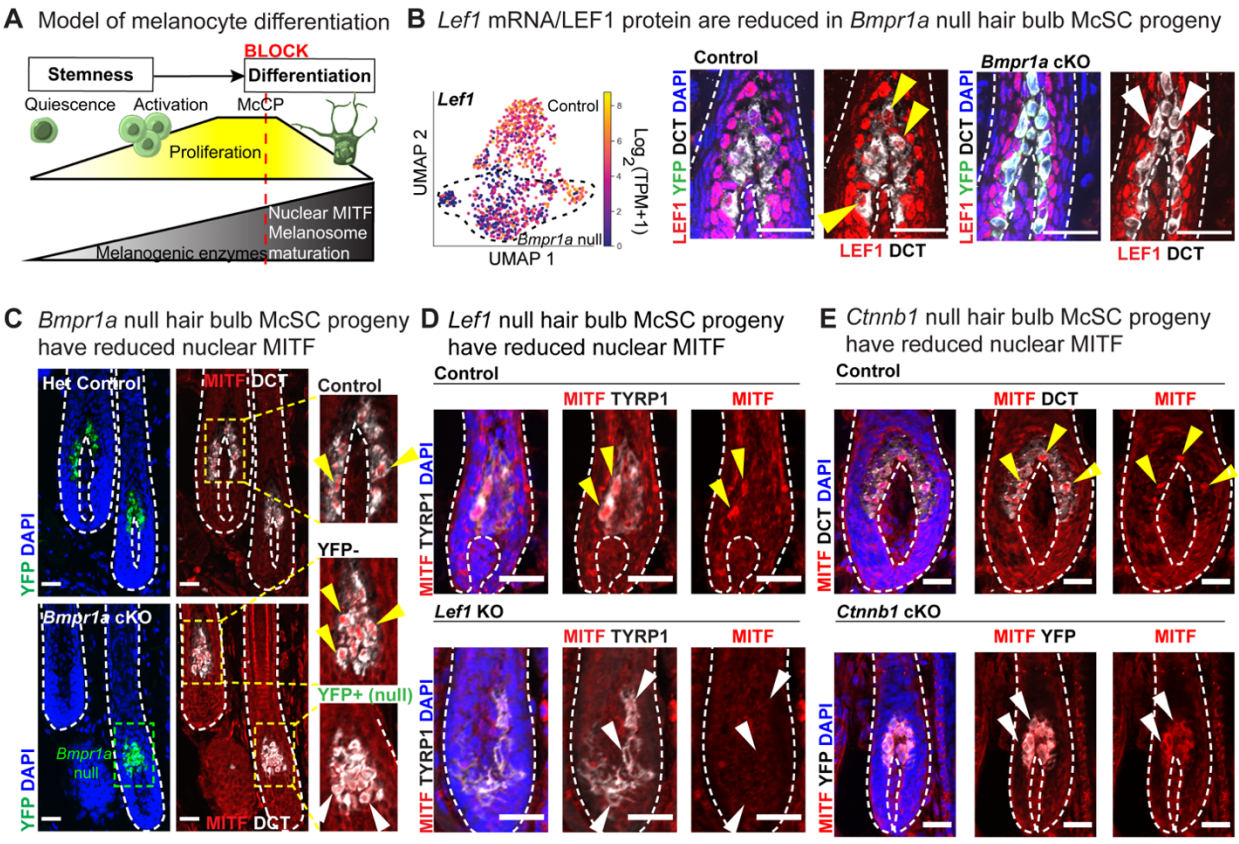

Figure 3.10 Nuclear LEF1 and MITF are reduced in differentiating *Bmpr1a* null cells. **(A)** Model of McSC lineage progression with the proposed timing of the differentiation block without BMP signaling. **(B)** *Lef1* mRNA expression (left) with IMF (right) in control and *Bmpr1a* null cells. Yellow arrows indicate presence and white arrows indicate reduction/absence of nuclear LEF1. **(C)** IMF images depicting MITF in control and *Bmpr1a* null cells in anagen 1 week after waxing. Enlarged areas show reduction (white arrows) of nuclear MITF in transduced (YFP^+) vs. un-transduced (YFP^-) as an internal control. **(D-E)** IMF images illustrating MITF levels in hair bulb McSC progeny of **(D)** control and *Lef1* KO (P4) mice and **(E)** *Ctnnb1* cKO and control mice whose HFs were analyzed 1 week post-waxing. Yellow arrows indicate presence and white arrows indicate reduction/absence of nuclear MITF. IMF scale bars=25μm.

2019). Therefore, given that *Bmpr1a* null cells also showed reduced LEF1, I wanted to investigate the link between BMPR1a signaling, WNT/LEF1, and MITF. Moreover, previous reports have indicated that LEF1 can physically interact with and regulate MITF (Dorsky et al., 2000; Saito et al., 2002, Takeda et al., 2000; Yasumoto et al., 2002).

To ask whether such an interaction might be occurring, I first examined McSC progeny in the hair bulbs of *Lef1* KO and *Ctnnb1* cKO mice and also found that these cells exhibited

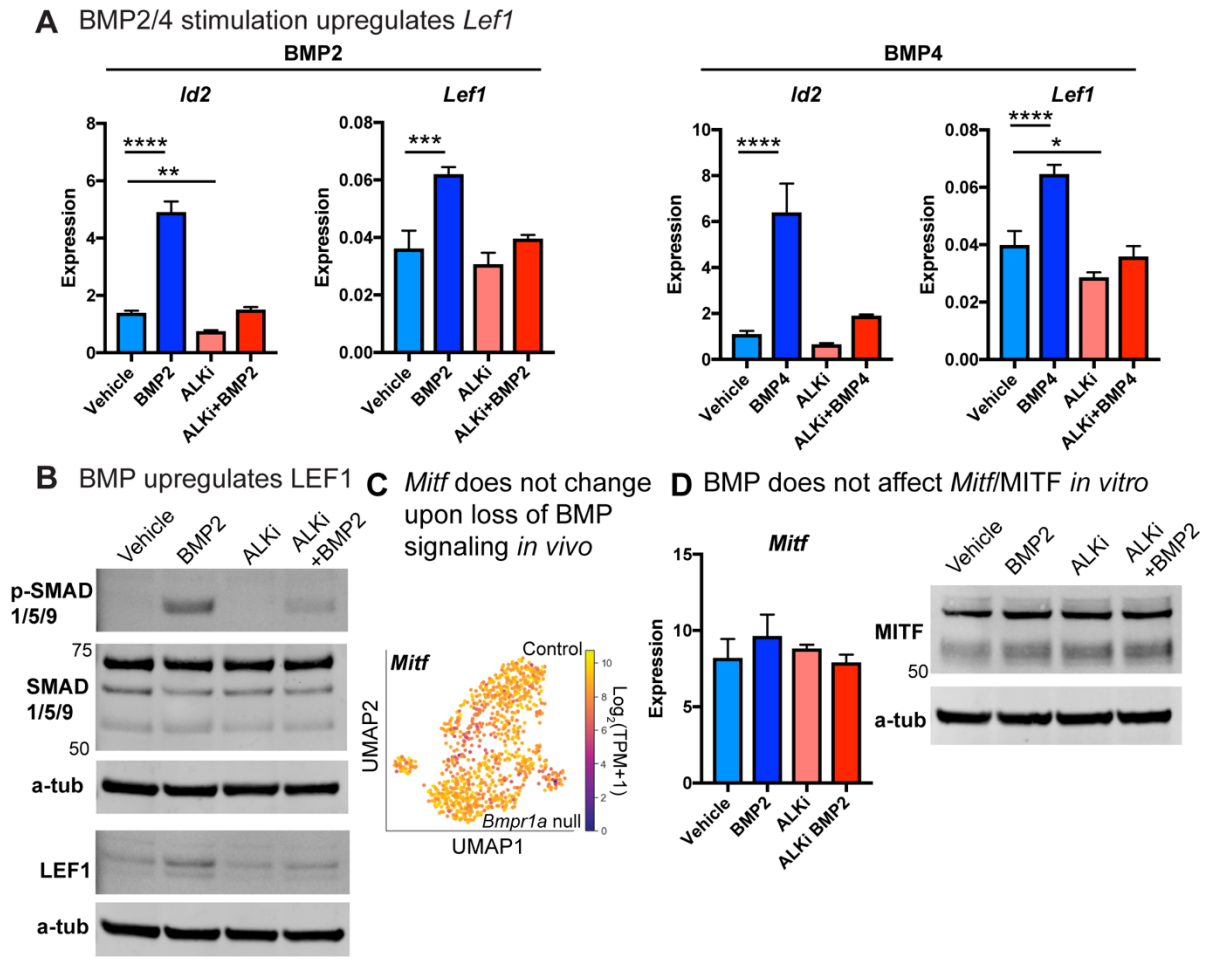

Figure 3.11 BMP-stimulated cells upregulate *Lef1*/LEF1. (A) *Id2* and *Lef1* mRNA levels by RT-qPCR after 30 hours of stimulation with 10 ng/mL recombinant BMP2 and BMP4 ± 250 nM ALK inhibitor (ALKi) [(BMP2 graphs: *Id2*, ****padj=0.0001, **padj=0.0084; *Lef1*, ***padj=0.0001) (BMP4 graphs: *Id2*, ****padj=0.0001, *Lef1*, ****padj=0.0001, *=0.0111 by ordinary one-way ANOVA, Dunnett's multiple comparisons test)]. **(B)** pSMAD1/5/9 and LEF1 protein levels by western blot after 48 hour treatment. **(C)** Expression plot of *Mitf* levels in control and *Bmpr1a* null cells. **(D)** *Mitf* levels by RT-qPCR after 30 hours of stimulation with 10 ng/mL recombinant BMP2 ± 250 nM ALKi, with MITF protein levels by western blot after 48 hour treatment.

diminished nuclear MITF **(Fig. 3.10 D-E)**, further suggesting a link between these signaling pathways and TFs. While cell culture experiments were limiting overall **(see Chapter 3.3.4.)**, I did find that upon BMP2/4 stimulation (ligands that are expressed in anagen skin *in vivo*), *Lef1* was upregulated. LEF1 protein levels were also increased at 48 hours of treatment with BMP2, as assessed by western blot. These trends were reversible upon treatment with the BMP receptor

(ALK) inhibitor K02288 **(Fig. 3.11 A-B)**. While *Mitf* mRNA was not changed during differentiation **(Fig. 3.11 C)** or upon BMP stimulation in culture **(Fig 3.11 D, left)**, *in vivo*, there was increased MITF protein upon intact BMPR1a signaling **(Fig. 3.10 C)**. However, in Melan-a2 cells, MITF levels were already high in untreated cells and did not change further upon BMP2 stimulation or K02288 inhibitor treatment **(Fig. 3.11 D, right)**, again underscoring the importance of studying this signaling cascade in the lineage in the physiological context.

To further investigate the possibility of such pathway intersection, genes with reduced expression in *Bmpr1a* null cells relative to control by scRNA-seq were scanned for TF motifs within their putative promoter regions (within 2.5 kb upstream of the transcription start site, TSS). To assess interplay between MITF and BMP-regulated LEF1 TFs, genes were classified as containing a MITF motif only, a LEF1 motif only, or both. In another analyses, to assess MITF and BMP-mediated pSMAD1/5/9 cooperation, genes were binned as containing a MITF motif only, a SMAD motif only, or both. These analyses revealed that genes with promotors harboring both MITF and LEF1 sites showed significantly lower expression than those with MITF alone; this preferential downregulation was not seen in genes with MITF and SMAD relative to MITF alone **(Fig. 3.12 A)**. Analyses of genes increased in *Bmpr1a* null cells did not indicate any enrichments **(Fig. 3.12 B)**. Strikingly, the BMP-regulated genes with both MITF and LEF1 sites (23 genes total) included those specifically involved in transport, transmembrane transport, melanin production, and melanosome organization, including *Mc1r*, *Oca2*, *Trpm1*, *Rab38*, and *Shroom2* **(Table 3.3;** see also Table S11 of Infarinato et al., 2020**)**. Together, these results suggested that downstream of BMPR1a signaling, LEF1 and MITF accumulate in the nucleus, where they may cooperate in the upregulation of differentiation-associated genes, particularly those involved in melanosome organization and transport.

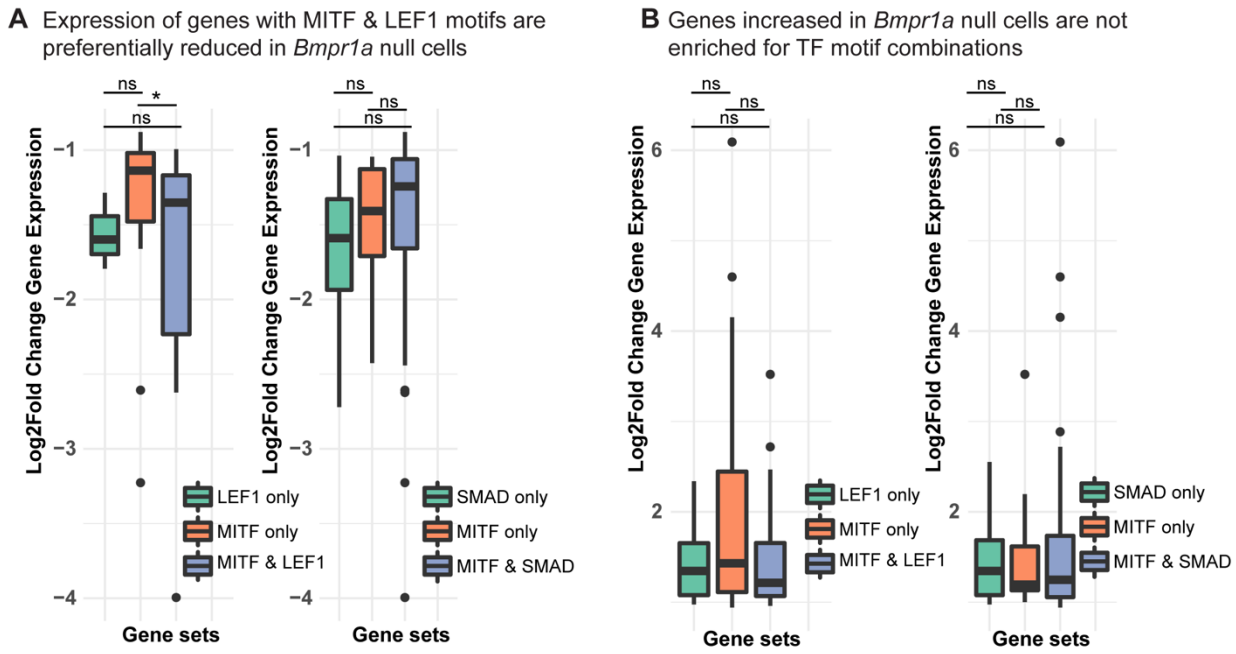

Figure 3.12 Motif analyses of putative promoter regions of BMPR1a-sensitive genes suggests cooperation between MITF and LEF1. Motif analysis of promotors within genes whose expression is either **(A)** reduced or **(B)** increased upon *Bmpr1a* loss. Box and whisker plots showing gene sets and the $\log_2$fold change gene expression in *Bmpr1a* null cells (*p=0.036 by Wilcoxon test).

3.3.7 Chromatin accesibility dynamics during the transition from McSC to melanocyte suggests cooperation between LEF1 and MITF in differentiation

To look for further evidence of that MITF and LEF1 cooperate in melanocyte differentiation *in vivo*, I lastly sought to interrogate the chromatin landscape of the lineage. Recent studies have indicated the importance of specific chromatin modifers in regulating McSC behavior (Koludrovic et al., 2015; Moon et al., 2017), but again, I wanted to take an unbiased approach to survey chromatin *in vivo*. I hypothesized that chromatin openness would change as McSCs underwent differentiation into melanocytes and that regions that gain accessibility during differentiation would contain TF binding motifs that play a role in this transition. To assay chromatin dynamics in the McSC lineage, I implemented Assay for Transposase-Accessible Chromatin with high-throughput sequencing (ATAC-seq), a technique that uses Tn5 transposase

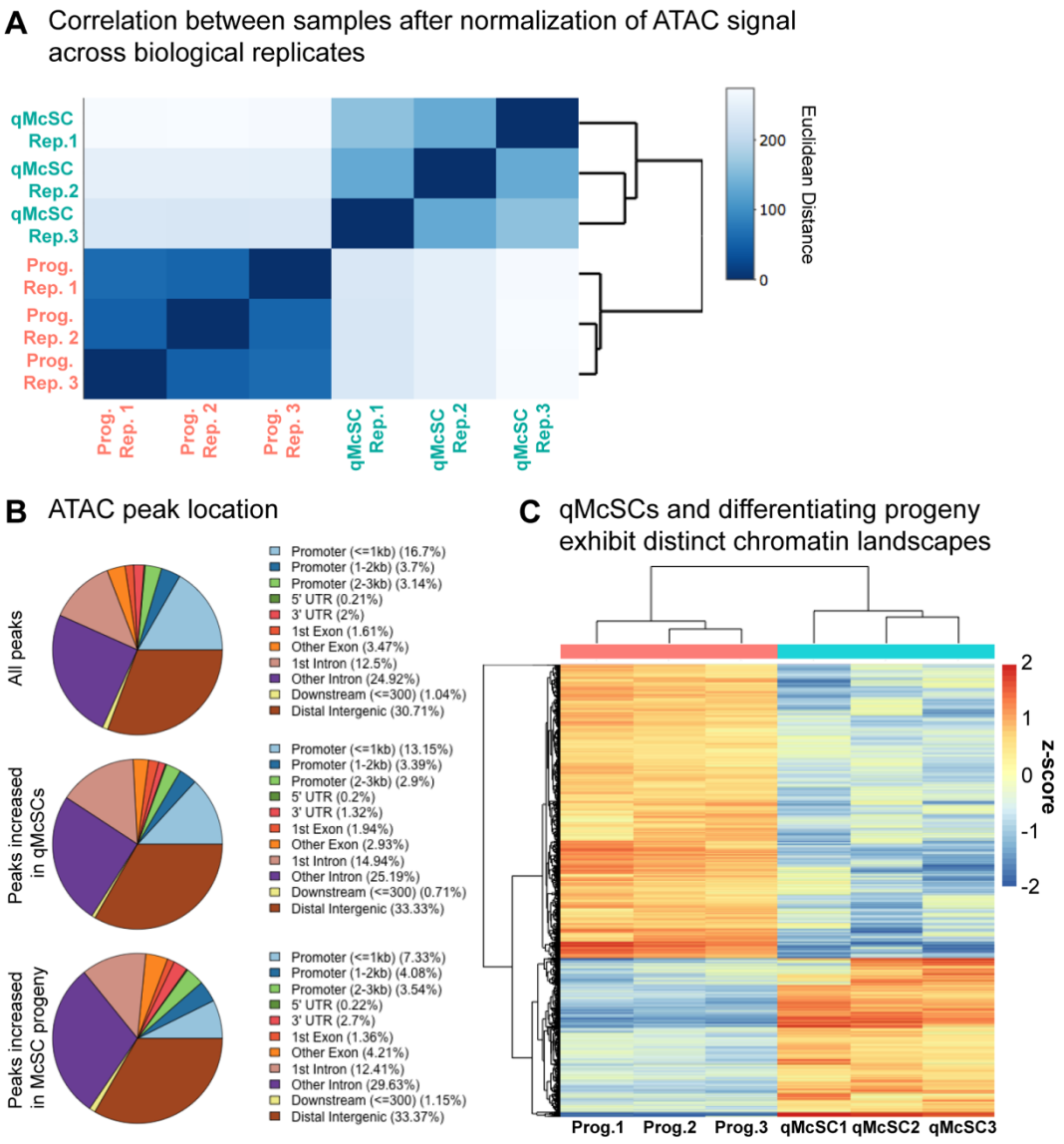

Figure 3.13 qMcSCs and their progeny exhibit differential chromatin accessibility. (A) Correlation matrix indicating similarity between biological replicates of ATAC-seq. **(B)** Location of ATAC peaks expressed as percentages. **(C)** Heatmap of differential peaks in qMcSCs versus their differentiating hair bulb progeny (prog.) ($Log_2FoldChange \geq 1$, $p \leq 0.05$).

to insert sequencing adaptors in regions of open chromatin that is suitable for low cell number input (≥10,000 cells) (Buenrostro et al., 2013). For this assay, I isolated qMcSCs from the telogen bulge and McCP/melanocyte progeny from the anagen VI hair bulbs of *Dct*-eGFP$^+$ mice to evaluate and compare chromatin states in stem and differentiating states.

These ATAC-seq data showed high reproducibility across biological replicates **(Fig. 3.13 A)**, with similar percentages of peaks within 50 kilobases (kbs) of canonical TSSs (28.2% for peaks increased by $\log_2$fold≥1 in qMcSCs; 26.4% for McSC progeny) and similarly distributed throughout promoters, gene bodies, and intergenic regions **(Fig. 3.13 B)**. To ask whether the chromatin landscape changes throughout differentiation, differential peak analysis was performed. This analysis indicated that indeed qMcSCs and their differentiating progeny exhibit strikingly distinct chromatin accessibility profiles (**Fig. 3.13C** [$\log_2$ fold change≥1, p≤0.05], see also Table S12 of Infarinato et al., 2020**)**, allowing for examination of chromatin regions containing BMP-sensitive genes by scRNA-seq as well as TF motifs within these dynamic regions.

Genes whose expression was diminished in *Bmpr1a* null cells showed increased accessibility in differentiation. Example gene tracks for *Gpr143* and *Oca2* are shown in **Fig. 3.14 A**. Notably, *Lef1* seemed to show chromatin remodeling as McSCs became differentiated, and some of the peaks that became more open in differentiating progeny contained SMAD motifs **(Fig. 3.14 B)**, supporting the notion that this TF gene might be a direct BMP target gene. Consistent with the timing of BMP signaling activity in the lineage, a number of these differential peaks associated with differentiation resided within the promoter/enhancer regions of genes downregulated upon *Bmpr1a* ablation **(Fig. 3.14 C)**.

To next ask what TFs might bind in these differentially accessible chromatin regions, unbiased TF motif analysis was performed for stem and differentiation-enhanced ATAC peaks. Strikingly, LEF/TCF and MITF (TFEB, TFE3, TFEC) family factors were the top most enriched factors in peaks increased in differentiation **(Fig. 3.15 A;** see also Table S13 of Infarinato et al., 2020**)**. Conversely, peaks increased in qMcSCs showed enrichment of SP/KLF and AP-1 family motifs, consistent with the enrichment of these factors by RNA-seq, as well as those expected to

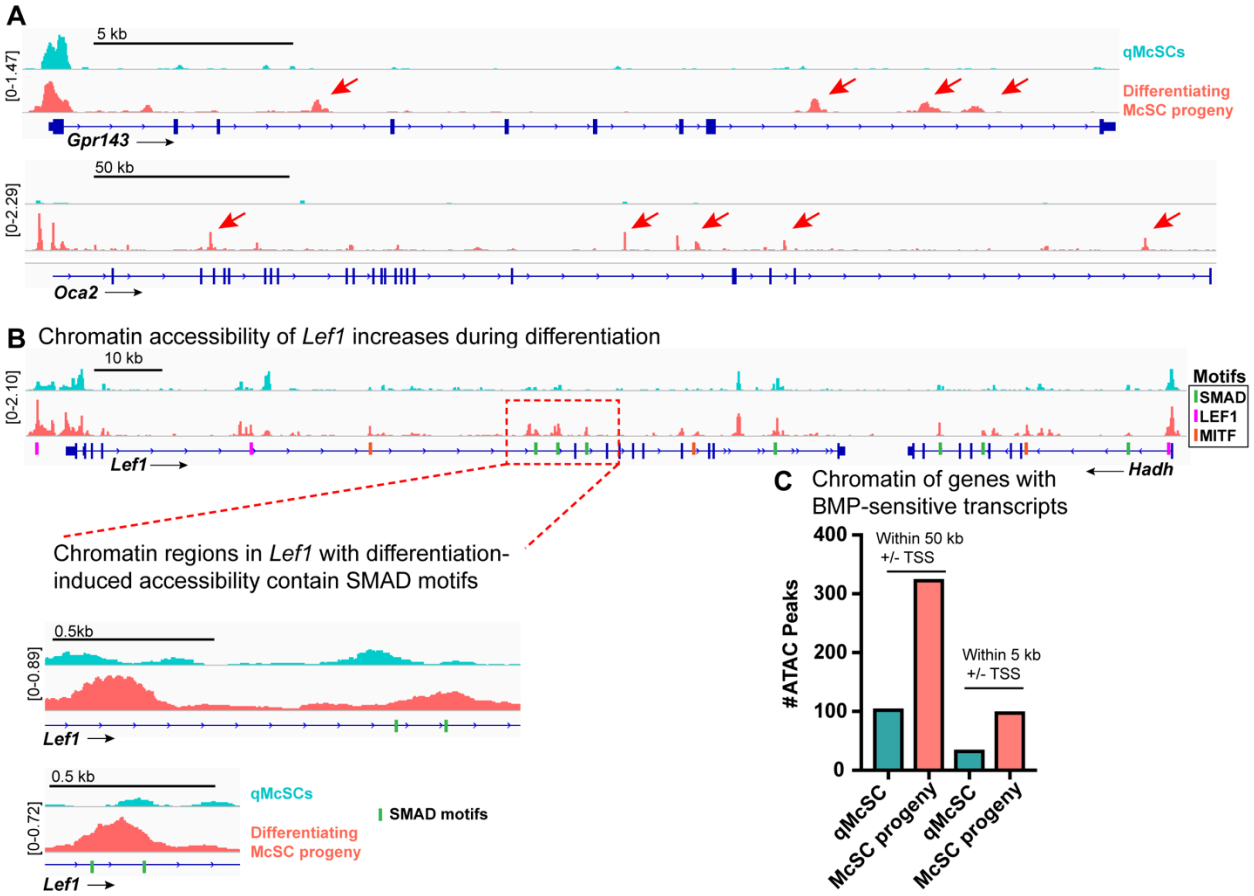

Figure 3.14 BMP-sensitive genes show increased accessibility in differentiation. (A) ATAC tracks showing differential peaks of select differentiation genes. **(B)** ATAC track of *Lef1* gene showing chromatin opening in differentiating progeny in regions with SMAD motifs, indicated by dashed red boxes. Merged (mean averaged) of three biological replicates are shown. Zoomed in views shown to bottom left within red dashed lines. **(C)** Number of peaks increased in either qMcSCs or their differentiating progeny within 5 or 50kb ± of the TSS of genes (80) whose expression is diminished upon loss of BMPR1a signaling by scRNA-seq.

play a role in SC biology, such as PAX3 and RBPJ. Motifs such as SOX10 were present in both qMcSC and differentiating progeny peaks, with no significant enrichment in either direction. Honing in specifically on the set of genes whose expression was diminished in *Bmpr1a* null cells, another motif analysis was performed on differentiation-enriched ATAC peaks within ±50 kb of the TSS for these differentially expressed genes (putative promoter and enhancer regions). Again, there was significant enrichment of binding motifs for LEF/TCF and MITF family factors **(Fig.**

3.15 B; Table 3.4; see also Table S14 of Infarinato et al., 2020**)**, further highlighting the importance of both LEF1 and MITF downstream of BMPR1a signaling in driving differentiation.

Lastly, to assess how BMP regulation via SMADs might impact chromatin dynamics, all differentiating progeny peaks were considered for genes whose expression was reduced in *Bmpr1a* null cells, as analysis of differentiation-enhanced peaks did not yield clear results for SMAD factors. In agreement with the predictive motif scanning of putative TSS regions **(Fig. 3.12)**, analysis of ATAC peaks in the differentiating progeny suggested that many genes involved in melanin biosynthesis, transport, and trafficking (i.e. *Mc1r, Rab38, Trpm1*, *Slc24a4*) may require cooperation of SMAD as well as MITF and LEF1 in controlling their lineage-specific activation **(Fig. 3.15 C**; see also Table S15 of Infarinato et al., 2020**)**. Overall, these data suggest that McSCs and their differentiating McCP/melanocyte progeny undergo chromatin rearrangement during differentiation and provide compelling evidence for not only the master regulator MITF but also LEF1 in promoting lineage maturation.

A Peaks up in progeny are enriched for LEF/TCF & MITF motifs

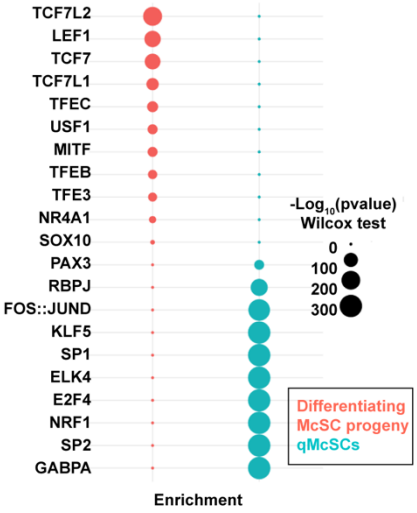

B Motifs enriched in peaks up in differentiating progeny near genes downregulated in *Bmpr1a* null

Motif	p-value
*TFEC	6.18E-05
***MITF**	**1.32E-04**
*TFEB	8.35E-04
**TCF7L2	9.34E-04
**TCF7	1.31E-03
*TFE3	1.62E-03
****LEF1**	**2.41E-02**

(within +/- 50 kb TSS)

C MITF, LEF1, and SMAD motifs within peaks in differentiating progeny near genes down-regulated in *Bmpr1a* null

Motifs	Genes (+/- 50 kb TSS)
LEF1 only	***Oca2***, *Sfrp4, Npy, Padi2*
LEF1 & MITF	*Slc26a2, Enpep, Ogdhl*
LEF1 & SMAD	***Shroom2***, ***Gpr143***, *Id2, Me1, Slc37a2, Nav2, Xpo6, Adam10, Amd1, Ephx1, Ftl1, Fabp5, Lgals3, Nr4a3, Pla2g15, Smpd1, Hhipl1, Rnf144b, Tubb3, Slc7a11, Ero1l, Egfl6, Fam129a, Pgm2l1*
LEF1, MITF, & SMAD	***Mc1r***, ***Rab38***, ***Trpm1***,***Slc24a4***, *Kif26b, Gpr137b, Eps8, Epdr1, Ctsd, S1pr3, Fech, Ptprs, Mtss1, Wfs1, Akap6, Itgb3, Atp6v0d2, Plxna4, Tacc1, Apold1, Ddah1, Scrn1, Sec14l1,Smchd1, 4930523C07Rik*
MITF only	*Frmd4a*
MITF & SMAD	*Ninj1, Tmem47, Tbx1, Insig1, Plxnd1*
SMAD only	***Slc45a2***, ***Tyrp1***, *Id3, Gsn, Calm1, Pitpnm2, Parm1, Tmem132d, Olfm2, D7Ertd443e, B3galt5, Asah1, Skil*

Figure 3.15 Motif analyses within ATAC peaks suggests cooperation of MITF, LEF1, and SMAD TFs at BMP-sensitive genes. (A) Plot expressing enrichment of select motifs in differential ATAC peaks between each cell type. Motifs with -Log_{10}(p-value) greater than 300 are expressed as a maximum of 300 here. **(B)** Motif analysis within peaks subset by the following parameters: peaks enriched in differentiating progeny relative to McSCs and 50 kb ± TSS of genes downregulated in *Bmpr1a* null cells. X. *=MITF family, **=LEF/TCF family. See also Table 3.4. **(C)** Motif analysis within differentiating McSC progeny peaks within 50 kb ± TSS of genes whose expression is diminished in *Bmpr1a* null cells. Table highlights LEF1, MITF, and SMAD(2, 3, and/or 4) motifs. Bolded genes specify those encoding proteins involved in melanogenesis.

3.3 Discussion

The temporal nature of my scRNA-seq dataset made it a powerful tool with which to elucidate the precise coordination of niche pathways and TF responses that might interact to achieve aMcSC and McCP proliferation and final melanocyte differentiation. Intrigued by evidence of converging BMP and WNT signaling downstream of McSC activation, I investigated the roles and intersection of these pathways in the lineage harnessing genetic mouse models, IMF and EM analyses, and scRNA and ATAC-seq. These studies revealed a newfound role for signaling through BMPR1a in driving cells past the McCP stage to fully mature melanocytes through nuclear accumulation of MITF and LEF1 to upregulate transcription of melanosome organization and transport genes.

Similar to the results of cell culture studies pertaining to BMP signaling, prior reports in animals were also difficult to resolve. Mice ectopically expressing the secreted BMP inhibitor noggin under the *Krt5* epidermal promoter had darker coats due to reduced expression of ASIP, which signals through MC1R to promote pheomelanin production (Sharov et al., 2005). At the same time, mice with melanocyte-specific deletion of *Bmpr2* had no phenotype unless on an activin A receptor type 2A (*Acvr2a*) full body KO background, in which case mice had gray hair (Han et al., 2012). In zebrafish, BMP signaling via growth differentiation factor (GDF6, also known as BMP13) suppresses melanocyte differentiation during development and in melanoma via downregulation of *mitfa* (an ortholog of *Mitf*). In implementing a conditional, lineage-specific ablation approach to delete *Bmpr1a*, a type I BMP receptor with preferential BMP ligand specificity, my approach allowed me to dissect the contribution of this pathway in lineage progression in the mammalian context, allowing for normal melanoblast specification and McSC establishment while preserving the native niche microenvironment. In this way, I could clearly demonstrate the BMP signaling is critical for normal melanocyte maturation, and in contrast to what has been described in zebrafish, promotes nuclear accumulation of MITF, as well as LEF1, to do so.

McSCs must coordinate their behavior with neighboring HFSCs, so because BMP (BMPR1a) signaling maintain HFSC quiescence (Adam et al., 2018; Genander et al., 2014; Kobielak et al., 2007), this pathway might have also been predicted to promote a quiescent state for McSCs in telogen. Surprisingly however, McSCs appear to be largely refractory to BMP signaling, as reflected by the paucity of nuclear pSMAD1/5/9 in these cells throughout the hair cycle. In *Bmpr1a* cKO mice, McSCs still became activated at early anagen, were able to generate differentiating progeny that populated the hair bulb, and then returned to quiescence later in

anagen. There are several possible scenarios that might explain these distinct responses of McSCs and HFSCs, from differential receptor expression to ligand availability. It is notable that these SCs occupy distinct locales within the niche; quiescent HFSCs flank the BMP-rich inner bulge, while qMcSCs reside near the base of the bulge where BMP levels lower (Hsu et al., 2011; Yang et al., 2017). TGF-β signaling is elevated at the bulge base (Oshimori and Fuchs, 2012), which could explain the preferential sensitivity of McSCs to this related signaling pathway during quiescence (Nishimura et al., 2010). Another interesting possibility is that in the McSC lineage, TGF-β and BMP signaling act in an antagonistic fashion, pushing cells towards stemness/quiescence and differentiation, respectively.

In considering how BMP intersects with WNT, while WNT/β-catenin signaling impacts McSC proliferation (Rabbani et al., 2011), BMP signaling functions after initial McCP specification, when cells are proliferative but show considerable signs of differentiation. In *Ctnnb1* cKO mice, nuclear pSMAD1/5/9 was still seen in McSC hair bulb progeny, suggesting that BMP signaling is not dependent on WNT signaling, but nuclear LEF1 was diminished in *Bmpr1a* null cells, suggesting WNT's reliance on BMP signaling downstream during melanocyte maturation. Placing BMP signaling upstream of *Lef1* expression and nuclear accumulation of LEF1 and MITF provided mechanistic understanding of the detrimental effects of loss of BMPR1a on pigment production, as well as their failure to progress appreciably past the immature McCP stage. While the "rheostat model" alone might explain why some MITF target genes were still expressed in *Bmpr1a null* cells (i.e. low levels induce expression of genes involved in survival and proliferation) and others are diminished (i.e. high levels induce genes involved in differentiation such as melanosome biogenesis and transport), these data also suggest cooperation with the TF LEF1 to completely achieve differentiation. While *Lef1* null lineage cells in the hair bulb showed

reduced nuclear MITF, the mechanism for how these two TFs might be coordinating their behavior it is not yet clear.

While some of BMP's effect on the lineage appear to be indirect, motif analysis of differentiating melanocyte ATAC peaks provides insight into genes that might be direct SMAD targets, such as *Slc45a2* and *Tyrp1* (SMAD sites only), but further studies are required to demonstrate such regulation. More interesting however was the reduced transcription of genes with both LEF1 and MITF in their putative promoter regions in *Bmpr1a* null cells, and the importance of these factors was reinforced by chromatin accessibility profiling of McSCs versus their differentiating progeny. These ATAC data also revealed that regions within the *Lef1* gene locus with SMAD motifs show enhanced accessibility upon differentiation, corroborating the finding that *Lef1* mRNAs are downregulated upon *Bmpr1a* ablation and suggesting that *Lef1* is likely a direct BMP target gene. Together, these data provide new insights into how BMP signals in this lineage, supporting a model whereby signaling through BMPR1a upregulates *Lef1*, and LEF1 then promotes nuclear accumulation of and cooperates with MITF to govern a critical cohort of melanocyte maturation genes.

CHAPTER 4:
SUMMARY AND PERSPECTIVES

4.1 Summary: new insights into McSC lineage progression and a key role for BMP signaling in melanocyte differentiation in the HF niche

Dissecting the molecular mechanisms that drive adult tissue SC behavior is of fundamental importance for our understanding of how the body maintains and replenishes itself. These same mechanisms can be disrupted in aging and disease. In my thesis research, I sought deeper understanding of McSCs and their dynamic lineage, generating a high-resolution characterization of the transcriptional programs that accompany lineage progression. Importantly, this work has yielded insight into the intermediate stages of McSC activation and McCP maturation and has uncovered that transcriptional heterogeneity increases over the course of the differentiation trajectory **(Chapter 2)**. Using conditional lineage-specific ablation in mice, I have demonstrated a role for BMPR1a signaling in driving complete differentiation, clarifying a role for this pathway in regulating McSC lineage progression in the HF niche that was not well appreciated or understood. Using single cell transcriptional profiling coupled with pseudotime analysis, I have unearthed the complex gene regulation downstream of this receptor and pinpointed where signaling acts in differentiation. Curiously, *Bmpr1a* null cells retain stemness markers, show elevated proliferation, and have a higher density of immature melanosomes. Importantly, BMPR1a signaling is necessary for the nuclear accumulation of master regulator MITF and WNT mediator LEF1. Investigating the substantial chromatin rearrangements that take place as cells transition from SCs to differentiated melanocytes, motif analyses further pointed to cooperation between MITF and LEF1 near BMP-sensitive genes **(Chapter 3)**. Altogether, my data support a model wherein McSCs are refractory to BMP until the McCP stage, when signaling promotes nuclear accumulation of MITF and SMAD-mediated upregulation of *Lef1*/LEF1; these two key TFs regulation transcription of genes required for terminal differentiation, involving the upregulation of melanosome and transport genes and the downregulation of stemness and proliferation genes.

In considering how these pathways fit into the broader field, McSCs seem to fall within the ranks of other tissue SC types such as HF, mesenchymal, and intestinal SCs, which also use the BMP pathway to coordinate differentiation (Adam et al., 2018; Beumer and Clevers, 2021; Chen et al., 2012; Genander et al., 2014; He et al., 2004). For instance, to promote differentiation and restrain proliferation, intestinal SCs undergo a switch from WNT to BMP signaling (Beumer and Clevers, 2021; He et al., 2004), whereas in McSCs, BMP seems to both promote differentiation, suppress proliferation, but also enhance WNT signaling through LEF1. Interestingly, in hippocampal neural SCs, BMP and WNT signaling also seem to converge at the level of LEF1 (Armenteros et al., 2018). These similarities raise questions about the role of other more universal signaling pathways associated with SC differentiation, particularly SHH signaling.

4.2 Outstanding questions: unraveling the complex mechanisms up- and downstream of BMPR1a in the tissue microenvironment

My results suggest that signaling downstream of BMPR1a leads to SMAD-mediated upregulation of *Lef1* mRNA and nuclear accumulation of LEF1 protein. While MITF is critical in promoting differentiation and appears to cooperate with LEF1 to do so, given that *Mitf* mRNA is not affected in *Bmpr1a* null cells, it is still not clear how BMP signaling induces accumulation of nuclear MITF post-transcriptionally. This is somewhat surprising, as LEF1 has been reported to activate transcription of *Mitf-M* in human cultured melanocytes (Takeda et al., 2002). In any case, in *Lef1* null cells, nuclear MITF is diminished, supporting interplay between these two factors. Previous studies have provided some possible avenues for how this coregulation might occur. For instance, LEF1 (but not TCF1) can physically interact with MITF/TFE3 TFs (Yasumoto et al., 2002). Perhaps such interactions might induce stabilization and nuclear localization of MITF. Alternatively, BMP-induced LEF1 might medicate enhanced WNT signaling, which has been

shown to stabilize MITF, driving upregulation of genes involved in multivesicular body biogenesis. These bodies further enhance WNT by sequestering β-catenin destruction complex proteins (Ploper et al., 2015).

Furthermore, BMPR1a phosphorylation can trigger both canonical and noncanonical signaling cascades, with different BMP ligands and receptor combinations activating different downstream mediators. It seems likely that *in vivo*, both arms are this cascade are stimulated simultaneously. While *Lef1* upregulation appears to occur through canonical BMP-SMAD signaling, MITF levels might be controlled via SMAD-independent noncanonical pathways, such as p38-MAPK, which can phosphorylate MITF in osteoclasts (Mansky et al., 2002). In cultured human melanocytes, BMP6 signals through p38 to induce melanogenesis (Singh et al., 2012). At the same time, this paper also demonstrated that BMP4 reduces melanin production, making it difficult to predict what the role of this signaling pathway would be in the native HF niche and highlighting the importance of complementary *in vivo* studies.

Reflecting further on the report by Singh et al. (2012) demonstrating the anti-melanogenic effect of BMP4 in culture, it is intriguing that I find that BMP4 (and BMP2) both induce upregulation of *Lef1*. While WNT signaling is critical for melanocyte differentiation (Rabanni et al., 2011), it is not yet completely clear to what extent reduced nuclear LEF1 drives the BMPR1a loss-of-function phenotype. While LEF1/TCF family motifs are enriched in differentiation-enhanced ATAC peaks **(Fig. 23A-B)**, it is possible that other TCF factors may be able to act in a functionally redundant manner. The *Lef1* KO mice do appear to have reduced hair pigmentation, but a conditional lineage-specific ablation approach would be ideal. To this end, I have been generating a *TyrCreER Lef1*^{floxed} (Zhou and Xue, 2012) *R26YFP*^{floedx} strain to investigate whether the hair graying phenotype is recapitulated. Skin from these mice will similarly be investigated

with IMF, and YFP$^+$ cells can be FACS purified to assess changes in transcription. To more conclusively define LEF1 targets, future ChIP-seq studies performed *in vivo* with techniques optimized for low cell input such as CUT&RUN (Skene and Henikoff, 2017) would be informative. One possibility to explore would be that LEF1 mediates target genes involved in proliferation. This fits with the finding that BMP4 (which in my hands upregulates *Lef1*) in downregulated during UV exposure (Singh et al., 2012). Perhaps this signal restrains proliferation in the HF bulb, but is downregulated upon UV in the epidermis to allow melanocytes to both proliferate and continue to produce melanin.

Finally, there is the question of which cells in the HF niche are providing the BMP ligands that McCP and melanocytes respond to during anagen. Autocrine signaling may be occurring, as McCP and melanocytes express *Bmp2* and *Bmp7* by scRNA-seq **(Fig. 8C-D)**, preferential ligands of BMPR1a (Wang et al., 2014). However, the skin is rich in BMPs emanating from several compartments. One immediate possible source is the HF matrix TACs, which would make sense in terms of coordinating the differentiation of these two SCs compartments so that pigment could be transferred to hair cells at the appropriate time. BMP also directly regulates a cohort of hair-specific genes in the proliferative progenitors of the hair shaft (Adam et al., 2018; Genander et al., 2014). Another candidate would be the *Krox20*$^+$ cells specifically, as these also provide SCF to promote melanocyte maturation and maintenance (Liao et al., 2017). BMPs also appear to be elevated at the apical region of the DP where proliferative precursors of both the hair shaft and the melanocytes reside (Yang et al., 2017). While it seems most likely that BMPs acting on the melanocyte lineage come from within the HF, other conceivable sources include the dermis, which exhibits cyclic expression of BMP2 and BMP4 or the adipose tissue that expresses BMP2 (Plikus et al., 2008), to which the anagen follicles gain proximity during downgrowth. In all probability,

several niche cell types producing different BMPs and extracellular regulators and the convergence of both canonical and noncanonical pathways with players like WNT converge to determine the outcome of BMPR1a signaling in the native microenvironment.

4.3 Future Directions

Studies investigating both specific pathways using genetic mouse models and global profiling methods in the melanocyte lineage in the HF have been critical for unraveling how McSCs transition through different cellular states in homeostasis. These in turn raise intriguing questions about how these genes and pathways act in phenotypic variation, aging, and diseases such as cancer. Pathways that regulate SC behavior often come into play in contexts outside of normal tissue regeneration. For example, the critical differentiation-promoting pathways MC1R and WNT/β-catenin are also necessary for McSC migration out of the HF niche to the epidermis during wounding (Chou et al., 2013; Sun et al., 2018). In melanoma, variants in MC1R, especially those resulting in fair skin and red hair, are associated with greater risk of developing cancer due not only to reduced pigmentation and UV-protection, but also because pheomelanin itself has carcinogenic properties (Mitra et al., 2012). Similarly, while its impacts on melanoma appear to be highly context-dependent, WNT/β-catenin is also a key player in melanoma (Gajos-Michniewicz and Czyz, 2020). Aging encompasses cumulative stress, injury, and inflammation over the course of an organism's lifetime, on top of homeostatic tissue demands. Here, I discuss three exciting avenues of inquiry that stem from my thesis work, exploring the possible roles of BMP signaling in color variation, age-related McSC decline, and melanoma.

4.3.1 Potential mediators of phenotypic diversity in hair pigmentation and patterning

The gray hair phenotype elicited by loss of *Bmpr1a* **(Fig. 3.3 A)** raises the question of whether this pathway might be altered in nature to achieve different skin and coat colors or contribute to pattern formation. In HFs, this could be accomplished through downregulation of BMPR1a cell surface expression during differentiation and or by differential ligand or inhibitor (i.e. noggin) production in the microenvironment. Whether BMPR1a signaling might affect melanoblast migration during embryonic development in some species, thus affecting pigmentation and patterning (as in SCF/c-KIT and EDN3/EDNRB mutant mice), is another possibility. Indeed, several of the genes upregulated in *Bmpr1a* null cells were related to migration and cell adhesion **(Fig. 3.6 B-C)**. At the same time, migration to the epidermis in adult mice in response to wounding or UV exposure is dependent on MC1R (Chou et al., 2013), which is downregulated in *Bmpr1a* cKO mice. Therefore, there are several potential mechanisms by which BMP could elicit phenotypic diversity in hair, fur, skin, and feathers.

While thoroughly investigating the status of epidermal melanocytes in the *Bmpr1a* cKO mice was beyond the scope of my study, I did not observe overt phenotypic differences in the ears, feet, or tail where these populations reside. There is reason to believe that such effects might only be seen upon UV exposure to enhance their basal activity. Singh et al. (2012) showed that upon UV exposure, human cultured melanocytes upregulate *Bmpr1a*, *Bmpr1b*, *Bmpr-II*, and *Bmp6*. Furthermore, their work suggests that different classes of BMPs can have opposing effects on melanogenesis, again highlighting the possibility of differential regulation of this pathway to achieve diverse colors and patterns.

4.3.2 Elevated BMP levels in aging skin and potential implications for hair graying

This deeper understanding of the role of BMP signaling in McSC differentiation into melanocytes in the HF raises an intriguing question: could perturbed BMP signaling occur throughout aging and contribute to hair graying? This is especially interesting in light of previous work in Fuchs Lab demonstrating that the production of BMPs in the skin increases with age in mice (Keyes et al., 2013). For aged HFSCs in the bulge, this results in increased pSMAD1/5/9 activity and longer periods of quiescence, leading to reduced hair growth (Keyes et al., 2013). Given this changing microenvironment and the importance of BMPR1a signaling in promoting melanocyte lineage differentiation under normal conditions, it is tempting to speculate that BMP might contribute to age-related hair graying. Indeed, while limited, there is some evidence linking increased WNT/β-catenin signaling in the skin to hair graying in mice (Zhang et al., 2017). These findings further suggest that pathways that normally regulate McSC lineage progression can be disrupted in age.

Hair graying can result from depletion or dysfunction of McSCs or McCP/melanocyte in the hair bulb. In actuality, a combination of issues might come into play as the long-lived McSCs and surrounding HF and skin microenvironment change during aging. In the case of BMP signaling, one might hypothesize that age-related hair graying might result from 1) increased BMP signaling causing ectopic activation of this pathway in bulge McSCs, driving their depletion and subsequent loss of their differentiating progeny, and or from 2) the impaired ability of McSC progeny to respond to BMP signaling, resulting in their failure to fully differentiate into pigment-producing cells, causing loss of color in the growing hair. These mechanisms could be investigated in mice, who like humans, exhibit age-associated hair graying; Zhang et al., (2017) observed graying at 34 months of age in C57/BL6 mice. Signs of ectopic activation of BMP signaling in

McSCs might result in pSMAD^{+} DCT^{+} McSCs and or differentiated (melanogenic) melanocytes in the bulge area. Impaired ability of differentiating progeny in aging follicles might elicit a phenotype reminiscent of *Bmpr1a* cKO mice, where anagen follicles with gray/white hair show DCT^{+} differentiating progeny in the hair bulb without nuclear pSMAD1/5/9, LEF1, or MITF. Cells from both conditions could be FACS purified to assess changes in receptor, BMP ligand, and downstream target gene expression in aged versus young adult mice.

Such studies in McSCs and their lineage and their response to BMPs throughout aging might shed light on disruptions that occur in other tissue SC types where BMP signaling is active. Furthermore, age-related deterioration of melanocyte function lessens their ability to produce melanin and provide UV protection, promoting epidermal aging and increasing the risk of skin cancer, rendering such investigations all the more important. If elevated BMP signaling in age does negatively impact McSCs (as has been shown for HFSCs), one could conceive of potentially using topical BMP inhibitors or intradermal injection of recombinant protein inhibitors as an anti-aging strategy to boost both hair growth and pigmentation.

4.3.3 BMPR1a as a possible switchboard for melanoma cells

Arguably one of the most exciting avenues opened up by this work are questions pertaining to how BMP might impact transformed cells of this lineage: melanoma. Not surprisingly, both pro- and anti-tumorigenic effects of this pathway have been described, but BMP has often been linked to melanoma invasiveness and migration (Braig and Bosserhoff, 2013; Gramann et al., 2019; Hsu et al., 2005; Rothhamer et al., 2005; Sinnberg et al., 2018; Venkatesan et al., 2018). For example, BMP2 is highly expressed in invasive melanoma cell lines, is thought to promote epithelial-mesenchymal transition, and is elevated in the blood of stage IV melanoma patients

(Sinnberg et al., 2018). Intriguingly, recent work in zebrafish melanoma has indicated that ligand-activated BMP signaling actually inhibits differentiation and cancer cell death (Venkatesan et al., 2018). This group further demonstrated that GDF6 is expressed in melanoma (but not in normal melanocytes) and acts through BMP receptors to maintain a neural crest signature through MITF inhibition. Furthermore, GDF6 expression in melanoma is inversely correlated with patient survival (Gramann et al., 2019).

However, my work demonstrates that in the mammalian physiological context, loss of BMP signaling suspends the melanocyte lineage in a committed progenitor-like state, where cells are proliferative but unable to fully differentiate. Therefore, one might hypothesize that melanoma cells could exploit this pathway to progress in malignancy, and that in certain contexts, being refractory to BMPR1a signaling could promote activated McSC/McCP-like characteristics. Perhaps in premalignant cells or early in tumor initiation, enhanced BMPR1a signaling might help to push cells towards a more differentiated ($MITF^{high}$ $LEF1^{high}$) and less proliferative state, blunting progression. As the tumor advances, however, cells could downregulate BMPR1a or its activating ligands to achieve an $MITF^{low\text{-}medium}$ $LEF1^{low\text{-}medium}$ state with less melanin production, more proliferation, and enhanced expression of stem and migratory genes. Support for such a scenario comes from familial cancer syndromes caused by germline mutations in *Bmpr1a*, such as Juvenile Polyposis and Cowden disease (Hsu et al., 2005; Zhou et al., 2001). These syndromes are characterized by benign overgrowths and increased susceptibility to cancer. Zhou et al. (2001) found that many *Bmpr1a* mutations in these patients were predicted to result in truncated receptors and diminished BMP signaling, reminiscent of the over-proliferation of McCP in *Bmpr1a* cKO mice. Therefore, BMPR1a might have both oncogenic and tumor suppressive roles, similar to reports where both pro- and anti-melanogenic or differentiation effects have been observed,

depending on the context (Bilodeau et al., 2001; Han et al., 2012; Jin et al., 2001; Kawakami et al., 2008; Park et al., 2009; Sharov et al., 2005; Singh et al., 2012; Yaar et al., 2006; Yang et al., 2014).

Indeed, related superfamily member TGF-β can enhance the proliferation of tumor-initiating cells when signaling is silenced, while simultaneously playing a powerful counter role in promoting invasion and metastasis (David et al., 2016; David and Massague, 2018; Guasch et al., 2007; Oshimori et al., 2015; Su et al., 2020). It is tempting to speculate that in melanoma, the juncture between immature McCP and differentiated melanocytes might become plastic through cells flipping their reliance on BMP signaling, depending on the stage of disease progression and particular microenvironment.

Future studies in mouse models of melanoma (to complement those performed in zebrafish) may illuminate whether mechanisms involving BMPR1a might be at work. If so, melanoma might conceivably be treated with BMP receptor agonists or antagonists. At the same time, in addition to BMPR1a and its downstream signaling, my extensive scRNA-seq of the lineage, in particular that of quiescent and activated McSCs and McCP, provides a wide range of genes and pathways whose role in both normal lineage and melanoma biology is yet to be determined.

CHAPTER 5:
MATERIALS AND METHODS

Mice

All mice were maintained in The Rockefeller University's Association for Assessment and Accreditation of Laboratory Animal Care (AAALAC)-accredited animal facility, the Comparative Bioscience Center. All mouse procedures were performed under Institutional Animal Care and Use Committee (IACUC)-approved laboratory protocols.

Dct-eGFP mice (Tg(Dct-EGFP)NY2Gsat/Mmucd, RRID:MMRRC_032849-UCD) were obtained from Mutant Mouse Resource and Research Center (MMRRC) at University of California at Davis and was donated to the MMRRC by Dr. Nathaniel Heintz of The Rockefeller University (GENSAT) (Gong et al., 2003). *Lef1*-RFP mice were generated previously in the Fuchs Lab by Rendl, et al. (2005). *Dct*-eGFP (mixed C57BL6/J, JAX#000664) males were crossed to CD1 females (CRL, Strain 022) to increase litter size and improve maternal care for mice used in qMcSC and aMcSC studies (*Dct*-eGFP$^+$ only). Background strain was kept as consistent as possible in generating *Dct*-eGFP$^+$ *Lef1*-RFP$^+$ mice, mating *Dct-eGFP* (mixed C57BL6/J) males with *Lef1*-RFP (CD1) females. *TyrCreER* (JAX#012328) (Bosenberg et al., 2006) mice were purchased from Jackson Laboratories and mated to in house colonies of *Bmpr1a floxed* (Mishina et al., 2002) *R26YFP floxed* (JAX#006148) (Srinivas et al., 2001) (mixed C57BL/6) mice. The *Lef1* KO strain (C57BL/6J) was obtained from Dr. Rudolf Grosschedl (Kratochwil et al., 1996). *Ctnnb1 floxed* (JAX#004152) (Brault et al., 2001) (C57BL/6J) were purchased from Jackson Laboratories.

For RNA and ATAC-seq experiments and IMF quantifications, male mice were used to eliminate sex-related differences, minimize variability in the hair cycle, and capture more cells per experiment. Male and female mice were used for IMF analysis (sex-matched for comparison), and female mice were used for *TyrCreER* *Bmpr1a*^{floxed} *R26YFP*^{floxed} 12 day post-waxing RT-qPCR.

Photographs of the gross phenotypes of mice were taken with iPhone 6, 7 Plus, and 11 Pro Max cameras and brightened in Fijj/ImageJ as necessary. Genotyping was performed using the primers listed in **Table 5.1** below.

Table 5.1 Genotyping Primer List

Primer Name	**Sequence 5' > 3'**
β-catenin 1	AAGGTAGAGTGATGAAAGTTGTT
β-catenin 2	CACCATGTCCTCTGTCCTATTC
β-catenin 3	TACACTATTGAATCACAGGGACTT
Bmpr1a Fx2 Forward	GCAGCTGCTGCTGCAGCCTCC
Bmpr1a Fx4_Reverse	TGGCTACAATTTGTCTCATGC
Dct(32849) F Forward)	GTGGGAATTTTGAGAGGAGAGGAAAG
GFPR2 Reverse	TAGCGGCTGAAGCACTGCA
Lef1-RFP Forward	CACCCTTGAGTTACCCCTCTG
Lef1-RFP Reverse	CCCTGAAAACTTTGCCCCCTC
Neo A	TGGAGAGGCTATTCGGCTATGAC
Neo B	AACTCGTCAAGAAGGCGATAGAAG
TyrCreER Forward	CAGGGTGTTATAAGCAATCCC
TyrCreER Reverse	CCTGGAAAATGCTTCTGTCCG
Rosa26YFP common	AAAGTCGCTCTGAGTTGTTAT
Rosa26YFP mutant	AAGACCGCGAAGAGTTTGTC
Rosa26YFP WT	GGAGCGGGAGAAATGGATATG

Animal procedures

EdU incorporation. To assess McSC proliferation by IMF, two 100 uL doses of 5 mg/mL 5-Ethynyl-2′-deoxyuridine (EdU) were administered by intraperitoneal injection (IP). Mice were euthanized and skin was collected 24 hours after the first dose of EdU. To quantify proliferation of McSCs and their differentiating progeny in the hair bulb in *TyrCreER Bmpr1a*^{floxed} *R26YF* ^{floxed} mice one week after waxing, animals were given 100-150 uL EdU by IP 4 hours prior to sacrifice and skin collection.

Tamoxifen treatment. Starting at P21 (weaning age), *TyrCreER Bmpr1a*^{floxed} *R26YFP*^{floxed} and *TyrCreER Ctnnb1*^{floxed} *R26YFP*^{floxed} mice were given 50uL 2% tamoxifen dissolved in Sigma corn oil by IP for seven consecutive days. In second telogen (P60-75), back skin was waxed under

isoflurane anesthesia. Buprenorphine was given for pain management, and nails were clipped to minimize scratching. To prevent fighting and injury of waxed skin, male mice were singly housed after the procedure until the time of euthanasia.

Fluorescence-activated Cell Sorting

To obtain single cell suspensions for FACS purification, mouse back skin was dissected and subjected to chemical and mechanical digestion. Telogen (P58-80 for qMcSCs) and anagen I-II (P21 for aMcSCs) skin was scraped with a dull scalpel to remove excess fat prior to rotating incubation in trypsin-EDTA (Gibco) hair side up at 37˚C for 45-60 minutes. Skin was then scraped with a dull scalpel against the direction of hair growth to release cells in the HFs. Anagen skin (P9-10 or 1 week or 12 days post waxing) was digested hair side up in 0.25% collagenase (Sigma) in HBSS (Gibco) at 37˚C for 25-30 minutes. DNAse (Roche, 1:200) and 5mM $MgCl_2$ was sometimes added to anagen skin preparations to minimize cell clumping. The skin was then scraped from the dermal side to preferentially release cells in the hair bulb. The suspensions were quenched with cold FACS buffer (5% FBS in 1X PBS), filtered, spun down, and incubated for 25 minutes on ice with primary antibodies. All antibodies used are listed in **Table 5.2**. For biotin-conjugated antibodies, cells were washed and incubated with streptavidin secondary antibody for 5-10 minutes on ice.

Table 5.2 FACS Antibody List

Antibody	Company, Catalogue #	Dilution
Ly-6A/E (Sca-1) PerCP-Cy5.5	eBioscience, 45-5981-82	1:1000
Ly-6A/E (Sca-1) APC-Cy7	BioLegend, 108126	1:1000
CD34 eFluor660	eBioscience, 50-0341	1:100
CD49f (α-6) BV421	BioLegend, 313624	1:100
CD49F (α-6) PE-Cy-7	BioLegend, 313621	1:100
CD117 (c-KIT) PE-Cy-7	eBioscience, 25-1171-82	1:100
Biotin-CD140a	BioLegend, 135910	1:150
Biotin-CD31	BioLegend, 102404	1:150
Biotin-CD45	BD, 553077	1:150
Streptavidin PE	eBioscience, 12-4317	1:1500
Streptavidin APC-Cy7	BD, 554063	1:500

DAPI was used for live/dead cell exclusion. For bulk RNA-seq and RT-qPCR, cells were sorted with a 70 um nozzle directly into TRIzol (ThermoFisher). For scRNA-seq, cells were sorted with a 100 um nozzle into 96 well plates, gating more conservatively to minimize the capture of contaminating cell types. Cells were sorted by the Flow Cytometry Resource Center of The Rockefeller University. Flow cytometry plots were generated using FlowJo to illustrate the strategies used to isolate each cell population. Manual compensation was performed for presentation of flow plots

Immunofluorescence

To prepare tissue for IMF analysis, mouse back skin was prefixed in 4% paraformaldehyde in PBS immediately after dissection for 30 minutes at room temperature or 1-2 hours at 4˚C. Tissue was then washed with 1X PBS and incubated while rotating in 30% sucrose in PBS at 4˚C overnight before embedding in OCT Compound. Frozen blocks were sectioned (10-18μm thickness) on a Leica cryostat and mounted on SuperFrost Plus slides (Thermo Fisher). Unstained slides were stored at -20˚C until further processing.

Slides were dried at room temperature before blocking for at least an hour in IMF staining buffer consisting of 5% normal donkey serum, 1% bovine serum albumin, 2% fish gelatin and 0.3% Triton X-100 in PBS. For TYR and MITF IMF, slides were additionally fixed in cold methanol at 20˚C for 20 minutes before blocking. Slides were incubated with primary antibodies diluted in IMF staining buffer (listed in **Table 5.3**) at 4˚C overnight and washed three times with PBS prior to incubation with secondary antibodies (Alexa Fluor-RRX, 488, or 647-conjugated, Life Technologies at 1:500 dilution) for an hour at room temperature. For EdU, the Click-iT EdU Alexa Fluor 647 Imaging Kit (C10340) was used before proceeding to secondary antibody staining. Slides were washed another three times before mounting with ProLong Antifade Gold with DAPI Mountant (Thermo Fisher). Counterstaining with DAPI in PBS was sometimes performed to enhance nuclear signal.

Table 5.3 Primary Immunofluorescence Antibody List

Antibody	Company, Catalogue #	Dilution
DCT (TYRP2, D-18)	Santa Cruz, sc-10451	1:200-250
TYRP1	Made by Fuchs Lab	1:100
Tyrosinase (PEP7)	Made by V.J. Hearing	1:750
CD104 (integrin β-4)	BD Pharmingen, #553745	1:100
PMEL (Anti-Melanoma gp100 [EP4863(2)])	Abcam, ab137078	1:750
GFP	Abcam, ab13970	1:2000
RFP	Made by Fuchs Lab	
Phospho-Smad1 (Ser463/465)/Smad5 (Ser463/465)/ Smad9 (Ser465/467) (D5B10)	Cell Signaling, #13820	1:100
Phospho-p38 MAPK (Thr180/Tyr182) (D3F9) XP	Cell Signaling, #4511	1:100
MITF	Abcam, ab122982	1:100
LEF1	Made by Fuchs Lab	1:250

Immunofluorescence Microscopy

IMF microscopy images were acquired with an Axio Observer.Z1 epifluorescence microscope with a Hamamatsu ORCA-ER camera (Hamamatsu Photonics) and with an ApoTome.2 (Carl Zeiss) slider using 20, 40, or 63X objectives and Zen software (Carl Zeiss).

Differential interference contrast (DIC) brightfield images were taken on the Axio Observer.Z1 using the Axiocam 305 camera (Zeiss). Images were processed by channel using Fiji/ImageJ using Brightness/Contrast where appropriate. Images with Z-stacks were displayed as max intensity projections. Optical density (OD) was determined with MetaMorph software (Molecular Devices), where $OD=\log_{10}$ (1/transmittance), and transmittance=transmitted light/incident light. Measurements were made of a single plane of DIC bright field image with Integrated Morphometry Analysis within a freehand drawn region outlining the DCT-stained region (based on maximum intensity projection).

Electron microscopy

Skin samples were fixed in 2% glutaraldehyde, 4% PFA, and 2 mM CaCl2 in 0.1 M sodium cacodylate buffer (pH 7.2) at room temperature for >1 hour, post-fixed in 1% osmium tetroxide, and processed for Epon embedding. Ultrathin sections (60–65 nm) were counterstained with uranyl acetate and lead citrate. Images were taken with a transmission electron microscope (Tecnai G2-12 FEI) equipped with a digital camera (AMT BioSprint29). For quantification, melanosomes were counted within hair bulb McSC progeny areas $\geq 10um^2$. These areas were outlined by hand by H. Amalia Pasolli, an expert in EM analysis of the skin. Melanosomes were scored as immature by the presence of striations/translucency and as mature (stage IV) if opaque. Measurements were expressed as melanosome number/cell area captured.

Cell Culture

The Melan-a2 mouse melanocyte cell line was generated by Sviderskaya, et al. (1995) and purchased from the Wellcome Trust Functional Genomics Cell Bank of St George's, University of London (http://anatomy.sgul.ac.uk/pages/). Cells were cultured in RPMI 1640 with L-glutamine supplemented with 10% FBS, 5% Penicillin-Streptomycin, 200 pM cholera toxin, and 200 nM

phorbol 12-myristate 13-acetate and grown at 7.5% CO_2. Cells were plated for experiments 24 hours before treatment in normal growth media, then serum starved at 0.5% FBS during the course of treatment (10 ng/mL recombinant human/murine/rat BMP2, murine BMP4, or human BMP6 (Peprotech) and or 250 nM ALK inhibitor K02288 (Tocris) in DMSO).

To generate a *Bmpr1a* KO Melan-a2 cell line with CRISPR, we first made a clonal parental cell line from a single Melan-a2 cell to minimize experimental variability. Predesigned gRNA was purchased from Integrated DNA Technologies (IDT) (control non-targeting and DesignID:Mm.Cas9.BMPR1A.1.AB *Bmpr1a*, Exon 9, 5'-CAUGACGCAUUAACACCGUCGUUUUAGAGCUAUGCU-3'). Cells were transfected with Lipofectamine RNAiMAX (ThermoFisher) to deliver ribonucleoproteins (RNPs) consisting of duplexed gRNA and tracrRNA-Atto550 with Alt-R S.p. Cas9 Nuclease V3 (IDT). Culture media was changed 12-24 hours post transfection, and then genomic DNA was extracted with QuickExtract (Lucigen). The cut site region was PCR amplified, and cutting efficiency was tested by T7 endonuclease assay (New England Biolabs). To generate the *Bmpr1a* KO cell line, the parental clonal cell line was transfected and single cells were sorted into 96 well plates from which cell lines were grown. Gene KO was confirmed by MiSeq and the rgenome.net Cas-analyzer tool. The relevant primers are listed in **Table 5.4** below.

Table 5.4 Primers used for *Bmpr1a* CRISPR KO *in Vitro*

Primer Name	Purpose	Sequence 5' > 3'
Sg_Ex9_CutSite_F1	*Bmpr1a* cut site PCR (T7 assay)	GGACTGTGTCGGATCAGCTAGG
Sg_Ex9_CutSite_R1	*Bmpr1a* cut site PCR (T7 assay)	TGTGTACCATCACACCCACTCA
BH_Seq_CutSite_F1	MiSeq validation of *Bmpr1a* KO (allows for barcoding, library prep)	TCGTCGGCAGCGTCAGATGTGTATAAGAG ACAGGGAGCTATTTGGTTATGCCAGGCTT
BH_Seq_CutSite_R1	MiSeq validation of *Bmpr1a* KO (allows for barcoding, library prep)	GTCTCGTGGGCTCGGAGATGTGTATAAGA GACAGGCTACACAACCATTTGAATCCACA

RT-qPCR

Cultured cells were washed with PBS and harvested by resuspending in TRI Reagent LS (Sigma); FACS purified cells were sorted directly into TRI Reagent LS. RNA was purified using the Direct-zol RNA MicroPrep kit (Zymo Research) according to the kit protocol. cDNA was made with the SuperScript VILO cDNA Synthesis Kit (ThermoFisher) and diluted before RT-qPCR, which was performed using SYBR Green PCR master mix (ThermoFisher). *Ppib2* was used as a housekeeping gene, and primer sequences are listed in **Table 5.5**.

Table 5.5 RT-qPCR Primer List

Primer Name	**Sequence 5' > 3'**
Gapdh Forward	GTCGTGGAGTCTACTGGTGTCTTCAC
Gapdh Reverse	GTTGTCATATTTCTCGTGGTTCACACCC
Bmpr1a Forward	GCTATTGCTCAGGACACTGC
Bmpr1a Reverse	TGGTTTCTCCCTGATCATCTT
Eps8 Forward	TCTTCACCACCCTATTCCCAG
Eps8 Reverse	CATCTTTCCGATCCAGCACGA
Id2 Forward	CTATCGTCAGCCTGCATCAC
Id2 Reverse	ATTCAGATGCCTGCAAGGAC
Kif26b Forward	TACACCATGATCGGAAGGGAC
Kif26b Reverse	CTTGAACAGCCAAGAAATAGCAC
Lef1 Forward	CGCTAAAGGAGAGTGCAGCTA
Lef1 Reverse	GCTGTCTCTCTTTCCGTGCT
Mitf Forward	ACTTTCCCTTATCCCATCCAC
Mitf Reverse	TGAGATCCAGAGTTGTCGTACA
Oca2 Forward	CCTGAACATACAGAGTTTGGCT
Oca2 Reverse	GAGCAGAGGAGTGTCTTCCTTA
Pax3 Forward	CCGGGGCAGAATTACCCAC
Pax3 Reverse	GCCGTTGATAAATACTCCTCCG
Ppib2 Forward	GTGAGCGCTTCCCAGATGAGA
Ppib2 Reverse	TGCCGGAGTCGACAATGATG
Rab38 Forward	GGGACATTGCTGGTCAAGAAA
Rab38 Reverse	GGCTTACCATTAGGGAGCGTT
Slc26a2 Forward	AGAGACGGGGCTTTTGATTTC
Slc26a2 Reverse	GGCACCAACAGGATACCCAC
Vimentin Forward	GAAATTGCAGGAGGAGATGC
Vimentin Reverse	TCCACTTTCCGTTCAAGGTC

Western blotting

Cultured cells were washed in cold 1X PBS, lysed in cold RIPA Buffer (Millipore) supplemented with protease and phosphatase inhibitors (Roche), and harvested by scraping. Cells were lysed for 30 minutes on ice with vortexing, centrifuged at 4°C for 10 minutes, and supernatant lysate was collected. Protein concentration was determined by BCA Assay (Pierce) read on a BioTek plate reader using a bovine serum albumin standard curve. Up to 50μg protein was loaded on NuPAGE 4-12% Bis-Tris Gels (Invitrogen) and run for 1 hour at 200V in NuPAGE MOPS SDS Running Buffer (Invitrogen). Protein was transferred at 30V overnight at 4°C onto PVDF membranes in NuPage Transfer Buffer (Invitrogen) with 20% methanol. Membranes were blocked in PBS-based blocking buffer (Odyssey) for at least 1 hour at room temperature before incubating with primary antibodies overnight at 4°C in blocking buffer supplemented with Tween-20. Membranes were washed several times in PBS with 0.1% Tween-20 before incubating with fluorescent secondary antibodies in blocking buffer supplemented with Tween-20 and SDS. Membranes were washed again before imaging on an Odyssey CLx machine (LI-COR). The primary and secondary antibodies and the dilutions used are listed in **Table 5.6**.

TABLE 5.6 Immunoblotting Antibody List

Antibody	Company, Catalogue #	Dilution
Phospho-Smad1 (Ser463/465)/Smad5 (Ser463/465)/ Smad9 (Ser465/467) (D5B10)	Cell Signaling, #13820	1:1000
SMAD1/5/9	Invitrogen, #PA1-41079	1:1000
LEF1 (C12A5)	Cell Signaling, #2230	1:1000
MITF (D5G7V)	Cell Signaling, #12590	1:1000
α-tubulin	Invitrogen, #T5168	1:10,000
Donkey anti-rabbit 800 (secondary)	LI-COR, #926-32213	1:10,000
Donkey anti-mouse 680 (secondary)	LI-COR, # 926-68072	1:10,000

Bulk RNA-seq

Cells were FACS purified into TRI Reagent LS, and total RNA was purified using the Direct-zol RNA MicroPrep kit (Zymo Research). For McSCs, cells from 4 male mice at P60 were pooled for Replicate 1, and cells from 4 male mice at P62 were pooled for Replicate 2. For differentiating McSC progeny in the hair bulb, cells from male P10 mice were also pooled: 3 mice for Replicate 1, 2 mice for Replicate 2, and 4 mice for Replicate 3. The Weill Cornell Medical College Genomic Core facility (New York, NY) performed quality control analysis and sequencing. Briefly, RNA quality was determined by Agilent 2100 Bioanalyzer, and cDNA libraries were prepared using the Illumina TrueSeq mRNA sample preparation kit (non-stranded, poly-A selection) and sequenced on an Illumina HiSeq 4000 instrument.

Single cell cDNA synthesis and library preparation

ScRNA-seq libraries were prepared using a slightly modified version of the Smart-seq2 protocol described by Picelli et al. (2014). Cells were FACS sorted into 96 well plates with 2μL lysis buffer containing Triton X-100, RNaseOUT (Invitrogen), Oligo dT30VN, dNTPs, and ERCC spike-ins. Plates were flash frozen in liquid nitrogen and stored at -80˚C until further processing. Plates were then thawed on ice before lysing at 72˚C for 3 minutes. The RNA was subject to reverse transcription (4U/μL Maxima H- transcriptase), template switching reaction, and whole transcriptome amplification. cDNA was purified with 7μL AMPure XP beads per well. To test for low quality libraries or empty wells, RT-qPCR for *Gapdh* was performed before proceeding. Illumina sequencing libraries were then prepared using the Nextera XT DNA library preparation kit (Illumina). After barcoding, samples were pooled and purified with MinElute PCR Purification Kit (Qiagen), then cleaned with 0.9X by volume AMPure XP beads (Beckman Coulter). Libraries were sequenced on an Illumina NextSeq 500 (75 bp paired-end read, mid-output).

ATAC library preparation

Cells were FACS purified using an 85μm nozzle for gentler sorting to improve viability. qMcSCs were isolated as described in Fig. 2.2 B from *Dct*-eGFP^{+} x CD1 2nd telogen skin at P60 (Replicate 1, cells from 3 male mice pooled) and P80 (Replicates 2 and 3, cells from 4 male mice pooled for each); differentiating progeny were isolated from *Dct*-eGFP^{+} (C57BL6/J background with some CD1) anagen skin at P9 (Replicate 1, cells from 1 male mouse, Replicates 2 and 3, cells from 2 male mice pooled for each) using the following FACS strategy: dump (CD31, CD45, CD140a)$^{-}$, Sca-1^{-}, CD34^{-}, eGFP^{high}, CD117^{+} cells). Library preparation was performed as described (Buenrostro et al., 2013) with some modifications. Briefly, sorted cells were washed with cold PBS, pelleted, and resuspended in cold lysis buffer (10 mM Tris-HCl, pH 7.4, 10 mM NaCl, 3 mM $MgCl_2$, 0.1% IGEPAL CA-630). Buffer was removed after centrifugation, then samples were incubated in the transposition reaction at 37°C for 30 minutes (Illumina Nextera DNA Preparation Kit, using 10uL TDE1 enzyme). The reaction was terminated by adding Tagmentation Clean Up buffer consisting of 300 mM EDTA and 900 mM NaCl. DNA was purified with the Qiagen MiniElute PCR purification kit, then PCR amplified with barcode identifiers for 12-18 cycles, and the products taken at three cycling times were tested by D1000 Tape Station (Agilent). Optimal samples were then pooled and bead purified for sequencing on NextSeq High Output 75 single read (40 x 40 bp paired end).

Schematics

Some graphics from SMART Servier Medical Art (https://smart.servier.com) were used to make to make schematics. Other illustrations were created with Adobe Illustrator and Microsoft PowerPoint.

Quantification and Statistical Analyses

Statistical tests for microscopy quantifications and RT-qPCR were performed with GraphPad Prism 7. Column data was first subject to D'Agostino and Pearson normality testing. For data without normal distribution, two-tailed Mann-Whitney test was used to compare two groups, and Kruskal-Wallis test with Dunn's with multiple comparisons was used to compare between more than two groups. For RT-qPCR, where n number was too low for normality testing, unpaired t test or ordinary one-way ANOVA with Dunnett's multiple comparison tests were performed.

Bulk RNA-seq analysis

Sequence and transcript coordinates for mouse mm10 UCSC genome and gene models were retrieved from the Bioconductor Bsgenome.Mmusculus.UCSC.mm10 (version 1.4.0) and TxDb.Mmusculus.UCSC.mm10.knownGene (version 3.4.0) Bioconductor libraries, respectively. Read length was 51bp. Transcript expressions were calculated using the Salmon quantification software (version 0.8.2) (Patro et al., 2017) and gene expression levels as TPMs and counts were obtained using Tximport (version 1.8.0) (Soneson et al., 2015). Normalization and rlog transformation of raw read counts in genes were performed using DESeq2 (version 1.20.0) (Love et al., 2014). Variability between samples was assessed with hierarchical clustering and heat maps of between sample distances implemented in the Pheatmap R package (1.0.10) as described by Love et al. (2014), and sample similarity is expressed as Euclidean distance. Published HFSC RNA-seq data from Ge et al. (2017) was obtained from Gene Expression Omnibus (GEO) accession #GSE89928 (GSM2656733 CL_BuA and GSM2656734 CL_BuB).

Single cell RNA-seq analysis

Sequence and transcript coordinates for mouse release M23 (GRCm38.p6) genome and gene models were downloaded from GENCODE (https://www.gencodegenes.org/mouse/release_M23.html). Adaptors were trimmed from reads using Skewer (version 0.2.2). Sequencing reads were aligned to the mouse reference genome combined with sequences for ERCC spike-ins as artificial chromosomes using STAR (version 2.5.2a) (Dobin et al., 2013) with default parameters for paired-end reads. Transcript expressions were calculated with Salmon (version 0.14.1) (Patro et al., 2017), and gene expression levels as TPMs and counts were obtained with Tximport (version 1.12.3) (Soneson et al., 2015). TPMs were transformed to $\log_2$(TPM+1). For downstream analyses, cells with <1,250 genes detected per cell and genes expressed in <5% of the cell population were removed. Cells expressing lower levels of *Dct* ($\log_2$(TPM+1) <6) and or those expressing the HF lineage gene *Krt15* ($\log_2$(TPM+1) >6) were excluded. After filtering, the number of cells in the dataset were as follows: qMcSCs n=104 cells (n=3 mice), aMcSCs n=193 cells (n=3 mice), McSC differentiating progeny (McCP/melanocytes) n=308 cells (n=2 mice), *Bmpr1a* WT control n=205 cells (n=1 mouse), *Bmpr1a* heterozygous n=304 cells (n=2 mice), and *Bmpr1a* null n=421 cells (n=2 mice).

Analyses and visualization of data were conducted in a Python environment built on the Numpy, SciPy, matplotlib, scikit-learn package and pandas libraries (Pedregosa et al., 2011). Batch effect variation between sequencing runs and biological replicates was assessed by examining the Euclidean distances between replicates within each hair cycle timepoint dataset versus across hair cycle timepoints, which showed closer relationships between replicates compared with variation between biologically distinct collection timepoints. PCA analysis of the only dataset with some evidence of replicate-specific clustering patterns (P10 anagen VI) captured

biologically relevant differences in gene expression separating these replicates, suggesting that these differences likely represent true biological variation between animals in this highly dynamic differentiating population, rather than technical batch effects.

To distinguish biological variability in gene expression from technical noise, a statistical model for identifying highly variable genes compared to ERCC spike-ins as described by Brennecke et al. (2013) was implemented. A custom script based on the methodology described by Brennecke et al., 2013 (in R version 3.6.1) was used to identify those genes with variation at least 10% above the technical variation with FDR less than 0.1.

To visualize the data and identify clusters, the highly variable gene dataset was centered and scaled, and PCA was performed. A Jack-straw approach for the first 100 components (based on Seurat v3.1.1) (Stuart et al., 2019) was implemented in R to calculate a statistical significance for each PC, and components with $p<0.05$ were retained for downstream analysis. Significant PCs were used as input for non-linear dimensionality reduction, performed using UMAP implemented in scikit-learn. A graph-based clustering approach based on building a kNN graph and clustering with the Louvain algorithm (with k set to $1/5^{th}$ of the dataset size, and resolution parameter of 1×10^{-4}) was implemented. Euclidean distance in PCA space served as input for both UMAP generation and Louvain clustering. In second level analysis, the same strategy was used for dimensionality reduction, clustering, and visualization, with variable genes and PCs determined separately for each of the main cell clusters (C1, C2, C3).

For pseudotime analysis, the same strategy for dimensionality reduction and clustering of each dataset was used, principal graph based on the community analysis was constructed, and a pseudotime values for each cell was computed using Monocle 3 (version 0.2.0) (Cao et al., 2019; Trapnell et al., 2014). To identify genes that change as a function of pseudotime, the "graph_test()"

function of Monocle 3 was used to implement Moran's *I* test. Genes were considered significantly changing here if they had a q-value<$1.0x10^{-4}$.

Differential gene expression was used to identify genes up- and downregulated in each cluster. Briefly, raw count matrices for the biologically variable genes within each dataset were used and applied to the DESeq2 package (version 1.24.0) (Love et al., 2014) using R. A negative binomial fit was used to model differential gene expression, the dataset was factored based on Louvain cluster assignments, and a threshold of 0.75 was used to construct Wald tests of significance. In general, genes were considered to be significantly differentially expressed if their $\log_2$(fold change) $\geq|1|$ and p-adjusted value (q) ≤ 0.05. Lowly expressed differential genes (baseMean expression ≤ 5) were discarded from visualization and further analysis. Expression levels of specific genes of interest were visualized as $\log_2$(TPM+1) values on UMAP plots. The "stemness" and "differentiation" signature gene sets used to generate global scores were the top 100 up- or down-regulated differentially expressed genes between McSCs (C1 and C2) and McSC differentiating progeny (C3). The "AddModuleScore" function from Seurat v3.1.1 was used to calculate the average expression levels of each gene set on a single cell level, subtracted by the aggregated expression of control feature sets, as originally described in Tirosh et al. (2016).

GO analyses of differentially expressed genes were performed using PANTHER Tools Overrepresentation Test (version 14.0), and annotated using the GO Biological Process Complete list (Mi et al., 2019; Thomas et al., 2006), with significant associations calculated by the Fisher's Exact test and multiple comparisons corrected for using FDR. Where indicated, GO analyses were also annotated using DAVID Bioinformatics Resources 6.8 "Functional Annotation," "BP Direct" lists (Huang et al., 2009a; Huang et al., 2009b).

Heatmaps were constructed in a Python environment built on the Numpy, SciPy, matplotlib, scikit-learn package and pandas libraries (Pedregosa et al., 2011). For specific GO annotations, the corresponding *Mus musculus* gene lists were obtained from AmiGO 2 through the Gene Ontology Consortium. Each GO gene list was used to filter the biologically variable genes associated with the dataset to generate normalized expression matrices, and genes characteristic of cell clusters (expressed in >50% of the cluster cells) were used for visualization. Each expression matrix was scaled and centered, and hierarchical linkages between genes was calculated based on pairwise correlation distances using the Farthest Point Algorithm. The matplotlib extension Seaborn visualization library (version 0.9.1) was used to create heatmaps using the clustermap() function with the previously generated gene-based hierarchical linkages fed in.

BMP or canonical WNT target gene lists were culled from mouse literature (Table S8 of Infarinato et al., 2020); to be included, target genes had to be validated as direct targets of the signaling pathway in at least two mesenchymal or epithelial tissues, and be expressed in our datasets. Cell cycle stage specific gene lists were obtained from Macosko et al. (2015). To generate a global proliferation gene set score, an amalgamated list of cell cycle stage-specific genes was used. The "AddModuleScore" function from Seurat v3.1.1 was used to calculate the average expression levels of each gene set on a single cell level, subtracted by the aggregated expression of control feature sets, as originally described in Tirosh et al. (2016). Gene set scores for each cell are color-coded on UMAP visualizations of the data or on violin plots binned by sub-cluster cell identity.

Promoter analysis of differentially expressed genes

HOMER genome-wide motif predictions were used to scan for LEF1, MITF, and SMAD motifs within 2.5 kb upstream of the TSS of genes that were significantly changed with padj≤0.05,

baseMean≥5 in the *Bmpr1a* null versus control cluster. Motifs had to be found in at least one TSS to be considered positive, then genes were then grouped based on the presence or absence of motifs. The difference in fold change between two groups was tested by Wilcoxon test with the null hypothesis that there is no difference in the distribution between the test groups. The results were plotted with R (3.6.1) and ggplot2.

ATAC-seq analysis

ATAC-seq reads are aligned to the mm10 genome from the Bsgenome.Mmusculus.UCSC.mm10 Bioconductor package (version 1.4.0) using Rsubread's align method in paired-end mode with fragments between 1 to 5000 base-pairs considered properly paired (Liao et al., 2013). Normalized, fragment signal bigWigs were created using the rtracklayer package. Peak calls were made with MACS2 software in BAMPE mode (Feng J et al., 2012; Zhang et al., 2008) and sequences under these peaks used with the motifMatcher Bioconductor package (Schep et al., 2014) and JASPAR motif database (Fornes et al., 2020) to identify known motifs within ATAC-seq peaks. Differential ATAC-seq signal was identified using the DESeq2 package (Ross-Innes CS et al., 2012; Love et al., 2014) and enrichment for motifs identified using the Limma packages geneSetTest function (Ritchie et al., 2015). Integrative Genomics Viewer (IGV) was used for gene track and peak visualization.

Data Availability

The bulk and scRNA-seq and ATAC-seq and code generated during this study are available at GEO [GSE147299/ https://www.ncbi.nlm.nih.gov/geo/query/acc.cgi?acc=GSE147299].

APPENDIX

Table 2.1 Select List of Differentially Expressed "Stemness" and "Differentiation" Genes from DESeq2 Comparison of C1 and C2 vs. C3 cells (see also Table S2 from Infarinato et al., 2020) *All values shown to three decimal points, ranked by padj value

"Stemness" Genes

Gene Name	baseMean	log2FoldChange	stat	pvalue	padj
Arid5a	55.144	4.415	22.643	1.626E-113	9.691E-111
Lmna	146.456	3.407	22.635	1.948E-113	1.045E-110
Socs3	13.928	6.498	22.422	2.401E-111	1.171E-108
Col12a1	118.818	4.992	22.246	1.240E-109	5.544E-107
Fosb	150.150	6.711	21.631	9.247E-104	2.918E-101
Fos	87.376	4.838	20.848	1.586E-96	4.254E-94
Gab1	25.657	3.804	20.358	3.926E-92	7.799E-90
Vim	72.713	3.279	20.097	7.909E-90	1.463E-87
C4b	25.086	7.613	19.317	3.885E-83	5.788E-81
Junb	27.407	3.956	19.001	1.684E-80	2.293E-78
Sulf2	20.808	3.583	19.000	1.710E-80	2.293E-78
Bcl2	10.713	3.669	18.904	1.062E-79	1.390E-77
Adgrg1	41.006	3.380	18.621	2.181E-77	2.785E-75
Sbno2	39.072	3.971	18.278	1.244E-74	1.517E-72
Atf3	28.740	6.009	17.848	2.983E-71	3.266E-69
Adamtsl4	15.394	4.034	17.785	9.193E-71	9.669E-69
Jun	66.969	3.507	17.525	9.208E-69	9.319E-67
Cubn	14.540	4.600	16.826	1.576E-63	1.432E-61
Nr4a1	80.646	4.142	16.670	2.179E-62	1.948E-60
Gm37352	40.083	3.819	16.024	8.620E-58	6.889E-56
Pde1c	10.661	3.741	16.024	8.733E-58	6.889E-56
Enpp2	55.947	2.522	15.761	5.739E-56	4.160E-54
Cyp2d22	10.102	5.271	15.700	1.513E-55	1.068E-53
Gucy1b1	7.253	4.439	15.649	3.374E-55	2.320E-53
Agrn	31.948	3.033	15.647	3.486E-55	2.367E-53
H2-Q4	7.623	4.878	15.362	2.928E-53	1.963E-51
Vmp1	18.806	2.835	15.252	1.593E-52	1.042E-50
Plagl1	20.224	2.952	15.011	6.193E-51	3.908E-49
H2-D1	34.118	2.518	14.878	4.582E-50	2.858E-48
Klf6	27.310	2.574	14.625	1.946E-48	1.200E-46
H2-K1	11.266	3.541	14.608	2.491E-48	1.519E-46
Dusp18	16.353	3.537	13.829	1.697E-43	9.100E-42
Sema5a	14.677	3.207	13.584	4.994E-42	2.601E-40
AW011738	6.590	4.229	13.497	1.621E-41	8.283E-40
Arid5b	17.312	2.854	13.422	4.516E-41	2.243E-39
Csrnp1	10.380	5.671	13.341	1.329E-40	6.481E-39

Prelp	12.471	3.857	13.335	1.457E-40	7.039E-39
Prex2	15.862	2.491	12.964	1.963E-38	8.925E-37
Col16a1	10.798	2.714	12.778	2.175E-37	9.484E-36
Ppp1r15a	10.229	3.946	12.691	6.609E-37	2.859E-35
Myo10	28.098	1.992	12.504	7.098E-36	2.952E-34
Auts2	10.411	2.411	12.404	2.498E-35	1.023E-33
Ahr	6.537	3.711	12.170	4.470E-34	1.725E-32
Gm37376	58.121	2.074	12.133	7.045E-34	2.699E-32
Egr1	62.819	3.795	11.999	3.593E-33	1.321E-31
Pax3	48.077	1.805	11.999	3.596E-33	1.321E-31
Myadm	30.894	2.455	11.964	5.494E-33	1.978E-31
4930402H24Rik	18.825	2.335	11.755	6.659E-32	2.304E-30
Glul	39.453	2.339	11.720	1.009E-31	3.446E-30
Idh2	15.207	1.945	11.588	4.747E-31	1.602E-29
Cd274	9.282	4.758	11.414	3.546E-30	1.168E-28
Rnf144a	7.449	2.695	11.414	3.549E-30	1.168E-28
Ets1	7.877	2.573	11.407	3.865E-30	1.264E-28
Igsf3	17.309	2.224	11.380	5.276E-30	1.715E-28
Arnt2	10.709	2.939	11.361	6.571E-30	2.098E-28
Pde4b	7.085	4.166	11.282	1.609E-29	5.076E-28
Irs2	14.342	2.594	11.164	6.135E-29	1.880E-27
Klf9	6.685	3.033	11.055	2.070E-28	6.168E-27
Plekhm2	11.478	2.322	10.892	1.254E-27	3.675E-26
Lpin1	8.887	2.650	10.793	3.714E-27	1.060E-25
Malat1	502.984	1.825	10.475	1.125E-25	3.010E-24
Slc27a1	8.518	3.511	10.405	2.362E-25	6.210E-24
Appl2	16.596	1.974	10.395	2.607E-25	6.788E-24
Ndrg1	10.186	3.455	10.201	1.968E-24	4.888E-23
Per1	13.888	2.415	10.155	3.141E-24	7.765E-23
Ubald1	9.929	2.399	10.101	5.496E-24	1.340E-22
Ahdc1	7.473	2.794	9.965	2.165E-23	5.208E-22
Gucy2f	6.645	4.889	9.948	2.575E-23	6.166E-22
Jmjd1c	23.048	2.013	9.895	4.376E-23	1.030E-21
Zfp36	13.266	2.802	9.892	4.526E-23	1.060E-21
Crebrf	7.724	2.661	9.821	9.139E-23	2.113E-21
Mdfic	8.493	3.271	9.813	9.898E-23	2.279E-21
Gm42418	1123.306	1.636	9.762	1.645E-22	3.770E-21
Ahnak	206.591	1.732	9.719	2.493E-22	5.666E-21
Lgals3	31.405	2.127	9.692	3.252E-22	7.329E-21
Cyr61	8.873	3.438	9.547	1.333E-21	2.942E-20
Ripk1	5.918	3.017	9.530	1.580E-21	3.474E-20
Sox6	14.469	2.013	9.339	9.712E-21	2.067E-19
Arhgef2	5.694	2.935	9.269	1.877E-20	3.963E-19
Irf2bpl	16.699	1.913	9.222	2.915E-20	6.133E-19

Mylk	6.477	3.079	9.219	2.993E-20	6.271E-19
Irgm1	6.763	3.368	9.140	6.248E-20	1.289E-18
B3gnt2	7.552	2.867	9.127	7.027E-20	1.444E-18
Fscn1	10.000	2.427	9.112	8.090E-20	1.644E-18
Fam214a	5.715	3.017	9.077	1.120E-19	2.267E-18
Cpne4	6.191	2.677	8.809	1.264E-18	2.456E-17
Erbb3	22.192	1.827	8.678	4.029E-18	7.610E-17
Sertad1	5.273	3.219	8.669	4.367E-18	8.197E-17
Usp53	5.278	2.413	8.665	4.531E-18	8.468E-17
Cdh1	17.249	2.097	8.647	5.269E-18	9.813E-17
Slc4a8	13.716	2.869	8.641	5.591E-18	1.038E-16
Inf2	12.312	2.138	8.484	2.172E-17	3.989E-16
Egr2	9.327	3.866	8.423	3.677E-17	6.687E-16
Pnrc1	5.159	2.176	8.410	4.092E-17	7.390E-16
Hmcn1	9.112	2.555	8.298	1.060E-16	1.889E-15
Clasp2	17.863	1.623	8.257	1.488E-16	2.634E-15
Hspa1b	5.479	3.023	8.218	2.064E-16	3.631E-15
Myc	11.202	2.442	8.021	1.049E-15	1.809E-14
Anxa1	10.648	2.033	7.971	1.579E-15	2.715E-14
Slc5a3	6.741	2.429	7.959	1.733E-15	2.970E-14
Capn6	7.353	2.810	7.953	1.825E-15	3.107E-14
Stard13	7.208	2.467	7.919	2.385E-15	4.036E-14
Myo1b	8.792	1.953	7.869	3.572E-15	6.024E-14
Rnf213	7.330	3.203	7.856	3.960E-15	6.658E-14
Zbtb20	22.953	1.899	7.798	6.288E-15	1.044E-13
Ier2	7.101	2.420	7.767	8.014E-15	1.323E-13
Klf4	6.010	2.633	7.719	1.175E-14	1.934E-13
Btg2	7.464	3.094	7.701	1.354E-14	2.214E-13
Fam102a	9.421	1.907	7.669	1.732E-14	2.815E-13
Cdc14a	11.719	1.851	7.629	2.357E-14	3.786E-13
Crip2	8.638	2.539	7.600	2.956E-14	4.719E-13
Ifrd1	9.497	2.103	7.547	4.462E-14	7.039E-13
Nfia	8.908	1.888	7.480	7.420E-14	1.154E-12
Anxa11	5.587	1.984	7.444	9.776E-14	1.516E-12
Brd2	28.751	1.508	7.435	1.043E-13	1.613E-12
Stat3	29.849	1.711	6.988	2.792E-12	3.952E-11
Mafk	5.844	2.550	6.968	3.225E-12	4.540E-11
Klf7	7.189	2.030	6.951	3.637E-12	5.081E-11
Ccnl1	10.458	1.676	6.929	4.225E-12	5.872E-11
Slc6a17	45.641	1.571	6.893	5.453E-12	7.558E-11
Lbh	21.268	1.417	6.884	5.799E-12	8.017E-11
Cttnbp2nl	11.579	1.797	6.850	7.367E-12	1.011E-10
Ncor2	17.038	1.553	6.806	1.003E-11	1.362E-10
Pvr	5.351	2.350	6.652	2.884E-11	3.811E-10

Wee1	5.202	2.350	6.628	3.397E-11	4.477E-10
Timp2	10.524	1.875	6.487	8.731E-11	1.126E-09
Txnip	9.183	2.174	6.451	1.109E-10	1.426E-09
Dnajb1	11.202	1.779	6.412	1.437E-10	1.831E-09
Gpx3	6.039	3.123	6.193	5.910E-10	7.355E-09
Prickle1	7.362	1.856	6.190	6.001E-10	7.452E-09
Cdh3	60.078	1.266	6.170	6.829E-10	8.420E-09
Stat2	5.309	2.221	6.118	9.458E-10	1.158E-08
Btg1	7.001	1.619	6.115	9.681E-10	1.183E-08
Ablim1	12.355	2.270	6.093	1.106E-09	1.342E-08
Tns2	5.817	2.340	6.067	1.307E-09	1.579E-08
Dclk2	9.641	1.950	6.024	1.701E-09	2.037E-08
Igf1r	11.076	1.730	5.911	3.397E-09	3.978E-08
Helz2	6.337	2.692	5.857	4.726E-09	5.487E-08
Foxo3	24.108	1.376	5.846	5.025E-09	5.809E-08
Arhgap39	6.371	1.858	5.841	5.192E-09	5.989E-08
Olfm1	6.949	1.879	5.839	5.262E-09	6.056E-08
Clk1	11.442	1.376	5.832	5.469E-09	6.268E-08
Klf5	6.257	2.215	5.829	5.574E-09	6.375E-08
Mtss1l	6.919	1.786	5.787	7.150E-09	8.092E-08
Syne2	14.479	1.781	5.773	7.800E-09	8.789E-08
Ctdsp2	14.459	1.432	5.740	9.495E-09	1.068E-07
Daam1	8.305	1.483	5.680	1.349E-08	1.508E-07
Abl2	6.802	2.083	5.662	1.498E-08	1.660E-07
Dusp10	6.494	2.063	5.629	1.817E-08	1.997E-07
Tra2a	6.074	1.552	5.607	2.059E-08	2.254E-07
Bahcc1	5.375	1.878	5.554	2.787E-08	3.002E-07
Cspg4	7.698	2.330	5.542	2.998E-08	3.223E-07
Eng	8.673	1.821	5.529	3.222E-08	3.436E-07
Osmr	6.130	2.552	5.478	4.307E-08	4.557E-07
Vamp2	7.659	1.627	5.469	4.532E-08	4.785E-07
B2m	23.617	1.278	5.468	4.558E-08	4.803E-07
Filip1l	5.907	1.956	5.397	6.786E-08	7.009E-07
Zfp521	8.923	1.716	5.351	8.742E-08	8.966E-07
Kdm6b	7.158	1.666	5.331	9.764E-08	9.938E-07
Ythdc1	5.326	1.649	5.317	1.053E-07	1.064E-06
Ankrd28	14.394	1.524	5.274	1.335E-07	1.334E-06
Rnd3	8.430	1.701	5.171	2.334E-07	2.310E-06
Fam129b	6.100	1.888	5.169	2.352E-07	2.324E-06
Rasa3	11.601	1.362	5.081	3.749E-07	3.650E-06
Eci2	7.965	1.373	5.073	3.907E-07	3.790E-06
Nfatc1	7.280	1.811	4.963	6.952E-07	6.612E-06
Slc41a1	8.065	1.898	4.955	7.220E-07	6.855E-06
Aff3	16.673	1.383	4.936	7.963E-07	7.534E-06

Foxk1	7.176	1.524	4.927	8.361E-07	7.895E-06
Lama3	6.114	2.287	4.920	8.644E-07	8.134E-06
Foxo4	5.458	1.777	4.905	9.325E-07	8.754E-06
Ncald	7.217	1.611	4.847	1.254E-06	1.161E-05
Ski	12.056	1.396	4.797	1.613E-06	1.481E-05
Nedd9	6.563	1.973	4.787	1.690E-06	1.549E-05
Sept8	18.038	1.331	4.762	1.917E-06	1.752E-05
Tor1aip1	5.699	1.584	4.698	2.623E-06	2.376E-05
Il6st	21.783	1.380	4.697	2.637E-06	2.385E-05
Slc15a4	8.742	1.445	4.635	3.565E-06	3.187E-05
Dennd1a	8.696	1.508	4.564	5.023E-06	4.431E-05
Timp3	14.275	1.844	4.537	5.693E-06	4.965E-05
Myo1e	8.208	1.457	4.523	6.101E-06	5.287E-05
Ano1	12.236	1.565	4.473	7.699E-06	6.566E-05
Itpr3	5.611	1.854	4.469	7.847E-06	6.670E-05
Dock5	12.603	1.368	4.437	9.116E-06	7.689E-05
Rnf31	6.219	1.675	4.388	1.142E-05	9.498E-05
Klhl21	10.514	1.412	4.388	1.144E-05	9.498E-05
Fosl2	17.573	1.658	4.354	1.337E-05	1.098E-04
Nr3c1	5.191	1.569	4.341	1.416E-05	1.153E-04
Akap8l	5.709	1.570	4.337	1.448E-05	1.176E-04
Chd6	12.734	1.328	4.323	1.542E-05	1.248E-04
Litaf	18.740	1.307	4.302	1.691E-05	1.364E-04
Gm47283	6.433	1.381	4.300	1.706E-05	1.374E-04
Mcl1	11.317	1.318	4.278	1.883E-05	1.514E-04
Sorbs1	14.388	1.279	4.187	2.830E-05	2.236E-04
Tnrc18	14.104	1.309	4.170	3.050E-05	2.395E-04
Rela	6.669	1.430	4.087	4.373E-05	3.366E-04
Tnrc6c	6.356	1.428	4.082	4.460E-05	3.428E-04
Srsf7	6.870	1.374	4.073	4.640E-05	3.555E-04
Mef2d	12.239	1.299	4.049	5.143E-05	3.919E-04
Eif1a	6.534	1.475	3.992	6.563E-05	4.958E-04
Zfp592	7.696	1.435	3.990	6.613E-05	4.989E-04
Ppp1r10	9.347	1.376	3.972	7.119E-05	5.333E-04
Numa1	15.785	1.224	3.868	1.097E-04	7.963E-04
Cavin1	8.194	1.474	3.854	1.162E-04	8.415E-04
Atf4	7.262	1.263	3.788	1.516E-04	1.088E-03
Prag1	6.107	1.537	3.753	1.751E-04	1.241E-03
Zc3hav1	12.967	1.283	3.750	1.767E-04	1.251E-03
Ptprj	33.028	1.145	3.740	1.843E-04	1.299E-03
Kmt2a	13.513	1.221	3.718	2.005E-04	1.406E-03
Serinc3	9.546	1.273	3.700	2.159E-04	1.502E-03
Tmbim1	11.073	1.330	3.699	2.166E-04	1.505E-03
Nfya	6.135	1.459	3.572	3.544E-04	2.413E-03

Hnrnph1	15.127	1.134	3.488	4.858E-04	3.266E-03
Tcaf1	6.691	1.477	3.485	4.925E-04	3.306E-03
Rsrp1	21.051	1.157	3.473	5.146E-04	3.442E-03
Nfat5	15.487	1.245	3.408	6.549E-04	4.342E-03
Inpp4a	6.688	1.359	3.384	7.140E-04	4.716E-03
Zfp36l1	16.266	1.154	3.360	7.782E-04	5.115E-03
Tmem94	10.442	1.263	3.317	9.111E-04	5.938E-03
Slc39a14	7.862	1.337	3.306	9.452E-04	6.145E-03
Trp53inp1	6.008	1.486	3.304	9.527E-04	6.187E-03
Nop58	5.996	1.297	3.303	9.578E-04	6.205E-03
Cd200	7.151	1.318	3.287	1.012E-03	6.537E-03
Arhgap21	6.993	1.300	3.281	1.035E-03	6.678E-03
Srsf5	18.657	1.085	3.264	1.098E-03	7.063E-03
St5	7.452	1.270	3.263	1.104E-03	7.091E-03
Ccnl2	16.447	1.134	3.200	1.376E-03	8.674E-03
Tmem2	7.672	1.473	3.159	1.584E-03	9.847E-03
Klhl24	8.578	1.203	3.157	1.596E-03	9.906E-03
Flrt3	6.383	1.445	3.080	2.071E-03	1.273E-02
Ccnt1	7.306	1.292	3.071	2.132E-03	1.307E-02
Ak3	14.646	1.119	3.069	2.150E-03	1.316E-02
Gnb4	5.303	1.280	3.047	2.314E-03	1.406E-02
Ezh1	5.726	1.302	3.041	2.360E-03	1.430E-02
Insr	7.007	1.263	3.029	2.457E-03	1.484E-02
Lrch3	9.251	1.200	3.013	2.587E-03	1.559E-02
Cic	17.692	1.110	2.961	3.063E-03	1.815E-02
Nsmf	5.126	1.337	2.917	3.533E-03	2.069E-02
Emp1	7.833	1.478	2.885	3.916E-03	2.266E-02
Dclk1	9.563	1.179	2.871	4.089E-03	2.358E-02
Plp1	29.369	1.143	2.812	4.918E-03	2.810E-02
Stat5a	7.246	1.260	2.807	4.998E-03	2.849E-02
Atf7	17.632	1.090	2.767	5.650E-03	3.178E-02
Stau1	8.643	1.153	2.748	5.993E-03	3.355E-02
Epc1	6.668	1.167	2.737	6.198E-03	3.452E-02
Rnf38	12.356	1.085	2.733	6.268E-03	3.486E-02
Cdk19	6.028	1.246	2.714	6.645E-03	3.671E-02
Vezf1	7.955	1.094	2.692	7.096E-03	3.912E-02
Gjc3	10.614	1.225	2.679	7.388E-03	4.060E-02
Cttnbp2	18.389	1.099	2.662	7.769E-03	4.256E-02
Gprc5b	5.951	1.276	2.644	8.192E-03	4.461E-02
Shc1	11.063	1.102	2.622	8.741E-03	4.726E-02

"Differentiation" Genes

Gene Name	baseMean	log2FoldChange	stat	pvalue	padj
Me1	5.949	-5.294	-28.378	3.787E-177	2.031E-173
Bmp7	7.113	-5.577	-27.983	2.625E-172	7.041E-169
Rab38	36.135	-4.501	-26.439	4.863E-154	8.695E-151
Fndc1	9.192	-5.408	-25.460	5.484E-143	7.354E-140
Krt31	10.680	-6.277	-25.386	3.570E-142	3.830E-139
Atp6v0d2	9.338	-5.567	-23.772	6.498E-125	5.809E-122
Tchh	5.797	-5.407	-23.695	4.057E-124	3.109E-121
Oca2	73.716	-5.738	-23.009	3.827E-117	2.566E-114
Krt35	7.450	-5.714	-22.051	9.300E-108	3.563E-105
Mlana	78.767	-3.484	-21.930	1.338E-106	4.784E-104
S100a1	13.154	-3.692	-21.830	1.205E-105	4.041E-103
Eps8	16.445	-4.366	-21.599	1.855E-103	5.527E-101
Krt87	6.819	-5.424	-20.750	1.215E-95	3.104E-93
Krt33a	5.928	-5.357	-20.731	1.815E-95	4.426E-93
Slc24a4	54.551	-4.934	-20.699	3.569E-95	7.976E-93
Col3a1	26.434	-7.492	-20.555	7.012E-94	1.504E-91
Trpm1	470.363	-3.906	-20.388	2.136E-92	4.407E-90
Slc24a5	62.002	-3.529	-19.983	7.690E-89	1.375E-86
Gja1	26.626	-4.017	-19.917	2.908E-88	5.031E-86
Krt71	6.121	-5.217	-19.713	1.655E-86	2.774E-84
Scrn1	10.022	-4.123	-19.484	1.491E-84	2.423E-82
Krtap8-1	5.647	-5.312	-19.471	1.920E-84	3.029E-82
Col1a1	29.560	-7.414	-19.329	3.076E-83	4.715E-81
Mc1r	58.927	-3.712	-18.263	1.645E-74	1.961E-72
Sparc	33.357	-3.393	-18.260	1.720E-74	2.006E-72
Dsp	10.583	-4.554	-18.124	2.074E-73	2.367E-71
Gapdh	62.801	-2.257	-18.009	1.664E-72	1.860E-70
Tyr	327.912	-2.814	-17.829	4.215E-71	4.522E-69
Krt73	5.689	-5.211	-17.535	7.798E-69	8.044E-67
Robo1	8.976	-3.526	-17.091	1.721E-65	1.678E-63
Slc7a8	65.248	-3.265	-17.021	5.784E-65	5.540E-63
Kif26b	36.268	-3.598	-16.540	1.906E-61	1.649E-59
Dlx3	5.215	-4.722	-16.402	1.854E-60	1.554E-58
Gfra1	5.868	-4.122	-16.363	3.524E-60	2.908E-58
Col1a2	14.692	-6.142	-16.015	1.009E-57	7.840E-56
Gpr143	14.238	-3.331	-15.747	7.180E-56	5.135E-54
Nrp2	5.385	-4.903	-15.306	6.981E-53	4.623E-51
Id2	13.214	-2.803	-15.158	6.689E-52	4.323E-50
Lama5	5.635	-5.205	-14.368	8.227E-47	4.903E-45
Ttc3	67.474	-2.118	-14.253	4.289E-46	2.528E-44
Ftl1	162.927	-1.893	-14.239	5.217E-46	3.042E-44

Dsc3	5.922	-4.197	-13.999	1.590E-44	8.990E-43
Loxl2	20.701	-3.680	-13.998	1.592E-44	8.990E-43
B3galt5	11.790	-3.401	-13.983	1.971E-44	1.101E-42
Wfs1	8.342	-3.715	-13.930	4.162E-44	2.302E-42
4931406C07Rik	13.232	-2.813	-13.831	1.654E-43	8.962E-42
Egfr	5.205	-4.316	-13.640	2.309E-42	1.214E-40
Tinagl1	10.895	-3.096	-13.528	1.074E-41	5.540E-40
Specc1	14.288	-2.797	-13.432	3.927E-41	1.969E-39
Epdr1	13.579	-2.807	-13.401	5.986E-41	2.946E-39
Bgn	7.995	-5.474	-13.263	3.806E-40	1.823E-38
Ctsd	69.512	-2.004	-13.179	1.160E-39	5.506E-38
Epb41	14.444	-2.665	-13.165	1.404E-39	6.604E-38
Slc45a2	73.810	-2.445	-13.019	9.590E-39	4.397E-37
Tyrp1	461.225	-2.095	-12.950	2.353E-38	1.061E-36
Myef2	12.641	-2.907	-12.942	2.606E-38	1.165E-36
Smpd1	12.130	-2.938	-12.815	1.352E-37	5.944E-36
Proser2	7.199	-2.960	-12.547	4.149E-36	1.766E-34
Eogt	26.872	-2.554	-12.533	4.917E-36	2.077E-34
Slc7a5	71.064	-2.437	-12.510	6.544E-36	2.742E-34
S1pr3	8.031	-3.958	-12.336	5.813E-35	2.344E-33
Ftl1-ps1	8.377	-2.060	-12.326	6.602E-35	2.643E-33
Psd3	5.579	-3.063	-12.321	6.987E-35	2.776E-33
Emp3	10.328	-2.378	-12.296	9.522E-35	3.755E-33
Lef1	6.964	-2.919	-12.255	1.587E-34	6.212E-33
Sema6d	24.896	-2.906	-12.222	2.384E-34	9.268E-33
Trp63	5.212	-4.120	-12.130	7.339E-34	2.792E-32
Mcc	9.669	-2.838	-12.118	8.457E-34	3.195E-32
Fstl1	5.362	-4.553	-12.040	2.192E-33	8.165E-32
Lpl	6.379	-3.075	-11.904	1.125E-32	4.023E-31
Aldoa	47.755	-2.082	-11.884	1.437E-32	5.070E-31
Ero1l	10.928	-2.852	-11.717	1.039E-31	3.527E-30
Calm1	36.639	-1.935	-11.560	6.588E-31	2.209E-29
Ccnd2	20.798	-2.467	-11.555	6.974E-31	2.324E-29
B4galt6	8.246	-2.522	-11.373	5.723E-30	1.849E-28
Pmel	828.372	-2.105	-11.137	8.312E-29	2.533E-27
Gne	13.552	-2.593	-11.135	8.428E-29	2.554E-27
Ctsh	9.624	-2.715	-11.134	8.583E-29	2.586E-27
mt-Nd1	223.043	-1.550	-11.093	1.363E-28	4.085E-27
Perp	9.169	-3.038	-10.982	4.661E-28	1.374E-26
Ptgds	168.727	-2.040	-10.882	1.401E-27	4.085E-26
Eno1	26.851	-2.102	-10.842	2.166E-27	6.246E-26
Rab32	8.393	-2.419	-10.774	4.572E-27	1.298E-25
Cd63	67.943	-1.663	-10.675	1.329E-26	3.676E-25
Fam210b	12.248	-2.360	-10.455	1.389E-25	3.689E-24

Adam10	28.836	-1.944	-10.441	1.605E-25	4.240E-24
Fbn1	11.778	-3.565	-10.399	2.515E-25	6.580E-24
Scd2	50.704	-2.024	-10.340	4.646E-25	1.192E-23
Atp6v0c	54.411	-1.601	-10.333	4.972E-25	1.270E-23
Pgam1	23.938	-1.956	-10.321	5.676E-25	1.443E-23
Pgk1	11.107	-2.153	-10.319	5.773E-25	1.461E-23
Txn1	10.913	-1.831	-10.217	1.669E-24	4.164E-23
Sfn	10.965	-3.161	-10.154	3.186E-24	7.840E-23
Trim29	6.449	-3.280	-10.128	4.167E-24	1.021E-22
Col6a3	7.149	-5.552	-9.998	1.558E-23	3.781E-22
G6pdx	7.145	-2.375	-9.940	2.786E-23	6.641E-22
Apold1	9.352	-2.445	-9.845	7.215E-23	1.683E-21
Car13	7.446	-2.520	-9.823	8.963E-23	2.081E-21
Ednrb	160.843	-1.774	-9.753	1.797E-22	4.103E-21
Soat1	8.138	-2.511	-9.693	3.233E-22	7.318E-21
Slc26a2	18.917	-2.334	-9.636	5.622E-22	1.251E-20
Mknk2	22.897	-1.958	-9.596	8.346E-22	1.850E-20
Gpr155	6.808	-2.788	-9.520	1.726E-21	3.778E-20
Bop1	15.551	-2.052	-9.439	3.765E-21	8.144E-20
Cyb5a	21.648	-1.749	-9.416	4.701E-21	1.013E-19
Ldha	43.659	-1.825	-9.289	1.556E-20	3.299E-19
Gstp1	103.798	-1.575	-9.115	7.839E-20	1.599E-18
Nckap5l	15.147	-1.938	-8.987	2.545E-19	5.074E-18
Emc8	9.628	-2.107	-8.974	2.850E-19	5.640E-18
Creg1	10.504	-2.168	-8.966	3.081E-19	6.076E-18
Igfbp4	5.085	-4.113	-8.955	3.386E-19	6.654E-18
Slc3a2	83.950	-1.639	-8.707	3.107E-18	5.889E-17
Prelid1	16.312	-1.704	-8.669	4.370E-18	8.197E-17
Lrp1	12.162	-3.558	-8.635	5.886E-18	1.089E-16
Npy	10.879	-2.297	-8.447	2.986E-17	5.448E-16
Pgam1-ps2	6.857	-2.107	-8.227	1.918E-16	3.384E-15
Nkd1	9.290	-2.237	-8.102	5.403E-16	9.349E-15
Lss	8.077	-2.181	-7.929	2.217E-15	3.763E-14
Ltbp4	5.401	-3.258	-7.840	4.497E-15	7.538E-14
Gng12	24.117	-1.614	-7.802	6.096E-15	1.016E-13
Fdps	9.143	-1.860	-7.650	2.012E-14	3.250E-13
Tfeb	17.831	-1.915	-7.592	3.146E-14	4.992E-13
Tnfrsf19	14.755	-2.019	-7.521	5.427E-14	8.536E-13
Postn	7.107	-3.890	-7.381	1.568E-13	2.389E-12
Met	31.235	-1.834	-7.376	1.632E-13	2.480E-12
mt-Nd2	39.935	-1.301	-7.275	3.461E-13	5.201E-12
Prdx1	27.925	-1.370	-7.219	5.242E-13	7.762E-12
mt-Nd5	205.636	-1.218	-7.205	5.815E-13	8.569E-12
Washc5	16.790	-1.650	-7.201	5.957E-13	8.754E-12

Pkm	29.267	-1.517	-7.092	1.318E-12	1.905E-11
Tnxb	5.156	-5.057	-7.021	2.202E-12	3.150E-11
Slc6a8	6.586	-1.954	-7.019	2.238E-12	3.193E-11
Adi1	16.713	-1.644	-7.006	2.454E-12	3.492E-11
Spg21	19.176	-1.521	-6.986	2.835E-12	4.002E-11
Jup	14.395	-2.011	-6.964	3.317E-12	4.658E-11
Ccser2	21.049	-1.657	-6.950	3.662E-12	5.102E-11
Lgals1	6.284	-1.812	-6.820	9.083E-12	1.237E-10
Ccnd1	6.354	-2.042	-6.801	1.041E-11	1.410E-10
Ptprf	10.028	-2.358	-6.798	1.060E-11	1.432E-10
Plxna1	21.205	-1.631	-6.769	1.294E-11	1.722E-10
Ptprs	37.029	-1.638	-6.702	2.051E-11	2.724E-10
Tacc1	62.024	-1.356	-6.679	2.407E-11	3.188E-10
Adgrl2	13.760	-1.639	-6.567	5.119E-11	6.730E-10
Fdft1	8.117	-1.868	-6.549	5.802E-11	7.573E-10
Atp5g3	12.941	-1.392	-6.507	7.650E-11	9.911E-10
Ago2	51.360	-1.372	-6.444	1.160E-10	1.489E-09
Tpi1	10.961	-1.542	-6.319	2.628E-10	3.325E-09
Acat2	5.603	-1.848	-6.310	2.788E-10	3.518E-09
mt-Nd4	83.133	-1.123	-6.180	6.400E-10	7.928E-09
Dpp7	11.172	-1.664	-6.084	1.175E-09	1.423E-08
Ctsb	55.171	-1.295	-6.065	1.320E-09	1.592E-08
Mylip	12.773	-1.708	-5.978	2.266E-09	2.677E-08
Naa60	6.304	-1.671	-5.960	2.520E-09	2.964E-08
Hr	5.416	-2.044	-5.891	3.843E-09	4.491E-08
Selenop	127.818	-1.279	-5.806	6.383E-09	7.269E-08
Cotl1	10.640	-1.551	-5.803	6.514E-09	7.403E-08
Atp6v1b2	46.930	-1.372	-5.800	6.615E-09	7.501E-08
Gjb2	11.511	-1.873	-5.636	1.743E-08	1.920E-07
Etv5	7.721	-1.741	-5.622	1.892E-08	2.076E-07
Atp6v1a	15.943	-1.463	-5.595	2.210E-08	2.409E-07
Mboat2	6.299	-1.677	-5.541	3.013E-08	3.232E-07
Akr1a1	45.817	-1.198	-5.539	3.038E-08	3.253E-07
Cux1	21.847	-1.447	-5.478	4.304E-08	4.557E-07
Cyfip2	8.078	-1.751	-5.460	4.754E-08	4.980E-07
Calr	34.881	-1.320	-5.419	5.980E-08	6.229E-07
Mmp2	5.926	-2.063	-5.411	6.258E-08	6.506E-07
Serp1	12.474	-1.477	-5.407	6.398E-08	6.638E-07
Nhs	7.542	-1.756	-5.378	7.539E-08	7.762E-07
mt-Co3	44.223	-1.716	-5.328	9.922E-08	1.008E-06
Uqcrq	5.475	-1.439	-5.236	1.645E-07	1.637E-06
Mapk6	13.518	-1.407	-5.223	1.757E-07	1.742E-06
Atp13a2	10.091	-1.578	-5.132	2.867E-07	2.816E-06
Xpo6	11.874	-1.433	-5.021	5.129E-07	4.948E-06

Ctsl	21.312	-1.445	-5.013	5.360E-07	5.153E-06
Npc1	22.438	-1.301	-4.979	6.404E-07	6.112E-06
Mfsd14b	15.041	-1.405	-4.970	6.687E-07	6.371E-06
Dhcr24	16.468	-1.418	-4.946	7.581E-07	7.184E-06
Nfatc2	7.994	-1.763	-4.863	1.154E-06	1.071E-05
Acaca	10.710	-1.522	-4.823	1.417E-06	1.304E-05
Gdi2	22.631	-1.222	-4.693	2.692E-06	2.427E-05
Ndufa4	5.170	-1.279	-4.571	4.858E-06	4.293E-05
Hmga1	10.756	-1.465	-4.562	5.073E-06	4.461E-05
Fn1	9.239	-2.358	-4.554	5.257E-06	4.608E-05
Plxna4	6.144	-1.731	-4.535	5.759E-06	5.006E-05
Tpp1	21.024	-1.229	-4.489	7.147E-06	6.134E-05
Ptprg	11.195	-1.473	-4.487	7.234E-06	6.183E-05
Ttyh3	5.029	-1.635	-4.462	8.133E-06	6.892E-05
Gabarap	21.998	-1.116	-4.427	9.567E-06	8.043E-05
Mdh1	6.828	-1.360	-4.426	9.615E-06	8.071E-05
Nadk	11.516	-1.393	-4.412	1.026E-05	8.588E-05
Igsf8	17.897	-1.310	-4.373	1.225E-05	1.011E-04
Anxa2	29.325	-1.236	-4.367	1.258E-05	1.035E-04
Mtpn	21.234	-1.236	-4.354	1.339E-05	1.098E-04
Cox6b1	5.866	-1.234	-4.351	1.353E-05	1.106E-04
Efnb1	5.009	-2.022	-4.334	1.467E-05	1.190E-04
Cox5b	8.944	-1.204	-4.253	2.111E-05	1.690E-04
Itm2c	7.761	-1.370	-4.239	2.244E-05	1.791E-04
Tspan10	32.480	-1.390	-4.166	3.103E-05	2.433E-04
Peg3	8.251	-2.372	-4.125	3.715E-05	2.892E-04
Fads1	10.290	-1.381	-4.070	4.706E-05	3.601E-04
Sec14l1	12.947	-1.382	-4.054	5.034E-05	3.841E-04
Ssbp4	8.985	-1.330	-3.959	7.529E-05	5.609E-04
Mgll	68.724	-1.176	-3.928	8.574E-05	6.326E-04
Plxna2	7.974	-1.610	-3.927	8.613E-05	6.347E-04
Pdia3	24.662	-1.209	-3.909	9.280E-05	6.810E-04
Pfn1	35.810	-1.125	-3.908	9.323E-05	6.831E-04
App	22.469	-1.140	-3.778	1.582E-04	1.133E-03
Flnb	9.753	-1.431	-3.767	1.652E-04	1.175E-03
Gpi1	19.997	-1.159	-3.758	1.714E-04	1.218E-03
Abhd2	18.951	-1.304	-3.745	1.803E-04	1.274E-03
Gpr137b	11.732	-1.257	-3.740	1.838E-04	1.298E-03
Bzw1	9.641	-1.240	-3.715	2.031E-04	1.422E-03
Aars	7.855	-1.290	-3.700	2.158E-04	1.502E-03
Frmd4a	24.534	-1.182	-3.606	3.109E-04	2.130E-03
Celsr2	6.953	-1.415	-3.510	4.481E-04	3.027E-03
Morf4l2	16.372	-1.181	-3.475	5.103E-04	3.417E-03
Megf9	6.859	-1.326	-3.390	6.998E-04	4.629E-03

Zfp266	11.279	-1.234	-3.337	8.460E-04	5.534E-03
Lpp	18.800	-1.131	-3.230	1.238E-03	7.857E-03
Krt5	5.730	-1.678	-3.209	1.330E-03	8.412E-03
Cdc42	22.128	-1.042	-3.205	1.353E-03	8.546E-03
Ddah1	11.903	-1.220	-3.168	1.535E-03	9.575E-03
Mfsd12	7.110	-1.314	-3.136	1.711E-03	1.059E-02
Gspt1	6.550	-1.201	-3.073	2.121E-03	1.302E-02
Slc39a10	8.785	-1.389	-3.062	2.202E-03	1.344E-02
Cfap54	17.314	-1.230	-3.036	2.401E-03	1.454E-02
Insig1	17.378	-1.217	-3.007	2.641E-03	1.588E-02
Otub1	7.441	-1.171	-2.995	2.745E-03	1.649E-02
Slc25a39	15.061	-1.144	-2.987	2.816E-03	1.684E-02
Cs	21.474	-1.082	-2.928	3.408E-03	2.006E-02
Pcdhgc3	10.486	-1.216	-2.893	3.813E-03	2.213E-02
Rab1	18.843	-1.044	-2.844	4.454E-03	2.555E-02
Mif	8.297	-1.107	-2.806	5.018E-03	2.857E-02
Syt4	18.630	-1.244	-2.799	5.119E-03	2.909E-02
Bsg	24.524	-1.010	-2.633	8.472E-03	4.604E-02
Plekha8	6.048	-1.246	-2.632	8.499E-03	4.614E-02
Gns	21.955	-1.066	-2.617	8.883E-03	4.794E-02
Rab7	22.837	-1.002	-2.608	9.109E-03	4.910E-02

Table 3.1: Select List of Differentially Expressed Genes for *Bmpr1a* Null vs. Control Differentiating Progeny Cells from DESeq2 (see also Table S9 from Infarinato et al., 2020)
*All values shown to three decimal points, ranked by padj value

Control Genes

Gene Name	baseMean	log2FoldChange	stat	pvalue	padj
Id2	7.898	-2.607	-20.584	3.800E-94	4.750E-91
Itgb3	9.372	-3.995	-18.555	7.370E-77	3.070E-74
Kif26b	22.271	-2.274	-15.807	2.770E-56	5.780E-54
Atp6v0d2	12.111	-3.226	-15.632	4.400E-55	7.330E-53
B3galt5	7.955	-2.442	-15.612	6.000E-55	9.370E-53
Slc24a4	50.652	-2.280	-14.714	5.270E-49	7.330E-47
Slc37a2	8.526	-2.720	-14.670	9.980E-49	1.310E-46
Rab38	21.841	-1.725	-14.252	4.380E-46	5.480E-44
Parm1	2.326	-3.240	-13.491	1.770E-41	1.930E-39
Ephx1	5.849	-2.623	-13.370	9.020E-41	9.020E-39
Fam129a	5.488	-2.425	-13.018	9.660E-39	9.290E-37
Oca2	69.508	-1.912	-12.831	1.100E-37	9.840E-36
Sfrp4	4.848	-3.244	-12.337	5.710E-35	4.600E-33
Hhipl1	1.524	-3.046	-12.206	2.900E-34	2.190E-32
Epdr1	13.772	-1.658	-11.832	2.680E-32	1.810E-30
Egfl6	2.722	-2.916	-11.491	1.460E-30	8.920E-29
Apold1	13.615	-1.661	-11.442	2.590E-30	1.500E-28
Ttll7	2.910	-2.638	-11.292	1.440E-29	8.160E-28
Gpr143	14.902	-1.508	-11.177	5.310E-29	2.890E-27
Wfs1	5.356	-2.360	-10.721	8.080E-27	4.210E-25
Id3	5.860	-2.191	-10.518	7.100E-26	3.350E-24
Pla2g15	4.387	-1.887	-9.574	1.030E-21	4.210E-20
Smpd1	12.327	-1.580	-9.510	1.900E-21	7.540E-20
Plxna4	1.222	-3.025	-8.667	4.440E-18	1.530E-16
Rnf144b	2.481	-2.257	-8.467	2.510E-17	7.950E-16
Nr4a3	6.251	-1.794	-8.377	5.420E-17	1.670E-15
Trpm1	410.843	-1.289	-8.343	7.230E-17	2.200E-15
Me1	2.851	-1.923	-8.307	9.830E-17	2.960E-15
Tmem47	1.496	-2.443	-8.257	1.500E-16	4.390E-15
Eps8	24.224	-1.461	-8.256	1.510E-16	4.390E-15
Ptprs	37.340	-1.272	-8.218	2.070E-16	5.890E-15
Scrn1	8.310	-1.468	-7.804	5.970E-15	1.610E-13
Ctsd	92.539	-1.118	-7.748	9.330E-15	2.460E-13
Ogdhl	0.879	-2.868	-7.593	3.120E-14	7.640E-13
Tmem151a	0.765	-2.899	-7.473	7.850E-14	1.900E-12
Calm1	37.219	-1.060	-7.457	8.850E-14	2.130E-12
Olfm2	0.925	-2.755	-7.268	3.650E-13	8.300E-12

Pgm2l1	1.171	-2.379	-7.126	1.030E-12	2.260E-11
Tubb3	2.056	-1.950	-6.838	8.030E-12	1.660E-10
Amd1	10.791	-1.243	-6.828	8.600E-12	1.760E-10
Ero1l	10.216	-1.436	-6.756	1.420E-11	2.800E-10
Lgals3	15.866	-1.342	-6.461	1.040E-10	1.900E-09
Loxl2	17.896	-1.599	-6.382	1.740E-10	3.140E-09
Ninj1	4.505	-1.285	-6.330	2.450E-10	4.350E-09
Sec14l1	7.433	-1.351	-6.214	5.170E-10	8.970E-09
Plekha8	6.285	-1.364	-6.185	6.210E-10	1.060E-08
Emc8	11.706	-1.156	-5.923	3.160E-09	5.030E-08
Frmd4a	21.442	-1.087	-5.778	7.550E-09	1.170E-07
Shroom2	8.931	-1.218	-5.597	2.190E-08	3.230E-07
Slc45a2	78.717	-1.037	-5.559	2.720E-08	3.980E-07
Ddah1	2.459	-1.605	-5.493	3.950E-08	5.610E-07
Gpr137b	16.132	-1.182	-5.281	1.290E-07	1.750E-06
Tacc1	43.830	-0.995	-5.028	4.960E-07	6.110E-06
Mc1r	53.287	-1.080	-4.878	1.070E-06	1.250E-05
Skil	4.166	-1.332	-4.876	1.080E-06	1.260E-05
4930523C07Rik	10.536	-1.705	-4.761	1.920E-06	2.170E-05
Plxnd1	5.716	-1.286	-4.735	2.190E-06	2.440E-05
Akap6	1.449	-1.764	-4.691	2.710E-06	2.990E-05
Mtss1	5.542	-1.230	-4.689	2.750E-06	3.010E-05
Gsn	11.730	-1.243	-4.617	3.890E-06	4.140E-05
Npy	9.681	-1.182	-4.522	6.140E-06	6.290E-05
Xpo6	9.495	-1.097	-4.464	8.040E-06	8.100E-05
Fabp5	4.452	-1.220	-4.421	9.810E-06	9.690E-05
Asah1	14.842	-1.045	-4.395	1.110E-05	1.079E-04
Adam10	26.366	-1.012	-3.933	8.400E-05	7.371E-04
Slc26a2	9.977	-1.155	-3.914	9.090E-05	7.915E-04
Nav2	54.383	-0.994	-3.813	1.375E-04	1.146E-03
Ftl1	179.829	-0.879	-3.559	3.727E-04	2.958E-03
Slc7a11	4.459	-1.454	-3.547	3.894E-04	3.081E-03
Enpep	3.716	-1.274	-3.514	4.420E-04	3.431E-03
Tbx1	0.518	-1.854	-3.491	4.806E-04	3.697E-03
D7Ertd443e	2.432	-1.322	-3.311	9.304E-04	6.861E-03
Smchd1	8.656	-1.048	-3.239	1.200E-03	8.670E-03
Padi2	1.569	-1.592	-3.160	1.578E-03	1.108E-02
Insig1	18.165	-1.022	-3.161	1.575E-03	1.108E-02
Fech	8.357	-0.986	-3.105	1.904E-03	1.319E-02
Tyrp1	474.390	-0.927	-3.104	1.912E-03	1.320E-02
S1pr3	27.483	-1.061	-3.058	2.231E-03	1.503E-02
Tmem132d	0.499	-1.836	-2.800	5.108E-03	3.201E-02
Pitpnm2	3.461	-1.127	-2.686	7.239E-03	4.361E-02

***Bmpr1a* Null Genes**

Gene Name	baseMean	log2FoldChange	stat	pvalue	padj
Vim	41.870	2.468	22.621	2.690E-113	6.730E-110
Car14	5.486	3.521	20.562	6.070E-94	5.060E-91
Cdh1	23.571	2.339	18.910	9.470E-80	5.920E-77
Sulf2	15.571	2.393	18.618	2.280E-77	1.140E-74
Cspg4	5.915	4.153	18.240	2.470E-74	8.830E-72
1700086L19Rik	5.761	4.086	17.620	1.720E-69	5.360E-67
Col12a1	13.728	4.599	17.317	3.510E-67	9.760E-65
C4b	13.450	6.092	16.789	2.940E-63	7.350E-61
Dbpht2	3.081	4.278	16.684	1.710E-62	3.890E-60
Phgdh	5.198	2.552	15.764	5.540E-56	1.060E-53
Sema5a	4.369	3.898	15.759	5.910E-56	1.060E-53
Agrn	12.374	2.483	15.389	1.940E-53	2.850E-51
Idh2	12.882	1.618	13.927	4.340E-44	5.170E-42
Capn6	6.652	2.577	13.651	1.990E-42	2.260E-40
Adamtsl4	7.509	2.420	13.395	6.440E-41	6.710E-39
Abca1	5.798	2.886	12.965	1.940E-38	1.800E-36
Acvr1c	11.597	2.719	12.583	2.610E-36	2.250E-34
Itpr3	3.253	2.570	12.469	1.110E-35	9.230E-34
Enpp2	21.418	1.761	12.292	1.000E-34	7.850E-33
Rnf144a	4.315	2.100	12.142	6.300E-34	4.630E-32
Lama3	7.727	2.372	12.124	7.840E-34	5.600E-32
Hs3st1	2.320	3.097	12.097	1.090E-33	7.600E-32
Txnip	3.631	3.026	11.614	3.510E-31	2.310E-29
Rnf213	4.482	3.008	11.551	7.290E-31	4.670E-29
Hmgcs2	3.685	3.816	11.502	1.280E-30	8.010E-29
Nfia	5.247	1.887	11.454	2.250E-30	1.340E-28
Wscd1	3.625	2.521	11.241	2.580E-29	1.430E-27
Auts2	7.103	1.747	10.769	4.830E-27	2.570E-25
Rapgef3	1.315	3.088	10.708	9.300E-27	4.750E-25
Gab1	4.366	2.226	10.692	1.110E-26	5.560E-25
Kcnn4	0.913	3.109	10.616	2.520E-26	1.240E-24
Maob	3.121	2.768	10.594	3.180E-26	1.530E-24
Prex2	11.572	1.642	10.382	3.000E-25	1.380E-23
Erbb3	14.885	1.701	10.381	3.030E-25	1.380E-23
Cubn	5.085	2.195	10.219	1.620E-24	7.250E-23
Filip1l	4.492	2.053	10.141	3.650E-24	1.600E-22
Pde4b	2.728	2.453	10.014	1.320E-23	5.710E-22
Gsta4	2.230	2.260	9.895	4.370E-23	1.850E-21
Vcan	2.847	3.315	9.627	6.150E-22	2.560E-20
Adgrg1	13.468	2.053	9.564	1.130E-21	4.560E-20
Slc27a1	2.432	2.991	9.496	2.180E-21	8.500E-20

Fscn1	2.341	2.787	9.307	1.310E-20	5.040E-19
Wnk4	1.664	2.555	9.242	2.420E-20	9.180E-19
Afap1l2	1.410	3.000	9.164	5.000E-20	1.870E-18
Rnase4	2.219	3.543	9.114	7.940E-20	2.920E-18
Gm47865	4.150	1.794	9.072	1.170E-19	4.220E-18
Klf5	1.468	2.426	9.054	1.380E-19	4.920E-18
Serpinb1a	1.311	2.555	8.710	3.030E-18	1.070E-16
Gucy2f	2.720	2.998	8.666	4.480E-18	1.530E-16
Ctdsp2	7.578	1.483	8.662	4.640E-18	1.570E-16
Sema3a	1.531	2.664	8.606	7.570E-18	2.520E-16
Arhgef10l	1.448	2.774	8.554	1.190E-17	3.910E-16
Fam102a	5.116	1.656	8.509	1.760E-17	5.710E-16
Bcl9l	3.033	1.910	8.489	2.080E-17	6.660E-16
Hspa1b	3.275	3.321	8.404	4.320E-17	1.350E-15
Zfhx3	1.342	2.645	8.305	1.000E-16	2.980E-15
Plk2	2.921	1.940	8.220	2.030E-16	5.850E-15
Plec	17.394	1.500	8.051	8.200E-16	2.300E-14
Gjb2	5.957	1.687	8.021	1.050E-15	2.920E-14
Tcf7l2	1.123	2.041	7.892	2.990E-15	8.200E-14
Pde1c	5.223	1.853	7.856	3.960E-15	1.080E-13
Col1a1	4.946	3.267	7.778	7.380E-15	1.960E-13
Ptk7	2.567	2.004	7.718	1.180E-14	3.070E-13
Fbln2	2.507	2.198	7.699	1.380E-14	3.550E-13
Ahr	2.459	2.028	7.692	1.440E-14	3.690E-13
Card10	1.526	2.520	7.679	1.600E-14	4.050E-13
Pmp22	4.151	1.786	7.657	1.900E-14	4.760E-13
Pde3a	5.504	1.539	7.615	2.640E-14	6.540E-13
Appl2	8.504	1.380	7.420	1.170E-13	2.780E-12
Celsr2	3.589	1.761	7.411	1.250E-13	2.960E-12
Iqgap2	4.866	1.548	7.367	1.740E-13	4.080E-12
Gad1	0.817	3.027	7.362	1.810E-13	4.190E-12
Lpin1	3.601	1.675	7.322	2.440E-13	5.590E-12
H2-K1	5.397	1.619	7.218	5.270E-13	1.190E-11
Timp3	2.150	2.474	7.172	7.380E-13	1.650E-11
Cdk6	1.303	2.592	7.150	8.700E-13	1.920E-11
Ifitm3	1.573	1.984	7.100	1.250E-12	2.720E-11
Tnfrsf21	0.991	3.194	7.047	1.830E-12	3.950E-11
Prickle1	4.690	1.708	6.984	2.870E-12	6.120E-11
Arsi	0.796	3.002	6.981	2.930E-12	6.210E-11
Ahnak	72.999	1.350	6.881	5.940E-12	1.250E-10
Notch1	14.054	1.435	6.852	7.280E-12	1.520E-10
St5	6.023	1.386	6.811	9.670E-12	1.970E-10
Dsp	1.614	3.327	6.788	1.140E-11	2.290E-10
Lrp5	3.248	1.680	6.773	1.260E-11	2.520E-10

Hspg2	8.690	1.654	6.771	1.280E-11	2.540E-10
Prelp	5.479	1.617	6.708	1.970E-11	3.850E-10
Igfbp4	1.270	3.135	6.704	2.030E-11	3.930E-10
Abcg1	1.003	2.785	6.688	2.260E-11	4.340E-10
Shisa2	0.884	2.233	6.682	2.360E-11	4.510E-10
Fam129b	1.931	1.852	6.664	2.660E-11	5.030E-10
Dhrs3	1.341	2.399	6.637	3.200E-11	6.020E-10
Zbtb20	10.713	1.444	6.563	5.280E-11	9.860E-10
Crybg1	1.260	2.835	6.510	7.540E-11	1.400E-09
Lrp1	3.141	2.712	6.476	9.420E-11	1.730E-09
Fgfr1	1.882	2.001	6.423	1.340E-10	2.420E-09
Nfib	5.165	1.346	6.359	2.030E-10	3.620E-09
Trdmt1	1.488	1.774	6.271	3.580E-10	6.300E-09
Hspa1a	3.635	2.941	6.244	4.260E-10	7.450E-09
Igf1r	2.761	1.636	6.211	5.280E-10	9.100E-09
Dcn	1.150	2.938	6.205	5.470E-10	9.370E-09
Ucp2	3.658	2.103	6.173	6.720E-10	1.130E-08
Jup	4.439	1.844	6.124	9.100E-10	1.530E-08
Gm47316	2.082	1.671	6.048	1.470E-09	2.440E-08
Cd82	1.799	1.710	6.031	1.630E-09	2.700E-08
Junb	3.315	1.945	6.014	1.810E-09	2.980E-08
Rnase1	1.255	2.319	6.012	1.830E-09	2.990E-08
Ptprf	1.632	2.933	5.991	2.080E-09	3.380E-08
Ehd2	1.041	2.368	5.964	2.470E-09	3.980E-08
Pik3ip1	0.891	2.176	5.959	2.530E-09	4.060E-08
Krt5	1.009	3.083	5.907	3.490E-09	5.520E-08
Col3a1	3.896	2.566	5.846	5.040E-09	7.920E-08
A230050P20Rik	1.318	2.087	5.802	6.560E-09	1.030E-07
Sgsh	0.813	2.365	5.782	7.360E-09	1.140E-07
Bmp1	2.241	1.655	5.765	8.150E-09	1.250E-07
Nfix	0.649	2.230	5.758	8.500E-09	1.300E-07
Arrb1	0.907	2.675	5.744	9.260E-09	1.400E-07
Rnd3	2.944	1.609	5.701	1.190E-08	1.800E-07
AW011738	2.570	1.708	5.648	1.620E-08	2.430E-07
Igsf3	7.390	1.242	5.601	2.130E-08	3.170E-07
Zfp469	1.559	2.047	5.561	2.680E-08	3.930E-07
Pax3	34.639	1.058	5.553	2.820E-08	4.090E-07
Gucy1b1	1.986	1.937	5.542	2.990E-08	4.320E-07
Perp	1.134	2.988	5.537	3.080E-08	4.430E-07
Tnrc18	6.437	1.283	5.532	3.160E-08	4.510E-07
Sox6	8.240	1.215	5.422	5.880E-08	8.300E-07
H2-T23	1.079	1.969	5.399	6.700E-08	9.410E-07
Egfr	1.329	3.040	5.375	7.650E-08	1.070E-06
Rgmb	3.530	1.373	5.359	8.350E-08	1.160E-06

Zfp36	2.569	1.793	5.317	1.060E-07	1.460E-06
Bgn	0.903	2.570	5.314	1.070E-07	1.470E-06
Myh14	1.230	1.826	5.295	1.190E-07	1.630E-06
Syne2	4.936	1.554	5.267	1.380E-07	1.870E-06
Phip	3.318	1.433	5.265	1.410E-07	1.890E-06
Wdr6	13.267	1.180	5.256	1.470E-07	1.960E-06
Thbs2	1.044	2.780	5.256	1.470E-07	1.960E-06
Krt17	1.184	3.411	5.245	1.560E-07	2.070E-06
Coq8a	2.480	1.579	5.236	1.650E-07	2.160E-06
H2-Q4	1.545	2.170	5.227	1.720E-07	2.260E-06
Olfml1	0.744	2.515	5.222	1.770E-07	2.300E-06
Zbtb44	1.564	1.683	5.214	1.850E-07	2.390E-06
Gas1	1.382	1.697	5.190	2.100E-07	2.710E-06
Col1a2	3.420	1.829	5.171	2.330E-07	2.980E-06
Inf2	6.419	1.256	5.165	2.400E-07	3.060E-06
Abca8a	1.121	2.029	5.160	2.470E-07	3.130E-06
Pik3c2b	0.682	2.381	5.156	2.520E-07	3.180E-06
Sfn	1.514	2.551	5.144	2.690E-07	3.380E-06
Dgka	0.803	2.101	5.121	3.040E-07	3.800E-06
Fos	18.196	1.695	5.109	3.240E-07	4.030E-06
Trim29	1.652	2.913	5.064	4.100E-07	5.080E-06
Slc43a3	0.748	2.049	5.013	5.370E-07	6.580E-06
Cntn1	0.766	2.492	5.011	5.410E-07	6.600E-06
Arnt2	6.599	1.223	5.009	5.460E-07	6.630E-06
Myo1b	7.567	1.148	4.969	6.740E-07	8.090E-06
Boc	1.485	1.724	4.968	6.750E-07	8.090E-06
Phldb1	1.890	1.791	4.968	6.770E-07	8.090E-06
Neo1	6.366	1.195	4.960	7.050E-07	8.400E-06
Gm37376	22.131	1.169	4.941	7.770E-07	9.210E-06
Arhgef2	1.857	1.853	4.901	9.520E-07	1.120E-05
Rarg	1.540	1.721	4.894	9.900E-07	1.160E-05
Nrbp2	1.800	1.593	4.858	1.190E-06	1.370E-05
Tgfbr3	2.008	1.709	4.838	1.310E-06	1.510E-05
Pde1b	1.026	2.124	4.772	1.820E-06	2.090E-05
Arsg	1.175	1.780	4.762	1.920E-06	2.170E-05
Hspb1	0.910	2.550	4.764	1.900E-06	2.170E-05
Pxdn	1.176	2.322	4.753	2.000E-06	2.260E-05
Efnb1	0.988	2.375	4.739	2.150E-06	2.410E-05
Dlx3	0.990	2.884	4.734	2.200E-06	2.450E-05
Atf3	1.229	2.598	4.724	2.310E-06	2.550E-05
Itgb4	0.936	3.059	4.662	3.130E-06	3.420E-05
Myc	5.541	1.408	4.657	3.200E-06	3.480E-05
Frmd4b	1.996	1.667	4.635	3.570E-06	3.860E-05
Tnxb	1.544	3.213	4.632	3.620E-06	3.900E-05

Serping1	0.955	2.701	4.630	3.660E-06	3.930E-05
Ppp1r9a	0.977	1.923	4.620	3.830E-06	4.090E-05
Sdc4	0.632	2.288	4.603	4.160E-06	4.410E-05
Crip2	1.287	1.627	4.580	4.640E-06	4.890E-05
Myo10	13.135	1.069	4.576	4.730E-06	4.970E-05
Fstl1	0.889	2.478	4.575	4.760E-06	4.980E-05
Col16a1	5.658	1.221	4.561	5.080E-06	5.270E-05
Kcna2	8.441	1.239	4.562	5.060E-06	5.270E-05
Trp63	1.044	3.010	4.555	5.230E-06	5.400E-05
Zfp618	0.644	2.098	4.547	5.430E-06	5.590E-05
Chd6	6.379	1.146	4.518	6.240E-06	6.370E-05
Pdzd2	0.878	2.447	4.496	6.920E-06	7.030E-05
Car5b	0.703	1.922	4.476	7.610E-06	7.700E-05
Bcl2	3.493	1.368	4.447	8.730E-06	8.760E-05
Cdc42ep1	0.712	2.309	4.444	8.840E-06	8.840E-05
Wdfy3	4.590	1.200	4.439	9.040E-06	8.970E-05
Col6a3	1.955	2.344	4.439	9.040E-06	8.970E-05
Col5a1	1.274	2.929	4.416	1.010E-05	9.900E-05
Per1	4.734	1.310	4.412	1.020E-05	1.000E-04
Sema3c	3.993	1.345	4.412	1.020E-05	1.000E-04
Cxcl14	0.907	1.858	4.391	1.130E-05	1.094E-04
Grik1	1.148	1.786	4.357	1.320E-05	1.274E-04
Plxna2	1.857	1.839	4.335	1.460E-05	1.399E-04
Rin3	1.342	1.570	4.325	1.530E-05	1.462E-04
Usp53	1.490	1.520	4.310	1.630E-05	1.557E-04
Pde7b	4.820	1.334	4.269	1.960E-05	1.866E-04
Coro2a	0.615	2.450	4.262	2.030E-05	1.922E-04
Nfkbiz	1.765	1.658	4.252	2.120E-05	1.997E-04
Cd200	2.346	1.417	4.248	2.160E-05	2.030E-04
Emp2	2.380	1.498	4.207	2.580E-05	2.410E-04
Dixdc1	0.560	2.044	4.208	2.580E-05	2.410E-04
Gng7	2.028	1.403	4.206	2.590E-05	2.411E-04
Casz1	1.083	2.853	4.200	2.670E-05	2.469E-04
Ece1	0.841	1.939	4.195	2.730E-05	2.516E-04
Arrdc3	1.975	1.511	4.191	2.780E-05	2.557E-04
Plxnb1	0.888	2.870	4.165	3.120E-05	2.855E-04
Ets1	3.729	1.222	4.128	3.660E-05	3.338E-04
Dock3	1.299	1.997	4.103	4.080E-05	3.705E-04
Eng	7.938	1.132	4.096	4.200E-05	3.809E-04
Clasp2	11.676	1.030	4.055	5.020E-05	4.528E-04
Epha2	1.162	1.864	4.053	5.070E-05	4.555E-04
Dapk1	0.640	2.095	4.040	5.350E-05	4.798E-04
Gas7	0.890	2.507	4.018	5.860E-05	5.236E-04
Shc1	7.619	1.079	4.017	5.900E-05	5.243E-04

Zfp704	6.247	1.105	4.016	5.910E-05	5.243E-04
Dpysl3	1.330	1.674	4.008	6.130E-05	5.412E-04
Irf6	0.576	2.247	3.972	7.130E-05	6.278E-04
Usp54	3.861	1.222	3.927	8.590E-05	7.511E-04
Cyp2d22	1.062	2.640	3.910	9.230E-05	8.015E-04
Prkd3	7.108	1.037	3.900	9.610E-05	8.291E-04
Tnik	4.403	1.156	3.900	9.620E-05	8.291E-04
Lama5	0.998	2.887	3.894	9.850E-05	8.460E-04
Ivns1abp	16.971	1.001	3.892	9.960E-05	8.524E-04
Fchsd2	2.839	1.248	3.887	1.017E-04	8.675E-04
Tet3	6.900	1.085	3.861	1.131E-04	9.617E-04
Oplah	0.791	1.788	3.853	1.167E-04	9.887E-04
Sox4	1.997	1.284	3.851	1.177E-04	9.945E-04
Ip6k3	0.630	2.396	3.850	1.182E-04	9.953E-04
Fat2	1.182	3.613	3.842	1.218E-04	1.022E-03
Bmp7	0.671	2.267	3.840	1.228E-04	1.027E-03
Heg1	0.797	2.365	3.805	1.420E-04	1.180E-03
Cpne4	7.224	1.149	3.783	1.551E-04	1.284E-03
Lrrtm2	2.306	1.416	3.764	1.670E-04	1.378E-03
Aldh1a3	1.047	2.794	3.715	2.034E-04	1.673E-03
Itga4	0.834	1.812	3.710	2.074E-04	1.700E-03
Stard9	1.665	1.562	3.680	2.328E-04	1.902E-03
S100a6	0.445	1.932	3.668	2.445E-04	1.991E-03
Erich3	0.527	1.955	3.667	2.453E-04	1.991E-03
Ltbp4	0.855	2.221	3.659	2.531E-04	2.048E-03
Lama1	3.146	1.288	3.638	2.747E-04	2.215E-03
Hap1	1.389	1.511	3.625	2.885E-04	2.319E-03
Capn5	0.694	1.774	3.616	2.987E-04	2.393E-03
Plpp3	1.069	1.602	3.614	3.010E-04	2.404E-03
Arid5b	3.077	1.252	3.596	3.230E-04	2.571E-03
Jarid2	5.474	1.111	3.538	4.038E-04	3.185E-03
Dsg3	0.822	3.107	3.535	4.078E-04	3.206E-03
Irf2bpl	6.785	1.077	3.532	4.123E-04	3.231E-03
Med12	9.431	1.008	3.515	4.398E-04	3.429E-03
Plekhn1	1.322	1.441	3.515	4.402E-04	3.429E-03
Malat1	234.342	1.048	3.510	4.481E-04	3.458E-03
Cobll1	1.808	1.353	3.510	4.478E-04	3.458E-03
P3h2	0.973	1.680	3.482	4.975E-04	3.815E-03
Xdh	0.523	1.908	3.480	5.007E-04	3.828E-03
Mmp14	8.685	1.013	3.476	5.093E-04	3.870E-03
Jag1	0.641	1.791	3.476	5.089E-04	3.870E-03
Xylt1	1.369	1.472	3.463	5.350E-04	4.053E-03
Gm9920	1.225	1.493	3.458	5.435E-04	4.105E-03
Plxna3	0.662	1.825	3.415	6.373E-04	4.799E-03

Krt75	0.991	3.367	3.390	6.986E-04	5.245E-03
Col6a1	0.784	2.762	3.384	7.134E-04	5.340E-03
Lad1	0.765	2.575	3.356	7.902E-04	5.897E-03
Hmcn1	6.280	1.175	3.352	8.019E-04	5.966E-03
Fancc	1.078	1.329	3.327	8.766E-04	6.503E-03
Jun	20.871	1.346	3.319	9.048E-04	6.693E-03
Cavin2	6.634	1.076	3.308	9.398E-04	6.910E-03
2610035D17Rik	0.431	1.722	3.297	9.789E-04	7.176E-03
Gm10800	0.857	1.684	3.291	9.992E-04	7.304E-03
Tns4	0.742	2.800	3.276	1.053E-03	7.675E-03
Numa1	7.433	1.021	3.272	1.067E-03	7.757E-03
Dsc3	0.769	2.654	3.265	1.095E-03	7.938E-03
Fcgrt	0.481	2.007	3.223	1.267E-03	9.127E-03
Nr1d1	1.525	1.359	3.218	1.289E-03	9.253E-03
Rab11fip5	1.006	1.540	3.218	1.292E-03	9.253E-03
Dclk2	4.867	1.194	3.189	1.426E-03	1.019E-02
Sipa1l3	5.703	1.052	3.185	1.448E-03	1.030E-02
Ica1	1.668	1.227	3.185	1.450E-03	1.030E-02
Maml3	2.888	1.162	3.167	1.540E-03	1.088E-02
Bambi	1.182	1.359	3.167	1.540E-03	1.088E-02
Prag1	2.685	1.203	3.156	1.598E-03	1.119E-02
Tram2	1.341	1.337	3.144	1.665E-03	1.162E-02
Adgra2	1.976	1.276	3.141	1.686E-03	1.174E-02
Col18a1	0.591	1.939	3.115	1.838E-03	1.276E-02
Gria4	0.971	1.694	3.098	1.946E-03	1.340E-02
Col14a1	0.656	2.324	3.089	2.010E-03	1.380E-02
Fn1	1.860	1.667	3.076	2.100E-03	1.438E-02
Klk1b22	0.481	1.737	3.075	2.106E-03	1.438E-02
Ogt	18.022	0.960	3.070	2.141E-03	1.459E-02
Tspan2	1.448	1.666	3.066	2.172E-03	1.476E-02
Fnbp1l	2.091	1.206	3.061	2.210E-03	1.497E-02
Slc39a14	2.910	1.176	3.059	2.223E-03	1.502E-02
Tubb2b	6.655	1.100	3.035	2.406E-03	1.617E-02
Insr	3.991	1.091	3.015	2.571E-03	1.723E-02
Egr3	0.632	2.215	3.012	2.597E-03	1.736E-02
Mpzl1	8.840	0.975	2.998	2.719E-03	1.813E-02
Obsl1	0.824	1.512	2.989	2.799E-03	1.861E-02
Zfp783	0.719	1.669	2.987	2.818E-03	1.869E-02
Rasgef1b	0.555	1.940	2.972	2.959E-03	1.952E-02
Col6a2	0.679	2.449	2.972	2.959E-03	1.952E-02
Bcam	0.542	2.339	2.969	2.989E-03	1.966E-02
Lifr	1.360	1.610	2.961	3.064E-03	2.011E-02
Axl	0.660	2.065	2.941	3.273E-03	2.142E-02
Grhl1	0.556	1.997	2.926	3.433E-03	2.241E-02

Arhgap32	8.589	1.002	2.921	3.487E-03	2.270E-02
Plp1	20.265	1.008	2.897	3.766E-03	2.445E-02
Unc5b	0.854	1.735	2.883	3.937E-03	2.550E-02
Efemp1	0.468	2.179	2.879	3.986E-03	2.575E-02
Sned1	0.669	1.879	2.864	4.184E-03	2.696E-02
Nfat5	6.552	1.022	2.854	4.315E-03	2.773E-02
Dock6	2.177	1.195	2.852	4.341E-03	2.783E-02
Slc15a2	0.680	1.604	2.848	4.397E-03	2.811E-02
Ablim1	4.048	1.379	2.846	4.430E-03	2.825E-02
Pkp1	0.490	2.192	2.844	4.456E-03	2.834E-02
Ahdc1	3.183	1.098	2.828	4.684E-03	2.972E-02
Notch2	11.131	0.982	2.823	4.750E-03	3.006E-02
Ndrg1	1.265	1.698	2.816	4.869E-03	3.074E-02
Gm44005	1.562	1.276	2.814	4.899E-03	3.085E-02
Fndc1	0.913	2.698	2.803	5.059E-03	3.178E-02
Dnm1	0.447	1.688	2.798	5.141E-03	3.213E-02
Sdc1	0.477	1.810	2.790	5.278E-03	3.284E-02
Wnt5a	0.597	2.262	2.789	5.281E-03	3.284E-02
Kmt2a	7.219	0.985	2.782	5.406E-03	3.354E-02
Gpc3	0.438	2.000	2.776	5.496E-03	3.401E-02
Frem2	0.929	1.581	2.772	5.576E-03	3.442E-02
Plcl1	0.638	1.574	2.765	5.688E-03	3.502E-02
Socs3	1.099	2.002	2.753	5.907E-03	3.629E-02
Olfm1	9.519	1.039	2.748	6.003E-03	3.670E-02
Arhgap21	3.441	1.049	2.748	6.004E-03	3.670E-02
Nup210	2.267	1.313	2.745	6.046E-03	3.687E-02
Klhl24	5.210	1.038	2.740	6.149E-03	3.740E-02
Nfic	11.088	0.941	2.725	6.437E-03	3.906E-02
Adamts1	2.871	1.337	2.720	6.529E-03	3.952E-02
Bahcc1	2.694	1.117	2.706	6.802E-03	4.107E-02
Per3	1.616	1.258	2.684	7.284E-03	4.377E-02
Emp1	1.130	1.410	2.681	7.335E-03	4.397E-02
Runx1	0.398	1.759	2.677	7.432E-03	4.434E-02
Spint2	0.362	1.823	2.677	7.427E-03	4.434E-02
Rassf2	0.613	1.472	2.674	7.490E-03	4.458E-02
Unkl	1.250	1.294	2.663	7.742E-03	4.597E-02
Btg2	0.493	1.946	2.661	7.782E-03	4.610E-02
Col4a1	0.688	2.453	2.659	7.833E-03	4.630E-02
Padi3	0.618	2.388	2.644	8.197E-03	4.833E-02
Vangl2	3.541	1.068	2.633	8.455E-03	4.974E-02
Tns1	0.683	2.247	2.631	8.509E-03	4.993E-02

Table 3.2: DAVID GO terms from Gene Lists in Table 3.1 (see also Table S9 from Infarinato et al., 2020)

DAVID GO Term Analysis Output: Statistical enrichment, GO Biological Process Complete

Control List

Term	Count	%	P-Value	Benjamini
melanin biosynthetic process	4	5	1.90E-05	1.30E-02
melanosome organization	4	5	2.40E-05	8.50E-03
negative regulation of sequence-specific DNA binding transcription factor activity	4	5	3.00E-03	5.00E-01
vagus nerve morphogenesis	2	2.5	8.30E-03	7.70E-01
positive regulation of keratinocyte apoptotic process	2	2.5	1.20E-02	8.30E-01
pigmentation	3	3.8	1.50E-02	8.30E-01
cellular protein modification process	3	3.8	1.60E-02	8.00E-01
visual perception	4	5	1.80E-02	8.00E-01
axon guidance	4	5	2.40E-02	8.50E-01
muscle organ development	3	3.8	2.80E-02	8.70E-01
cellular aromatic compound metabolic process	2	2.5	2.90E-02	8.50E-01
regulation of axon extension involved in axon guidance	2	2.5	2.90E-02	8.50E-01
semicircular canal morphogenesis	2	2.5	2.90E-02	8.50E-01
epithelial cell differentiation	3	3.8	3.20E-02	8.50E-01
cerebral cortex development	3	3.8	3.20E-02	8.30E-01
positive regulation of feeding behavior	2	2.5	3.30E-02	8.10E-01
positive regulation of ryanodine-sensitive calcium-release channel activity	2	2.5	3.30E-02	8.10E-01
transport	14	17.5	3.60E-02	8.20E-01
inner ear morphogenesis	3	3.8	3.60E-02	8.00E-01
response to endoplasmic reticulum stress	3	3.8	4.00E-02	8.10E-01
regulation of cell migration	3	3.8	4.10E-02	8.00E-01
positive regulation of smooth muscle cell proliferation	3	3.8	4.40E-02	8.10E-01
branchiomotor neuron axon guidance	2	2.5	4.50E-02	8.00E-01
semaphorin-plexin signaling pathway involved in axon guidance	2	2.5	5.30E-02	8.40E-01
lens fiber cell differentiation	2	2.5	5.30E-02	8.40E-01
multicellular organism development	9	11.2	6.30E-02	8.70E-01
cell proliferation	4	5	6.30E-02	8.70E-01
barbed-end actin filament capping	2	2.5	6.40E-02	8.60E-01
transmembrane transport	5	6.2	6.50E-02	8.50E-01
angiogenesis	4	5	7.70E-02	8.90E-01
developmental pigmentation	2	2.5	8.00E-02	8.90E-01
melanocyte differentiation	2	2.5	8.00E-02	8.90E-01

extracellular matrix organization	3	3.8	8.10E-02	8.80E-01
tissue regeneration	2	2.5	8.70E-02	8.90E-01
positive regulation of angiogenesis	3	3.8	9.00E-02	8.90E-01
middle ear morphogenesis	2	2.5	9.50E-02	9.00E-01
actin filament polymerization	2	2.5	9.50E-02	9.00E-01
endothelial cell migration	2	2.5	9.90E-02	9.00E-01

***Bmpr1a* Null List**

Term	Count	%	P-Value	Benjamini
cell adhesion	36	10.7	1.00E-12	2.30E-09
positive regulation of transcription from RNA polymerase II promoter	46	13.7	3.60E-09	4.10E-06
positive regulation of transcription, DNA-templated	32	9.5	2.60E-08	2.00E-05
skin development	10	3	6.50E-07	3.70E-04
wound healing	12	3.6	7.00E-07	3.20E-04
positive regulation of cell proliferation	28	8.3	9.90E-07	3.70E-04
angiogenesis	18	5.4	1.00E-06	3.30E-04
cell migration	16	4.8	1.30E-06	3.70E-04
neural tube development	9	2.7	2.50E-06	6.30E-04
single organismal cell-cell adhesion	12	3.6	2.80E-06	6.40E-04
canonical Wnt signaling pathway	11	3.3	3.30E-06	6.70E-04
blood vessel development	10	3	3.70E-06	7.00E-04
negative regulation of cell proliferation	22	6.5	3.90E-06	6.90E-04
negative regulation of transcription from RNA polymerase II promoter	32	9.5	4.30E-06	7.00E-04
regulation of cell migration	10	3	7.30E-06	1.10E-03
axon guidance	13	3.9	1.20E-05	1.60E-03
skeletal muscle cell differentiation	8	2.4	4.40E-05	5.90E-03
intracellular signal transduction	20	6	7.70E-05	9.70E-03
endodermal cell differentiation	6	1.8	9.00E-05	1.10E-02
blood vessel remodeling	7	2.1	9.30E-05	1.00E-02
response to mechanical stimulus	8	2.4	1.10E-04	1.20E-02
glycosaminoglycan biosynthetic process	6	1.8	1.10E-04	1.10E-02
negative regulation of neuron projection development	8	2.4	1.20E-04	1.20E-02
organ morphogenesis	10	3	1.20E-04	1.10E-02
cAMP catabolic process	5	1.5	1.40E-04	1.20E-02
extracellular matrix organization	10	3	1.70E-04	1.50E-02
heart development	15	4.5	2.00E-04	1.70E-02
response to cAMP	7	2.1	2.40E-04	2.00E-02
multicellular organism development	35	10.4	2.50E-04	1.90E-02
protein heterotrimerization	5	1.5	2.80E-04	2.10E-02
semaphorin-plexin signaling pathway	6	1.8	2.80E-04	2.00E-02
neural tube closure	9	2.7	2.90E-04	2.00E-02

transforming growth factor beta receptor signaling pathway	8	2.4	3.20E-04	2.20E-02
positive regulation of BMP signaling pathway	6	1.8	3.70E-04	2.40E-02
cell-matrix adhesion	8	2.4	4.10E-04	2.60E-02
positive regulation of mesenchymal cell proliferation	6	1.8	4.20E-04	2.60E-02
cell motility	5	1.5	4.20E-04	2.60E-02
cell cycle arrest	8	2.4	5.20E-04	3.00E-02
collagen fibril organization	6	1.8	5.40E-04	3.10E-02
skeletal system development	9	2.7	5.60E-04	3.10E-02
regulation of transcription from RNA polymerase II promoter	18	5.4	6.10E-04	3.30E-02
regulation of cell proliferation	13	3.9	6.40E-04	3.40E-02
circadian regulation of gene expression	7	2.1	6.50E-04	3.40E-02
keratinocyte differentiation	8	2.4	6.90E-04	3.50E-02
epidermis development	7	2.1	7.10E-04	3.50E-02
positive regulation of catenin import into nucleus	4	1.2	7.70E-04	3.70E-02
post-anal tail morphogenesis	5	1.5	8.50E-04	4.00E-02
negative regulation of axon extension involved in axon guidance	5	1.5	9.90E-04	4.60E-02
regulation of embryonic development	4	1.2	1.00E-03	4.60E-02
semaphorin-plexin signaling pathway involved in axon guidance	4	1.2	1.30E-03	5.80E-02
negative regulation of fibroblast growth factor receptor signaling pathway	4	1.2	1.30E-03	5.80E-02
cardiac septum morphogenesis	4	1.2	1.30E-03	5.80E-02
regulation of angiogenesis	5	1.5	1.30E-03	5.70E-02
ureteric bud development	6	1.8	1.40E-03	6.00E-02
lung development	9	2.7	1.50E-03	6.10E-02
branching involved in salivary gland morphogenesis	4	1.2	2.00E-03	8.20E-02
negative regulation of apoptotic process	21	6.2	2.20E-03	8.70E-02
in utero embryonic development	14	4.2	2.30E-03	8.90E-02
nervous system development	16	4.8	2.60E-03	9.70E-02
protein phosphorylation	21	6.2	2.70E-03	1.00E-01
positive regulation of epithelial to mesenchymal transition	5	1.5	2.70E-03	1.00E-01
positive regulation of neuron projection development	9	2.7	2.90E-03	1.00E-01
desmosome organization	3	0.9	2.90E-03	1.00E-01
negative regulation of vascular endothelial growth factor signaling pathway	3	0.9	2.90E-03	1.00E-01
hemidesmosome assembly	3	0.9	2.90E-03	1.00E-01
positive regulation of cell migration	11	3.3	3.00E-03	1.00E-01
neuron projection development	9	2.7	3.00E-03	1.00E-01
hair follicle morphogenesis	5	1.5	3.10E-03	1.00E-01
branching morphogenesis of an epithelial tube	5	1.5	3.40E-03	1.10E-01
establishment of planar polarity	4	1.2	3.50E-03	1.10E-01

digestive tract morphogenesis	4	1.2	3.50E-03	1.10E-01
bone remodeling	4	1.2	3.50E-03	1.10E-01
coronary vasculature development	5	1.5	3.80E-03	1.20E-01
response to toxic substance	7	2.1	3.80E-03	1.20E-01
retinal blood vessel morphogenesis	3	0.9	4.30E-03	1.30E-01
collagen biosynthetic process	3	0.9	4.30E-03	1.30E-01
odontogenesis of dentin-containing tooth	6	1.8	4.70E-03	1.40E-01
embryonic limb morphogenesis	6	1.8	4.70E-03	1.40E-01
neuron projection morphogenesis	6	1.8	4.70E-03	1.40E-01
face development	4	1.2	4.70E-03	1.40E-01
positive regulation of protein phosphorylation	10	3	4.90E-03	1.40E-01
patterning of blood vessels	5	1.5	5.00E-03	1.40E-01
cellular response to retinoic acid	6	1.8	5.40E-03	1.50E-01
positive regulation of fibroblast proliferation	6	1.8	5.40E-03	1.50E-01
cell-cell adhesion	10	3	5.90E-03	1.60E-01
response to corticosteroid	3	0.9	6.00E-03	1.60E-01
cardiac atrium morphogenesis	3	0.9	6.00E-03	1.60E-01
Notch signaling pathway	8	2.4	6.20E-03	1.70E-01
liver development	7	2.1	6.20E-03	1.70E-01
cellular response to vascular endothelial growth factor stimulus	4	1.2	6.30E-03	1.60E-01
positive regulation of DNA replication	5	1.5	6.50E-03	1.70E-01
positive regulation of protein binding	6	1.8	6.50E-03	1.70E-01
signal transduction	35	10.4	6.70E-03	1.70E-01
epidermal growth factor receptor signaling pathway	5	1.5	7.60E-03	1.90E-01
neuron apoptotic process	5	1.5	7.60E-03	1.90E-01
pericardium morphogenesis	3	0.9	7.90E-03	1.90E-01
positive regulation of extracellular matrix disassembly	3	0.9	7.90E-03	1.90E-01
somatic stem cell population maintenance	5	1.5	8.20E-03	2.00E-01
Rho protein signal transduction	5	1.5	8.20E-03	2.00E-01
negative regulation of epithelial cell proliferation	6	1.8	8.30E-03	2.00E-01
response to estradiol	7	2.1	8.40E-03	2.00E-01
venous blood vessel morphogenesis	3	0.9	1.00E-02	2.30E-01
establishment of epithelial cell apical/basal polarity	3	0.9	1.00E-02	2.30E-01
heart trabecula morphogenesis	3	0.9	1.00E-02	2.30E-01
negative chemotaxis	4	1.2	1.00E-02	2.30E-01
cellular response to amino acid stimulus	8	2.4	1.00E-02	2.30E-01
neural crest cell migration	5	1.5	1.00E-02	2.30E-01
activation of MAPK activity	6	1.8	1.00E-02	2.30E-01
positive regulation of epithelial cell proliferation	6	1.8	1.00E-02	2.30E-01
aging	9	2.7	1.10E-02	2.30E-01
regulation of cell shape	8	2.4	1.10E-02	2.30E-01
establishment or maintenance of cell polarity	4	1.2	1.10E-02	2.30E-01
collagen metabolic process	3	0.9	1.20E-02	2.50E-01

embryonic eye morphogenesis	3	0.9	1.20E-02	2.50E-01
response to cytokine	6	1.8	1.30E-02	2.70E-01
liver regeneration	4	1.2	1.40E-02	2.70E-01
sprouting angiogenesis	4	1.2	1.40E-02	2.70E-01
positive regulation of mitotic nuclear division	4	1.2	1.40E-02	2.70E-01
positive regulation of apoptotic process	13	3.9	1.40E-02	2.80E-01
post-embryonic development	7	2.1	1.50E-02	2.80E-01
actin filament organization	6	1.8	1.50E-02	2.80E-01
cellular response to fibroblast growth factor stimulus	4	1.2	1.50E-02	2.80E-01
response to radiation	4	1.2	1.50E-02	2.80E-01
extracellular fibril organization	3	0.9	1.50E-02	2.80E-01
bleb assembly	3	0.9	1.50E-02	2.80E-01
astrocyte differentiation	3	0.9	1.50E-02	2.80E-01
negative regulation of neuron migration	3	0.9	1.50E-02	2.80E-01
pulmonary valve morphogenesis	3	0.9	1.50E-02	2.80E-01
salivary gland morphogenesis	3	0.9	1.50E-02	2.80E-01
branchiomotor neuron axon guidance	3	0.9	1.50E-02	2.80E-01
limb bud formation	3	0.9	1.50E-02	2.80E-01
skin morphogenesis	3	0.9	1.50E-02	2.80E-01
negative regulation of protein phosphorylation	6	1.8	1.50E-02	2.90E-01
organ regeneration	5	1.5	1.60E-02	3.00E-01
bone development	5	1.5	1.60E-02	3.00E-01
positive regulation of filopodium assembly	4	1.2	1.60E-02	3.00E-01
regulation of ERK1 and ERK2 cascade	4	1.2	1.60E-02	3.00E-01
prostate gland epithelium morphogenesis	3	0.9	1.80E-02	3.20E-01
morphogenesis of an epithelial sheet	3	0.9	1.80E-02	3.20E-01
cell differentiation	23	6.8	1.80E-02	3.20E-01
response to hydrogen peroxide	5	1.5	1.80E-02	3.20E-01
positive regulation of angiogenesis	7	2.1	1.90E-02	3.30E-01
cholesterol metabolic process	6	1.8	1.90E-02	3.30E-01
receptor-mediated endocytosis	5	1.5	2.00E-02	3.40E-01
cardiac epithelial to mesenchymal transition	3	0.9	2.10E-02	3.40E-01
planar cell polarity pathway involved in neural tube closure	3	0.9	2.10E-02	3.40E-01
fibroblast migration	3	0.9	2.10E-02	3.40E-01
cardiac right ventricle morphogenesis	3	0.9	2.10E-02	3.40E-01
cellular response to transforming growth factor beta stimulus	5	1.5	2.10E-02	3.50E-01
negative regulation of neuron apoptotic process	8	2.4	2.20E-02	3.50E-01
actin filament bundle assembly	4	1.2	2.30E-02	3.60E-01
blood vessel morphogenesis	4	1.2	2.30E-02	3.60E-01
heart looping	5	1.5	2.30E-02	3.60E-01
neuron differentiation	7	2.1	2.40E-02	3.70E-01
vasculogenesis involved in coronary vascular morphogenesis	3	0.9	2.40E-02	3.70E-01

kidney morphogenesis	3	0.9	2.40E-02	3.70E-01
cellular response to epidermal growth factor stimulus	4	1.2	2.40E-02	3.70E-01
ossification	6	1.8	2.60E-02	3.90E-01
kidney development	7	2.1	2.60E-02	3.90E-01
positive regulation of protein kinase B signaling	6	1.8	2.70E-02	4.00E-01
establishment of epithelial cell polarity	3	0.9	2.70E-02	4.00E-01
Wnt signaling pathway, planar cell polarity pathway	3	0.9	2.70E-02	4.00E-01
positive regulation of cholesterol efflux	3	0.9	2.70E-02	4.00E-01
inner ear development	5	1.5	2.80E-02	4.00E-01
positive regulation of canonical Wnt signaling pathway	5	1.5	2.90E-02	4.10E-01
cell communication	4	1.2	3.00E-02	4.20E-01
transmembrane receptor protein tyrosine kinase signaling pathway	6	1.8	3.00E-02	4.20E-01
response to calcium ion	5	1.5	3.10E-02	4.20E-01
vasculogenesis	5	1.5	3.10E-02	4.20E-01
positive regulation of cell size	3	0.9	3.10E-02	4.20E-01
positive regulation of histone H3-K4 methylation	3	0.9	3.10E-02	4.20E-01
positive regulation of cartilage development	3	0.9	3.10E-02	4.20E-01
histone H3-K4 trimethylation	3	0.9	3.10E-02	4.20E-01
positive regulation of peptidyl-tyrosine phosphorylation	6	1.8	3.10E-02	4.20E-01
substrate adhesion-dependent cell spreading	4	1.2	3.20E-02	4.30E-01
regulation of growth	5	1.5	3.20E-02	4.30E-01
negative regulation of canonical Wnt signaling pathway	6	1.8	3.30E-02	4.30E-01
sensory perception of sound	7	2.1	3.40E-02	4.40E-01
transcription from RNA polymerase II promoter	7	2.1	3.40E-02	4.40E-01
regulation of transcription, DNA-templated	52	15.5	3.40E-02	4.40E-01
ventricular trabecula myocardium morphogenesis	3	0.9	3.40E-02	4.40E-01
astrocyte development	3	0.9	3.40E-02	4.40E-01
positive regulation of meiotic cell cycle	2	0.6	3.40E-02	4.40E-01
canonical Wnt signaling pathway involved in positive regulation of wound healing	2	0.6	3.40E-02	4.40E-01
extrinsic apoptotic signaling pathway in absence of ligand	4	1.2	3.60E-02	4.50E-01
transcription, DNA-templated	44	13.1	3.80E-02	4.70E-01
positive regulation of protein export from nucleus	3	0.9	3.80E-02	4.70E-01
smooth muscle tissue development	3	0.9	3.80E-02	4.70E-01
pharyngeal system development	3	0.9	3.80E-02	4.70E-01
definitive hemopoiesis	3	0.9	3.80E-02	4.70E-01
axonal fasciculation	3	0.9	3.80E-02	4.70E-01
establishment of protein localization to plasma membrane	4	1.2	3.80E-02	4.70E-01
phosphorylation	18	5.4	3.90E-02	4.70E-01

positive regulation of peptidyl-serine phosphorylation	5	1.5	4.00E-02	4.70E-01
embryonic skeletal system development	4	1.2	4.10E-02	4.80E-01
establishment of skin barrier	3	0.9	4.20E-02	4.90E-01
negative regulation of neuron differentiation	5	1.5	4.30E-02	4.90E-01
SMAD protein signal transduction	5	1.5	4.50E-02	5.10E-01
chondrocyte differentiation	4	1.2	4.60E-02	5.10E-01
spleen development	4	1.2	4.60E-02	5.10E-01
positive regulation of cell differentiation	4	1.2	4.60E-02	5.10E-01
anterior/posterior pattern specification	6	1.8	4.60E-02	5.10E-01
regulation of microtubule cytoskeleton organization	3	0.9	4.60E-02	5.10E-01
positive regulation of cell-cell adhesion	3	0.9	4.60E-02	5.10E-01
camera-type eye development	5	1.5	4.70E-02	5.10E-01
osteoblast differentiation	6	1.8	4.70E-02	5.10E-01
positive regulation of smooth muscle cell proliferation	5	1.5	5.10E-02	5.30E-01
negative regulation of cell death	5	1.5	5.10E-02	5.30E-01
positive regulation of cysteine-type endopeptidase activity involved in apoptotic process	4	1.2	5.10E-02	5.30E-01
branching involved in ureteric bud morphogenesis	4	1.2	5.10E-02	5.30E-01
glial cell differentiation	3	0.9	5.10E-02	5.30E-01
embryonic hemopoiesis	3	0.9	5.10E-02	5.30E-01
positive regulation of focal adhesion assembly	3	0.9	5.10E-02	5.30E-01
intermediate filament organization	3	0.9	5.10E-02	5.30E-01
convergent extension	2	0.6	5.10E-02	5.30E-01
distal tubule development	2	0.6	5.10E-02	5.30E-01
transforming growth factor beta receptor complex assembly	2	0.6	5.10E-02	5.30E-01
planar cell polarity pathway involved in axis elongation	2	0.6	5.10E-02	5.30E-01
epicardial cell to mesenchymal cell transition	2	0.6	5.10E-02	5.30E-01
regulation of epidermal cell division	2	0.6	5.10E-02	5.30E-01
positive regulation of TRAIL-activated apoptotic signaling pathway	2	0.6	5.10E-02	5.30E-01
regulation of gluconeogenesis by regulation of transcription from RNA polymerase II promoter	2	0.6	5.10E-02	5.30E-01
regulation of developmental process	2	0.6	5.10E-02	5.30E-01
heparan sulfate proteoglycan metabolic process	2	0.6	5.10E-02	5.30E-01
cell morphogenesis	5	1.5	5.20E-02	5.40E-01
cell development	4	1.2	5.30E-02	5.40E-01
cell growth	4	1.2	5.30E-02	5.40E-01
cartilage development	5	1.5	5.40E-02	5.50E-01
regulation of actin cytoskeleton organization	4	1.2	5.60E-02	5.60E-01
regulation of apoptotic process	8	2.4	5.90E-02	5.70E-01
membrane depolarization	3	0.9	6.00E-02	5.80E-01
cochlea morphogenesis	3	0.9	6.00E-02	5.80E-01

regulation of insulin secretion involved in cellular response to glucose stimulus	3	0.9	6.00E-02	5.80E-01
positive regulation of cardiac muscle cell proliferation	3	0.9	6.00E-02	5.80E-01
palate development	5	1.5	6.10E-02	5.80E-01
hair follicle development	4	1.2	6.10E-02	5.80E-01
actin cytoskeleton reorganization	4	1.2	6.10E-02	5.80E-01
hemopoiesis	5	1.5	6.30E-02	5.90E-01
cellular response to calcium ion	4	1.2	6.40E-02	6.00E-01
middle ear morphogenesis	3	0.9	6.50E-02	5.90E-01
decidualization	3	0.9	6.50E-02	5.90E-01
homophilic cell adhesion via plasma membrane adhesion molecules	7	2.1	6.50E-02	6.00E-01
cellular response to insulin stimulus	5	1.5	6.70E-02	6.00E-01
intrinsic apoptotic signaling pathway in response to DNA damage	4	1.2	6.70E-02	6.00E-01
outflow tract morphogenesis	4	1.2	6.70E-02	6.00E-01
negative regulation of prostatic bud formation	2	0.6	6.80E-02	6.00E-01
positive regulation of extracellular exosome assembly	2	0.6	6.80E-02	6.00E-01
response to high density lipoprotein particle	2	0.6	6.80E-02	6.00E-01
response to human chorionic gonadotropin	2	0.6	6.80E-02	6.00E-01
cell migration involved in endocardial cushion formation	2	0.6	6.80E-02	6.00E-01
transformation of host cell by virus	2	0.6	6.80E-02	6.00E-01
heterochromatin assembly	2	0.6	6.80E-02	6.00E-01
central nervous system development	5	1.5	6.90E-02	6.10E-01
response to light stimulus	3	0.9	6.90E-02	6.10E-01
positive regulation of peptidyl-threonine phosphorylation	3	0.9	6.90E-02	6.10E-01
morphogenesis of an epithelium	3	0.9	6.90E-02	6.10E-01
neuronal stem cell population maintenance	3	0.9	6.90E-02	6.10E-01
positive regulation of cell growth	5	1.5	7.20E-02	6.20E-01
response to drug	11	3.3	7.20E-02	6.20E-01
rhythmic process	6	1.8	7.30E-02	6.20E-01
negative regulation of osteoblast differentiation	4	1.2	7.30E-02	6.20E-01
somitogenesis	4	1.2	7.30E-02	6.20E-01
negative regulation of neurogenesis	3	0.9	7.40E-02	6.20E-01
release of cytochrome c from mitochondria	3	0.9	7.40E-02	6.20E-01
ovarian follicle development	4	1.2	7.70E-02	6.30E-01
inflammatory response	11	3.3	7.80E-02	6.40E-01
Wnt signaling pathway	8	2.4	7.90E-02	6.40E-01
integrin-mediated signaling pathway	5	1.5	7.90E-02	6.40E-01
adrenal gland development	3	0.9	7.90E-02	6.40E-01
positive regulation of Rho protein signal transduction	3	0.9	7.90E-02	6.40E-01

negative regulation of transcription, DNA-templated	16	4.8	8.00E-02	6.40E-01
response to wounding	4	1.2	8.00E-02	6.40E-01
response to oxidative stress	6	1.8	8.20E-02	6.50E-01
brain development	8	2.4	8.30E-02	6.50E-01
convergent extension involved in organogenesis	2	0.6	8.40E-02	6.50E-01
axis elongation	2	0.6	8.40E-02	6.50E-01
diterpenoid metabolic process	2	0.6	8.40E-02	6.50E-01
cell-substrate junction assembly	2	0.6	8.40E-02	6.50E-01
cellular response to indole-3-methanol	2	0.6	8.40E-02	6.50E-01
urinary bladder development	2	0.6	8.40E-02	6.50E-01
eye morphogenesis	2	0.6	8.40E-02	6.50E-01
dichotomous subdivision of terminal units involved in salivary gland branching	2	0.6	8.40E-02	6.50E-01
ciliary body morphogenesis	2	0.6	8.40E-02	6.50E-01
morphogenesis of a polarized epithelium	2	0.6	8.40E-02	6.50E-01
positive regulation of basement membrane assembly involved in embryonic body morphogenesis	2	0.6	8.40E-02	6.50E-01
regulation of oligodendrocyte differentiation	2	0.6	8.40E-02	6.50E-01
myelination	4	1.2	8.60E-02	6.60E-01
cell surface receptor signaling pathway	8	2.4	8.80E-02	6.60E-01
regulation of gene expression	10	3	8.90E-02	6.70E-01
positive regulation of gene expression	12	3.6	8.90E-02	6.70E-01
cell proliferation	8	2.4	8.90E-02	6.70E-01
osteoclast differentiation	3	0.9	9.00E-02	6.70E-01
negative regulation of mitotic cell cycle	3	0.9	9.00E-02	6.70E-01
protein localization to plasma membrane	4	1.2	9.30E-02	6.80E-01
regulation of protein phosphorylation	4	1.2	9.30E-02	6.80E-01
regulation of blood pressure	4	1.2	9.30E-02	6.80E-01
cell aging	3	0.9	9.50E-02	6.80E-01
response to progesterone	3	0.9	9.50E-02	6.80E-01
pituitary gland development	3	0.9	9.50E-02	6.80E-01
endochondral ossification	3	0.9	9.50E-02	6.80E-01
neuron projection guidance	2	0.6	1.00E-01	7.00E-01
response to aluminum ion	2	0.6	1.00E-01	7.00E-01
notochord morphogenesis	2	0.6	1.00E-01	7.00E-01
interleukin-4 secretion	2	0.6	1.00E-01	7.00E-01
bundle of His cell-Purkinje myocyte adhesion involved in cell communication	2	0.6	1.00E-01	7.00E-01
muscular septum morphogenesis	2	0.6	1.00E-01	7.00E-01
positive regulation of endothelial cell chemotaxis	2	0.6	1.00E-01	7.00E-01
positive regulation of transcription of Notch receptor target	2	0.6	1.00E-01	7.00E-01
intracellular cholesterol transport	2	0.6	1.00E-01	7.00E-01
trigeminal nerve structural organization	2	0.6	1.00E-01	7.00E-01

glial cell development	2	0.6	1.00E-01	7.00E-01
planar cell polarity pathway involved in axon guidance	2	0.6	1.00E-01	7.00E-01
salivary gland cavitation	2	0.6	1.00E-01	7.00E-01
positive regulation of protein kinase activity	4	1.2	1.00E-01	7.00E-01
positive regulation of phosphatidylinositol 3-kinase signaling	4	1.2	1.00E-01	7.00E-01

Table 3.3: List of Genes with Reduced Expression in *Bmpr1a* Null Differentiating Progeny Cells (padj≤0.05, baseMean≥5) with MITF and LEF1 Motifs Within Their Putative Promoter Region (see also Table S11 from Infarinato et al., 2020)

Itgb3
Ephx1
B3galt5
Fam129a
Slc24a4
Kif26b
Id3
Oca2
Rab38
Eps8
Plekha8
Sec14l1
Trpm1
Amd1
Gsn
Shroom2
Gpr137b
Slc26a2
Xpo6
Frmd4a
Mc1r
Asah1
Nav2

Table 3.4: Motif Analysis of ATAC Peaks Increased in Differentiating Progeny Proximal to Genes Whose Expression is Diminished in *Bmpr1a* Null Cells (see also Table S14 from Infarinato et al., 2020)
*Values shown to three decimal points, where applicable

Motif	Expected	Observed	Obs/Exp	P-value
NR2F1	39.105	62	1.585	2.824E-06
MAFG::NFE2L1	108.882	116	1.065	7.989E-06
USF1	40.514	61	1.506	1.526E-05
TFEC	27.381	45	1.643	6.182E-05
USF2	30.671	48	1.565	9.500E-05
MITF	24.811	41	1.652	1.323E-04
TFEB	27.342	41	1.500	8.354E-04
TCF7L2	64.483	75	1.163	9.346E-04
Tcf7	58.028	69	1.189	1.319E-03
Rarb	32.239	45	1.396	1.598E-03
TFE3	31.288	44	1.406	1.625E-03
Arnt	49.484	61	1.233	1.829E-03
SOX13	28.956	41	1.416	2.257E-03
NEUROD1	40.694	52	1.278	3.003E-03
Sox2	42.263	53	1.254	3.725E-03
TFAP4	27.031	38	1.406	3.887E-03
HEY2	13.105	22	1.679	4.444E-03
Creb3l2	15.987	25	1.564	6.098E-03
MEIS3	24.178	34	1.406	6.625E-03
CREB1	24.439	34	1.391	7.674E-03
Sox6	67.102	72	1.073	7.807E-03
SOX15	55.966	63	1.126	8.382E-03
RARA	27.526	37	1.344	8.546E-03
Bhlha15	10.968	18	1.641	1.124E-02
ZSCAN4	46.305	54	1.166	1.166E-02
Rhox11	16.133	24	1.488	1.240E-02
NRL	26.689	35	1.311	1.493E-02
Ddit3::Cebpa	12.235	19	1.553	1.611E-02
MAX::MYC	21.232	29	1.366	1.748E-02
Nr2f6(var.2)	31.292	39	1.246	1.928E-02
ZBED1	2.110	5	2.370	1.970E-02
MEIS1	29.436	37	1.257	2.095E-02
TEAD1	30.485	38	1.247	2.117E-02
NR4A2	31.587	39	1.235	2.179E-02

OLIG3	7.770	13	1.673	2.189E-02
MYC	20.736	28	1.350	2.212E-02
RXRB	31.711	39	1.230	2.292E-02
Esrrg	28.641	36	1.257	2.304E-02
LEF1	59.559	63	1.058	2.418E-02
SRF	9.472	15	1.584	2.425E-02
Hnf4a	27.799	35	1.259	2.479E-02
Sox3	93.604	87	0.929	2.587E-02
SOX10	72.044	72	0.999	2.791E-02
NR2F2	36.604	43	1.175	2.911E-02
RUNX1	72.331	72	0.995	2.979E-02
SIX2	31.336	38	1.213	2.987E-02
SREBF2(var.2)	14.895	21	1.410	3.034E-02
NKX2-3	21.439	28	1.306	3.156E-02
MYCN	15.058	21	1.395	3.345E-02
NR4A1	27.553	34	1.234	3.426E-02
PRDM1	37.126	43	1.158	3.490E-02
Gmeb1	3.094	6	1.939	3.587E-02
SPIC	41.730	47	1.126	3.641E-02
Twist2	16.235	22	1.355	3.905E-02
ZNF263	242.212	154	0.636	3.913E-02
TBX19	10.109	15	1.484	3.954E-02
Hic1	23.930	30	1.254	4.042E-02
RORA	29.027	35	1.206	4.091E-02
ESRRB	29.093	35	1.203	4.197E-02
BHLHE41	11.996	17	1.417	4.453E-02
Mlxip	15.582	21	1.348	4.501E-02
Srebf1(var.2)	17.442	23	1.319	4.536E-02
Hoxc9	20.290	26	1.281	4.551E-02
PBX1	16.715	22	1.316	5.033E-02
NFIC	44.166	48	1.087	5.323E-02
CLOCK	9.690	14	1.445	5.330E-02
Rarg	27.729	33	1.190	5.479E-02
ZNF143	33.031	38	1.150	5.503E-02
Rarb(var.2)	28.787	34	1.181	5.515E-02
FOXH1	23.754	29	1.221	5.697E-02
Npas2	16.968	22	1.297	5.713E-02
Pax6	13.313	18	1.352	5.771E-02
MZF1	244.565	153	0.626	5.908E-02

SIX1	22.927	28	1.221	6.110E-02
TEAD3	33.454	38	1.136	6.320E-02
HEY1	13.482	18	1.335	6.340E-02
MYB	23.068	28	1.214	6.466E-02
Hmx1	20.118	25	1.243	6.503E-02
NKX2-8	25.138	30	1.193	6.590E-02
NFIA	27.225	32	1.175	6.658E-02
RARA(var.2)	31.464	36	1.144	6.685E-02
NFKB1	14.518	19	1.309	6.769E-02
Nr5a2	52.350	54	1.032	6.798E-02
MAFK	27.381	32	1.169	7.038E-02
MEIS2	24.301	29	1.193	7.056E-02
Pou5f1::Sox2	39.439	43	1.090	7.144E-02
MAFG	16.531	21	1.270	7.285E-02
MSC	31.747	36	1.134	7.328E-02
Nr1h3::Rxra	29.728	34	1.144	7.636E-02
MLX	13.871	18	1.298	7.791E-02
BHLHE40	12.110	16	1.321	8.043E-02
TCF7L1	52.127	53	1.017	8.604E-02
TEAD2	33.599	37	1.101	9.235E-02
RXRG	31.440	35	1.113	9.327E-02
ONECUT3	20.021	24	1.199	9.373E-02
Gfi1	28.284	32	1.131	9.533E-02
EBF1	29.495	33	1.119	9.969E-02
Hoxa9	20.196	24	1.188	1.004E-01
Alx4	17.258	21	1.217	1.007E-01
EOMES	21.259	25	1.176	1.027E-01
Hes2	13.518	17	1.258	1.035E-01
THAP1	37.658	40	1.062	1.113E-01
BARX1	14.659	18	1.228	1.136E-01
DMRT3	14.692	18	1.225	1.152E-01
MAX	17.693	21	1.187	1.202E-01
Esrra	27.991	31	1.108	1.211E-01
Id2	16.784	20	1.192	1.236E-01
Gfi1b	45.179	46	1.018	1.242E-01
Pitx1	15.873	19	1.197	1.267E-01
POU2F2	32.520	35	1.076	1.270E-01
BHLHE23	7.589	10	1.318	1.278E-01
VENTX	7.593	10	1.317	1.281E-01

OLIG1	6.730	9	1.337	1.282E-01
Lhx4	14.985	18	1.201	1.308E-01
RORA(var.2)	20.980	24	1.144	1.335E-01
MLXIPL	13.130	16	1.219	1.337E-01
STAT1::STAT2	85.134	75	0.881	1.359E-01
OLIG2	6.827	9	1.318	1.366E-01
NEUROG2	11.337	14	1.235	1.386E-01
Atoh1	7.746	10	1.291	1.406E-01
RORB	21.221	24	1.131	1.449E-01
mix-a	27.650	30	1.085	1.500E-01
Nkx3-1	19.323	22	1.139	1.518E-01
SPI1	41.325	42	1.016	1.527E-01
Mafb	25.631	28	1.092	1.556E-01
Dux	9.750	12	1.231	1.572E-01
MYF6	24.638	27	1.096	1.587E-01
SOX8	26.825	29	1.081	1.610E-01
BHLHE22	6.220	8	1.286	1.613E-01
MNT	16.498	19	1.152	1.617E-01
MAFF	30.211	32	1.059	1.659E-01
BCL6B	29.160	31	1.063	1.682E-01
MEF2D	29.212	31	1.061	1.704E-01
ZNF354C	89.960	77	0.856	1.708E-01
Bcl6	50.464	49	0.971	1.710E-01
JUN	32.657	34	1.041	1.749E-01
RUNX3	28.276	30	1.061	1.777E-01
HES5	11.885	14	1.178	1.779E-01
JUN::JUNB(var.2)	15.811	18	1.138	1.807E-01
RARA::RXRA	32.890	34	1.034	1.849E-01
PBX2	29.555	31	1.049	1.860E-01
Nr2e3	29.567	31	1.048	1.865E-01
Mecom	27.409	29	1.058	1.885E-01
HNF4G	54.907	52	0.947	1.899E-01
TGIF2	23.151	25	1.080	1.906E-01
Nkx2-5(var.2)	36.477	37	1.014	1.910E-01
PRRX1	21.089	23	1.091	1.927E-01
UNCX	21.089	23	1.091	1.927E-01
CDX1	27.510	29	1.054	1.935E-01
TGIF1	23.216	25	1.077	1.941E-01
TEAD4	31.979	33	1.032	1.946E-01

Myod1	67.261	61	0.907	1.961E-01
GSC2	11.163	13	1.165	1.962E-01
HIC2	29.776	31	1.041	1.964E-01
Znf423	27.619	29	1.050	1.989E-01
TWIST1	35.544	36	1.013	2.006E-01
HSF1	25.481	27	1.060	2.009E-01
Arntl	18.177	20	1.100	2.037E-01
Crx	22.335	24	1.075	2.040E-01
TAL1::TCF3	25.604	27	1.055	2.075E-01
NFATC2	54.229	51	0.940	2.105E-01
IRF9	32.404	33	1.018	2.144E-01
HOXC13	16.330	18	1.102	2.163E-01
POU6F1	14.351	16	1.115	2.180E-01
Tcf12	66.629	60	0.901	2.187E-01
Sox1	16.400	18	1.098	2.213E-01
SOX9	22.661	24	1.059	2.233E-01
NEUROD2	5.875	7	1.191	2.234E-01
Nr2f6	36.247	36	0.993	2.323E-01
SREBF2	23.983	25	1.042	2.384E-01
NR1A4::RXRA	14.623	16	1.094	2.393E-01
NFAT5	36.477	36	0.987	2.431E-01
GCM1	11.704	13	1.111	2.437E-01
NKX3-2	17.789	19	1.068	2.479E-01
JUND(var.2)	29.669	30	1.011	2.482E-01
BATF3	15.753	17	1.079	2.489E-01
GSC	10.788	12	1.112	2.491E-01
ZNF282	26.401	27	1.023	2.524E-01
PKNOX2	29.867	30	1.004	2.590E-01
MXI1	20.066	21	1.047	2.614E-01
Lhx8	19.048	20	1.050	2.638E-01
HOXC12	9.016	10	1.109	2.652E-01
Sox17	24.443	25	1.023	2.668E-01
LBX1	22.278	23	1.032	2.670E-01
TBR1	20.152	21	1.042	2.674E-01
PKNOX1	25.597	26	1.016	2.704E-01
NFIL3	15.025	16	1.065	2.725E-01
GMEB2	3.544	4	1.129	2.750E-01
Dlx2	15.113	16	1.059	2.798E-01
MAF::NFE2	42.072	40	0.951	2.803E-01

Crem	7.246	8	1.104	2.809E-01
Spz1	24.692	25	1.012	2.827E-01
Stat6	40.938	39	0.953	2.845E-01
TFAP2A(var.3)	30.330	30	0.989	2.852E-01
EWSR1-FLI1	134.215	99	0.738	2.888E-01
TFAP2B(var.3)	34.015	33	0.970	2.973E-01
MEF2B	23.872	24	1.005	3.011E-01
NFKB2	14.351	15	1.045	3.027E-01
Rxra	31.835	31	0.974	3.056E-01
Nobox	16.458	17	1.033	3.065E-01
PAX4	13.453	14	1.041	3.141E-01
HSF4	25.288	25	0.989	3.221E-01
Sox11	29.926	29	0.969	3.293E-01
LHX6	15.706	16	1.019	3.316E-01
TBX1	32.328	31	0.959	3.343E-01
SHOX	20.009	20	1.000	3.366E-01
Prrx2	20.009	20	1.000	3.366E-01
LHX9	20.009	20	1.000	3.366E-01
RAX2	20.009	20	1.000	3.366E-01
IRF2	33.567	32	0.953	3.382E-01
FOXA1	43.274	40	0.924	3.383E-01
VDR	24.458	24	0.981	3.415E-01
SOX4	29.078	28	0.963	3.481E-01
EVX2	13.832	14	1.012	3.506E-01
NFATC1	30.286	29	0.958	3.516E-01
ELF5	33.821	32	0.946	3.530E-01
LHX2	19.167	19	0.991	3.554E-01
SMAD2::SMAD3::SMAD4	55.306	49	0.886	3.562E-01
Foxq1	30.457	29	0.952	3.623E-01
TFAP2C(var.3)	29.413	28	0.952	3.696E-01
PROX1	9.933	10	1.007	3.711E-01
FOXF2	26.022	25	0.961	3.724E-01
GCM2	7.965	8	1.004	3.756E-01
HNF1B	16.220	16	0.986	3.781E-01
RREB1	108.233	83	0.767	3.799E-01
RFX3	18.387	18	0.979	3.804E-01
Myog	69.897	59	0.844	3.815E-01
FOS::JUN(var.2)	18.432	18	0.977	3.842E-01
NFIX	22.821	22	0.964	3.844E-01

Neurog1	8.035	8	0.996	3.849E-01
Pparg::Rxra	67.251	57	0.848	3.909E-01
Alx1	18.513	18	0.972	3.911E-01
STAT3	60.313	52	0.862	3.954E-01
MIXL1	21.866	21	0.960	3.964E-01
NR4A2::RXRA	13.284	13	0.979	4.003E-01
Sox5	18.632	18	0.966	4.013E-01
BARHL2	7.166	7	0.977	4.030E-01
RELB	19.759	19	0.962	4.043E-01
RXRA::VDR	17.593	17	0.966	4.053E-01
TFAP2A(var.2)	45.920	41	0.893	4.077E-01
JUNB(var.2)	11.281	11	0.975	4.088E-01
T	10.250	10	0.976	4.089E-01
ISX	18.758	18	0.960	4.121E-01
Shox2	18.758	18	0.960	4.121E-01
Stat5a::Stat5b	47.312	42	0.888	4.130E-01
E2F1	4.278	4	0.935	4.148E-01
ZBTB18	43.559	39	0.895	4.175E-01
BACH2	55.356	48	0.867	4.181E-01
Dmbx1	11.384	11	0.966	4.205E-01
Nfe2l2	41.152	37	0.899	4.235E-01
IRF4	20.017	19	0.949	4.258E-01
MEF2A	32.737	30	0.916	4.318E-01
NFATC3	30.382	28	0.922	4.329E-01
LMX1A	23.521	22	0.935	4.377E-01
LMX1B	23.521	22	0.935	4.377E-01
HOXC11	8.429	8	0.949	4.379E-01
VSX1	16.880	16	0.948	4.387E-01
VSX2	16.880	16	0.948	4.387E-01
RHOXF1	20.174	19	0.942	4.389E-01
CREB3L1	12.603	12	0.952	4.395E-01
JDP2(var.2)	17.981	17	0.945	4.397E-01
Dlx1	17.999	17	0.944	4.414E-01
TFAP2C(var.2)	37.749	34	0.901	4.415E-01
STAT1	42.755	38	0.889	4.421E-01
TBX20	23.666	22	0.930	4.488E-01
LBX2	19.226	18	0.936	4.524E-01
POU4F2	28.363	26	0.917	4.551E-01
ATF7	13.821	13	0.941	4.558E-01

SOX21	22.634	21	0.928	4.567E-01
HSF2	27.256	25	0.917	4.593E-01
DBP	8.610	8	0.929	4.622E-01
PAX7	8.614	8	0.929	4.627E-01
Lhx3	27.307	25	0.916	4.628E-01
RAX	19.368	18	0.929	4.646E-01
SMAD3	10.731	10	0.932	4.662E-01
NR1H4	19.398	18	0.928	4.671E-01
PITX3	18.325	17	0.928	4.703E-01
Foxd3	66.774	55	0.824	4.872E-01
ONECUT1	8.799	8	0.909	4.873E-01
Hoxa11	9.908	9	0.908	4.944E-01
ISL2	17.494	16	0.915	4.950E-01
CDX2	31.364	28	0.893	4.974E-01
RORC	19.752	18	0.911	4.974E-01
HOXD12	8.880	8	0.901	4.978E-01
CREB3	9.937	9	0.906	4.979E-01
TFAP2B	40.023	35	0.874	5.004E-01
CEBPD	5.772	5	0.866	5.014E-01
REST	45.265	39	0.862	5.071E-01
RUNX2	26.797	24	0.896	5.096E-01
TFAP2A	42.768	37	0.865	5.115E-01
FOSL1::JUN(var.2)	12.217	11	0.900	5.142E-01
GSX2	30.437	27	0.887	5.153E-01
HES7	11.273	10	0.887	5.296E-01
NOTO	17.881	16	0.895	5.299E-01
FOSB::JUN	17.962	16	0.891	5.371E-01
E2F8	19.137	17	0.888	5.412E-01
XBP1	8.146	7	0.859	5.415E-01
HLF	11.384	10	0.878	5.422E-01
RFX4	19.163	17	0.887	5.434E-01
EN1	14.692	13	0.885	5.442E-01
ATF4	15.837	14	0.884	5.475E-01
LIN54	27.416	24	0.875	5.533E-01
Rarg(var.2)	29.811	26	0.872	5.535E-01
TBX21	21.613	19	0.879	5.569E-01
TFAP2C	39.777	34	0.855	5.576E-01
Atf1	5.073	4	0.788	5.603E-01
PBX3	47.630	40	0.840	5.609E-01

MGA	22.832	20	0.876	5.617E-01
TBX15	22.832	20	0.876	5.617E-01
ALX3	25.203	22	0.873	5.642E-01
IRF8	22.870	20	0.875	5.647E-01
HLTF	12.696	11	0.866	5.660E-01
Foxa2	39.944	34	0.851	5.669E-01
Pou2f3	28.830	25	0.867	5.682E-01
Barhl1	18.328	16	0.873	5.693E-01
SPIB	84.186	65	0.772	5.693E-01
HOXA5	14.949	13	0.870	5.694E-01
POU3F2	31.284	27	0.863	5.705E-01
NR1H2::RXRA	31.316	27	0.862	5.725E-01
MEOX2	29.023	25	0.861	5.811E-01
FOSB::JUNB(var.2)	13.972	12	0.859	5.831E-01
DUX4	19.658	17	0.865	5.851E-01
HOXB2	24.362	21	0.862	5.887E-01
EVX1	12.965	11	0.848	5.941E-01
ELF3	26.828	23	0.857	5.952E-01
ZBTB7C	15.258	13	0.852	5.988E-01
GBX2	18.769	16	0.852	6.068E-01
GSX1	24.634	21	0.852	6.084E-01
Rfx1	34.396	29	0.843	6.101E-01
FOSL2::JUN(var.2)	21.131	18	0.852	6.103E-01
Hmx3	24.696	21	0.850	6.128E-01
SREBF1	23.513	20	0.851	6.129E-01
SNAI2	36.974	31	0.838	6.138E-01
NFIC::TLX1	39.593	33	0.833	6.176E-01
IRF7	38.345	32	0.835	6.194E-01
Hoxd3	27.194	23	0.846	6.200E-01
Tcf21	26.064	22	0.844	6.249E-01
RFX2	16.685	14	0.839	6.251E-01
POU3F4	23.723	20	0.843	6.282E-01
SP1	153.810	101	0.657	6.326E-01
TBP	16.784	14	0.834	6.337E-01
CEBPG	7.753	6	0.774	6.345E-01
NKX6-2	23.823	20	0.840	6.353E-01
NHLH1	39.982	33	0.825	6.383E-01
TP53	21.500	18	0.837	6.385E-01
ZNF740	41.401	34	0.821	6.446E-01

SP2	137.597	93	0.676	6.474E-01
Hoxd8	30.128	25	0.830	6.517E-01
MSX1	14.692	12	0.817	6.519E-01
MSX2	14.692	12	0.817	6.519E-01
BSX	14.692	12	0.817	6.519E-01
Arid5a	13.551	11	0.812	6.522E-01
Hoxb5	24.071	20	0.831	6.528E-01
MNX1	33.967	28	0.824	6.578E-01
Ar	15.914	13	0.817	6.581E-01
GBX1	15.914	13	0.817	6.581E-01
Creb5	16.023	13	0.811	6.675E-01
FOXB1	34.181	28	0.819	6.698E-01
TCF4	31.679	26	0.821	6.703E-01
MTF1	17.240	14	0.812	6.720E-01
RBPJ	67.193	52	0.774	6.760E-01
FOSL2::JUND(var.2)	19.647	16	0.814	6.766E-01
FOSL2::JUNB(var.2)	13.821	11	0.796	6.773E-01
HMBOX1	11.554	9	0.779	6.807E-01
Smad4	26.972	22	0.816	6.844E-01
KLF4	54.477	43	0.789	6.865E-01
HOXC10	12.782	10	0.782	6.881E-01
Stat4	53.170	42	0.790	6.902E-01
Bach1::Mafk	46.340	37	0.798	6.909E-01
OTX2	14.034	11	0.784	6.964E-01
HOXA2	17.564	14	0.797	6.978E-01
NR3C1	14.073	11	0.782	6.999E-01
HOXB13	32.243	26	0.806	7.022E-01
Six3	9.479	7	0.738	7.041E-01
POU5F1B	24.869	20	0.804	7.058E-01
GATA2	21.274	17	0.799	7.080E-01
POU3F3	32.368	26	0.803	7.090E-01
HOXB3	24.942	20	0.802	7.104E-01
IRF3	48.215	38	0.788	7.136E-01
DUXA	17.774	14	0.788	7.138E-01
MEF2C	49.757	39	0.784	7.207E-01
Arx	15.527	12	0.773	7.232E-01
ESX1	19.167	15	0.783	7.284E-01
HOXA13	32.737	26	0.794	7.286E-01
HOXD13	32.870	26	0.791	7.354E-01

ONECUT2	12.153	9	0.741	7.369E-01
POU3F1	31.675	25	0.789	7.394E-01
IRF1	125.912	85	0.675	7.406E-01
Ahr::Arnt	55.911	43	0.769	7.420E-01
NR2C2	54.590	42	0.769	7.457E-01
TCF3	29.294	23	0.785	7.470E-01
OTX1	2.695	1	0.371	7.482E-01
RARA::RXRG	31.923	25	0.783	7.520E-01
PLAG1	49.185	38	0.773	7.528E-01
MEOX1	22.051	17	0.771	7.585E-01
TFAP2B(var.2)	41.228	32	0.776	7.604E-01
VAX1	22.104	17	0.769	7.617E-01
VAX2	22.104	17	0.769	7.617E-01
Msx3	22.134	17	0.768	7.635E-01
CUX2	4.067	2	0.492	7.666E-01
ESR1	17.328	13	0.750	7.677E-01
PPARG	23.445	18	0.768	7.682E-01
Nr2e1	31.013	24	0.774	7.701E-01
SRY	23.532	18	0.765	7.732E-01
Pax2	7.794	5	0.641	7.743E-01
GATA6	23.597	18	0.763	7.768E-01
Hmx2	23.628	18	0.762	7.785E-01
KLF13	27.389	21	0.767	7.791E-01
NR3C2	13.878	10	0.721	7.799E-01
HOXD11	10.307	7	0.679	7.835E-01
FOXK1	31.312	24	0.766	7.844E-01
IRF5	16.407	12	0.731	7.873E-01
ZBTB7B	12.847	9	0.701	7.931E-01
CUX1	4.278	2	0.468	7.951E-01
GRHL2	29.003	22	0.759	7.961E-01
EMX2	15.327	11	0.718	7.965E-01
DLX6	16.550	12	0.725	7.966E-01
Ascl2	49.062	37	0.754	7.990E-01
GLI2	17.822	13	0.729	7.996E-01
PAX9	10.508	7	0.666	8.002E-01
RELA	27.881	21	0.753	8.033E-01
FOSL1::JUND(var.2)	11.768	8	0.680	8.034E-01
GATA3	20.481	15	0.732	8.105E-01
FIGLA	23.003	17	0.739	8.118E-01

Dlx4	14.341	10	0.697	8.122E-01
PAX3	8.205	5	0.609	8.129E-01
ASCL1	73.555	53	0.721	8.228E-01
FOXP2	45.653	34	0.745	8.245E-01
ZNF24	34.936	26	0.744	8.277E-01
HOXA10	32.340	24	0.742	8.289E-01
RFX5	18.362	13	0.708	8.306E-01
Dlx3	18.399	13	0.707	8.326E-01
Tcfl5	9.715	6	0.618	8.342E-01
PDX1	18.643	13	0.697	8.453E-01
REL	24.992	18	0.720	8.457E-01
MZF1(var.2)	43.760	32	0.731	8.520E-01
PPARA::RXRA	32.962	24	0.728	8.523E-01
CEBPE	7.457	4	0.536	8.553E-01
PAX1	10.025	6	0.599	8.559E-01
TP73	21.398	15	0.701	8.559E-01
NKX6-1	23.964	17	0.709	8.564E-01
FOXD1	22.718	16	0.704	8.579E-01
FOXO3	22.718	16	0.704	8.579E-01
KLF9	100.397	68	0.677	8.589E-01
TEF	8.810	5	0.568	8.600E-01
SCRT2	21.594	15	0.695	8.645E-01
EMX1	19.107	13	0.680	8.673E-01
HESX1	16.564	11	0.664	8.674E-01
Gata1	28.296	20	0.707	8.733E-01
EHF	24.416	17	0.696	8.743E-01
GLIS3	16.726	11	0.658	8.750E-01
TP63	16.810	11	0.654	8.788E-01
E2F3	3.710	1	0.270	8.827E-01
E2F7	13.080	8	0.612	8.843E-01
ZEB1	43.572	31	0.711	8.853E-01
POU6F2	24.750	17	0.687	8.864E-01
JUN(var.2)	55.143	39	0.707	8.880E-01
POU1F1	32.789	23	0.701	8.897E-01
CEBPB	7.968	4	0.502	8.902E-01
JUND	51.009	36	0.706	8.931E-01
SPDEF	11.967	7	0.585	8.932E-01
FOXI1	30.302	21	0.693	8.952E-01
FOXL1	30.302	21	0.693	8.952E-01

FOXD2	30.302	21	0.693	8.952E-01
FOXO4	30.302	21	0.693	8.952E-01
FOXO6	30.302	21	0.693	8.952E-01
FOXP3	30.302	21	0.693	8.952E-01
PROP1	21.116	14	0.663	8.960E-01
Arid3a	140.131	87	0.621	8.973E-01
MYBL2	3.904	1	0.256	8.992E-01
FOXP1	30.520	21	0.688	9.014E-01
POU2F1	27.940	19	0.680	9.039E-01
HIF1A	8.216	4	0.487	9.043E-01
ZNF384	84.438	57	0.675	9.063E-01
MYBL1	4.019	1	0.249	9.079E-01
CEBPA	24.144	16	0.663	9.092E-01
GLIS1	11.057	6	0.543	9.119E-01
YY1	32.311	22	0.681	9.130E-01
HNF1A	21.651	14	0.647	9.136E-01
TBX2	21.696	14	0.645	9.150E-01
YY2	8.436	4	0.474	9.155E-01
FOXC1	37.935	26	0.685	9.162E-01
ARNT::HIF1A	7.142	3	0.420	9.202E-01
FOSL1::JUNB	48.080	33	0.686	9.210E-01
Atf3	8.572	4	0.467	9.218E-01
EN2	12.707	7	0.551	9.243E-01
POU5F1	31.587	21	0.665	9.276E-01
GATA1::TAL1	20.856	13	0.623	9.288E-01
PAX5	13.062	7	0.536	9.362E-01
KLF16	114.026	72	0.631	9.362E-01
SP3	112.302	71	0.632	9.378E-01
GATA5	18.558	11	0.593	9.387E-01
ESR2	39.693	26	0.655	9.478E-01
GRHL1	14.917	8	0.536	9.495E-01
Hand1::Tcf3	28.629	18	0.629	9.498E-01
Hoxd9	34.254	22	0.642	9.509E-01
FOXC2	56.153	37	0.659	9.517E-01
NFYA	23.300	14	0.601	9.528E-01
Zfx	57.913	38	0.656	9.542E-01
FOXG1	26.138	16	0.612	9.543E-01
Foxj2	26.138	16	0.612	9.543E-01
POU4F3	29.027	18	0.620	9.562E-01

SP8	92.714	59	0.636	9.568E-01
FOSL2	52.167	34	0.652	9.575E-01
ZNF410	15.378	8	0.520	9.595E-01
FOSL1	55.456	36	0.649	9.602E-01
CENPB	5.063	1	0.198	9.603E-01
INSM1	42.246	27	0.639	9.619E-01
E2F2	6.848	2	0.292	9.646E-01
POU4F1	29.776	18	0.605	9.663E-01
Hes1	14.391	7	0.486	9.673E-01
Foxo1	48.868	31	0.634	9.688E-01
FOS	54.957	35	0.637	9.691E-01
ID4	30.168	18	0.597	9.707E-01
FOXK2	31.935	19	0.595	9.740E-01
Gata4	24.823	14	0.564	9.742E-01
FOS::JUN	48.369	30	0.620	9.763E-01
TFCP2	10.575	4	0.378	9.768E-01
ELF4	25.284	14	0.554	9.786E-01
E2F6	72.768	45	0.618	9.802E-01
Foxj3	45.985	28	0.609	9.803E-01
ELF1	22.684	12	0.529	9.810E-01
FOSL2::JUNB	44.650	27	0.605	9.813E-01
SP4	74.715	46	0.616	9.814E-01
ETV6	31.424	18	0.573	9.815E-01
GLIS2	18.550	9	0.485	9.829E-01
Phox2b	20.140	10	0.497	9.839E-01
Nkx2-5	24.573	13	0.529	9.844E-01
JUNB	54.509	33	0.605	9.847E-01
FOS::JUND	54.554	33	0.605	9.849E-01
FOSB::JUNB	43.978	26	0.591	9.856E-01
Klf1	77.697	47	0.605	9.861E-01
Arid3b	29.290	16	0.546	9.864E-01
TBX4	19.174	9	0.469	9.875E-01
TBX5	19.174	9	0.469	9.875E-01
KLF5	144.201	81	0.562	9.877E-01
FOSL1::JUN	53.791	32	0.595	9.880E-01
NFYB	23.704	12	0.506	9.881E-01
FOSL2::JUN	49.259	29	0.589	9.884E-01
TFDP1	23.926	12	0.502	9.892E-01
ZBTB33	10.222	3	0.293	9.899E-01

JUN::JUNB	35.993	20	0.556	9.900E-01
BATF::JUN	45.372	26	0.573	9.909E-01
FOS::JUNB	42.708	24	0.562	9.921E-01
SCRT1	21.594	10	0.463	9.922E-01
FOSL2::JUND	44.526	25	0.561	9.928E-01
KLF14	54.120	31	0.573	9.932E-01
FOSL1::JUND	47.866	27	0.564	9.933E-01
PHOX2A	21.991	10	0.455	9.936E-01
Klf12	51.338	29	0.565	9.940E-01
ERF	22.327	10	0.448	9.946E-01
NFE2	33.967	17	0.500	9.964E-01
JDP2	38.793	20	0.516	9.966E-01
EGR2	24.247	10	0.412	9.981E-01
ELK4	29.598	13	0.439	9.985E-01
ETV3	16.964	5	0.295	9.990E-01
EGR3	42.517	20	0.470	9.993E-01
ETV2	23.148	8	0.346	9.995E-01
HINFP	12.775	2	0.157	9.997E-01
ETV1	14.873	3	0.202	9.997E-01
ZBTB7A	37.832	16	0.423	9.997E-01
ZIC4	31.384	12	0.382	9.998E-01
ZIC1	33.446	13	0.389	9.998E-01
ERG	19.412	5	0.258	9.998E-01
Gabpa	27.035	9	0.333	9.999E-01
EGR1	23.727	7	0.295	9.999E-01
EGR4	36.063	14	0.388	9.999E-01
ELK1	16.264	3	0.184	9.999E-01
ZIC3	31.412	11	0.350	9.999E-01
ELK3	16.733	3	0.179	9.999E-01
FEV	17.807	3	0.168	1.000E+00
E2F4	31.344	10	0.319	1.000E+00
ETV4	15.815	2	0.126	1.000E+00
ETS1	20.646	4	0.194	1.000E+00
ETV5	14.030	1	0.071	1.000E+00
FLI1	20.017	3	0.150	1.000E+00
CTCFL	86.496	36	0.416	1.000E+00
NRF1	31.519	7	0.222	1.000E+00
CTCF	104.673	43	0.411	1.000E+00

REFERENCES

Adam, R.C., Yang, H., Ge, Y., Lien, W.H., Wang, P., Zhao, Y., Polak, L., Levorse, J., Baksh, S.C., Zheng, D., et al. 2018. Temporal Layer of Signaling Effectors Drives Chromatin Remodeling during Hair Follicle Stem Cell Lineage Progression. *Cell Stem Cell* 22(3):398-413.

Adameyko, I., Lallemend, F., Aquino, J. B., Pereira, J. A., Topilko, P., Müller, T., Fritz, N., Beljajeva, A., Mochii, M., Liste, I. et al. 2009. Schwann cell precursors from nerve innervation are a cellular origin of melanocytes in skin. *Cell* 139, 366-379.

Alexandrov, L.B., Nik-Zainal, S., Wedge, D.C., Aparicio, S.A., Behjati, S., Biankin, A.V., Bignell, G.R., Bolli, N., Borg, A., Børresen-Dale, A.L., et al. 2012. Signatures of mutational processes in human cancer. *Nature* 500(7463):415-21.

Armenteros, T., Andreu, Z., Hortigüela, R., Lie, D.C., Mira, H. 2018. BMP and WNT signalling cooperate through LEF1 in the neuronal specification of adult hippocampal neural stem and progenitor cells. *Sci. Rep.* 8, 9241.

Becht, E., McInnes, L., Healy, J., Dutertre, C.-A., Kwok, I.W.H., Ng, L.G., Ginhoux, F., Newell, E.W. 2019. Dimensionality reduction for visualizing single-cell data using UMAP. *Nat. Biotechnol.* 37, 38–44.

Belmadani, A., Jung, H., Ren, D., Miller, R.J. 2009. The chemokine SDF-1/CXCL12 regulates the migration of melanocyte progenitors in mouse hair follicles. *Differentiation* 77(4):395-411.

Belote, R.L., Le, D., Maynard, A., Lang, U.E., Sinclair, A., Planells-Palop, V., Baskin, L., Tward, A.D., Darmanis, S., Judson-Torres, R.L.. 2020. Human melanocyte development and melanoma dedifferentiation at single cell resolution. bioRxiv 2020.05.25.115287.

Bergqvist, C., Ezzedine, K. 2020. Vitiligo: A Review. *Dermatology* 236(6):571-592.

Beumer, J., Clevers, H. 2021. Cell fate specification and differentiation in the adult mammalian intestine. *Nat Rev Mol Cell Biol.* 22(1):39-53.

Bilodeau, M. L., Greulich, J.D., Hullinger, R.L., Bertolotto C., Ballotti, R., Andrisani, O.M. 2001. BMP-2 stimulates tyrosinase gene expression and melanogenesis in differentiated melanocytes. *Pigment Cell Res.* 14(5):328-36.

Blondel, V.D., Guillaume, J-L., Lambiotte, R., Lefebvre, E. 2008. Fast unfolding of communities in large networks. *Journal of Statistical Mechanics: Theory and Experiment* 2008 (10): P10008.

Boiko, A.D., Razorenova, O.V., van de Rijn, M., Swetter, S.M., Johnson, D.L., Ly, D.P., Butler, P.D., Yang, G.P., Joshua B, Kaplan M.J., et al. 2010. Human melanoma-initiating cells express neural crest nerve growth factor receptor CD271. *Nature* 466(7302):133-7.

Bosenberg, M., Muthusamy, V., Curley, D.P., Wang, Z., Hobbs, C., Nelson, B., Nogueira C., Horner, J.W. 2nd, Depinho, R., Chin, L. 2006. Characterization of melanocyte-specific inducible Cre recombinase transgenic mice. *Genesis* 44(5):262-7.

Botchkareva, N.V., Khlgatian, M., Longley, B.J., Botchkarev, V.A., Gilchrest, B.A. 2001. SCF/c-kit signaling is required for cyclic regeneration of the hair pigmentation unit. *FASEB J* 15(3):645-58.

Braig, S., Bosserhoff, A.K. 2013. Death inducer-obliterator 1 (Dido1) is a BMP target gene and promotes BMP-induced melanoma progression. *Oncogene* **32**(7):837-48.

Brault, V., Moore, R., Kutsch, S., Ishibashi, M., Rowitch, D.H., McMahon, A.P., Sommer, L., Boussadia, O., Kemler, R. 2001. Inactivation of the beta-catenin gene by Wnt1-Cre-mediated deletion results in dramatic brain malformation and failure of craniofacial development. *Development* 128(8):1253-64.

Brennecke, P., Anders, S., Kim, J.K., Kołodziejczyk, A.A, Zhang, X., Proserpio, V., Baying, B., Benes, V., Teichmann, S.A., Marioni, J.C., Heisler, M.G. 2013. Accounting for technical noise in single-cell RNA-seq experiments. *Nat. Methods* 10(11):1093-5.

Buenrostro, J.D., Giresi, P.G., Zaba, L.C., Chang, H.Y., Greenleaf, W.J. 2013. Transposition of native chromatin for multimodal regulatory analysis and personal epigenomics. *Nat. Methods* 10(12): 1213–1218.

Cao, J., Spielmann, M., Qiu, X., Huang, X., Ibrahim, D.M., Hill, A.J., Zhang, F., Mundlos, S., Christiansen, L., Steemers, F.J., et al. 2019. The single-cell transcriptional landscape of mammalian organogenesis. *Nature* **566**, 496–502.

Caro T, Mallarino R. 2020. Coloration in Mammals. *Trends Ecol Evol.* 35(4):357-366.

Carreira, S., Goodall, J., Denat, L., Rodriguez, M., Nuciforo, P., Hoek, K.S., Testori, A., Larue, L., Goding, C.R. 2006. Mitf regulation of Dia1 controls melanoma proliferation and invasiveness. *Genes Dev.* 20(24): 3426–3439.

Chang, C.Y., Pasolli, H.A., Giannopoulou, E.G., Guasch, G., Gronostajski, R.M., Elemento, O., Fuchs, E. 2013. NFIB is a governor of epithelial-melanocyte stem cell behavior in a shared niche. *Nature* 495(7439):98-102.

Cheli, Y., Giuliano, S., Botton, T., Rocchi, S., Hofman, V., Hofman, P., Bahadoran, P., Bertolotto, C., Ballotti, R. 2011. Mitf is the key molecular switch between mouse or human melanoma initiating cells and their differentiated progeny. *Oncogene* 30(20):2307-18.

Chen, G., Deng, C., Li, Y.P. 2012. TGF-β and BMP signaling in osteoblast differentiation and bone formation. *Int J Biol Sci.* 8(2):272-88.

David, C.J., Huang, Y.H., Chen, M., Su, J., Zou, Y., Bardeesy, N., Iacobuzio-Donahue, C.A., Massague, J. 2016. TGF-β Tumor Suppression through a Lethal EMT. *Cell* 164(5):1015-30.

David, C.J., Massague, J. 2018. Contextual determinants of TGFβ action in development, immunity and cancer. *Nat. Rev. Mol. Cell Biol*. 19(7):419-435.

Davis, L.E., Shalin, S.C., Tackett, A.J. 2019. Current state of melanoma diagnosis and treatment. *Cancer Biol Ther.* 20(11):1366-1379.

Dobin, A., Davis, C.A., Schlesinger, F., Drenkow, J., Zaleski, C., Jha, S., Batut, P., Chaisson, M., Gingeras, T.R. 2013. STAR: ultrafast universal RNA-seq aligner. *Bioinformatics* 29(1):15-21.

Dorsky, R.I., Raible, D.W., Moon, R.T. 2000. Direct regulation of nacre, a zebrafish MITF homolog required for pigment cell formation, by the Wnt pathway. *Genes Dev.* 14(2):158-62.

Enshell-Seijffers, D., Lindon, C., Wu, E., Taketo, M. M., Morgan, B.A. 2010. β-Catenin activity in the dermal papilla of the hair follicle regulates pigment-type switching. *Proc. Natl. Acad. Sci.USA* 107(50):21564-9.

Erickson, C.A., Goins, T.L. 1995. Avian neural crest cells can migrate in the dorsolateral path only if they are specified as melanocytes. *Development* 121(3):915-24.

Fang, D., Nguyen, T.K., Leishear, K., Finko, R., Kulp, A.N., Hotz, S., Van Belle, P.A., Xu, X., Elder, D.E., Herlyn, M. 2005. A tumorigenic subpopulation with stem cell properties in melanomas. *Cancer Res.* 65(20):9328-37.

Fazio, M., van Rooijen, E., Dang, M., van de Hoek, G., Ablain, J., Mito, J.K., Yang, S., Thomas, A., Michael J, Fabo T, et al. 2021. SATB2 induction of a neural crest mesenchyme-like program drives melanoma invasion and drug resistance. *Elife* 10:e64370.

Feng, J., Liu, T., Qin, B., Zhang, Y., Liu, X. S. 2012. Identifying ChIP-seq enrichment using MACS. *Nat. Protoc.* 7(9):1728-40.

Filoni, A., Mariano, M., Cameli, N. 2019. Melasma: How hormones can modulate skin pigmentation. *J Cosmet Dermatol*. 18(2):458-463.

Fornes, O., Castro-Mondragon, J.A., Khan, A., van der Lee, R., Zhang, X., Richmond, P.A., Modi, B.P., Correard, S., Gheorghe, M., Baranašić, D., et al. 2020. JASPAR 2020: update of the open-access database of transcription factor binding profiles. *Nucleic Acids Res.* 8;48(D1):D87-D92.

Gajos-Michniewicz, A., Czyz, M. 2020. WNT Signaling in Melanoma. *Int J Mol Sci.* 21(14):4852.

Ge, Y., Gomez, N.C., Adam, R.C., Nikolova, M., Yang, H., Verma, A., Lu, C.P., Polak L., Yuan, S., Elemento, O., et al. 2017. Stem Cell Lineage Infidelity Drives Wound Repair and Cancer. *Cell* 169(4):636-650.

Genander, M., Cook, P.J., Ramsköld, D., Keyes, B.E., Mertz, A.F., Sandberg, R., Fuchs, E. 2014. BMP Signaling and Its pSMAD1/5 Target Genes Differentially Regulate Hair Follicle Stem Cell Lineages. *Cell Stem Cell* 15(5): 619–633.

Glover, J.D., Knolle, S., Wells, K.L., Liu, D., Jackson, I.J., Mort, R.L., Headon, D.J. 2015. Maintenance of distinct melanocyte populations in the interfollicular epidermis. *Pigment Cell Melanoma Res.* 28(4):476-80.

Goding, C.R., Arnheiter, H. 2019. MITF – the first 25 years. *Genes Dev.* 33: 983-1007.

Gong, S., Zheng, C., Doughty, M.L., Losos, K., Didkovsky, N., Schambra, U.B., Nowak, N.J., Joyner, A., Leblanc, G., Hatten, et al. 2003. A gene expression atlas of the central nervous system based on bacterial artificial chromosomes. *Nature* 425(6961):917-25.

Gonzales, K., & Fuchs, E. (2017). Skin and Its Regenerative Powers: An Alliance between Stem Cells and Their Niche. *Developmental Cell* 43(4), 387–401.

Gramann, A.K., Venkatesan, A.M., Guerin, M., Ceol, C.J. 2019. Regulation of zebrafish melanocyte development by ligand-dependent BMP signaling. *Elife* 2019;8:e50047.

Guasch, G., Schober, M., Pasolli, H.A., Conn, E.B., Polak, L., Fuchs, E. 2007. Loss of TGFbeta signaling destabilizes homeostasis and promotes squamous cell carcinomas in stratified epithelia. *Cancer Cell* 12(4):313-27.

Gupta, P.B., Kuperwasser, C., Brunet, J.P., Ramaswamy, S., Kuo, W.L., Gray, J.W., Naber, S.P., Weinberg, R.A. 2005. The melanocyte differentiation program predisposes to metastasis after neoplastic transformation. *Nat Genet.* 37(10):1047-54.

Han, R., Beppu, H., Lee, Y.K., Georgopoulos, K., Larue, L., Li, E., Weiner, L., Brissette J. L. A pair of transmembrane receptors essential for the retention and pigmentation of hair. *Genesis*. 2012;50(11):783-800. doi:10.1002/dvg.22039

Hari, L., Brault, V., Kleber, M., Lee, H.Y., Ille, F., Leimeroth, R., Paratore, C., Suter, U., Kemler, R., and Sommer, L. 2002. Lineage-specific requirements of beta-catenin in neural crest development. *J. Cell Biol.* 159, 867–880.

Hari, L., Miescher, I., Shakhova, O., Suter, U., Chin, L., Taketo, M., Richardson, W.D., Kessaris, N., Sommer, L. 2012. Temporal control of neural crest lineage generation by Wnt/β-catenin signaling. *Development* 139(12):2107-17.

Harris, M.L., Buac, K., Shakhova, O., Hakami, R.M., Wegner, M., Sommer, L., Pavan, W.J.. 2013. A dual role for SOX10 in the maintenance of the postnatal melanocyte lineage and the differentiation of melanocyte stem cell progenitors. *PLoS Genet.* 9(7):e1003644.

Harris, M.L., Fufa, T.D., Palmer, J.W., Joshi, S.S., Larson, D.M., Incao, A., Gildea, D.E., Trivedi, N.S., Lee, A.N., Day, C-P, et al. 2018. A direct link between MITF, innate immunity, and hair graying. PLoS Biol 16(5): e2003648.

Hayward, N.K., Wilmott, J.S., Waddell, N., Johansson, P.A., Field, M.A., Nones, K., Patch, A.M., Kakavand, H., Alexandrov, L.B., Burke, H., et al. 2017. Whole-genome landscapes of major melanoma subtypes. *Nature* 545(7653):175-180.

He, X.C., Zhang, J., Tong, W.G., Tawfik, O., Ross, J., Scoville, D.H., Tian, Q., Zeng, X., He, X., Wiedemann, L.M., et al. 2004. BMP signaling inhibits intestinal stem cell self-renewal through suppression of Wnt-beta-catenin signaling. *Nat Genet.* 36(10):1117-21.

Hsu, M.Y., Rovinsky, S., Penmatcha, S., Herlyn, M., Muirhead, D. 2005. Bone morphogenetic proteins in melanoma: angel or devil? *Cancer Metastasis Rev.* 24(2):251-63.

Hsu, Y-C., Pasolli, H.A., Fuchs, Elaine. 2011. Dynamics Between Stem Cells, Niche and Progeny in the Hair Follicle. *Cell* 144(1): 92–105.

Hsu, Y-C., Li, L., Fuchs, E. 2014. Transit-Amplifying Cells Orchestrate Stem Cell Activity and Tissue Regeneration. *Cell* 157(4):935-49.

Huang, da W., Sherman, B.T., Lempicki, R.A. 2009. Bioinformatics enrichment tools: paths toward the comprehensive functional analysis of large gene lists. *Nucleic Acids Res.* 37(1):1-13.

Huang, da W., Sherman, B.T., Lempicki, R.A. 2009. Systematic and integrative analysis of large gene lists using DAVID Bioinformatics Resources. *Nature Protoc.* 4(1):44-57.

Ikeya, M., Lee, S.M., Johnson, J.E., McMahon, A.P., Takada, S. 1997. Wnt signalling required for expansion of neural crest and CNS progenitors. *Nature* 389(6654):966-70.

Inaba, M., Chuong, C.M. 2020. Avian Pigment Pattern Formation: Developmental Control of Macro- (Across the Body) and Micro- (Within a Feather) Level of Pigment Patterns. *Front Cell Dev Biol.* 8:620.

Infarinato, N.R., Stewart, K.S., Yang, Y., Gomez, N.C., Pasolli, H.A., Hidalgo, L., Polak, L., Carroll, T.S., Fuchs, E. 2020. BMP signaling: at the gate between activated melanocyte stem cells and differentiation. *Genes & Development*, 34(23-24):1713-1734.

Ito, N., Ito, T., Kromminga, A., Bettermann, A., Takigawa, M., Kees, F., Straub, R.H., Paus, R. 2005. Human hair follicles display a functional equivalent of the hypothalamic-pituitary-adrenal axis and synthesize cortisol. *FASEB J* 19(10):1332-4.

Jin, E.J., Erickson, C.A., Takada, S., Burrus, L.W. 2001. Wnt and BMP Signaling Govern Lineage Segregation of Melanocytes in the Avian Embryo. *Dev. Biol.* 233(1):22-37.

Johansson, J.A., Marie, K.L., Lu, Y., Brombin, A., Santoriello, C., Zeng, Z., Zich, J., Gautier, P., von Kriegsheim, A., Brunsdon, H., et al. 2020. PRL3-DDX21 Transcriptional Control of Endolysosomal Genes Restricts Melanocyte Stem Cell Differentiation. *Dev Cell* 54(3):317-332.e9.

Jordan, S.A., Jackson, I.J. 2000. MGF (KIT ligand) is a chemokinetic factor for melanoblast migration into hair follicles. *Dev Biol.* 225(2):424-36.

Joshi, S.S., Tandukar, B., Pan, L., Huang, J.M., Livak, F., Smith, B.J., Hodges, T., Mahurkar, A.A., Hornyak, T.J. 2019. CD34 defines melanocyte stem cell subpopulations with distinct regenerative properties. *Plos Genetics* 15(4):e1008034.

Kapp, F.G., Perlin, J.R., Hagedorn, E.J., Gansner, J.M., Schwarz, D.E., O'Connell, L.A., Johnson, N.S., Amemiya, C., Fisher, D.E., Wölfle, U., et al. 2018. Protection from UV light is an evolutionarily conserved feature of the haematopoietic niche. *Nature* 558(7710):445-448.

Kaufman, C.K., Mosimann, C., Fan, Z.P., Yang, S., Thomas, A.J., Ablain, J., Tan, J.L., Fogley, R.D., van Rooijen, E., Hagedorn, E.J., et al. 2016. A zebrafish melanoma model reveals emergence of neural crest identity during melanoma initiation. *Science* 351(6272):aad2197.

Kawakami, T., Kimura, S., Kawa, Y., Kato, M., Mizoguchi, M., Soma, Y. 2008. BMP-4 upregulates Kit expression in mouse melanoblasts prior to the Kit-dependent cycle of melanogenesis. *J. Invest. Dermatol.* 128(5):1220-6.

Keyes, B.E., Segala, J.P., Heller, E., Lien, W-H., Chang, C.-Y., Guoc, X., Oristian, D.S., Zheng, D., Fuchs, E. 2013. Nfatc1 orchestrates aging in hair follicle stem cells. *Proc Natl Acad Sci USA* 110(51):E4950-9.

Kobielak, K., Stokes, N., de la Cruz, J., Polak, L., Fuchs, E. 2007. Loss of a quiescent niche but not follicle stem cells in the absence of bone morphogenetic protein signaling. *Proc. Natl. Acad. Sci. USA*, 104(24):10063-8.

Köhler, C., Nittner, D., Rambow, F., Radaelli, E., Stanchi, F., Vandamme, N., Baggiolini, A., Sommer, L., Berx, G., van den Oord, J.J., et al. 2017. Mouse Cutaneous Melanoma Induced by Mutant BRaf Arises from Expansion and Dedifferentiation of Mature Pigmented Melanocytes. *Cell Stem Cell* 21(5):679-693.e6.

Koludrovic, D., Laurette, P., Strub, T., Keime, C., Le Coz, M., Coassolo, S., Mengus, G., Larue, L., Davidson, I. 2015. Chromatin-Remodelling Complex NURF Is Essential for Differentiation of Adult Melanocyte Stem Cells. *PLoS Genet.* Oct 6;11(10):e1005555.

Kratochwil, K., Dull, M., Fariñas, I., Galceran, J., Grosschedl, J. 1996. *Lef* 1 expression is activated by BMP-4 and regulates inductive tissue interactions in tooth and hair development. *Genes Dev.* 10(11):1382-94.

Landsberg, J., Kohlmeyer, J., Renn, M., Bald, T., Rogava, M., Cron, M., Fatho, M., Lennerz, V., Wölfel, T., Hölzel, M., et al. 2012. Melanomas resist T-cell therapy through inflammation-induced reversible dedifferentiation. *Nature* 490(7420):412-6.

Lang, D., Lu, M.M., Huang, L., Engleka, K.A., Zhang, M., Chu, E.Y., Lipner, S., Skoultchi, A., Millar, S.E., Epstein, J.A. 2005. Pax3 functions at a nodal point in melanocyte stem cell differentiation. *Nature* 433(7028):884-7.

Larue, L., de Vuyst, F., Delmas, V. 2013. Modeling melanoblast development. *Cell Mol Life Sci.* 70(6):1067-79.

Lee, H.O., Levorse, J.M., Shin, M.K. 2003. The endothelin receptor-B is required for the migration of neural crest-derived melanocyte and enteric neuron precursors. *Dev Biol.* 259(1):162-75.

Li, A., Ma, Y., Yu, X., Mort, R.L., Lindsay, C.R., Stevenson, D., Strathdee, D., Insall, R.H., Chernoff, J., Snapper, S.B., et al. 2011. Rac1 drives melanoblast organization during mouse development by orchestrating pseudopod- driven motility and cell-cycle progression. *Dev Cell* 21(4):722-34.

Liao, C., Booker, R.C., Morrison, S., Le, L.Q. 2017. Identification of hair shaft progenitors that create a niche for hair pigmentation. *Genes Dev.* 31(8):744-756.

Liao, Y., Smyth, G.K., Shi, W. 2013. The Subread aligner: fast, accurate and scalable read mapping by seed-and-vote. *Nucleic Acids Res.* 41(10): e108.

Lin, J.Y., Fisher, D.E. 2007. Melanocyte biology and skin pigmentation. *Nature* 445(7130):843-50.

Lin, S. J., Foley, J., Jiang, T. X., Yeh, C. Y., Wu, P., Foley, A., Yen, C. M., Huang, Y. C., Cheng, H. C., Chen, C. F., et al. 2013. Topology of feather melanocyte progenitor niche allows complex pigment patterns to emerge. *Science* 340(6139), 1442–1445.

Liu, N., Matsumura, H., Kato, T., Ichinose, S., Takada, A., Namiki, T., Asakawa, K., Morinaga, H., Mohri, Y., De, et al. 2019. Stem cell competition orchestrates skin homeostasis and ageing. *Nature* 568(7752):344-350.

Love, M.I., Huber, W., Anders, S. 2014. Moderated estimation of fold change and dispersion for RNA-seq data with DESeq2. *Genome Biol.* 15(12):550.

Lu, Z., Xie, Y., Huang, H., Jiang, K., Zhou, B., Wang, F., Chen, T. 2020. Hair follicle stem cells regulate retinoid metabolism to maintain the self-renewal niche for melanocyte stem cells. *Elife* Jan 3;9:e52712.

Luciani, F., Champeval, D., Herbette, A., Denat, L., Aylaj, B., Martinozzi, S., Ballotti, R., Kemler, R., Goding, C.R., De Vuyst, F., et al. 2011. Biological and mathematical modeling of melanocyte development. *Development* 138(18):3943-54.

Macosko, E.Z., Basu, A., Satija, R., Nemesh, J., Shekhar, K., Goldman, M., Tirosh, I., Bialas, A.R., Kamitaki, N., Martersteck, E.M., et al. 2015. Highly Parallel Genome-wide Expression Profiling of Individual Cells Using Nanoliter Droplets. *Cell* 161(5):1202-1214.

Mallarino, R., Henegar, C., Mirasierra, M., Manceau, M., Schradin, C., Vallejo, M., Beronja, S., Barsh, G.S., Hoekstra, H. 2016. Developmental mechanisms of stripe patterns in rodents. *Nature* 539, 518–523.

Marks, M.S., Seabra, M.C. 2001. The melanosome: membrane dynamics in black and white. *Nat. Rev. Mol. Cell Biol.* 2(10):738-48.

Mansky, K.C., Sankar, U., Han, J., Ostrowski, M.C. 2002. Microphthalmia transcription factor is a target of the p38 MAPK pathway in response to receptor activator of NF-kappa B ligand signaling. *J Biol Chem.* 277(13):11077-83.

Marie, K.L., Sassano, A., Yang, H.H., Michalowski, A.M., Michael, H.T., Guo, T., Tsai, Y.C., Weissman, A.M., Lee, M.P., Jenkins, L.M., et al. 2020. Melanoblast transcriptome analysis reveals pathways promoting melanoma metastasis. *Nat Commun*. 11(1):333.

Matsumura, H., Mohri, Y., Binh, N.T., Morinaga, H., Fukuda, M., Ito, M., Kurata, S., Hoeijmakers, J., Nishimura, E.K. 2016. Hair follicle aging is driven by transepidermal elimination of stem cells via COL17A1 proteolysis. *Science* 351(6273):aad4395.

Maurus, K., Hufnagel, A., Geiger, F., Graf, S., Berking, C., Heinemann, A., Paschen, A., Kneitz, S., Stigloher, C., Geissinger, E., et al. 2017. The AP-1 transcription factor FOSL1 causes melanocyte reprogramming and transformation. *Oncogene* 36(36):5110-5121.

Mi, H., Muruganujan, A., Ebert, D., Huang, X., Thomas, P.D. 2019. PANTHER version 14: more genomes, a new PANTHER GO-slim and improvements in enrichment analysis tools. *Nucleic Acids Res.* 47(Database issue):D419-D426.

Mishina, Y., Hanks, M.C., Miura, S., Tallquist, M.D., Behringer, R.R. 2002. Generation of Bmpr/Alk3 conditional knockout mice. *Genesis* 32(2):69–72.

Mitra, D., Luo, X., Morgan, A., Wang, J., Hoang, M.P., Lo, J., Guerrero, C.R., Lennerz, J.K., Mihm, M.C., Wargo, J.A., et al. 2012. An ultraviolet-radiation-independent pathway to melanoma carcinogenesis in the red hair/fair skin background. *Nature* 491(7424):449-53.

Moon, H., Donahue, L.R., Choi, E., Scumpia, P.O., Lowry, W.E., Grenier, J.K., Zhu, J., White, A.C. 2017. Melanocyte stem cell activation and translocation initiate cutaneous melanoma in response to UV exposure. *Cell Stem Cell* 21, 665-678.

Moriyama, M., Osawa, M., Mak, S.S., Ohtsuka, T., Yamamoto, N., Han, H., Delmas, V., Kageyama, R., Beermann, F., Larue, L., et al. 2006. Notch signaling via Hes1 transcription factor maintains survival of melanoblasts and melanocyte stem cells. *J Cell Biol.* 173(3):333-9.

Mort, R.L., Jackson, I.J., Patton, E.E. 2015. The melanocyte lineage in development and disease. *Development* 142(4): 620:632.

Nishimura, E.K., Granter, S.R., Fisher, D.E. 2005. Mechanisms of hair graying: incomplete melanocyte stem cell maintenance in the niche. *Science* 307(5710):720-4.

Nishimura, E.K., Jordan, S.A., Oshima, H., Yoshida, H., Osawa, M., Moriyama, M., Jackson, I.J., Barrandon, Y., Nishikawa, S. 2002. Dominant role of the niche in melanocyte stem-cell fate determination. *Nature* 416(6883):854-60.

Nishimura, E.K., Suzuki, M., Igras, V., Du, J., Lonning, S., Miyachi, Y., Roes, J., Beermann, F., Fisher, D.E. 2010. Key roles for transforming growth factor beta in melanocyte stem cell maintenance. *Cell Stem Cell* 6(2):130-40.

Nishimura, E.K. 2011. Melanocyte stem cells: a melanocyte reservoir in hair follicles for hair and skin pigmentation. *Pigment Cell Melanoma Res.* 24(3):401-10.

Nusse, R., Clevers, H. Wnt/β-Catenin Signaling, Disease, and Emerging Therapeutic Modalities. *Cell* 169(6):985-999.

Okamoto, N., Aoto, T., Uhara, H., Yamazaki, S., Akutsu, H., Umezawa, A., Nakauchi, H., Miyachi, Y., Saida, T., Nishimura, E. K. 2014. A melanocyte-melanoma precursor niche in sweat glands of volar skin. *Pigment Cell Melanoma Res.* 27, 1039-1050.

Osawa, M., Egawa, G., Mak, S.S., Moriyama, M., Freter, R., Yonetani, S., Beermann, F., Nishikawa, S. 2005. Molecular characterization of melanocyte stem cells in their niche. *Development* 132(24):5589-99.

Oshimori, N., Fuchs, E. 2012. Paracrine TGF-β signaling counterbalances BMP-mediated repression in hair follicle stem cell activation. *Cell Stem Cell* 10(1):63-75.

Oshimori, N., Oristian, D., Fuchs, E. 2015. TGF-β promotes heterogeneity and drug resistance in squamous cell carcinoma. *Cell* 160(5):963-976.

Park, H-Y., Wu, C., Yaar, M., Stachur, C.M., Kosmadaki, M., Gilchrest, B.A. 2009. Role of BMP-4 and Its Signaling Pathways in Cultured Human Melanocytes. *Int. J. Cell Biol.* 2009: 750482.

Patro, R., Duggal, G., Love, M.I., Irizarry, R.A., Kingsford, C. 2017. Salmon provides fast and bias-aware quantification of transcript expression. *Nat. Methods* 14(4):417-419.

Pedregosa, F., Varoquaux, G., Gramfort, A., Michel, V., Thirion, B., Grisel, O., Blondel, M., Prettenhofer, P., Weiss, R., Dubourg, V. et al. 2011. Scikit-learn: Machine Learning in Python. *Journal of Machine Learning Research* 12, 2825-2830.

Picelli S, Björklund ÅK, Faridani OR, Sagasser S, Winberg G, Sandberg R. 2013. Smart-seq2 for sensitive full-length transcriptome profiling in single cells. *Nature Methods* 11:1096-8.

Picelli, S., Faridani, O.R., Bjorklund, A.K., Winberg, G., Sagasser, S., Sandberg, R. 2014. Full-length RNA-seq from single cells using Smart-seq2. *Nat. Protoc.* 9(1):171-81.

Plikus, M.V., Mayer, J.A., de la Cruz, D., Baker, R.E., Maini, P.K., Maxson, R., Chuong, C.M. 2008. Cyclic dermal BMP signalling regulates stem cell activation during hair regeneration. *Nature* 451(7176):340-4.

Ploper, D., Taelman, V.F., Robert, L., Perez, B.S., Titz, B., Chen, H.W., Graeber, T.G., von Euw, E., Ribas, A., De Robertis, E.M. 2015. MITF drives endolysosomal biogenesis and potentiates Wnt signaling in melanoma cells. *Proc. Natl. Acad. Sci. USA* 112(5):E420-9.

Potterf, S., Furumura, M., Dunn, K. Arnheiter, H., Pavan, W.J. 2000. Transcription factor hierarchy in Waardenburg syndrome: regulation of MITF expression by SOX10 and PAX3. *Hum Genet* 107, 1–6.

Price, E.R., Fisher, D.E. 2001. Sensorineural deafness and pigmentation genes: melanocytes and the Mitf transcriptional network. *Neuron* 30(1):15-8.

Rabbani, P., Takeo, M., Chou, W., Myung, P., Bosenberg, M., Chin, L., Taketo, M.M., Ito, M. 2011. Coordinated activation of Wnt in epithelial and melanocyte stem cells initiates pigmented hair regeneration. *Cell* 145(6):941-955.

Rendl, M., Lewis, L., Fuchs, E. 2005. Molecular dissection of mesenchymal-epithelial interactions in the hair follicle. *PLoS Biol.* 3(11):e331.

Riesenberg, S., Groetchen, A., Siddaway, R., Bald, T., Reinhardt, J., Smorra, D., Kohlmeyer, J., Renn, M., Phung, B., Aymans, P., et al. 2015. MITF and c-Jun antagonism interconnects melanoma dedifferentiation with pro-inflammatory cytokine responsiveness and myeloid cell recruitment. *Nat Commun.* 6:8755.

Ritchie, M.E., Phipson, B., Wu, D., Hu, Y., Law, C.W., Shi, W., Smyth, G.K. 2015. Limma powers differential expression analyses for RNA-sequencing and microarray studies. *Nucleic Acids Research,* 43(7), e47.

Roesch, A., Fukunaga-Kalabis, M., Schmidt, E.C., Zabierowski, S.E., Brafford, P.A., Vultur, A., Basu, D., Gimotty, P., Vogt, T., Herlyn, M. 2010. A temporarily distinct subpopulation of slow-cycling melanoma cells is required for continuous tumor growth. *Cell* 141(4):583-94.

Ross-Innes, C.S., Stark, R., Teschendorff, A.E., Holmes, K.A., Ali, H.R., Dunning, M.J., Brown, G.D., Gojis, O., Ellis, I.O., Green, A.R., et al. 2012. Differential oestrogen receptor binding is associated with clinical outcome in breast cancer. *Nature* 481(7381):389-93.

Rothhammer, T., Poser, I., Soncin, F., Bataille, F., Moser, M., Bosserhoff, A.K. 2005. Bone morphogenic proteins are overexpressed in malignant melanoma and promote cell invasion and migration. *Cancer Res.* 65:448-456.

Saito, H., Yasumoto, K., Takeda, K., Takahashi, K., Fukuzaki, A., Orikasa, S., Shibahara, S. 2002. Melanocyte-specific microphthalmia-associated transcription factor isoform activates its own gene promoter through physical interactions with lymphoid-enhancing factor 1. *J. Biol. Chem.* 277(32):28787-94.

Santoriello, C., Sporrij, A., Yang, S., Flynn, R.A., Henriques, T., Dorjsuren, B., Custo Greig, E., McCall, W., Stanhope, M.E., Fazio M, et al. 2020. RNA helicase DDX21 mediates nucleotide stress responses in neural crest and melanoma cells. *Nat Cell Biol.* 22(4):372-379.

Schadendorf, D., van Akkooi, A.C.J., Berking, C., Griewank, K.G., Gutzmer, R., Hauschild, A., Stang, A., Roesch, A., Ugurel, S. 2018. Melanoma. *Lancet* 392: 971-84.

Schatton, T., Murphy, G.F., Frank, N.Y., Yamaura, K., Waaga-Gasser, A.M., Gasser, M., Zhan, Q., Jordan, S., Duncan, L.M., Weishaupt, C., et al. 2008. Identification of cells initiating human melanomas. *Nature* 451(7176):345-9.

Schep, A., Bioconductor team. 2014. BSgenome.Mmusculus.UCSC.mm10: Full genome sequences for Mus musculus (UCSC version mm10). R package version 1.4.0. motifmatchr: Fast Motif Matching in R. R package version 1.10.0.

Schouwey, K., Delmas, V., Larue, L., Zimber-Strobl, U., Strobl, L.J., Radtke, F., Beermann, F. 2007. Notch1 and Notch2 receptors influence progressive hair graying in a dose-dependent manner. *Dev Dyn.* 236(1):282-9.

Shin, M., Levorse, J., Ingram, R., Tilghman, S.M.. 1999. The temporal requirement for endothelin receptor-B signalling during neural crest development. *Nature* 402, 496–501.

Sharma, P., Allison, J.P. 2015. The future of immune checkpoint therapy. *Science* 348(6230):56-61.

Sharov, A.A., Fessing, M., Atoyan, R., Sharova, T.Y., Haskell-Luevano, C., Weiner, L., Funa, K., Brissette, J.L., Gilchrest, B.A., Botchkarev, V.A. 2005. Bone morphogenetic protein (BMP) signaling controls hair pigmentation by means of cross-talk with the melanocortin receptor-1 pathway. *Proc. Natl. Acad. Sci. USA* 102(1):93-8.

Singh, S.K., Abbas, W.A., Tobin, D.J. 2012. Bone morphogenetic proteins differentially regulate pigmentation in human skin cells. *J. Cell Science* 125: 4306-4319.

Sinnberg, T., Niessner, H., Levesque, M.P., Dettweiler, C., Garbe, C., Busch, C. 2018. Embryonic bone morphogenetic protein and nodal induce invasion in melanocytes and melanoma cells. *Biol. Open.* 7(6).

Skene, P.J., Henikoff, S. 2017. An efficient targeted nuclease strategy for high-resolution mapping of DNA binding sites. *Elife* Jan 16;6:e21856.

Soneson, C., Love, M.I., Robinson, M.D. 2015. Differential analyses for RNA-seq: transcript-level estimates improve gene-level inferences. *F1000Res.* 4:1521

Srinivas, S., Watanabe, T., Lin, C.S., William, C.M., Tanabe, Y., Jessell, T.M., Costantini, F. 2001. Cre reporter strains produced by targeted insertion of EYFP and ECFP into the ROSA26 locus. *BMC Dev. Biol.* 1(1):4.

Staricco, R.G. 1959. Amelanotic melanocytes in the outer sheath of the human hair follicle. *J Invest Dermatol*. 33:295-7.

Strauss, D.C., Thomas, J.M. 2010. Transmission of donor melanoma by organ transplantation. *Lancet Oncol.* 11(8):790-6.

Stuart, T., Butler, A., Hoffman, P., Hafemeister, C., Papalexi, E., Mauck, W.M. 3rd, Hao, Y., Stoeckius, M., Smibert, P., Satija, R. 2019. Comprehensive Integration of Single-Cell Data. *Cell* 177(7):1888-1902.

Su, J., Morgani, S.M., David, C.J., Wang, Q., Er, E.E., Huang, Y.H., Basnet, H., Zou, Y., Shu, W., Soni RK, et al. 2020. TGF-β orchestrates fibrogenic and developmental EMTs via the RAS effector RREB1. *Nature* 577(7791):566-571.

Sun, Q., Lee, W., Mohri, Y., Takeo, M., Lim, C.H., Xu, X., Myung, P., Atit, R.P., Taketo, M.M., Moubarak, R.S., et al. 2019. A novel mouse model demonstrates that oncogenic melanocyte stem cells engender melanoma resembling human disease. *Nat. Commun.* 10(1):5023

Suzuki, I., Cone, R.D., Im, S., Nordlund, J., Abdel-Malek, Z.A. 1996. Binding of melanotropic hormones to the melanocortin receptor MC1R on human melanocytes stimulates proliferation and melanogenesis. *Endocrinology* 137(5):1627-33.

Sviderskaya E.V., Wakeling, W.F., Bennett, D.C. 1995. A cloned, immortal line of murine melanoblasts inducible to differentiate to melanocytes. *Development* 121(5):1547-57.

Tabone-Eglinger, S., Wehrle-Haller, M., Aebischer, N., Jacquier, M.C., Wehrle-Haller, B. 2012. Membrane-bound Kit ligand regulates melanocyte adhesion and survival, providing physical interaction with an intraepithelial niche. *FASEB J* 26(9):3738-53.

Takeda, K., Yasumoto, K., Takada, R., Takada, S., Watanabe, K., Udono, T., Saito, H., Takahashi, K., Shibahara, S. 2000. Induction of melanocyte-specific microphthalmia-associated transcription factor by Wnt-3a. *J. Biol. Chem.* 275(19):14013-6.

Takeo, M., Lee, W., Rabbani, P., Sun, Q., Hu, H., Lim, C.H., Manga, P., Ito, M. 2016. EdnrB governs regenerative response of melanocyte stem cells by crosstalk with Wnt signaling. *Cell Rep.* 15(6):1291-302.

Tanimura, S., Tadokoro, Y., Inomata, K., Binh, N.T., Nishie, W., Yamazaki, S., Nakauchi, H., Tanaka, Y., McMillan, J.R., Sawamura, D., et al. 2011. Hair follicle stem cells provide a functional niche for melanocyte stem cells. *Cell Stem Cell* 8(2):177-87.

Thomas, A.J., Erickson, C.A. 2008. The making of a melanocyte: the specification of melanoblasts from the neural crest. *Pigment Cell Melanoma Res.* 21(6):598-610.

Thomas, A.J., Erickson, C.A.2009. FOXD3 regulates the lineage switch between neural crest-derived glial cells and pigment cells by repressing MITF through a non-canonical mechanism. *Development* 136(11):1849-58.

Thomas, P.D., Kejariwal, A., Guo, N., Mi, H., Campbell, M.J., Muruganujan, A., Lazareva-Ulitsky, B. 2006. Applications for protein sequence–function evolution data: mRNA/protein expression analysis and coding SNP scoring tools. *Nucleic Acids Res.* 34(Web Server issue): W645–W650.

Tirosh, I., Izar, B., Prakadan, S.M., Wadsworth, M.H. 2nd, Treacy, D., Trombetta, J.J., Rotem, A., Rodman, C., Lian, C., Murphy, G., et al. 2016. Dissecting the multicellular ecosystem of metastatic melanoma by single-cell RNA-seq. *Science* 352(6282):189-96.

Tobin, D.J., Hagen, E., Botchkarev, V.A., Paus, R. 1998. Do hair bulb melanocytes undergo apoptosis during hair follicle regression (catagen)? *J Invest Dermatol.* 111(6):941-7.

Trapnell, C., Cacchiarelli, D., Grimsby, J., Pokharel, P., Li, S., Morse, M., Lennon, N.J., Livak, K.J., Mikkelsen, T.S., Rinn, J.L. 2014. Pseudo-temporal ordering of individual cells reveals dynamics and regulators of cell fate decisions. *Nat. Biotechnol.* 32(4): 381–386.

Trucco, L.D., Mundra, P.A., Hogan, K., Garcia-Martinez, P., Viros, A., Mandal, A.K., Macagno, N., Gaudy-Marqueste, C., Allan, D., Baenke, F., et al. 2019. Ultraviolet radiation-induced DNA damage is prognostic for outcome in melanoma. *Nat Med.* 25(2):221-224.

Ubellacker, J.M., Tasdogan, A., Ramesh, V., Shen, B., Mitchell, E.C., Martin-Sandoval, M.S., Gu, Z., McCormick, M.L., Durham, A.B., Spitz, D.R., et al. 2020. Lymph protects metastasizing melanoma cells from ferroptosis. *Nature* 585(7823):113-118.

Ueno, M., Aoto, T., Mohri, Y., Yokozeki, H., Nishimura, E. K. 2014. Coupling of the radiosensitivity of melanocyte stem cells to their dormancy during the hair cycle. *Pigment Cell Melanoma Res.* 27(4):540-51.

Valluet, A., Druillennec, S., Barbotin, C., Dorard, C., Monsoro-Burq, A.H., Larcher, M., Pouponnot, C., Baccarini, M., Larue, L., Eychène, A. 2012. B-Raf and C-Raf are required for melanocyte stem cell self-maintenance. *Cell Rep.* 2(4):774-80.

van Genderen, C., Okamura, R.M., Fariñas. I., Quo, R.G., Parslow, T.G., Bruhn, L., Grosschedl, R. 1994. Development of several organs that require inductive epithelial-mesenchymal interactions is impaired in LEF-1-deficient mice. *Genes Dev.* 8(22):2691-703.

van Velthoven C.T.J., Rando T.A. 2019. Stem Cell Quiescence: Dynamism, Restraint, and Cellular Idling. *Cell Stem Cell* 24(2):213-225.

Venkatesan, A.M., Vyas, R., Gramann, A.K., Dresser, K., Gujja, S., Bhatnagar, S., Chhangawala, S., Gomes, C.B.F., Xi, H.S., Lian, C.G., et al. 2018. Ligand-activated BMP signaling inhibits cell differentiation and death to promote melanoma. J. *Clin. Invest.* 128(1): 294-308.

Wang, R.N., Green, J., Wang, Z., Deng, Y., Qiao, M., Peabody, M., Zhang, Q., Ye, J., Yan. Z., Denduluri S., et al. 2014. Bone Morphogenetic Protein (BMP) signaling in development and human diseases. *Genes Dis.* 1(1):87-105.

Wood, J.M., Decker, H., Hartmann, H., Chavan, B., Rokos, H., Spencer, J.D., Hasse, S., Thornton, M.J., Shalbaf, M., Paus, R., et al. 2009. Senile hair graying: H2O2-mediated oxidative stress affects human hair color by blunting methionine sulfoxide repair. FASEB J., 23(7):2065-75.

Yaar, M., Wu, C., Park, H.Y., Panova, I., Schutz, G., Gilchrest, B.A. 2006. Bone morphogenetic protein-4, a novel modulator of melanogenesis. *J. Biol. Chem.* 281(35):25307-14.

Yang, H., Adam, R.C., Ge, Y., Hua, Z.L., Fuchs E. 2017. Epithelial-Mesenchymal Micro-niches Govern Stem Cell Lineage Choices. *Cell* 169(3):483-496.

Yang, J., Wang, J., Pan, L., Li, H., Rao, C., Zhang, X., Niu, G., Qu, J., Hou, L. 2014. BMP4 is required for the initial expression of MITF in melanocyte precursor differentiation from embryonic stem cells. *Exp. Cell Res.* 320(1):54-61.

Yasumoto, K., Takeda, K., Saito, H., Watanabe, K., Takahashi, K., Shibahara, S. 2002. Microphthalmia-associated transcription factor interacts with LEF-1, a mediator of Wnt signaling. *EMBO J.* 21(11):2703-14.

Yoshida, H., Kunisada, T., Kusakabe, M., Nishikawa, S., Nishikawa, S.I. 1996. Distinct stages of melanocyte differentiation revealed by analysis of nonuniform pigmentation patterns. *Development* 122(4):1207-14.

Yoshida, H., Hayashi, S., Shultz, L.D., Yamamura, K., Nishikawa, S., Nishikawa, S., Kunisada, T. 1996. Neural and skin cell-specific expression pattern conferred by steel factor regulatory sequence in transgenic mice. *Dev. Dyn*. 207, 222–232.

Zhang, B., Ma, S., Rachmin, I., He, M., Baral, P., Choi, S., Gonçalves, W.A., Shwartz, Y, Fast, E.M., Su, Y., et al. 2020. Hyperactivation of sympathetic nerves drives depletion of melanocyte stem cells. *Nature* 577(7792):676-681.

Zhang, Y., Liu T, Meyer C.A., Eeckhoute, J., Johnson, D.S., Bernstein, B.E., Nusbaum, C., Myers, R.M., Brown, M., Li, W., Liu, X.S. 2008. Model-based analysis of ChIP-Seq (MACS). *Genome Biol.* 9(9):R137

Zhang, Z., Lei, M., Xin, H., Hu, C., Yang, T., Xing, Y., Li, Y., Guo, H., Lian, X., Deng, F. 2017. Wnt/β-catenin signaling promotes aging-associated hair graying in mice. *Oncotarget* 8(41):69316-69327

Zhou, X., Xue, H.H. 2012. Cutting edge: generation of memory precursors and functional memory CD8+ T cells depends on T cell factor-1 and lymphoid enhancer-binding factor-1. *J Immunol.* 189(6):2722-6

Zhou, X.P., Woodford-Richens, K., Lehtonen, R., Kurose, K., Aldred, M., Hampel, H., Launonen, V., Virta, S., Pilarski, R., Salovaara, R., et al. 2001. Germline mutations in BMPR1A/ALK3 cause a subset of cases of juvenile polyposis syndrome and of Cowden and Bannayan-Riley-Ruvalcaba syndromes. *Am J Hum Genet.* 69(4):704-11.